

ADA 260 966

BNL-48106
INFORMAL REPORT

Advanced Zinc Phosphate Conversion and Pre-Ceramic
Polymetallosiloxane Coatings For Corrosion Protection
of Steel and Aluminum, and Characteristics of
Polyphenyletheretherketone-Based Materials

das

Final Report

T. Sugama and N.R. Carciello

July 1992

Prepared for:
U.S. Army Research Office
P.O. Box 12211
Research Triangle Park, NC 27709

Energy Efficiency and Conservation Division

DEPARTMENT OF APPLIED SCIENCE

BROOKHAVEN NATIONAL LABORATORY
UPTON, LONG ISLAND, NEW YORK 11973

bnl
ccw

DISCLAIMER

This report was prepared as an account of work sponsored by an agency of the United States Government. Neither the United States Government nor any agency thereof, nor any of their employees, nor any of their contractors, subcontractors, or their employees makes any warranty, express or implied, or assumes any legal liability or responsibility for the accuracy, completeness, or usefulness of any information, apparatus, product or process disclosed, or represents that its use would not infringe privately owned rights. Reference herein to any specific commercial product, process, or service by trade name, trademark, manufacturer, or otherwise, does not necessarily constitute or imply its endorsement, recommendation, or favoring by the United States Government or any agency thereof. The views and opinions of authors expressed herein do not necessarily state or reflect those of the United States Government or any agency, contractor, or subcontractor thereof.

Advanced Zinc Phosphate Conversion and Pre-Ceramic Polymetallosiloxane
Coatings For Corrosion Protection of Steel and Aluminum, and
Characteristics of Polyphenyletheretherketone-Based Materials

Final Report

T. Sugama and N.R. Carciello

July 1992

Prepared for the
U.S. Army Research Office
P.O. Box 12211
Research Triangle Park, NC 27709

Energy Efficiency and Conservation Division
Department of Applied Science
Brookhaven National Laboratory
Upton, New York 11973

This work was performed under the auspices of the U.S. Department of
Energy, Washington, D.C. Under Contract No. DE-AC02-76CH00016

REPORT DOCUMENTATION PAGE			Form Approved OMB No. 0704-0188	
<small>Public reporting burden for this collection of information is estimated to average 1 hour per response, including the time for reviewing instructions, searching existing data sources, gathering and maintaining the data needed, and completing and reviewing the collection of information. Send comments regarding this burden estimate or any other aspect of this collection of information, including suggestions for reducing this burden, to Washington Headquarters Services, Directorate for Information Operations and Reports, 1215 Jefferson Davis Highway, Suite 1204, Arlington, VA 22202-4302, and to the Office of Management and Budget, Paperwork Reduction Project (0704-0188), Washington, DC 20503.</small>				
1. AGENCY USE ONLY (Leave blank)		2. REPORT DATE 09/24/92		3. REPORT TYPE AND DATES COVERED
4. TITLE AND SUBTITLE Advanced Zinc Phosphate Conversion and Pre-Ceramic Polymetallosiloxane Coatings for Corrosion Protection of Steel and Aluminum, and Characteristics of Polyphenyletheretherketone-Based Materials				5. FUNDING NUMBERS
6. AUTHOR(S) T. Sugama and N.R. Carciello				
7. PERFORMING ORGANIZATION NAME(S) AND ADDRESS(ES) Associated Universities, Inc. Brookhaven National Laboratory Upton, NY 11973				8. PERFORMING ORGANIZATION REPORT NUMBER
9. SPONSORING/MONITORING AGENCY NAME(S) AND ADDRESS(ES) U. S. Army Research Office P. O. Box 12211 Research Triangle Park, NC 27709-2211				10. SPONSORING/MONITORING AGENCY REPORT NUMBER
11. SUPPLEMENTARY NOTES The view, opinions and/or findings contained in this report are those of the author(s) and should not be construed as an official Department of the Army position, policy, or decision, unless so designated by other documentation.				
12a. DISTRIBUTION/AVAILABILITY STATEMENT Approved for public release; distribution unlimited.				12b. DISTRIBUTION CODE
13. ABSTRACT (Maximum 200 words) The characteristics of anhydrous zinc phosphate (Zn-Ph) coatings deposited by immersing the steel in transition Co, Ni, and Mn cation-incorporated phosphating solutions were investigated. Two important features for the anhydrous 340°C-heated Zn-Ph were addressed. One was to determine if the electron trapping behavior of Co^{2+} and Ni^{2+} ions adsorbed in the crystal lattices acts to inhibit the cathodic reaction on the Zn-Ph, and the second was to determine the less susceptibility of the $\alpha\text{-Zn}_3(\text{PO}_4)_2$ phase to alkali-induced dissolution. The factors governing the film-forming performance of pre-ceramic polymetallosiloxane (PMS) coatings for aluminum (Al) substrate surfaces were investigated. Four factors were important in obtaining a good film: 1) the formation of organopolymetallosiloxane at sintering temperatures of 150°C; 2) the pyrolytic conversion at 350°C into an amorphous PMS network structure in which the Si-O-M linkage were moderately enhanced; 3) the non-crystalline phases; and 4) the formation of interfacial oxane bond between PMS and Al oxide. The formation of well-crystallized polyphenyletheretherketone (PEEK) in the vicinity of silica aggregates was found in the molded body made in N_2 . Such a PEEK crystalline structure contributed significantly to the thermal and hydrothermal stabilities of mortar specimens at temperatures up to 200°C, and the resistance in 5 wt% H_2SO_4 solution at 80°C.				
14. SUBJECT TERMS anhydrous zinc phosphate, steel, corrosion, polymetallosiloxane, aluminum, polyphenyletheretherketone				15. NUMBER OF PAGES 10
				16. PRICE CODE
17. SECURITY CLASSIFICATION OF REPORT UNCLASSIFIED	18. SECURITY CLASSIFICATION OF THIS PAGE UNCLASSIFIED	19. SECURITY CLASSIFICATION OF ABSTRACT UNCLASSIFIED	20. LIMITATION OF ABSTRACT UL	

STATEMENT OF WORK

Under U.S. Army Research Office (ARO) sponsorship, on Contract Numbers, MIPR-AR0102-89, 103-90, 119-91 and 157-92, Brookhaven National Laboratory (BNL) performed research on three topics:

- 1) Advanced zinc phosphate conversion coatings,
- 2) Synthesis and characteristics of pre-ceramic polymetallosiloxane coating films, and
- 3) Crystalline polyphenyletheretherketone (PEEK) - based materials.

Major research activities within each of these topics are described below.

1. Advanced Zinc Phosphate Conversion Coatings

The major phase in the insoluble zinc phosphate (Zn·Ph) conversion coatings, which is responsible for improved corrosion protection, was identified to be the same $\text{Zn}_3(\text{PO}_4)_2 \cdot 2\text{H}_2\text{O}$, as that used as a starting material. From the viewpoint of crystal molecular structure, because Zn·Ph layers contain a certain amount of crystallized water, it should be considered that when thermal barrier organic topcoat systems, such as polyimide [1,2], polybenzimidazoles [2], polyquinoxalines [3,4], and polyphenylene sulphide [4], are applied directly to the Zn·Ph surface, high-temperature treatment of the topcoats to form solid polymer films will lead to interfacial disbondment and separation brought about by the dehydration of the Zn·Ph. This failure is associated with the formation of weak boundary layers, resulting in poor corrosion protection. It was very important, therefore, to gain fundamental knowledge regarding the thermal degradation and phase transformation of Zn·Ph at an elevated temperature, before studying the interfacial chemical nature between the high-temperature performance polymers and the crystalline Zn·Ph. On the other hand, during the corrosion of iron and steel in a near neutral aqueous environment, the cathodic half reaction in terms of the oxygen reduction reaction, is $\text{H}_2\text{O} + 1/2 \text{O}_2 + 2\text{e}^- = 2 \text{OH}^-$. A shortcoming of Zn·Ph coatings as a barrier to the corrosion of steel is that the hydroxyl ions generated by this cathodic reaction [5] induce dissolution of the coating layers. A lower susceptibility of Zn·Ph to alkali dissolution also minimizes cathodic delamination rates for polymeric topcoat films. Thus, it was very important in assessing anticorrosive coatings to estimate the extent of alkali dissolution of Zn·Ph.

The ionic and/or elemental cobalt and nickel atoms are well-known inhibitors of the cathodic reaction of electrogalvanized steel [6-9]. The mechanism of this inhibition of corrosion was described by Leidheiser and Suzuki [10] as being due to the electron trapping reactions, M^{2+} (M: Co and Ni) + $2\text{e}^- = \text{M}^0$, of such atoms doped in the zinc oxide lattice. The M^{2+} ions favorably trap the electrons evolved from the anodic reaction, $\text{Zn}^0 - 2\text{e}^- \longrightarrow \text{Zn}^{2+}$, occurring at the oxide/solution interface, thereby inhibiting the cathodic reaction.

Accordingly, the emphasis of our present study was directed towards developing and characterizing advanced hydrous and anhydrous Zn·Ph containing the Co and Ni atoms, and poly(acrylic)acid, p(AA), which is a polyelectrolyte macromolecule species. The advanced Zn·Ph coatings will inhibit oxygen reduction reactions and minimize the rate of cathodic delamination of high-temperature performance polymer topcoats from phosphated steels.

2. Synthesis of Pre-Ceramic Polymetallosiloxane Coating Films

Ceramic coatings have not yet been widely used on aluminum and magnesium alloys, and on other low melting-point metal substrates because of two main reasons. First, coatings must adhere well and have an appropriate expansion coefficient, especially during temperature cycling, otherwise the coating will separate from the substrate. Second, many ceramic coatings must be applied and processed at high temperature ($>1000^{\circ}\text{C}$), using expensive and time-consuming methods, such as chemical vapor deposition.

To solve these problems with conventional ceramic coatings, our work was focused upon the synthesis of pre-ceramic inorganic polymetallosiloxane (PMS) polymers, and upon the characteristics of the synthesized PMS as corrosion-protective coatings on aluminum substrates.

The use of metal alkoxides, $\text{M}(\text{OR})_4$ (where M is Ti, Zr, Ge, Al, B, La, and Sn, R is CH_3 , C_2H_5 , C_3H_7 or C_4H_9), as a means of enhancing the network connectivity and, hence, the extent of three-dimensional crosslinking of polymeric organosilanes synthesized using sol-gel techniques in terms of hydrolysis-polycondensation processes, was investigated previously [11, 12]. These authors reported that the incorporation of $\text{M}(\text{OR})_4$ into the organosilane system improved mechanical properties such as the modulus of elasticity and tensile strength of the organosiloxane polymer. Huang et al. also reported that the addition of excessive amounts of $\text{M}(\text{OR})_4$ to the systems results in large reductions in the elongation at the failure point of the polymers [13]. All of these studies were performed at temperatures up to 220°C .

An inorganic polysilane formed by a sol-gel polycondensation process involving tetraethylorthosilicate, $\text{Si}(\text{OC}_2\text{H}_5)_4$, is presently used as a binder in inorganic zinc-rich primers, which act to inhibit the corrosion of metals [14]. The major characteristics of these cured inorganic zinc primer films are their excellent adhesion to metallic substrates, thermal stability, resistance to ultraviolet light and weathering, and abrasion. As a result, they appear promising for use as reliable underlying structures to which organic topcoats can be applied.

On the basis of the above information, our attention was focused on the characteristics of polymeric materials synthesized through hydrolysis-condensation reactions of $\text{M}(\text{OR})_4$ -incorporated organosilane monomeric mixtures over the temperature range $100\text{--}500^{\circ}\text{C}$. When film fabrication temperatures $\geq 300^{\circ}\text{C}$ are considered, it can be assumed that a large number of carbon-containing groups will be eliminated pyrolytically from the polymer network structures as a result of elevated temperature. Hence, attention was given to the pyrolytic changes in the conformation of M compound-modified organosilane polymers. Such conformational changes and their processes, as a function of temperature,

may be different, depending on the species of organosilane and the proportions of organosilane to $M(OR)_4$ used as original starting materials.

To obtain such information, we examined three topics. First, emphasis was placed on the pyrolytic conformational changes and the mechanisms of Ti compound-modified organosilane polymers formed at various $Ti(OR)_4$ to organosilane monomer ratios. In this study, the 3-glycidoxypropyltrimethoxysilane (GPS) examined by previous investigators [11,12] was used. The observed conformational changes were correlated with alterations in the surface morphology, changes in surface chemical composition and chemical states of the Ti compound-modified GPS coating films overlayed on aluminum substrates at temperatures up to 500°C. The ability of the coatings formed at temperatures ranging from 100°C to 500°C to inhibit the pitting corrosion of aluminum was studied secondly. The third research topic focused on the use of other metal alkoxide species, such as $Al(OC_3H_7)_3$, and $Zr(OC_3H_7)_4$. In addition, the fabrication of thin films (thickness $<1\mu m$), which may form microcrack-free coatings, because of lower rates of volatility and pyrolysis, was also considered. Finally, based upon fundamental knowledge obtained from the above studies, efforts were then focused on the fabrication of good coating films and the evaluation of their corrosion protective performance.

3. Crystalline Polyphenyletheretherketone (PEEK) - Based Materials

The melt crystallized polyaryl polymers, such as polyphenylenesulphide (PPS), $\left(\text{C}_6\text{H}_4\text{-S} \right)_n$, polyphenyletheretherketone (PEEK), $\left(\text{C}_6\text{H}_4\text{-C(=O)-C}_6\text{H}_4\text{-O-C}_6\text{H}_4\text{-O} \right)_n$, and polyphenyletherketone (PEK), $\left(\text{C}_6\text{H}_4\text{-C(=O)-C}_6\text{H}_4\text{-O} \right)_n$, have common chemical features consisting of aromatic backbone chains coupled with oxygen, ketone, and/or sulphur. When these linear polymers are left in an oven at a temperature above their melting point of $> 280^\circ\text{C}$, chain extension of the main phenyl groups caused by melting leads to molecular orientation, which is reflected in the crystallization of the polymers during cooling from the melting temperature to a lower temperature [15-17]. Such crystallization behavior of the polyaryls gives them specific desirable characteristics as adhesives, such as high temperature stability, high radiation, chemical, and hydrothermal resistance, and good mechanical and dielectric properties. Thus, polyaryls have become of increasing interest for applications in coatings, as adhesives, and in composites.

Our particular interest was to investigate the thermal, hydrothermal, and chemical durabilities of PEEK polymer mortar specimens, which were prepared by the melting-cooling processes of PEEK powder-sand mixtures. In addition, the thermal characteristics, crystalline behavior, and change in chemical structure of the PEEK neat cements under air or N_2 environments were also explored.

SUMMARY OF RESULTS

1. Advanced Zinc Phosphate Conversion Coatings

Advanced Zn·Ph conversion coatings can be prepared by immersing steel in Co^{2+} and Ni^{2+} ion-incorporated p(AA)-zinc phosphate solution systems. The formation of M^{2+} (M: Co and Ni)-p(AA) salt complexes containing $-\text{COO}^- \text{M}^{2+} -\text{OOC}-$ groups played an important role in accelerating and promoting the growth and development of Zn·Ph crystal layers over the steel, and also introduced amorphous Fe-rich phosphate conversion layers in the vicinity of Fe_2O_3 substrates. The electron trapping behavior of the M^{2+} ions dissociated from the complex formations and M hydroxides in the NaCl solution inhibited cathodic reactions, thereby resulting in an extended lifetime for the Zn·Ph, which serves to provide corrosion protection for steel. In the final stages of the conversion process, the crystal phase of Ni system-derived conversion coatings consisted of zinc orthophosphate dihydrate, $[\text{Zn}_3(\text{PO}_4)_2 \cdot 2\text{H}_2\text{O}]$ as the major component and hopeite, $[\text{Zn}_3(\text{PO}_4)_2 \cdot 4\text{H}_2\text{O}]$ as the minor one. The uniform coverage of $\text{Zn}_3(\text{PO}_4)_2 \cdot 2\text{H}_2\text{O}$ -hopeite interlocked crystals over the steel may reduce the rate of corrosion.

In thermal dehydration processes at 340°C , a hopeite $\rightarrow \gamma\text{-Zn}_3(\text{PO}_4)_2$ phase transition occurs. In contrast, the $\text{Zn}_3(\text{PO}_4)_2 \cdot 2\text{H}_2\text{O}$ was preferentially converted into the $\alpha\text{-Zn}_3(\text{PO}_4)_2$ phase which has a alkali dissolution rate considerably lower than that of the γ -phase. This results in a minimized cathodic delamination rate of polymeric films from α -phase steel substrates.

When high-temperature performance PPS polymer coatings were directly applied to cold-rolled steel surfaces, the chemical reaction at 350°C between the Fe_2O_3 at the outermost surfaces of the steel and the PPS in air led to the formation of FeSO_4 at the critical interfacial zones. Although the intermediate FeSO_4 layers, as interfacial reaction products, play an important role in developing bond strength at the PPS/steel joint, the alkali-catalyzed hydrolysis of FeSO_4 caused by the cathodic reaction, $\text{H}_2\text{O} + 1/2\text{O}_2 + 2\text{e}^- = 2\text{OH}^-$, at any defects in the coating film, caused catastrophic cathodic delamination of the PPS film from the steel. Therefore, to avoid the direct contact of PPS with steel, a p(AA)-modified Zn·Ph conversion coating was deposited on the steel surfaces. Before applying the PPS, the $\text{Zn}_3(\text{PO}_4)_2 \cdot 2\text{H}_2\text{O}$ as a major phase of the Zn·Ph layers was converted into an $\alpha\text{-Zn}_3(\text{PO}_4)_3$ phase by thermal dehydration at 350°C . This thermal treatment also promoted the transformation of the poly(acid) structure within the p(AA) into the poly(acid)anhydride, and the oxidation of free Fe atoms dissociated from the steel surfaces during the precipitation of the crystalline Zn·Ph coating. We found that SO_2 emitted from the PPS at the PPS-to-Zn·Ph boundary regions preferentially reacts with the oxidized Fe compounds, rather than with Zn and P atoms in the Zn·Ph crystals. Such a gas-solid interaction between SO_2 and the oxidized Fe compound at 350°C caused the formation of a FeS reaction product. In addition, the two different interactions were recognized: one was the polymer-to-polymer reaction between the PPS and the poly(acid)anhydride existing at the outer surface of the Zn·Ph layers; the other was the mechanical interlocking associated with the mechanical anchoring of the PPS polymer, which resulted from the penetration of the melted polymer into the open surface microstructure of the Zn·Ph layers. These physico-chemical factors,

contributing to the development of adhesion force at the PPS/Zn·Ph interfaces, were essentially responsible for a high lap-shear bond strength on the phosphated metal-to-phosphated metal PPS specimens.

Once a cathodic reaction occurs at a defect in the PPS/Zn·Ph system, the action of NaOH derived from the cathodic reaction results in the dissolution and hydrolysis of the anhydrous Zn·Ph and FeS interaction product. Such an alkali-induced dissociation resulted in the formation of the Na-related sulfur compounds, such as Na-sulphide, Na-sulphite, and Na-sulphate. However, the rate of cathodic delamination of PPS for the PPS/Zn·Ph system was considerably lower than that for the PPS/steel system.

Based upon this information, additional work to continue its development is needed. Topics requiring additional work are as follows: 1) steel surface preparation requirements for achieving a rapid deposition of Zn·Ph crystals, 2) the application of Zn·Ph to galvanized steel surfaces, and 3) an evaluation of other high-temperature performance polymers such as polyimide, polybenzimidazole and polyphenyletheretherketone, as a topcoating material for Zn·Ph.

2. Synthesis of Pre-Ceramic Polymetallosiloxane Coating Films

Inorganic amorphous polymetallosiloxane, PMS, can be synthesized through hydrolysis-polycondensation-pyrolysis reactions of sol-precursor solution systems consisting of N-[3-(triethoxysilyl) propyl]-4,5-dihydroimidazole (TSPI) and $M(OC_3H_7)_n$ (M: Zr, Ti and Al, n: 3 or 4) as a film-forming reagent, HCl as a hydrolysis catalyst, and CH_3OH and water as a liquor medium. During this study of corrosion-protective thin films for low melting point aluminum substrates, the following seven items could be conclusively generalized as the major physico-chemical factors governing the film-forming behavior of PMS under the sol precursor (25°C) → sintering (150°C) → annealing (350°C) processes:

- 1) During the sol-film forming stage, adding HCl to the mixtures of TSPI and $M(OC_3H_7)_n$ induces the formation of hydroxylated metals, the Cl-substituted end groups in the monomeric organosilane, and the separation of imidazole derivatives from TSPI.
- 2) In the sintering process of sol films at 150°C, the formation of metal oxide polyorganosiloxane bond formed by the dechlorinating reaction between the Cl attached to propyl carbon in organosilane and the proton in the hydroxylated Zr or Ti compounds, played an important role in weight loss of the film.
- 3) Referring to 2), the Al hydroxide, derived from $Al(OC_3H_7)_3$ in which the trivalent ion is the principal oxidation state, preferentially reacts with hydroxylated organosilane to form the Al-O-Si linkage at a low temperature. However, this linkage was broken when the sintered film was annealed at 350°C, thereby creating large stress cracks and a high weight loss of the film.

- 4) The pyrolysis of Ti and Zr oxides-incorporated polyorganosiloxane compounds led to the formation of Ti and Zr oxides-crosslinked with polysiloxane, while also eliminating carbonaceous groups and Cl compounds from the sintered materials. These crosslinked network structures served to minimize the development of stress cracks in the films pyrolyzed at 350°C.
- 5) Although a certain amount of crystalline anatase particles were present in the amorphous polytitanosiloxane (PTS) coatings, the moderate crosslinking effects of Ti oxides and the densification of the M-O-Si linkage provided the most effective coating film in this study.
- 6) The identification of covalent oxane bonds at the interfaces between the PTS and the alkali-etched aluminum substrate illustrates the possibility of strong adhesion forces.
- 7) Referring to 4), 5), and 6), the integrated assignments of these factors were correlated directly to good corrosion resistance of aluminum alloys in NaCl solutions.

All the information described above was obtained from experiments with the sol precursor solution in the presence of acid catalysts. As described by several investigators [18,19], the microstructure of the film can be altered by varying the rate of polymerization of sol particles; namely, the extent of growth of the polymeric sol in an aqueous medium depended primarily on the pH of the precursor solution. When acid-type catalysts were added to the solution, the sol consisted of entangled linear polymers. By contrast, a highly condensed sol consisting of randomly branched chains was prepared by incorporating base-type catalysts. Xerogel films derived from the acidic sol precursor system had a continuous, dense microstructure, while the base-type system results in the formation of globular structures consisting of aggregations of randomly grown individual clusters. Therefore, additional work will focus on an investigation of the characteristics of fractal PMS cluster coating films derived from two-step, acid-base-catalyzed precursors consisting of N-[3-(triethoxysilyl)propyl]-4,5-dihydroimidazole (TSPI), M(OR)_n, methanol, and water, over a broad pH range of 1.0 to 13.0.

3. Crystalline Polyphenyletheretherketone (PEEK)-Based Materials

When melt crystallized polyphenyletheretherketone (PEEK) thermoplastic polymer was used as a high-temperature performance cementitious material, the degree of crystallinity of PEEK was dependent upon gaseous environment present at the polymer melting temperature of > 340°C. Namely, a well-formed PEEK crystal neat cement was assembled by melting-cooling processes in N₂ gas, whereas the oxygen-catalyzed deformation of PEEK structures in air led to a low rate of crystallinity, reflecting a poor thermal stability of cement. With regard to the PEEK mortar specimens made by the same process of the packed PEEK powder-silica sand mixtures at temperatures ranging from 400°C to 25°C, the microstructure of PEEK developed in the vicinity to the SiO₂ sand surfaces in N₂ was characterized by the growth of the crystals possessing transcrystalline textures. The creation of such spherulites at the interfaces

may be due to the nucleation of crystalline PEEK by the SiO_2 . No spherulitic growths were found at the PEEK- SiO_2 interfaces prepared in air. As a result of the formation of well-crystallized PEEK, mortar specimens not only have excellent thermal and hydrothermal stabilities at temperatures up to 200°C , but also maintain strength when exposed in 5 wt% H_2SO_4 at 80°C .

Considering that PEEK is currently utilized as a binder in high performance fiber-reinforced polymer composites, additional work to formulate composite systems will be directed towards, 1) crystallinity-related studies, 2) phase compositions, 3) adhesive mechanisms, and 4) microstructure developments, within PEEK layers adjacent to the fibers.

LIST OF PROGRAM PRESENTATIONS, PUBLICATIONS, AND PATENTS

Papers Presented

T. Sugama, Polyacrylic Acid-Modified Zinc Phosphate Conversion Coatings for Corrosion Protection of Steel. Proceedings of the 1989 Tri-Service Conference on Corrosion, Atlantic City, New Jersey, October 17-19, 1989.

T. Sugama, Sol-Gel Derived Polytitanosiloxane Coatings. Proceedings of Corrosion 90, Las Vegas, Nevada, April 23-27, 1990.

T. Sugama, Polymer-Modified Conversion Coatings. Workshop on Surface Science and Technology, Ann Arbor, Michigan, November 7-9, 1990.

T. Sugama, Fractal Polyzirconosiloxane Cluster Coatings. Proceedings of the 1991 Tri-Service Conference on Corrosion, Plymouth, MA, May 11-14, 1992.

Published

T. Sugama, L.E. Kukacka, and N. Carciello, Polytitanosiloxane Coatings Derived from $Ti(OC_2H_5)_4$ - Modified Organosilane Precursors. Progress in Organic Coatings, Vol. 18, 173-196 (1990).

T. Sugama and J. Pak, Characteristics of Transition Metal-Adsorbed Anhydrous Zinc Phosphate Coatings as Corrosion Barriers for Steels. Materials and Manufacturing Processes, Vol. 6, 227-239 (1991).

T. Sugama, L.E. Kukacka, N. Carciello, and J.B. Warren, Influence of the High Temperature Treatment of Zinc Phosphate Conversion Coatings. Journal of Materials Science, Vol. 26, 1045-1050 (1991).

T. Sugama, N. Carciello, and C. Taylor, Pyrogenic Polygermanosiloxane Coatings for Aluminum Substrates. Journal of Non-Crystalline Solids, Vol. 134, 58-70 (1991).

T. Sugama and C. Taylor, Chemical Degradation of Pyrogenic Polytitanosiloxane Coatings. Materials Letters, Vol. 11, 187-192 (1991).

T. Sugama and N.R. Carciello, Interface of Polyphenylene Sulphide-to-Metal Joints. Int. J. Adhesion and Adhesives, Vol. 11, 97-104 (1991).

T. Sugama and R. Broyer, Advanced Poly(acrylic) acid - Modified Zinc Phosphate Conversion Coatings: Use of Cobalt and Nickel Cations. Surface and Coatings Technology, Vol. 50, 89-95 (1992).

T. Sugama, N.R. Carciello, and M. Miura, Adhesion of Crystalline Polyphenyletheretherketon (PEEK) in Metal-to-Metal Joints. Int. J. Adhesion and Adhesives, Vol. 12, 27-37 (1992).

T. Sugama, and N.R. Carciello, Corrosion Protection of Steel and Bond Durability at Polyphenylene Sulfide-to-Anhydrous Zinc Phosphate Interfaces. J. Applied Polymer Science, Vol 45, 1291-1301 (1992).

T. Sugama and C. Taylor, Pyrolysis-Induced Polymetallosiloxane Coatings for Aluminum Substrates. Journal of Materials Science, Vol. 27, 1723-1734 (1992).

Issued Patents

T. Sugama, Polyacid Macromolecule Primers. United States Patent Number 4,889,718 on Dec. 26, 1989.

T. Sugama, Solid-Gel Precursor Solutions and Methods for the Fabrication of Polymetallosiloxane Coating Films. United States Patent Number 5,110,863 on May 5, 1992.

ACKNOWLEDGMENTS

The authors wish to acknowledge the support and guidance received from Dr. Robert R. Reeber of the U.S. Army Research Office, Research Triangle Park, NC.

REFERENCES

1. C.E. Sroog, J. Polym. Sci., Macromol. Rev. 11, (1976) 161.
2. H. Vogel and C.S. Marvel, J. Polym. Sci. 50, (1961) 511.
3. J.K. Stille and J.R. Williams, *ibid.* B2, (1964) 209.
4. R.W. Lenz, et al., *ibid.* 50, (1962) 351.
5. T. Sugama, L.E. Kukacka, N. Carciello and J.B. Warren, J. Coating Tech. 61, (1989) 43.
6. T. Adaniya, Sheet Metal Industry, 55, (1978) 73.
7. T. Adaniya and M. Ohmura, Metal, 31, (1977) 1100..
8. L.F.G. Williams, Surface Technology, 5, (1977) 105.
9. M. Kurachi, K. Fujiwara, and T. Tanaka, Proceedings of Congress International Union Electrodeposition Surface Finishing, Basel, (1972) 152.
10. H. Leidheiser, Jr. and I. Suzuki, Journal of Electrochemical Society, 128, (1981) 241.
11. G. Philipp and H. Schmidt, J. Non-Cryst. Solids, 63, (1984) 283.
12. H. Schmidt, J. Non-Cryst. Solids, 73, (1985) 681.
13. H.H. Huang, R.H. Glaser, and G.L. Wilkes, in M. Zeldin, K.J. Wynne, and H.R. Allcock (eds.), Inorganic and Organometallic Polymers, ACS Symp. Ser. No. 360, Am. Chem. Soc., Washington, DC, 1988, p. 354.
14. R.F. Brady, Jr., J. Protect. Coat. Linings, 4, (1987) 42.
15. R.W. Lenz, C.E. Handlovity, and H.A. Smith, J. Polymer Science, 58, (1961) 351.
16. P.C. Dawson and D.J. Blundell, Polymer, 21, (1980) 577.
17. A.J. Waddon, M.J. Hill, A. Keller, and D.J. Blundell, J. Materials Science, 22, (1987) 1173.
18. C.J. Brinker and G.W. Scherer, J. Non-Cryst. Solids, 70, (1985) 301.
19. J. Livage, M. Henry, and C. Sanchez, Prog. Solid State Chem., 18, (1988), 259.

APPENDIX A

ZINC PHOSPHATE CONVERSION COATINGS - RELATED PUBLICATIONS

CHARACTERISTICS OF TRANSITION METAL-ADSORBED ANHYDROUS ZINC PHOSPHATE COATINGS AS CORROSION BARRIERS FOR STEELS

T. Sugama

Brookhaven National Laboratory

Department of Applied Science

Energy Efficiency and Conservation Division

Upton, New York 11973

J. Pak

Washington College

Department of Chemistry

Chestertown, Maryland 21620

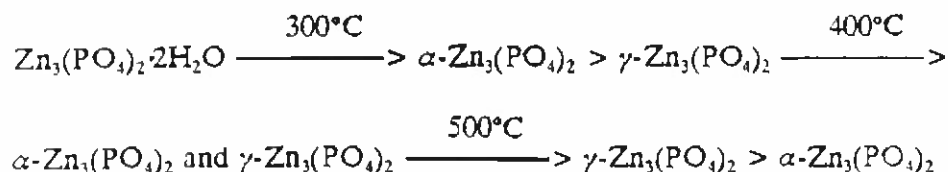
ABSTRACT

In attempting to develop anhydrous zinc phosphate (Zn-Ph) conversion coatings suitable for use with a high-temperature performance polyphenylene sulfide (PPS) topcoat, the characteristics of Zn-Ph deposited by immersing the steel in transition Co, Ni, and Mn cation-incorporated phosphating solutions were investigated. Two important features for the anhydrous 340°C-heated Zn-Ph were addressed. One was to determine if the electron trapping behavior of Co^{2+} and Ni^{2+} ions adsorbed in the crystal lattices acts to inhibit the cathodic reaction on the Zn-Ph, and the second was to determine the less susceptibility of the $\alpha\text{-Zn}_3(\text{PO}_4)_2$ phase to alkali-induced dissolution. The former affects the lifetime of the Zn-Ph layer as a barrier to corrosion of steel, and the latter reflects on the reduction of cathodic delamination rate of the PPS film from the α phase-steel substrate.

INTRODUCTION

Interfacial delamination will occur when organic topcoating systems, such as polyimide, polyphenylene sulfide, and polyquinoxalines, are applied directly to crystalline zinc phosphate (Zn-Ph) hydrate conversion coatings on steel. During treatment of the topcoat with high temperature to form a solid polymer film, separation is brought about by the dehydration of hydrous Zn-Ph crystals. On the

assumption that such a failure may occur at the polymer-Zn·Ph interface. Our previous work (1) focused on the effects of anhydrous Zn·Ph phases induced through a preheating-dehydration treatment, before depositing the topcoats. The phase transition versus temperature kinetics for the thermal dehydration of zinc orthophosphate dihydrate ($\text{Zn}_3(\text{PO}_4)_2 \cdot 2\text{H}_2\text{O}$) processes are as follows:



During the corrosion of iron and steel in a near neutral aqueous environment, the cathodic half reaction in terms of the oxygen reduction reaction, is $\text{H}_2\text{O} + \frac{1}{2} \text{O}_2 + 2\text{e}^- = 2 \text{OH}^-$. A shortcoming of Zn·Ph coatings as a barrier to the corrosion of steel is that the hydroxyl ions generated by this cathodic reaction (2) induce dissolution of the coating layers. A lower susceptibility of Zn·Ph to alkali dissolution also minimizes cathodic delamination rates for polymeric topcoat films. Thus, it was very important in assessing anticorrosive coatings to estimate the extent of alkali dissolution of Zn·Ph. We estimated this by comparing the rates of phosphorous dissociation from the crystal layers after exposure to 0.1M NaOH solution. The magnitude of susceptibility of hydrated and unhydrated Zn·Ph phases to alkali-induced dissolution was in the order of $\text{Zn}_3(\text{PO}_4)_2 \cdot 2\text{H}_2\text{O} > \gamma\text{-Zn}_3(\text{PO}_4)_2 > \alpha\text{-Zn}_3(\text{PO}_4)_2$. However, the formed $\gamma\text{-Zn}_3(\text{PO}_4)_2$ phase was found to afford poor protection because of the formation of numerous microcracks on the crystal faces caused by the $\alpha \longrightarrow \gamma$ -phase transition at 500°C .

Our experimental work was directed towards developing advanced anhydrous Zn·Ph conversion coatings which inhibit oxygen reduction reactions and minimize alkali dissolution. Particular attention was given to the characteristics of Zn·Ph modified with ionic and/or elemental cobalt and nickel atoms. These elements are well-known inhibitors of the cathodic reaction of electrogalvanized steel (3-6). The mechanism of this inhibition of corrosion was described by Leidheiser (7) as being due to the electron trapping reactions, M^{2+} (M: Co and Ni) + $2\text{e}^- = \text{M}^0$, of such atoms doped in the zinc oxide lattice. The M^{2+} ions favorably trap the electrons evolved from the anodic reaction, $\text{Zn}^0 - 2\text{e}^- \longrightarrow \text{Zn}^{2+}$, occurring at the oxide/solution interface, thereby inhibiting the cathodic reaction. The samples employed in these studies were prepared by dipping galvanized steel into an aqueous solution containing Co and Ni ions.

In our study, a different process was used to incorporate the metallic elements into an anhydrous Zn·Ph layer. We introduced the Co and Ni atoms into the crystal surface and/or layer simultaneously while the embryonic Zn·Ph crystals were growing on the steel surface. Hence, the samples were made by immersing the steel into the zinc phosphating solution containing Co and Ni ions at 80°C . For comparison with these atoms, two other elements, manganese and calcium, were evaluated.

Cathodic delamination studies of high temperature-cured polyphenylene sulfide (PPS) - coated anhydrous Zn·Ph specimens were also performed to delineate the

role of the phase composition of anhydrous Zn-Ph in reducing the delamination rates of PPS topcoat from the Zn-Ph.

EXPERIMENTAL

Materials

The metal substrate used was AISI 1010 cold-rolled steel supplied by the Denman and Davis Co. The steel contained 0.08-0.13 wt% C, 0.30-0.60 wt% Mn, 0.04 wt% P, and 0.05 wt% S. The unmodified zinc phosphating liquid used consisted of 1.3 wt% zinc orthophosphate dihydrate ($\text{Zn}_3(\text{PO})_2 \cdot 2\text{H}_2\text{O}$), 2.7 wt% H_3PO_4 , and 96.0 wt% water. In the modification of this standard formulation, four metal nitrate hydrates, $\text{Co}(\text{NO}_3)_2 \cdot 6\text{H}_2\text{O}$, $\text{Ni}(\text{NO}_3)_2 \cdot 6\text{H}_2\text{O}$, $\text{Mn}(\text{NO}_3)_2 \cdot 4\text{H}_2\text{O}$, and $\text{Ca}(\text{NO}_3)_2 \cdot 4\text{H}_2\text{O}$, supplied by Aldrich Chemical Company, Inc., were employed as a source of ionic and/or elemental Co, Ni, Mn, and Ca atoms. These metal compounds were added to the phosphating solution at a concentration of 1.0% by weight of the mass of the solution, and then stirred until they were completely dissolved.

Polyphenylene sulfide (PPS), supplied by the Phillips 66 Company, was used as a high-temperature performance polymer topcoat. The "as-received" PPS was a finely divided, tan-colored powder having a low molecular weight and high melt-flow, with a melting point of 288°C. The PPS polymer film was deposited on the dehydrated Zn-Ph surfaces in the following way. First, the Zn-Ph-coated steel was dipped into a PPS slurry consisting of 45 wt% PPS and 55 wt% isopropyl alcohol at 25°C. The coated specimens were preheated in an oven at 300°C for 3 hr, and then cured at 350°C for 2 hr.

In preparing the sample, the steel surfaces were wiped with acetone-soaked tissues to remove any mill oil contaminating the surface. The steel then was immersed for up to 30 min in the modified and unmodified conversion solutions described above at a temperature of 80°C for 30 min.

Measurements

The Zn-Ph-coated steel surfaces were examined with scanning electron microscopy (SEM) having an energy-dispersion X-ray spectrometry (EDX) attachment. The Zn-Ph crystal layers deposited on the steel surfaces scraped off to study the phase transition. They were then ground to a size of 325 mesh (0.044 mm) for thermogravimetric analysis (TGA), infrared (IR) spectroscopy, and x-ray powder diffraction (XRD).

X-ray photoelectron spectroscopy (XPS) was used to identify the chemical states and elemental compositions at the outermost surface site of ionic and/or elemental metals-incorporated Zn-Ph layers. The spectrometer was a V.G. Scientific ESCA 3 MK II using $K\alpha$ X-rays. The vacuum in the analyzer chamber of the instrument was maintained at 10^{-9} Torr throughout the experiments.

Corrosion measurements were made in an EG & G Princeton Applied Research Model 362-1. The specimen was mounted in a holder and then inserted into a EG & G Model K47 electrochemical cell. The tests were conducted in the aerated 0.5M NaCl solution at 25°C, and the exposed surface area of the specimens was 1.0 cm². The cathodic and anodic polarization curves were determined at a scan rate of 0.5 mV/sec in the corrosion potential range of -1.2 to -0.3 volts.

The cathodic delamination tests for the PPS-coated anhydrous Zn-Ph specimens were conducted in an air-covered 0.5M NaCl solution, using an applied potential of -1.5 volts vs SCE, for 3 days. This procedure is described in reference (8). A defect of approximately 1 mm was made using a drill bit. After exposure, the specimens were removed from the cell and allowed to dry. The PPS coating was removed by cutting, revealing a delaminated region, which appeared as a light gray area adjacent to the defect.

RESULTS AND DISCUSSION

Microstructure and Phase Transition

Fig.1 shows SEM micrographs for crystalline Zn-Ph microstructure deposited on steel substrates by immersing them into unmodified and modified zinc phosphating solutions. A quantitative analysis can be made of any element which exists at depths of several microns from the solid surface using the EDX spectrum in conjunction with SEM inspection. In this case, we adopted an element ratio of selected atom-to-Zn peak counts per 30 sec as a quantitative evaluation. The results from these conversion coatings are shown in Table 1. The thickness of the conversion coatings adhering to the substrates was determined using a surface profile measuring system. These results also are shown in Table 1. A standard Zn-Ph coating (see Fig.1-a) made with an unmodified solution is characterized by microstructure features which indicate a topography of interlocking rectangular-shape crystals precipitated on the steel. Compared with this, the crystal morphology resulting from the inclusion of Co in the phosphating solution showed (see Fig.1-b) packed, plate-like crystals of a size $>30\text{ }\mu\text{m}$. The EDX data (see Table 1) for the Co-Zn-Ph system indicated an Fe-to-Zn ratio of 0.42, which was markedly lower than that of the control. In contrast, the P-to-Zn ratios were similar. Since Fe can only originate from the steel substrate, it is possible that the presence of Co atoms at the beginning of crystal growth controls the release of Fe ions from the steel surface.

The microstructure for the Ni system-derived conversion coating (Fig.1-c) revealed a dense morphology of wide, plate-like crystals coexisting with small block-type crystals. The P/Zn and Fe/Zn ratios were almost equal to those for the Co system. A high Mn/Zn ratio of 0.15 was detected for the Mn system-derived coating (Table 1), thereby suggesting that an appreciable amount of Mn can be introduced into the crystal. The SEM micrograph (d) for this system revealed an image resembling that of the Co system. Although the data are not presented in any of the figures, the SEM morphology for the Ca-containing conversion coating was quite

similar to that for the control. However, no indication of Ca was found in EDX spectrum.

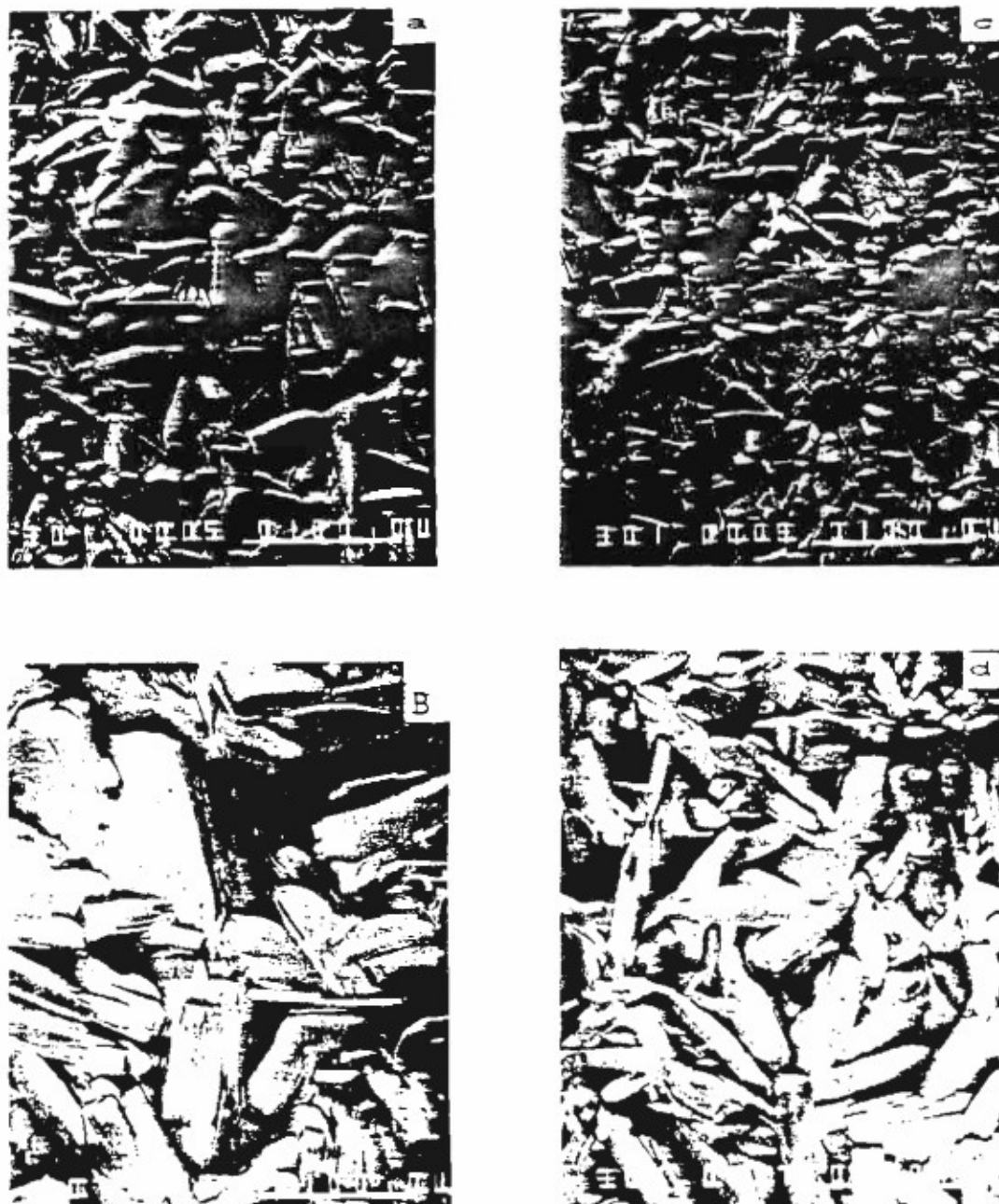


Figure 1. SEM images for conversion coatings derived from unmodified (a), and Co-(b), Ni-(c), and Mn-(d) modified zinc phosphating solutions.

Based upon these results, we conclude that the magnitude of diffusion and migration of these transition metal species in the crystal layer is in the following order: $Mn > Co > Ni$.

The XRD data (Table 2) indicated that only two crystal phases were distinguishable; hopeite ($Zn_3(PO_4)_2 \cdot 4H_2O$) (9), and zinc orthophosphate dihydrate ($Zn_3(PO_4)_2 \cdot 2H_2O$) (10). There was no evidence for the presence of the transition metal-related oxide, hydroxide, or phosphate compounds. The relative proportions of the $Zn_3(PO_4)_2 \cdot 4H_2O$ to $Zn_3(PO_4)_2 \cdot 2H_2O$ are likely to depend upon the metallic species added to the solution. Hence, the unmodified solution yields a phase composition consisting of dihydrate-based Zn·Ph as a major component and hopeite as a minor one. When Co-, Ni-, and Mn- modified solutions are used, they seem to promote the preferential precipitation of a single hopeite crystal layer. The data for the Ca system suggested an almost equal proportion of dihydrate - to tetrahydrate - based Zn·Ph phases.

From the above results and the EDX data, it is reasonable to conclude that the metallic species embedded in the crystal layers are present as ionic and elemental metals, as well as colloidal oxides or hydroxides.

TGA curves for powder samples dried at 80°C are depicted in Fig.2. The temperature of the onset of decomposition was obtained by finding the intersection point of the two linear extrapolations. The curves for all of the samples indicate the

TABLE I
The thickness and EDX Quantitative Analysis
for Unmodified and Modified
Zn·Ph Conversion Coating Surfaces

System	Thickness, μm	P/Zn	Intensity Count Ratio,				
			Fe/Zn	Co/Zn	Ni/Zn	Mn/Zn	Ca/Zn
Zn·Ph	12.5	0.82	0.56	-	-	-	-
Co-Zn·Ph	17.5	0.84	0.42	0.08	-	-	-
Ni-Zn·Ph	21.8	0.87	0.40	-	0.03	-	-
Mn-Zn·Ph	12.5	0.93	0.30	-	-	0.15	-
Ca-Zn·Ph	17.5	0.81	1.21	-	-	-	-

presence of two thermal decomposition stages; the first occurs at a temperature between -150° and $-180^\circ C$, and the second in the range from -330° to $-340^\circ C$. The first decomposition stage is possibly associated with liberation of water chemisorbed to the crystal faces, and the latter may be due to the removal of

crystallized water. Above 340°C, the curves level off, implying that the conversion from hydration to dehydration phases was essentially completed. At 340°C, the total weight loss for the control Zn·Ph was 9.1%; the Ca system-induced Zn·Ph exhibited a similar value. Somewhat higher weight losses (~11.3%) were measured for the other Zn·Ph systems. A possible interpretation for this finding is that the degree of weight loss occurring during dehydration depends mainly on the number of crystallized water molecules which react with free water to form hydrogen bonds. This reflects the fact that the affinity of the hopeite phase, which contains four crystallized H_2O , for water is higher than that of the dihydrate-based Zn·Ph phase. Thus, the major factors affecting the weight loss at temperatures up to 340°C are: 1) the amount of water trapped by hydrogen bonding in the crystal layers, and 2) the number of molecules of crystallized water.

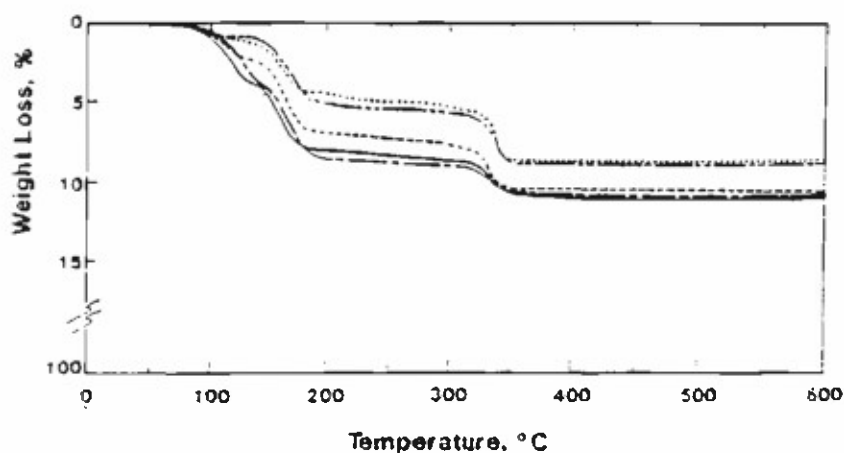


Figure 2. TGA curves of conversion coatings derived from the unmodified (— · — · —), and Co (- - - - -), Ni (— · — · —), Mn (————), and Ca (.)- modified phosphating solutions.

Therefore, it is reasonable to assume that such dehydration of Zn·Ph beneath high-temperature PPS topcoat systems may lead to disbandment at the PPS/ Zn·Ph interface, the extent of which may depend on the amount of crystallized water in the Zn·Ph. The influence of Co, Ni, and Mn systems-induced hopeite conversion coatings on the magnitude of disbandment might be greater than that of $Zn_3(PO_4)_2 \cdot 2H_2O$ coatings derived from the Ca-modified and unmodified phosphating solutions. Assuming that this concept is correct, interfacial disbandment can be avoided by converting the hydrated conversion coatings into thermally stable anhydrous phases before depositing the PPS polymers.

Once again, XRD analyses were carried out to identify the phase present in the dehydrated Zn-Ph after heating for 2 hr at 340°C. Table 2 summarizes the XRD data. The samples consisted essentially of two anhydrous Zn-Ph components, α -

TABLE 2
XRD Phase Compositions and Transformations
for Unmodified and Modified Zn-Ph Conversion
Coatings at 80°C and 340°C

System	Phases present at 80°C		Phases present at 340°C	
	Major	Minor	Major	Minor
Zn-Ph	$\text{Zn}_3(\text{PO}_4)_2 \cdot 2\text{H}_2\text{O}$	$\text{Zn}_3(\text{PO}_4)_2 \cdot 4\text{H}_2\text{O}$	α - and γ - $\text{Zn}_3(\text{PO}_4)_2$	
Co-Zn-Ph	$\text{Zn}_3(\text{PO}_4)_2 \cdot 4\text{H}_2\text{O}$	-	γ - $\text{Zn}_3(\text{PO}_4)_2$	α - $\text{Zn}_3(\text{PO}_4)_2$
Ni-Zn-Ph	$\text{Zn}_3(\text{PO}_4)_2 \cdot 4\text{H}_2\text{O}$	-	α - $\text{Zn}_3(\text{PO}_4)_2$	γ - $\text{Zn}_3(\text{PO}_4)_2$
Mn-Zn-Ph	$\text{Zn}_3(\text{PO}_4)_2 \cdot 4\text{H}_2\text{O}$	-	γ - $\text{Zn}_3(\text{PO}_4)_2$	α - $\text{Zn}_3(\text{PO}_4)_2$
Ca-Zn-Ph	$\text{Zn}_3(\text{PO}_4)_2 \cdot 4\text{H}_2\text{O}$ and $\text{Zn}_3(\text{PO}_4)_2 \cdot 2\text{H}_2\text{O}$	-	α - and γ - $\text{Zn}_3(\text{PO}_4)_2$	-

phase and γ -phase - $\text{Zn}_3(\text{PO}_4)_2$. No evidence was found for the presence of crystalline Co, Ni, Mn, and Ca compounds in these XRD tracings. For the control, the anhydrous α - and γ -phases are present as major components. The predominant component for the Co- and Mn- Zn-Ph systems was the γ -phase, suggesting that the transformations to α - and γ -phases are related to the original phases formed at 80°C. Namely, the conversion of hopeite at 340°C to the γ -phase rather than the α -phase is favored, with the exception of the Ni-Zn-Ph system.

Corrosion Protection

To determine if metal atoms incorporated into anhydrous Zn-Ph layers inhibit cathodic reactions, we focused upon the chemical states of 340°C-oxidized transition metal species incorporated into anhydrous crystal lattices, and the chemical transformation and conversion of the oxidized metal compounds after exposure to 0.1 M NaOH. XPS was used to obtain the information. XPS high-resolution spectra for the $\text{Co}_{2p3/2}$, $\text{Ni}_{2p3/2}$, and $\text{Mn}_{2p3/2}$ core levels of Co-, Ni- and Mn-incorporated Zn-Ph sample surfaces were determined. Fig.3 shows data taken before and after exposure to the NaOH. For the unexposed samples, the spectra for the Co sample has a major peak at 782.7 eV which corresponds to the Co in the CoO (11,12) formed by the oxidation of the Co atom during dehydration of Zn-Ph upon heating in air at 340°C. The peak emerging at 856.7 eV for the Ni sample reveals the presence of nickel oxide (NiO) (13,14). The formation of pyrolusite (MnO_2) at the surface of the oxidized Mn sample can be recognized by the main signal at 642.5 eV in the $\text{Mn}_{2p3/2}$ region (14).

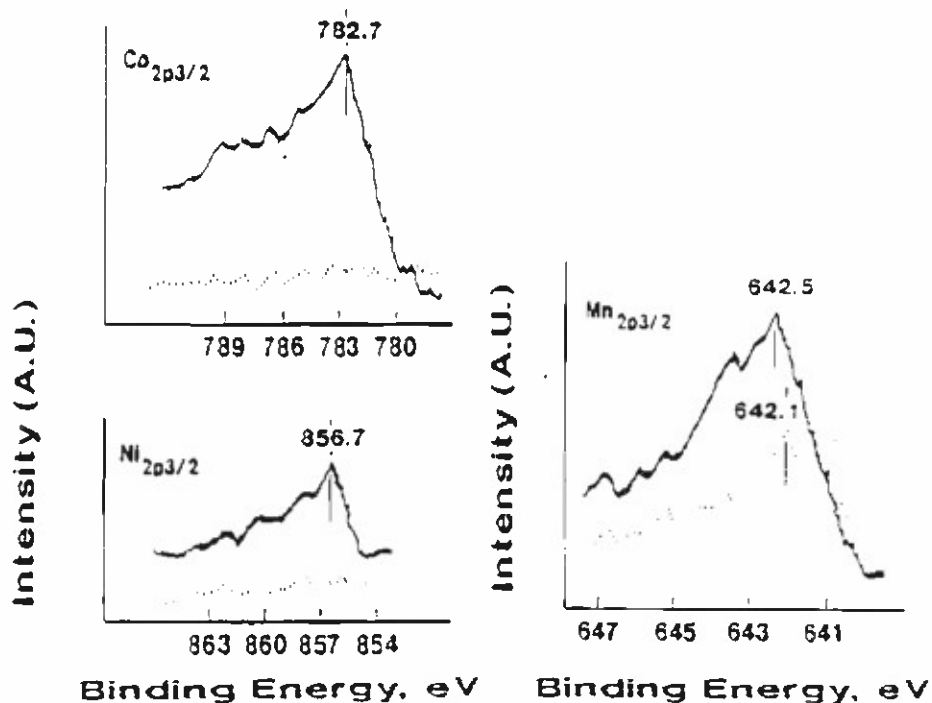


Figure 3. XPS high-resolution spectra in $\text{Co}_{2p3/2}$, $\text{Ni}_{2p3/2}$, and $\text{Mn}_{2p3/2}$ regions for transition metals-adsorbed Zn-Ph surfaces before (—) and after (....) exposure to NaOH.

After exposure to NaOH, no pronounced peaks were found. This finding implies that Co and Ni atoms precipitate on the outermost surface sites of the Zn-Ph layers, but do not diffuse into the layers. Therefore, NaOH-induced dissolution of the coating surfaces completely eliminates these atoms. In contrast, the spectrum from the sample containing Mn atoms, the most diffusible ionic species used, clearly shows a conspicuous signal intensity at the BE position of 642.1 eV that may be due to the formation of manganate hydroxides ($\text{MnO}(\text{OH})$ and $\text{Mn}(\text{OH})_3$) induced by alkali-catalyzed hydrolysis of MnO_2 (15).

Fig.4 shows typical cathodic polarization curves of log current density versus potential for the metal oxides-adsorbed and unadsorbed Zn-Ph anhydride samples in an aerated 0.5M NaCl solution. Comparison with the curve for the unadsorbed Zn-Ph sample, shows that the current density for the CoO-adsorbed Zn-Ph sample in the potential region between the -1.1 and -0.9 V was significantly less. The next lowest current density for the same potential region was obtained from coatings containing Ni oxides in the crystal lattices. In contrast, MnO_2 existing on the Zn-Ph

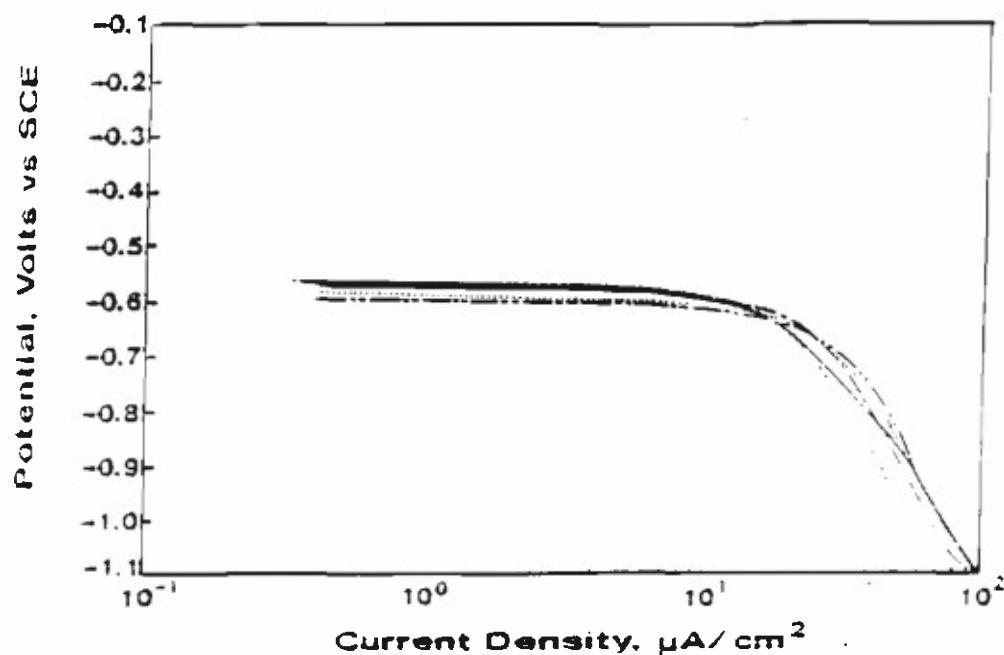


Figure 4. Comparisons of cathodic polarization curves for 340°C-treated unmodified (— · — · —), and Co (· · · · ·), Ni(— · — · —), Mn(———), and Ca (· · · · ·) - modified Zn-Ph coatings.

surface seems to play no role in shifting the current density to a lower value. Since the lower current density is attributed to a lower hydrogen reaction, this result confirms that the oxygen reduction reaction, $\text{H}_2\text{O} + \frac{1}{2} \text{O}_2 + 2\text{e}^- = 2 \text{OH}^-$, of the Zn-Ph-coated steel, was inhibited by incorporating CoO, and NiO into the Zn-Ph.

An important question that remains is which one of two $\text{Zn}_3(\text{PO}_4)_2$ phases, α and γ , is less susceptible to alkali-induced dissolution. To address this question, metal oxide-incorporated and unincorporated Zn-Ph samples were exposed to 0.1M NaOH for up to 48 hrs. The weight loss caused by the alkali dissolution of Zn-Ph was measured as a function of the exposure times. The results from these samples are summarized in Table 3. The weight loss is greater when the γ - $\text{Zn}_3(\text{PO}_4)_2$ phase is present as major crystal component, clearly showing that the γ -phase is considerably more susceptible to alkali dissolution, compared to the α -phase.

These results were related directly to the rates of cathodic delamination of PPS topcoat films from the Zn-Ph-deposited steels. The cathodic delamination tests for the PPS-coated Zn-Ph specimens were conducted in an air-covered 0.5M NaCl solution using an applied potential of -1.5 Volts vs SCE for 3 days. A 1 mm defect was made using a drill bit.

These test results are reported in Table 4. As expected, the PPS-to-Co- and Mn-Zn-Ph joint systems exhibited rapid delamination upon exposure, because of the

high degree of NaOH-induced dissolution of the γ - $\text{Zn}_3(\text{PO}_4)_2$ phase. In comparison, a markedly less PPS-delamination was observed with the Ni-, and Ca-Zn·Ph, and control conversion coatings containing α - $\text{Zn}_3(\text{PO}_4)_2$ as the major phase. For instance, the delaminated area of PPS film from the unmodified Zn·Ph was only 0.03 mm², compared with 2.54 mm² for the PPS-to- γ phase joint systems.

TABLE 3
Effect of Anhydrous Crystal Phase on the
Decrease in Weight Loss of Zn·Ph Caused by
NaOH-Induced Dissolution

System	Phase		1 hr	Weight Loss, %		
	Major	Minor		5 hr	24 hr	48 hr
Zn·Ph	α - and γ - $\text{Zn}_3(\text{PO}_4)_2$	--	0.060	0.164	0.206	0.221
Co-Zn·Ph	γ - $\text{Zn}_3(\text{PO}_4)_2$	α - $\text{Zn}_3(\text{PO}_4)_2$	0.066	0.189	0.234	0.257
Ni-Zn·Ph	α - $\text{Zn}_3(\text{PO}_4)_2$	γ - $\text{Zn}_3(\text{PO}_4)_2$	0.061	0.152	0.175	0.197
Mn-Zn·Ph	γ - $\text{Zn}_3(\text{PO}_4)_2$	α - $\text{Zn}_3(\text{PO}_4)_2$	0.066	0.187	0.233	0.255
Ca-Zn·Ph	α - and γ - $\text{Zn}_3(\text{PO}_4)_2$	--	0.060	0.160	0.200	0.217

TABLE 4
Comparison Between the Cathodically Delaminated Areas of
PPS/Unmodified Zn·Ph and/Modified Zn·Ph Interfaces
After Exposure to 0.5M NaCl Solution for 3 Days

System PPS	Delaminated Area, mm ²
Zn·Ph	0.03
Co-Zn·Ph	2.54
Ni-Zn·Ph	0.13
Mn-Zn·Ph	2.54
Ca-Zn·Ph	0.03

CONCLUSIONS

We investigated characteristics of dehydrated Zn-Ph crystal conversion coatings suitable for the application of high-temperature performance PPS polymer topcoats. The results led us to the following conclusions.

1. The dissolution of a certain amount of Co, Ni and Mn nitrate hydrates in the zinc phosphating solution results in the preferential precipitation of a hopeite phase ($\text{Zn}_3(\text{PO}_4)_2 \cdot 4\text{H}_2\text{O}$) on the steel's surface at 80°C.
2. The magnitude of diffusion and migration of transition ionic and elemental metals in the Zn-Ph crystal lattices was in the order $\text{Mn} > \text{Co} > \text{Ni}$.
3. Referring to 1), the addition of Ca nitrate hydrate resulted in the presence of mix phases of both zinc orthophosphate dihydrate ($\text{Zn}_3(\text{PO}_4)_2 \cdot 2\text{H}_2\text{O}$) and hopeite, the same as those derived from the unmodified phosphating solution. However, there was no evidence of adsorption of Ca atoms on the crystal lattices.
4. During thermal dehydration at 340°C, the hopeite $\rightarrow \gamma\text{-Zn}_3(\text{PO}_4)_2$ phase transition predominates in all but the Ni-incorporated hopeite. In contrast, the $\text{Zn}_3(\text{PO}_4)_2 \cdot 2\text{H}_2\text{O}$ was preferentially converted into the $\alpha\text{-Zn}_3(\text{PO}_4)_2$ phase.
5. The oxidized chemical states of Co, Ni, and Mn atoms on the surface of 340°C-heated Zn-Ph anhydride were identified as CoO, NiO, and MnO_2 .
6. The electron trapping behavior of Co^{2+} and Ni^{2+} ions dissociated from the metal oxide compounds in NaCl solution inhibits the cathodic reaction on the Zn-Ph surface, thereby extending the lifetime of the Zn-Ph which provides protection against corrosion to steels.
7. The degree of alkali dissolution of the $\alpha\text{-Zn}_3(\text{PO}_4)_2$ phase was considerably lower than that of the γ -phase. This difference reflected directly on the minimized cathodic delamination rate of PPS film from the α -phase steel substrates.

ACKNOWLEDGMENT

Jim Pak gratefully acknowledges support from the Department of Energy's Division of University and Industry Programs, Office of Energy Research, as a participant in the Science and Engineering Research Semester (SERS) Program.

REFERENCES

1. Sugama, T., L.E. Kukacka, N. Carciello, and J.B. Warren, Journal of Materials Science, Vol.26, No.4, pp.1045-1050, (1991).

2. Sugama, T., L.E. Kukacka, N. Carciello, and J.B., Warren, *Journal of Coating Technology*, Vol.61, No.43, (1989).
3. Adaniya, T., *Sheet Metal Industry*, Vol.55, No.73, (1978).
4. Adaniya, T. and M. Ohmura, *Metal*, Vol.31, No.1100, (1977).
5. Williams, L.F.G., *Surface Technology*, Vol.5, No.105, (1977).
6. Kurachi, M., K. Fujiwara, and T. Tanaka, *Proceedings of Congress International Union Electrodeposition Surface Finishing*, Basel, No.152, (1972).
7. Leidheiser, H., Jr., and I. Suzuki, *Journal of Electrochemical Society*, Vol.128, No.241, (1981).
8. Sommer, A.J. and H. Leidheiser, Jr., *Corrosion*, Vol.43, No.661, (1987).
9. Joint Committee on Powder Diffraction Standards, Card 33-1474, (1984).
10. Joint Committee on Powder Diffraction Standards, Card 30-1491, (1984).
11. Kim, K.S., *Physics Reviews B*, Vol.11, No.2177, (1975).
12. McIntyre, N.S. and M.G. Cook, *Analytical Chemistry*, Vol.47, No.2208, (1975).
13. Kim, K.S. and R.E. Davis, *Journal of Electron Spectroscopy*, Vol.1, No.251, (1973).
14. Kim, K.S., W.E. Baitinger, J.W. Amy, and N. Winograd, *Journal of Electron Spectroscopy*, Vol.5, No.351, (1974).
15. Oku, M. and K. Hirokawa, *Journal of Electron Spectroscopy*, Vol.8, No.475, (1976).

Influence of the high temperature treatment of zinc phosphate conversion coatings on the corrosion protection of steel

T. SUGAMA, L. E. KUKACKA, N. CARCIELLO, J. B. WARREN

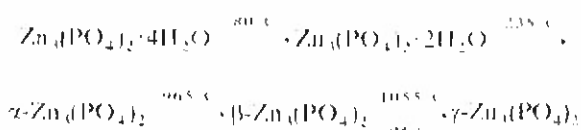
Process Sciences Division, Department of Applied Science, Brookhaven National Laboratory, Upton, New York 11973, USA

An anhydrous α - $\text{Zn}_3(\text{PO}_4)_2$ phase converted by the dehydration of hydrous zinc phosphate, $\text{Zn}_3(\text{PO}_4)_2 \cdot 2\text{H}_2\text{O}$, crystal coatings in air at a temperature of approximately 300 °C, significantly enhances the corrosion resistance of steel, and also reduces the susceptibility of the crystals to alkaline dissolution. A subsequent $\alpha \rightarrow \gamma$ phase transition at approximately 500 °C results in a poor protection behaviour, because of the formation of numerous microcracks on the crystal faces.

1. Introduction

Earlier work at Brookhaven National Laboratory (BNL) indicated that crystalline conversion coatings deposited on steel surfaces through a dissolution-re-crystallization process of the original zinc orthophosphate dihydrate [$\text{Zn}_3(\text{PO}_4)_2 \cdot 2\text{H}_2\text{O}$], not only enhance the corrosion protection of steel, but also significantly improve the adherence properties to organic topcoatings [1, 2]. The major phase in the insoluble conversion coatings, which is responsible for these improvements, was identified to be the same $\text{Zn}_3(\text{PO}_4)_2 \cdot 2\text{H}_2\text{O}$ (Zn·Ph) as that used as a convertible material.

From the viewpoint of crystal molecular structure, since Zn·Ph layers contain a certain amount of crystallized water, it should be considered that when thermal barrier organic topecoat systems such as polyimide [3], polybenzimidazoles [4], polyquinoxalines [5], and polyphenylene sulphide [6], are applied directly to the Zn·Ph surface, high-temperature treatment of the topecoats to form solid polymer films will lead to interfacial disbondment and separation brought about by the dehydration of the Zn·Ph. This failure is associated with the formation of weak boundary layers, resulting in poor corrosion protection. It is very important, therefore, to gain fundamental knowledge regarding the thermal degradation and behaviour of Zn·Ph, prior to studying the interfacial chemical nature between the high-temperature performance polymers and the crystalline Zn·Ph. As already reported by Kojima, *et al.* [7], the phase transition of hopeite, $\text{Zn}_3(\text{PO}_4)_2 \cdot 4\text{H}_2\text{O}$, with increased temperature in nitrogen gas, occurs through the following processes



These authors also indicated that a similar phase transition was observed in hot air.

The aim of the present study was, therefore, to determine the correlation between the phase transition or conformation of the $\text{Zn}_3(\text{PO}_4)_2 \cdot 2\text{H}_2\text{O}$ phase, as a function of temperature, and to understand how the thermally transformed phases protect steel from corrosion. In order to obtain this information, Zn·Phs precipitated on steel were exposed to air at temperatures up to 500 °C. Electrochemical testing of the converted phases was then conducted to provide data on the corrosion protection. Since cathodic delamination occurring at polymer-conversion coating interfaces is due mainly to alkaline dissolution of the phosphate coating [8], the extent of dissolution was also investigated. This was accomplished after soaking the different crystal phases in a 0.1 M NaOH solution at 25 °C.

2. Experimental procedure

2.1. Materials

The metal substrate used was a high strength cold-rolled sheet steel supplied by the Bethlehem Steel Corporation. The steel contained 0.06 wt % C, 0.6 wt % Mn, 0.6 wt % Si, and 0.07 wt % P. The formulation for the zinc phosphating liquid used in this study consisted of 1.3 wt % zinc orthophosphate dihydrate, 2.6 wt % H_2PO_4^- , and 96.1 wt % water.

The Zn·Ph conversion coatings were prepared in accordance with the following sequence. As the first step in the preparation, the steel surface was wiped with acetone-soaked tissues to remove any surface contamination due to mill oil. The steel was then immersed for up to 20 min in the conversion solution described above at a temperature of 80 °C. After immersion, the surface was rinsed with water, and then dried in an oven at 60 °C for 30 min.

2.2. Measurements

In order to study the phase transition and conversion of Zn·Ph coatings as a function of temperature up to 500 °C in air, the Zn·Ph crystal layers deposited on the steel surfaces were removed by scraping. They were then ground to a size of 325 mesh (0.044 mm) for use in analyses performed using the combined techniques of thermogravimetric analysis (TGA) coupled with differential thermal analysis (DTA), infrared (IR) spectroscopy, and X-ray powder diffraction (XRD).

The electrochemical testing for data on corrosion was performed with an EG & C Princeton Applied Research Model 362-1 Corrosion Measurement System. The electrolyte was a 0.5 M sodium chloride solution made from distilled water and reagent grade salt. The specimen was mounted in a holder and then inserted into a EG & G Model K47 electrochemical cell. The tests were conducted in the aerated 0.5 M NaCl solution at 25 °C, and the exposed surface area of the specimens was 1.0 cm². The cathodic and anodic polarization curves were determined at a scan rate of 0.5 mV sec⁻¹ in the corrosion potential range of -1.2 to 0.3 V.

Alterations to the surface microtopography images and the changes in surface chemical components of the heat-treated Zn·Ph coatings before and after exposure to a 0.1 M NaOH solution for 1 hr, were explored using AMR 10 nm scanning electron microscopy (SEM) associated with TN-2000 energy-dispersion X-ray spectrometry (EDX).

3. Results and discussion

Fig. 1 shows typical TGA-DTA curves for a powdered Zn·Ph sample after drying at 60 °C for 24 h. The curve

indicates that heating to 170 °C results in a weight loss of approximately 4%. Based upon the broad endothermic peak on the DTA curve at the same temperature, the weight loss is likely to be due to the removal of evaporable water such as free water and water adsorbed on the crystal. The curve also illustrates a manifestation of the kinetics of the elimination of non-evaporable water upon heating the Zn·Ph compounds. The reduction in weight of approximately 8% which occurs over the temperature range 170 to 350 °C is probably associated with the liberation of crystallized water existing in the Zn·Ph compounds, and this loss appears to be related directly to the prominent DTA endothermic peak at 345 °C. Beyond approximately 400 °C, the weight loss curve seems to level off, thereby suggesting that the conversion of the hydrous Zn·Ph compound into an anhydrous one is completed at approximately that temperature.

In addition to the TGA-DTA studies, IR and XRD analyses were also performed, and these data are shown in Figs 2 and 3, respectively. An estimate of the rate of liberation of crystallized water from the Zn·Ph compounds as a function of temperature, was made by plotting the variations in IR absorbance with temperature at a frequency of 1610 cm⁻¹ which reveals the H-O-H bending vibration of water of crystallization (see Fig. 2). As is evident from the absorbance against temperature curve, the absorbance decreased rapidly upon heating to 300 °C and beyond this temperature, levelled off. This suggests that to a large extent, the dehydration of Zn·Ph occurs in air at temperatures less than 300 °C. In fact, the XRD pattern (see Fig. 3 300 °C) for the diffraction range 0.256 to 0.371 nm, clearly indicates the formation of anhydrous α -Zn₃(PO₄)₂ as the major phase and anhydrous

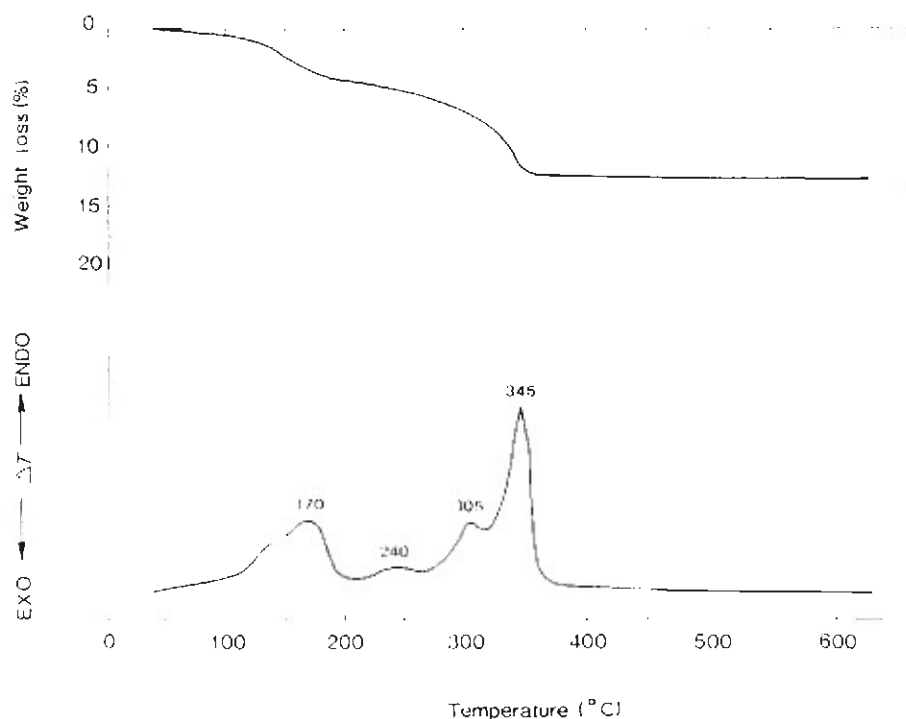


Figure 1. Typical TGA-DTA curves for zinc phosphate conversion coatings deposited on steel surfaces.

γ - $\text{Zn}_3(\text{PO}_4)_2$ as a minor phase. All of XRD lines for samples treated at temperature $< 200^\circ\text{C}$ are associated with the original $\text{Zn}_3(\text{PO}_4)_2 \cdot 2\text{H}_2\text{O}$ phase. This implies that the conversion into the anhydrous phases occurs at a temperature ranging from 200 to 300°C .

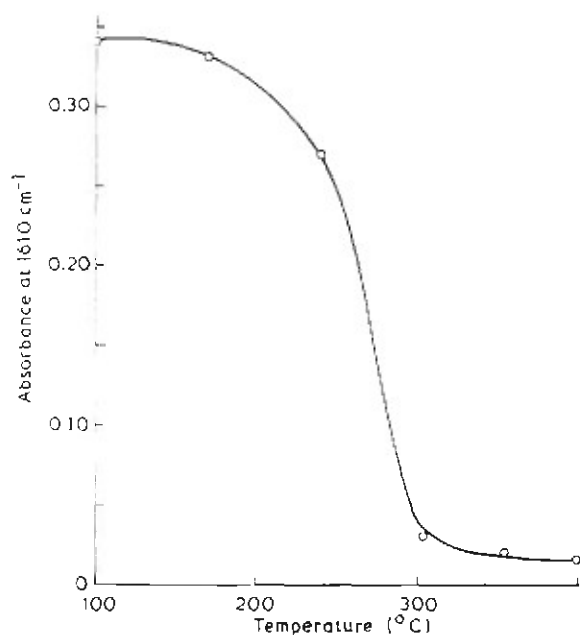


Figure 2 Changes in IR absorbance of H-O-H at 1610 cm^{-1} as a function of temperature for zinc phosphate coatings deposited on steel surfaces.

As indicated by the presence of a weak diffraction line at 0.293 nm which ascribes to the hydrous $\text{Zn}\cdot\text{Ph}$ compounds, the hydrous \rightarrow anhydrous conversion was not, however, complete at 300°C . This line disappeared when the sample was oven-heated at 400°C for 1 h. At 500°C , the tracing indicates the growth of line intensities at 0.279 and 0.343 nm , and weak peaks at 0.307 , 0.315 , and 0.360 nm . Since the former two intense lines represent the presence of a relatively large amount of γ - $\text{Zn}_3(\text{PO}_4)_2$, it appears that heat treatment at 500°C promotes $\alpha \rightarrow \gamma$ phase transition processes. Based upon the above information, a summary of the phase transition of $\text{Zn}_3(\text{PO}_4)_2 \cdot 2\text{H}_2\text{O}$ at temperatures up to 500°C is given in Table I. The resulting phase transitions are quite different from those obtained during an earlier study by Kojima [7] of the thermal deterioration of hopeite, $\text{Zn}_3(\text{PO}_4)_2 \cdot 4\text{H}_2\text{O}$. While the former undergoes the following conversion processes at relatively low temperatures, up to 500°C : $\text{Zn}_3(\text{PO}_4)_2 \cdot 2\text{H}_2\text{O} \rightarrow \alpha\text{-Zn}_3(\text{PO}_4)_2 \rightarrow \gamma\text{-Zn}_3(\text{PO}_4)_2$, and the α phase derived from hopeite is transformed to the β phase rather than the γ phase.

Electrochemical corrosion tests were performed to investigate how the various conversion phases affect the ability of the crystal coatings to protect the steel from corrosion. This protective ability was estimated by making comparisons between the corrosion potential, E_{corr} , values obtained from the potential axis at the transition point from the cathodic to anodic sites on the electrochemical polarization curves. As summarized in Table I, no appreciable changes in the E_{corr}

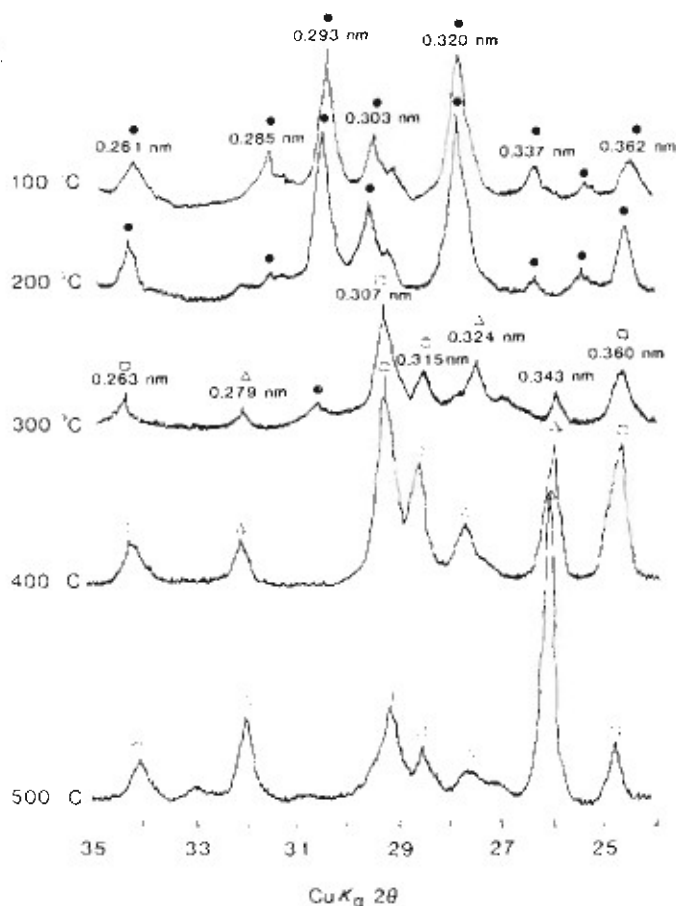


Figure 3 XRD patterns of 100, 200, 300, 400, and 500°C treated $\text{Zn}\cdot\text{Ph}$ layers: $\text{Zn}_3(\text{PO}_4)_2 \cdot 2\text{H}_2\text{O}$ (●), $\alpha\text{-Zn}_3(\text{PO}_4)_2$ (○) and $\gamma\text{-Zn}_3(\text{PO}_4)_2$ (△).

TABLE 1 Phase changes in conversion coating with E_{corr}

Temperature (°C)	Phase		E_{corr}^a (V)
	Major	Minor	
100	$\text{Zn}_3(\text{PO}_4)_2 \cdot 2\text{H}_2\text{O}$		-0.573
200	$\text{Zn}_3(\text{PO}_4)_2 \cdot 2\text{H}_2\text{O}$		-0.572
300	$\alpha\text{-Zn}_3(\text{PO}_4)_2$	$\gamma\text{-Zn}_3(\text{PO}_4)_2$	-0.572
400	α and $\gamma\text{-Zn}_3(\text{PO}_4)_2$		-0.600
500	$\gamma\text{-Zn}_3(\text{PO}_4)_2$	$\gamma\text{-Zn}_3(\text{PO}_4)_2$	-0.657

^a In aerated 0.5 M NaCl solution.

values for samples treated at temperatures up to 300 °C were observed. A shift in E_{corr} to a more negative site occurred when the samples were baked at 400 °C, thereby indicating that the hybrid layers of $\alpha\text{-Zn}_3(\text{PO}_4)_2$ and $\gamma\text{-Zn}_3(\text{PO}_4)_2$ have less corrosion resistance. A further increase in the treatment temperature to 500 °C resulted in a significant reduction in E_{corr} . Thus, it was found that the corrosion-protective ability of the Zn·Ph layers is dependent upon the extent of the conversion from the α phase to the γ phase, but independent of the dehydration and elimination of crystallized water in the Zn·Ph layers which occurs at a temperature of approximately 300 °C in air. The possible reason for the poor protective behaviour of the Zn·Ph layers containing the γ phase is the increased porosity of the crystal layers. This can be seen in the SEM images shown in Fig. 4. Namely, the SEM micrograph at the bottom of the figure which is of a 500 °C-treated sample surface indicates the presence of numerous microcracks on the crystal flates. Fig. 4 also gives the results of elemental intensity count ratios for iron or phosphorus to zinc atoms obtained by EDX quantitative analyses. These results show that the P/Zn ratio decreases with increased temperature and that no significant changes occur in the Fe/Zn ratio at temperatures up to 500 °C. This implies that some of the phosphorus atoms are eliminated as a result of heating in air.

Fig. 5 shows SEM micrographs and accompanying EDX elemental analyses for the heat-treated samples after exposure to a 0.1 M NaOH solution for 1 h. From the viewpoint of surface topographies, the SEM image for the exposed 100 °C-samples reveals a random distribution of roundish microcrystals. The alteration to a roundish shape from the original angular shape appears to be due to dissolution of the crystal caused by the attack of the NaOH solution. In connection with this, the EDX P/Zn ratio was reduced significantly from that of the corresponding unexposed sample (see Fig. 4—100 °C). It is clear that a large amount of phosphate was removed by the alkaline dissolution of the Zn·Ph crystals. In contrast, the Fe/Zn ratio changed very little.

The extent of the alkaline dissolution of the Zn·Ph can be estimated from the amount of reduction in the P/Zn ratios as determined by comparisons of the EDX quantitative data for samples before and after exposure. Attention was, therefore, given to the changes in the P/Zn ratio of the samples as a function of temperature. The resulting EDX data indicate that



Figure 4 SEM photographs (a) 100, (b) 300, and (c) 500 °C treated Zn·Ph surfaces.

Element	Before exposure intensity ratio Zn		
	100 °C	300 °C	500 °C
Iron	0.85	0.79	0.86
Zinc	1.00	1.00	1.00
Phosphorus	0.96	0.86	0.81

the P/Zn ratios for the exposed samples were lower than for unexposed ones, and the magnitude depends primarily on the treatment temperature; namely, the reduction rate conspicuously decreases with an



Figure 5. SEM images and EXD data for thermally treated Zn·Ph surfaces after exposure to 0.1 M NaOH for 1 hr: (a) 100 °C, (b) 300 °C, (c) 500 °C.

Element	After exposure to NaOH intensity ratio Zn		
	100 °C	300 °C	500 °C
Iron	0.81	0.62	0.84
Zinc	1.00	1.00	1.00
Phosphorus	0.48	0.72	0.82

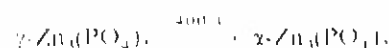
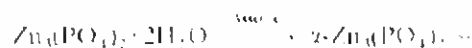
increase in treatment temperature. However, at 500 °C, the P/Zn ratios for samples before and after exposure were essentially the same, thereby suggesting that γ phase-rich crystal layers are less susceptible to

alkaline dissolution. Thus, the magnitude of alkaline dissolution for the Zn·Ph compounds seems to be in the order of $\text{Zn}_3(\text{PO}_4)_2 \cdot 2\text{H}_2\text{O} > \alpha\text{-Zn}_3(\text{PO}_4)_2 > \gamma\text{-Zn}_3(\text{PO}_4)_2$.

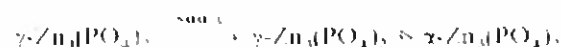
Polarization curves for 100, 300 and 500 °C treated samples after exposure to a 0.1 M NaOH solution for 1 h are given in Fig. 6. The shape of the curves represents the transition from cathodic polarization at the onset of the most negative potential to the anodic polarization curves at the end of the lower negative potential. The potential axis at the transition point from cathodic to anodic curves is normalized as the corrosion potential, E_{corr} . These polarization behaviours were determined in an aerated 0.5 M NaCl solution at 25 °C. Comparisons of the cathodic polarization areas for the 300 and 500 °C treated samples with that for the 100 °C treated sample indicated the following: (1) at 500 °C, the short-term steady-state current value in the potential region between -1.0 and -1.1 V is considerably higher, (2) heat treatment at 300 °C shifts the E_{corr} to a more positive site and decreases the current density at the potential axis, and (3) treatment at 500 °C decreases E_{corr} and enhances the current density in the vicinity of E_{corr} . Although the 500 °C treated Zn·Ph is less susceptible to alkaline dissolution, the higher current density (observation (1) above) is indicative of high oxygen reduction kinetics which occur under the coating. The reason for this enhanced oxygen reduction reaction, $\text{H}_2\text{O} + \frac{1}{2}\text{O}_2 + 2\text{e}^- = 2\text{OH}^-$, in an aerated NaCl solution may be due to the increased porosity of the coating caused by the $\alpha \rightarrow \gamma$ phase transitions during heating at 500 °C, thereby resulting in a poor protective performance. In addition, a coating exhibiting a poor protective nature would be expected to display a lower E_{corr} and a higher current density. This is in agreement with observation (3). With regards to observation (2), the conversion to an anhydrous α phase at 300 °C yields a more stable layer and inhibits the oxygen reduction reaction. It appears that this relates directly with the low-rate of alkaline dissolution.

4. Conclusions

The water of crystallization in the $\text{Zn}_3(\text{PO}_4)_2 \cdot 2\text{H}_2\text{O}$ major phase of Zn·Ph conversion coatings deposited on steel surfaces through dissolution-recrystallization processes using zinc orthophosphate dihydrate powders is eliminated by heating in air at temperature between 300 and 400 °C. The kinetics for the thermal dehydration of the hydrous crystal coatings are related directly to the following phase transition at temperatures up to 500 °C:



and



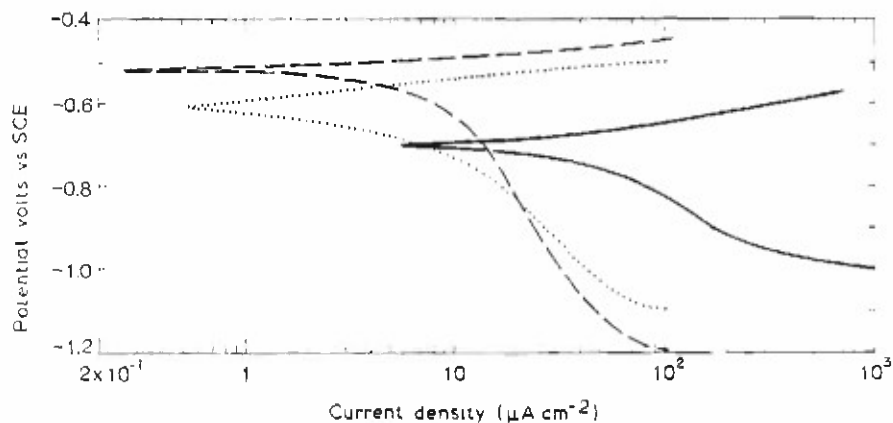


Figure 6. Polarization curves for 100°C (·····), 300°C (---), 500°C (—) treated zinc phosphated steels after immersion in 0.1 M NaOH.

When the corrosion-protective ability of these conversion phases was studied, it was determined that anhydrous α phase-rich crystal layers yielded at 300°C had the same protective ability as hydrous conversion coatings. Heat treatment at 500°C as a means of producing γ phase-rich coatings, however, led to a poor protective behaviour. This was due to an increase in the number of microcracks on the crystal faces caused by $\alpha \rightarrow \gamma$ phase transition. This suggests that the corrosion-protective ability of Zn-Ph layers at high temperatures is dependent on the extent of the conversion from α to γ phases, but independent of the dehydration and elimination of crystallized water in the Zn-Ph layers.

The anhydrous α and γ phases were also found to be less susceptible to alkaline dissolution of Zn-Ph crystals, thereby resulting in a lower rate of phosphorus dissociation from the crystal layers. The microcrack-free α phase layers at 300°C yielded the best protection performance for the crystal-covered steel systems upon exposure to a NaOH solution.

Acknowledgements

This work was performed under the auspices of the US Department of Energy, Washington, DC under con-

tract DE-ACO2-76CH00016 and supported by the US Army Research Office Program MIPR-ARO-103-88.

References

1. T. SUGAMA, L. E. KUKACKA, N. CARCIELLO and J. B. WARREN, *J. Coatings Tech.*, **61** (1989) 43.
2. T. SUGAMA, L. E. KUKACKA, N. CARCIELLO and J. B. WARREN, *J. Mater. Sci.*, **19** (1984) 4045.
3. C. F. SROOG, *J. Polym. Sci., Macromol. Rev.*, **11** (1976) 161.
4. H. VOGEL and C. S. MARVEL, *J. Polym. Sci.*, **50** (1961) 511.
5. J. K. STILLE and J. R. WILLIAMS, *ibid.*, **B2** (1964) 209.
6. R. W. LENZ, et al., *ibid.*, **50** (1962) 351.
7. R. KOJIMA, H. OKITA and Y. MATSU SHIMA, *Tetsu to Hagane*, **66** (1980) 924 (Japanese).
8. V. J. SOMMER and H. L. LEIDHEISER, Jr., *Corrosion*, **43** (1987) 661.

Received 9 December 1988
and accepted 31 May 1989

Advanced poly(acrylic)acid-modified zinc phosphate conversion coatings: use of cobalt and nickel cations

T. Sugama

Energy Efficiency and Conservation Division, Department of Applied Science, Brookhaven National Laboratory, Upton, NY 11973 (USA)

R. Broyer

Department of Science, Union High School, North Third St. Union, NJ 07083 (USA)

(Received October 16, 1990; accepted in final form July 16, 1991)

Abstract

The incorporation of cobalt (Co^{2+}) and nickel (Ni^{2+}) ions in a poly(acrylic)acid (p(AA))-modified zinc phosphate solution promoted the growth and development of crystalline zinc phosphate ($\text{Zn}\cdot\text{Ph}$) conversion coatings deposited on steel surfaces. This enhancement was due primarily to the preferential uptake of Co^{2+} and Ni^{2+} ions by p(AA), to form the Co- and Ni-OOC- salt complexes, rather than complexes with zinc ions. The electron trapping behaviors of Co^{2+} and Ni^{2+} dissociated from the salt complexes, and the hydroxides in the NaCl solution inhibited the cathodic reaction on $\text{Zn}\cdot\text{Ph}$. In particular, the conversion coatings derived from the nickel-modified phosphate solution were characterized by the formation of a coating consisting of hopeite as a major crystal phase, zinc orthophosphate dihydrate as a minor phase, and an amorphous iron-rich phosphate phase; this coating provided an extensive coverage over the steel, which contributed to protecting it from corrosion.

1. Introduction

Zinc phosphate ($\text{Zn}\cdot\text{Ph}$) conversion coatings, which are prepared by immersing steel substrates in a solution of zinc phosphate, have been widely applied as corrosion barriers for steel. As part of work to develop advanced $\text{Zn}\cdot\text{Ph}$ coatings, our particular focus was placed on the modifications of $\text{Zn}\cdot\text{Ph}$ by incorporating the organic polyelectrolyte macromolecule containing proton-donating pendant groups, such as carboxylic and sulfuric acids [1–3]. Our data indicated that the segmental chemisorption of functional polyelectrolyte on small phosphate crystals at the beginning of the precipitation of $\text{Zn}\cdot\text{Ph}$ not only acts to array a uniformly packed fine crystal morphology brought about by suppressing and delaying crystal growth but also significantly improves the stiffness and ductility of the normally brittle $\text{Zn}\cdot\text{Ph}$ layers. The major reason for these changes was associated with the formation of the carboxylate or sulfonate-linked zinc complexes, consisting of a charge-transferring bond at polyelectrolyte- $\text{Zn}\cdot\text{Ph}$ interfaces. The most recent study [4] on the enhancement of the corrosion-protective ability of unmodified $\text{Zn}\cdot\text{Ph}$ demonstrated that the adsorption of Co^{2+} and Ni^{2+} ions on the crystal faces extends the durability of $\text{Zn}\cdot\text{Ph}$. The reason for the extended durability was due primarily

to the electron-trapping behavior of such ionic species, which inhibits the cathodic reaction on the uncoated parts of the steel surfaces. However, there were no polyelectrolytes in the cobalt and nickel ions incorporated in the zinc phosphate solutions.

Accordingly, the emphasis of our present study was directed towards characterizing $\text{Zn}\cdot\text{Ph}$ derived from the cobalt and nickel ion-zinc phosphate solutions containing poly(acrylic)acid (p(AA)) which is a polyelectrolyte macromolecule species. The research had the following three objectives: (1) to explore the influence of segmental chemisorption of p(AA), which will react with cobalt and nickel ions adsorbed to $\text{Zn}\cdot\text{Ph}$ crystal surfaces, on the development and growth of crystals at the beginning of the precipitation of conversion coating to the steel surface, (2) to investigate the crystal phase as a function of cobalt-to-nickel ratios and (3) to assess the ability of the finally assembled crystal layers to protect the steel against corrosion.

2. Experimental details

2.1. Materials

The metal substrate used was AISI 1010 cold-rolled steel supplied by the Deman and Davis Co. The steel

contained 0.08–0.13 wt.% C, 0.30–0.60 wt.% Mn, 0.04 wt.% P and 0.05 wt.% S. The formulation for the unmodified zinc phosphate liquid was 1.3 wt.% zinc orthophosphate dihydrate [$\text{Zn}_3(\text{PO}_4)_2 \cdot 2\text{H}_2\text{O}$], 2.7 wt.% H_3PO_4 and 96.0 wt.% H_2O . In modifying this standard formulation, two metal nitrate hydrates, $\text{Co}(\text{NO}_3)_2 \cdot 6\text{H}_2\text{O}$ and $\text{Ni}(\text{NO}_3)_2 \cdot 6\text{H}_2\text{O}$ supplied by Aldrich Chemical Company, Inc., and 25% p(AA) colloidal solution obtained from Rohm and Hass Company, were employed as a source of the ionic cobalt and nickel atoms and the polyelectrolyte. The concentrations of these metal compounds and p(AA) (molecular weight of about 60 000) added to the zinc phosphate solution were 1.0 wt.% and 0.5 wt.% of the total standard solution respectively. Five different ratios of $\text{Co}(\text{NO}_3)_2 \cdot 6\text{H}_2\text{O}$ to $\text{Ni}(\text{NO}_3)_2 \cdot 6\text{H}_2\text{O}$ (100 to 0, 75 to 25, 50 to 50, 25 to 75 and 0 to 100 by weight) were used to compare their protective effects against corrosion. Although an alkaline immersion or spray is generally accepted to clean the metal surfaces, in this study the steel surfaces were wiped with acetone-soaked tissues to remove any surface contamination from mill oil. The steel then was immersed for up to 20 min in these modified and unmodified conversion solutions at a temperature of 80 °C.

2.2. Measurements

X-ray photoelectron spectroscopy (XPS) was used to identify the chemical states and elemental compositions at the outermost surface site of the p(AA)-Zn-Ph layers. The spectrometer used was a V.G. Scientific ESCA 3MK II with an Al $K\alpha$ (1486.6 eV) X-ray source. The surfaces of conversion coatings were examined by scanning electron microscopy (SEM) with an energy-dispersive X-ray spectrometry (EDXS) attachment. The Zn-Ph crystal layers were scraped from the steel surfaces to study the phase compositions. They were then ground to a size of 325 mesh (0.044 mm) for X-ray powder diffraction (XRD). Measurements of corrosion were made in an EG&G Princeton Applied Research model 362-1 corrosion measurement system. The specimen was mounted in a holder and then inserted into an EG&G model K47 electrochemical cell. The tests were conducted in an aerated 0.5 M NaCl solution at 25 °C, and the exposed surface area of the specimens was 1.0 cm². The cathodic polarization curves were determined at a scan rate of 0.5 mV s⁻¹ in the potential range from -1.2 to -0.2 V.

3. Results and discussion

3.1. Coating layers formed in the initial periods of Zn-Ph conversion process

To investigate the effect of Co^{2+} , Ni^{2+} and p(AA) additives on the promotion of crystal growth at the

initial stage of Zn-Ph precipitation, the steel samples were immersed for only 5 min and the conversion products explored using XPS and SEM-EDXS. Table 1 summarizes the XPS data on changes in the elemental composition of the sample surface as a function of the $\text{Co}(\text{NO}_3)_2 \cdot 6\text{H}_2\text{O}$ -to- $\text{Ni}(\text{NO}_3)_2 \cdot 6\text{H}_2\text{O}$ ratio. For all the samples, the principal element occupying the outermost surface sites was oxygen, in the concentration range 43–55 at.%, and the second predominant element was carbon, corresponding to the hydrocarbon in p(AA) chemisorbed and diffused on the conversion product surfaces. By comparison with the elemental composition of the control sample, denoted as the 0-to-0 ratio, the cobalt-modified sample (100-to-0 ratio) was characterized by a conspicuous increase in the concentration of zinc and phosphorus atoms, with a concomitant reduction in the content of iron atoms which is representative of both the steel substrate and the iron-based conversion products. Since zinc and phosphorus atoms directly reflect the precipitation of Zn-Ph on the steel, we believe that the Co^{2+} ions dissolved in the phosphating solution promote the precipitation of Zn-Ph crystals. The data further indicated that the zinc and phosphorus concentrations tend to decrease gradually as the cobalt-to-nickel ratio was lowered. In contrast, the iron concentration increases with decreasing cobalt-to-nickel ratio. The chemical states and compounds in the conversion products of these samples were identified from the deconvoluted curve of the high resolution XPS spectra of C 1s, Ni 2p, P 2p and Fe 2p_{3/2} signals. To set a scale in all the XPS spectra, the binding energy (BE) was calibrated with the C 1s of the principal hydrocarbon-type carbon peak fixed at 285.0 eV as an internal reference standard. The resulting spectra are shown in Figs. 1 and 2. Curves a, b, c, d and e correspond to samples with cobalt-to-nickel ratios of 0 to 0, 100 to 0, 50 to 50, 25 to 75 and 0 to 100 respectively. In the C 1s regions (see Fig. 1), the spectrum of the control sample (curve a) reveals the three resolvable Gaussian components at BE of 285.0, 288.1 and 288.9 eV. The main peak at 285.0 eV as a principal component is attributable to the hydrocarbons in the main chain

TABLE 1. Surface chemical compositions of unmodified and of cobalt- and nickel-modified conversion coatings at the beginning of precipitation of Zn-Ph

$\text{Co}(\text{NO}_3)_2 \cdot 6\text{H}_2\text{O}$ -to- $\text{Ni}(\text{NO}_3)_2 \cdot 6\text{H}_2\text{O}$ ratio	Concentration (at.%)				
	P	C	O	Fe	Zn
0 to 0	4.1	29.7	55.0	9.4	1.7
100 to 0	12.2	24.8	51.6	4.8	6.5
75 to 25	12.7	25.9	50.6	4.8	6.0
50 to 50	10.9	33.3	43.3	7.3	4.9
0 to 100	10.7	32.7	44.6	7.7	4.3

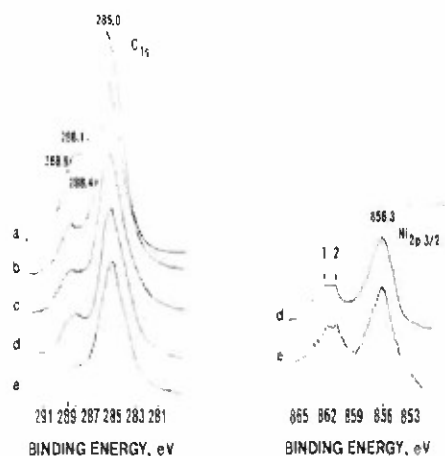


Fig. 1. NPS high resolution spectra in C 1s and Ni 2p_{3/2} regions for a control sample (curve a) and modified Zn·Ph conversion coatings, with various cobalt-to-nickel ratios (curve b, 100 to 0; curve c, 50 to 50; curve d, 25 to 75; curve e, 0 to 100).

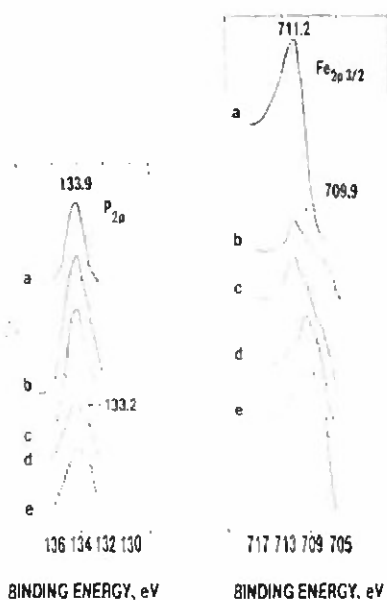


Fig. 2. P 2p and Fe 2p_{3/2} regions for a control sample (curve a) and Zn·Ph samples with various cobalt-to-nickel ratios (curve b, 100 to 0; curve c, 50 to 50; curve d, 25 to 75; curve e, 0 to 100).

of p(AA). The peak emerging at 288.1 eV in a high BE area can be ascribed to the carbon in the $-\text{COO}^- \text{Zn}^{2+} \text{OOC}-$ salt complex formation [3, 5], and 288.9 eV is due to carbon originating from the carboxylic acid, COOH, in the p(AA) [6]. The spectra for all of the cobalt- and nickel-incorporated Zn·Ph samples show a slight shift in the salt complex-related peak to a higher BE site compared to that of the control. The assignments of the shifted peak at 288.4 eV appear to be due to the Co- and Ni-OOC salt complexes. In fact, the O 1s core level (not shown)

had a strong peak at 531.4 eV, which was ascribed to the formation of COO-metal complexes. This finding strongly suggested that the functional COOH groups in the p(AA) preferentially react with the cobalt and nickel ions to precipitate the salt complex, rather than reacting with the zinc ions. The data were further supported by comparisons of the peak area ratio between C(COO-Co and COO-Ni) at 288.4 eV and C($-\text{CH}_2-$) at 285.0 eV. The resulting ratios for the 100-to-0, 50-to-50, 25-to-75 and 0-to-100 samples were 0.28, 0.26, 0.23 and 0.19 respectively, thereby demonstrating that the uptake of cobalt by COOH groups is much higher than that of nickel. Thus the extent of reactivity of these metal ions with p(AA) appears to be in the following order: cobalt > nickel > zinc. We offer no interpretation of the Co 2p_{3/2} peak in the BE ranging from 777 to 783 eV, because of the interference of the iron Auger line. The Ni 2p_{3/2} region (Fig. 1) for the 25-to-75 and 0-to-100 samples has a symmetric signal peak at 856.3 eV and a strong broad satellite band (shown by arrow 1 and arrow 2). According to McIntyre and Cook [7], this signal feature is associated with the nickel in Ni(OH)₂. In the P 2p core level spectra (see Fig. 2), the curve for the control sample reveals only a single peak at 133.9 eV, reflecting the phosphorus in the Zn·Ph precipitated on the steel. The intensity of this peak markedly increased as the control solution was modified by Co²⁺ ions. Since such an intense peak represents the deposition of a large amount of Zn·Ph, it is clear that cobalt ions have a significant effect on the acceleration of crystal growth and precipitation. A possible interpretation for this acceleration, taking into account the data from C 1s spectra, is that the preferential uptake of Co²⁺ ions by the p(AA) macromolecule, rather than Zn²⁺ ions, leads to numerous free zinc ions in the phosphate solutions. Hence, the role that Zn-p(AA) complexed formations play in controlling a crystal growth and in arraying a dense microstructure of fine Zn·Ph crystals is inhibited by the formation of Co-p(AA) salt complexes. For the samples (see P 2p, curve d) in which more than half the cobalt ions were replaced by nickel ions, the signal feature indicated the appearance of a new component at a low BE site of 133.2 eV, although the principal line of phosphorus in Zn·Ph is still present. The further growth of this new peak was observed in curve e in which the cobalt ions were completely replaced by nickel ions. To ascertain the assignment of this additional line, we investigated the Fe 2p_{3/2} region (Fig. 2). The peak at the position of 711.2 eV in the control is referable to the iron in the iron oxide, Fe₂O₃, forming on the top surface of the steel [8]. By comparison, the Fe 2p_{3/2} curve of the cobalt-modified 100-to-0 ratio sample is distinctive, namely an additional weak line at 709.9 eV, separate from the main line, appears in the spectrum.

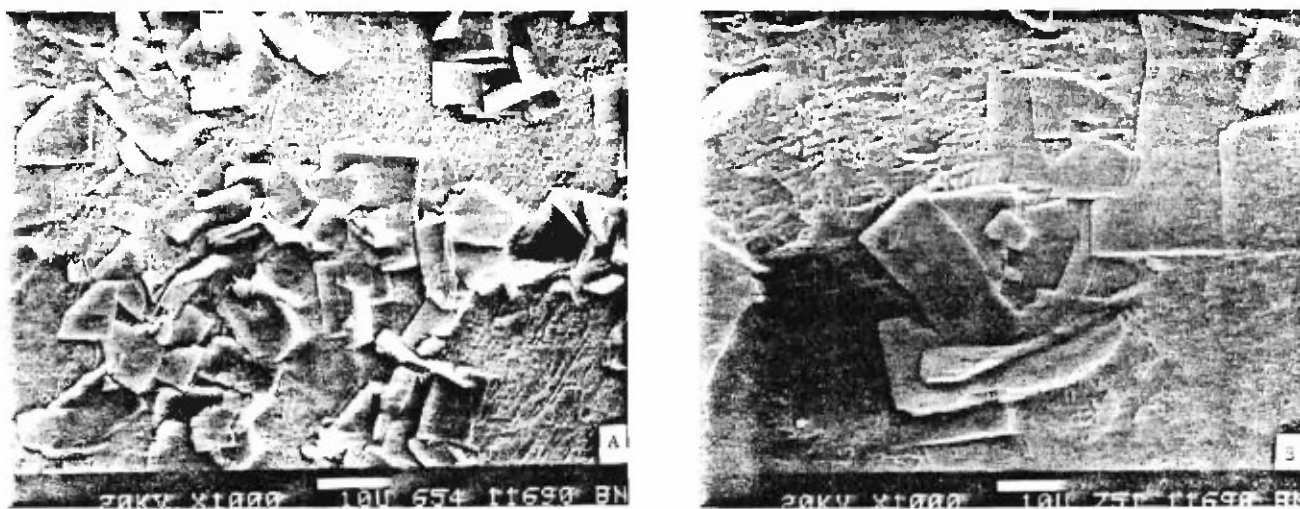


Fig. 3. SEM micrographs for (A) a control sample and (B) a cobalt-modified Zn·Ph coating precipitated on a steel surface in the early periods of the conversion processes.

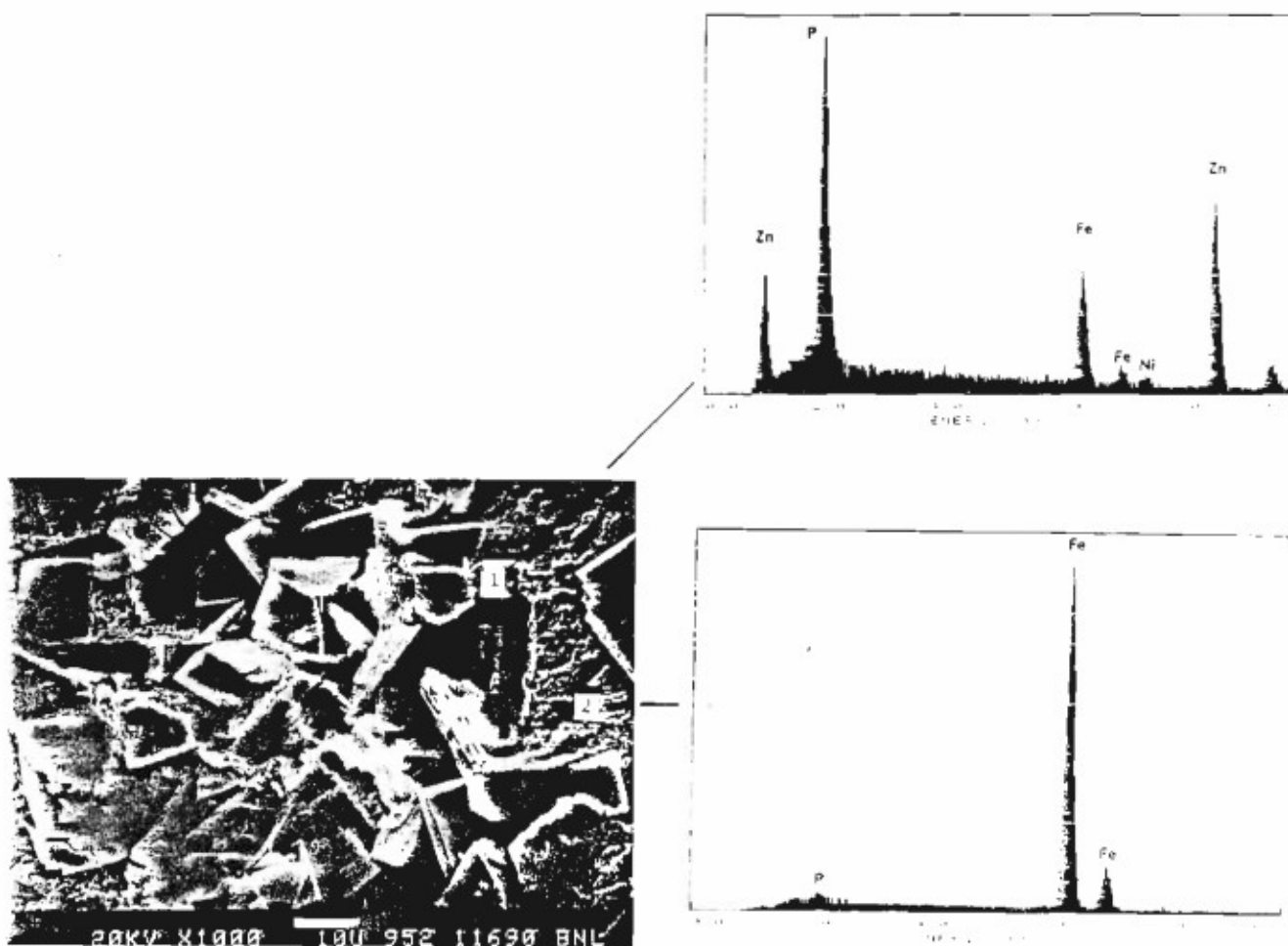


Fig. 4. SEM and EDXS spectra for nickel-modified Zn·Ph conversion coatings in the initial precipitation stages.

The intensity of this new line dramatically increases in proportion to the amount of nickel present. The growing new peak at 709.9 eV for samples with a 25-to-75 and 0-to-100 ratio eventually become the principal line. In contrast, the line intensity at 711.2 eV, originating from the iron in Fe_2O_3 , which is the main oxidized component of steel surfaces, is significantly reduced as the cobalt-to-nickel ratio decreases. In conjunction with an additional line at 133.2 eV in the P 2p region, we believe that the new peak emerging at 709.9 eV directly reflects the formation of iron phosphates. From these data, it is reasonable to assume that incorporating nickel ions into the p(AA)-modified zinc phosphate solution promotes the rate of conversion into the iron phosphates precipitating on the Fe_2O_3 layers. However, the precise phase of the precipitated iron phosphate compounds is unclear.

Figure 3 shows SEM micrographs coupled with EDXS spectra for the crystalline Zn·Ph microstructure deposited on steel substrates after immersion for 5 min in control solutions, and in cobalt-modified zinc phosphate solutions at 80 °C. At the start of Zn·Ph crystal growth, a standard Zn·Ph coating (Fig. 3(A)), made with the unmodified solution, was characterized by an irregular precipitation of rectangular-shaped plate crystals on the Fe_2O_3 surfaces. As expected, the crystal morphology of conversion coatings derived from cobalt-modified solution can be discriminated from that of the standard coatings; in the former (see Fig. 3(B)), we observed the precipitation of large well-formed plate-like crystals over 20 μm in size. This change was due to the effect of cobalt ions causing an increase in the rate of the Zn·Ph crystal growth and development. The particular microstructural feature of the nickel-system-derived conversion coatings was a dense morphology with wide plate crystals coexisting with small block-type crystals (Fig. 4). The EDXS spectrum for the large crystals (marked 1) is indicative of the formation of Zn·Ph containing a large amount of iron and a small amount of nickel. Location 2, which is

identical with an area not covered by crystals, was also inspected using EDXS. As is evident from the spectrum that contains a strong iron signal and weak phosphorus signal, the areas not covered with Zn·Ph deposits are composed of an amorphous iron-rich phosphate compound superimposed on the Fe_2O_3 layers. No nickel was found in area 2. These results from the microprobe were in good agreement with the XPS analyses.

Figure 5 presents typical cathodic polarization curves of the logarithm of current density *vs.* potential for the control sample and the 100-to-0, 50-to-50 and 0-to-100 ratio samples in an aerated 0.5 M NaCl solution. By comparison with the curve for the control, the striking characteristics of the cathodic curves for all the cobalt- and nickel-modified Zn·Ph samples are as follows: (1) a considerable reduction in current density in the potential region between -0.95 and -0.80 V and (2) a large shift in E_{corr} to less negative potentials.

With reference to characteristic (1), the indication of low current density is attributed to an inhibition of the cathodic reaction, particularly the oxygen reduction reaction: $\text{H}_2\text{O} + \frac{1}{2}\text{O}_2 + 2\text{e}^- = 2\text{OH}^-$. Thus such a reaction appears to be inhibited by incorporating the cobalt- and nickel-complexed p(AA) macromolecule and cobalt and nickel hydroxides into the Zn·Ph layers. The possible interpretation for this cathodic inhibition mechanism is that, when the p(AA) salt complexes containing $-\text{COO}^- - \text{M}^{2+} - \text{OOC}-$ groups ($\text{M} \equiv \text{Co}$ and Ni) and $\text{M}(\text{OH})_2$ in the conversion coatings come in contact with the NaCl solution, the sodium ions promote the breakage of the $\text{M}-\text{OOC}$ bonds. The breakage could be associated with an ion substitution of M for Na [3]. Hence the free transition M^{2+} ions isolated from the organic complex structure and dissociated by the hydrolysis of M hydroxide compounds in NaCl solution virtually stay in the crystal layers. Simultaneously, the anodic reaction $\text{Fe}^0 - 2\text{e}^- \rightarrow \text{Fe}^{2+}$, which is directly related to the corrosion of steel, may occur at the Zn·Ph-steel interfaces. On the assumption that this reaction process is correct, the electrons 2e^- generated by the anodic reaction of iron in the steel will then preferentially react with the M^{2+} ions. This reaction can be described as the electron-trapping reaction [9] $\text{M}^{2+} + 2\text{e}^- = \text{M}^0$. We believe that such an electron-trapping behavior of Co^{2+} and Ni^{2+} ions contributes to the extended lifetimes of Zn·Ph, which serves as a corrosion barrier for the steel. The curves also indicated that the effect of Co^{2+} on trapping activity is higher than that of Ni^{2+} .

Characteristic (2) directly reflects the degree of coverage of conversion coatings on the entire steel surface, namely a good coverage providing a continuous non-porous coating corresponds to the E_{corr} value at a less negative site. The consequent E_{corr} values for the control, 100-to-0, 50-to-50 and 0-to-100 samples were -0.66 V,

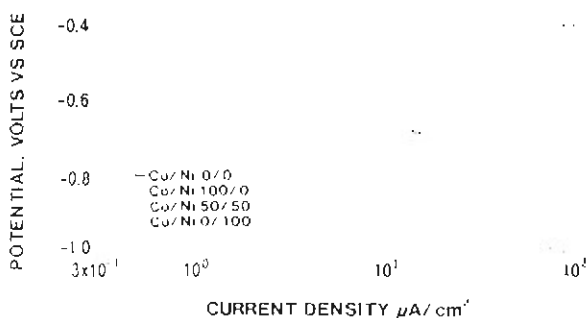


Fig. 5 Comparison of cathodic polarization curves for unmodified coatings and for cobalt- and nickel-modified Zn·Ph conversion coatings at the beginning of precipitation of Zn·Ph.

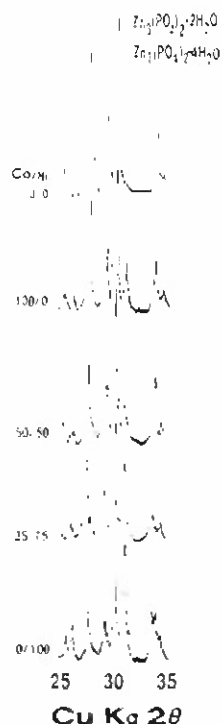


Fig. 6. XRD patterns for conversion coatings derived from unmodified and from cobalt- and nickel-modified zinc phosphate solutions.

−0.57 V, −0.55 V and −0.53 V respectively. Consequently, the most effective coverage of conversion coatings, which provide corrosion protection of steel, seem to be those prepared with nickel-modified phosphate solutions. This finding strongly suggests that good protection performance of conversion coating systems is due to two important factors: (1) a high degree of

coverage by packed crystal layers consisting of large and fine crystal particles and (2) the formation of amorphous iron-rich phosphate compounds in the vicinity of Fe_2O_3 .

3.2. Coating layers formed in the terminal stages of the conversion process

Figure 6 illustrates the XRD phase compositions of crystalline conversion coatings prepared by immersing the steel for 20 min in the unmodified and modified phosphate solutions at 80 °C. Only two crystal phases were distinguishable: zinc orthophosphate dihydrate ($\text{Zn}_3(\text{PO}_4)_2 \cdot 2\text{H}_2\text{O}$) and hopeite ($\text{Zn}_3(\text{PO}_4)_2 \cdot 4\text{H}_2\text{O}$). Interestingly, the data showed that the proportions of single $\text{Zn}_3(\text{PO}_4)_2 \cdot 2\text{H}_2\text{O}$ formation derived from the control solution system (cobalt-to-nickel ratio, 0-to-0) tend to be replaced by hopeite formation as the cobalt-to-nickel ratio was decreased. In fact, the major phase for the nickel-system-derived conversion coating (0-to-100 ratio) was identical with hopeite. The microstructural view of well-converted crystal compounds for the nickel-modified Zn·Ph disclosed an interlocking topography of growing crystals which uniformly covered the steel surfaces (Fig. 7). The feature of EDXS spectrum for a part of the crystal denoted as site 3 was almost the same as that of the crystals (see spectrum for site 1 in Fig. 4) formed at the beginning of the conversion process. All the findings were correlated directly with the evaluation of E_{corr} value for the conversion coatings deposited on the steels after immersion for 10 min and 20 min respectively. The variation in E_{corr} of the samples as a function of cobalt-to-nickel ratio is given in Fig. 8. The data clearly show that E_{corr} increases with a decreasing ratio of cobalt to nickel. This finding suggested that the degree of coverage by Zn·Ph derived from nickel-incorporated phosphate so-



Fig. 7. SEM-EDXS data of well-converted Zn·Ph coatings derived from nickel-modified phosphate solution.

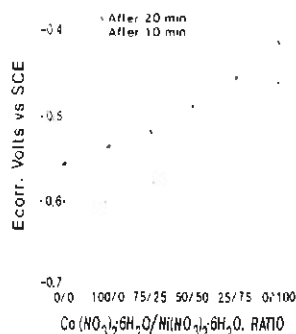


Fig. 8. Variations in corrosion potential value E_{corr} as a function of cobalt-to-nickel ratio for Zn·Ph-covered steel samples prepared by immersion for 10 and 20 min.

lation is higher than that from cobalt-incorporated solution. Also an immersion time of 20 min rather than of 10 min leads to a better coverage of the coatings.

4. Conclusions

The advanced Zn·Ph conversion coatings can be prepared by immersing the steel in the Co^{2+} - and Ni^{2+} -ion-incorporated p(AA)-zinc phosphate solution systems. The formation of M^{2+} ($\text{M} \equiv \text{Co}$ and Ni)-p(AA) salt complexes containing $-\text{COO}^- - \text{M}^{2+} - \text{OOC}-$ groups played an important role in accelerating and promoting the growth and development of Zn·Ph crystal layers over the steel and also introduced the amorphous iron-rich phosphate conversion layers in the vicinity of Fe_2O_3 substrates. The electron-trapping behavior of the M^{2+} ions dissociated from the complex formations and M hydroxides in the NaCl solution inhibited the cathodic reaction. In the final stages of the conversion process, the crystal phase of nickel-system-derived conversion coatings consisted of hopeite ($\text{Zn}_3(\text{PO}_4)_2 \cdot 4\text{H}_2\text{O}$) as the

major component and zinc orthophosphate dihydrate ($\text{Zn}_3(\text{PO}_4)_2 \cdot 2\text{H}_2\text{O}$) as the minor component. The uniform coverage of hopeite- $\text{Zn}_3(\text{PO}_4)_2 \cdot 2\text{H}_2\text{O}$ interlocked crystals over the steel may result in a reduction in the rate of corrosion.

Acknowledgments

Rina Broyer gratefully acknowledges support from the Department of Energy's Division of University and Industry Programs, Office of Energy Research, as a 1990 participant in the Teacher Research Associate Appointment Program. This work was performed under the auspices of the U.S. Department of Energy, Washington, DC, under Contract DE-ACO2-76CH00016 and supported by the U.S. Army Research Office Program MIPR-ARO-103-90.

References

1. T. Sugama, L. E. Kukacka, N. Carciello and J. B. Warren, *J. Mater. Sci.*, **23** (1988) 101.
2. T. Sugama, in L. H. Lee (ed.), *Adhesives, Sealants, and Coating for Space and Harsh Environments*, Plenum, New York, Vol. 37, *Polym. Sci. Technol.*, 1988, p. 405.
3. T. Sugama, L. E. Kukacka, N. Carciello and J. B. Warren, *J. Coat. Technol.*, **61** (1989) 43.
4. T. Sugama and J. Pak, *Adv. Mater. Manuf. Proc.*, **6** (2) (1991) 227.
5. U. Gelius, P. F. Heden, J. Hedman, B. J. Linder, R. Maune, R. Nordberg, C. Nordling and K. Siegbahn, *Phys. Scr.*, **2** (1970) 70.
6. T. Sugama, L. E. Kukacka, C. R. Clayton and H. C. Hua, *J. Adhes. Sci. Technol.*, **1** (4) (1987) 265.
7. N. S. McIntyre and M. G. Cook, *Anal. Chem.*, **47** (13) (1975) 2208.
8. N. S. McIntyre and D. G. Zetaruck, *Anal. Chem.*, **49** (11) (1977) 1521.
9. H. Leidheiser, Jr., and I. Suzuki, *J. Electrochem. Soc.*, **128** (1981) 241.

Corrosion Protection of Steel and Bond Durability at Polyphenylene Sulfide-to-Anhydrous Zinc Phosphate Interfaces

T. SUGAMA* and N. R. CARCIELLO

Energy Efficiency and Conservation Division, Department of Applied Science,
Brookhaven National Laboratory, Upton, New York 11973

SYNOPSIS

To enhance the performance of high-temperature polyphenylene sulfide (PPS) coating in protecting steels from corrosion, the cold-rolled steel surfaces were prepared with anhydrous zinc phosphate (Zn·Ph) conversion coatings containing poly(acid)anhydride as an interfacial tailoring material. The factors contributing to the formation of a good bond at the PPS/Zn·Ph joints were as follows: (1) the chemical reaction of PPS with Fe_2O_3 in the Zn·Ph layers, (2) PPS-to-poly(acid)anhydride interaction, and (3) the mechanical interlocking between PPS and the rough Zn·Ph crystal surfaces. Although such interfacial bond structures provide a superior durability of PPS/Zn·Ph joints against a hot H_2SO_4 solution, the cathodic reaction, $\text{H}_2\text{O} + \frac{1}{2}\text{O}_2 + 2\text{e}^- = 2\text{OH}^-$, occurring at any defect in the PPS/Zn·Ph joint system when NaCl is present will lead to the delamination of the PPS film from the phosphated steel. This cathodic delamination was due mainly to alkali-induced dissolution of Zn·Ph layers. However, the rate of delamination for the PPS/Zn·Ph systems was considerably lower compared with that for the PPS/steel system in the absence of Zn·Ph.

INTRODUCTION

In our recent studies on the interfacial bonding between polyphenylene sulfide (PPS) coatings and metal substrates, such as cold-rolled, stainless, and galvanized steels, we found that the degree of bond strength of PPS-to-metal joints depended primarily on the species of sulfur-related interfacial reaction products generated by the gas-solid chemical reaction between the metal oxides present at the outermost surface site of substrates and the SO_2 and SO_3 gases emitted from PPS at a high temperature of 350°C .¹ The order of these reaction compounds, which play an important role in developing bond strength, was $\text{Fe}_4(\text{SO}_4)_3 > \text{FeSO}_4 > \text{FeS}$. However, although such S-related iron reaction compounds significantly improved bond strength, it is well

known²⁻⁴ that these compounds commonly act to promote the corrosion rate of steels. To avoid the direct contact of PPS with steel, we also investigated the effectiveness of zinc phosphate (Zn·Ph) conversion coatings, deposited on the steel surfaces, in decreasing the cathodic delamination rate of PPS film from the zinc-phosphated steels.⁵ The cathodic reaction, in terms of the oxygen reduction reaction occurring at the corrosion sites of steel in a near-neutral aqueous environment, is $\text{H}_2\text{O} + \frac{1}{2}\text{O}_2 + 2\text{e}^- = 2\text{OH}^-$. The large number of hydroxyl ions generated by this cathodic reaction creates a high pH environment underneath the PPS layers. The attack of alkali solution on the crystalline Zn·Ph coating layer frequently causes its dissolution, thereby resulting in a high rate of delamination of the PPS film. Our previous investigation suggested that the anhydrous $\alpha\text{-Zn}_3(\text{PO}_4)_2$ phase derived from thermal dehydration of the original Zn·Ph hydrate phase has a low susceptibility to alkali-catalyzed dissolution.⁶

* To whom correspondence should be addressed.

Accordingly, the emphasis of this article was directed toward obtaining a better understanding and visualization of the chemical changes at the PPS-to- α phase interfacial contact zones, which are important in improving the durability of adhesive bond and reducing the rate of cathodic delamination of PPS film. For comparison, the interface of PPS-to-cold-rolled steel was also explored.

EXPERIMENTAL

Materials

The metal substrate used was AISI 1010 cold-rolled steel containing 0.08–0.13 wt % C, 0.3–0.6 wt % Mn, 0.04 wt % P, and 0.05 wt % S. The formulation of the zinc phosphate liquid was 1.3 wt % zinc orthophosphate dihydrate [$\text{Zn}_3(\text{PO}_4)_2 \cdot 2\text{H}_2\text{O}$], 2.6 wt % H_3PO_4 , 2.0 wt % [25% poly(acrylic) acid, p(AA)], 1.0 wt % $\text{Ni}(\text{NO}_3)_2 \cdot 6\text{H}_2\text{O}$, and 93.1 wt % water. The average molecular weight of p(AA) polyelectrolyte, supplied by Rohm and Hass Company, was $\approx 60,000$.

In preparing the zinc phosphate (Zn·Ph) samples, the steel surfaces were wiped with acetone-soaked tissues to remove any surface contamination from mill oil. The steel then was immersed for up to 20 min in the Zn·Ph conversion solutions at a temperature of 80°C. Finally, the deposited Zn·Ph layers were baked in an oven at 350°C for 2 h to prepare the anhydrous Zn·Ph layers.

PPS powder for the slurry coating was supplied by the Phillips 66 Company. The as-received PPS was a finely divided, tan powder having a high melt flow with a melting point of 288°C. The PPS film was deposited on the surfaces of the cold-rolled steel and Zn·Ph-treated steel substrate in the following way. First, the substrates were dipped into a PPS slurry consisting of 45 wt % PPS and 55 wt % isopropylalcohol at 25°C. Then, the slurry-coated substrates were preheated in the air at 300°C for 3 h to trigger the fusion of the PPS powder and, at the same time, the volatilization of the isopropylalcohol liquid phase. To assemble the crosslinked and extended macromolecular structures, the fused PPS was finally heated in air at 350°C for 2 h.

Measurements

The chemical compositions and states present on a bond-failure site at the interfaces of PPS/substrate

joint systems were explored using X-ray photoelectron spectroscopy (XPS), scanning electron microscopy (SEM), and energy-dispersion X-ray spectrometry (EDX). The XPS used was a V.G. Scientific ESCA 3MK II. The excitation radiation was provided by an Al $K\alpha$ (1486.6 eV) X-ray source, operated at a constant power of 200 W. The vacuum in the analyzer chamber of the instrument was maintained at 10^{-9} Torr. The atomic concentrations and ratios for the respective chemical elements were determined by comparing the XPS peak areas, which were obtained from the differential cross-sections for core-level excitation. To set a scale in all the high-resolution XPS spectra, the binding peak was fixed at 285.0 eV as an internal reference. A curve-deconvolution technique was employed to find the individual chemical states from the high-resolution spectra of each element. All measurements were made at an electron take-off angle of 38°, which corresponds to an analysis depth of ≈ 5 nm.⁷ EDX is extremely useful for the quantitative analysis of any elements that exist on a surface solid layer up to ≈ 2 μm in thickness.

The cathodic delamination tests for the PPS-coated anhydrous Zn·Ph specimens were conducted in an air-covered 1.0 M NaCl solution using an applied potential of -1.5 V vs. SCE for up to 8 days (see Fig. 1). Thickness of Zn·Ph layer deposited on the steel substrates with the 100×100 mm square area was determined to be approximately 30 μm using a surface profile measuring system. PPS thickness overlaid on the Zn·Ph was approximately 2 mil. The total area of film that comes into contact with NaCl solution was 6.0×10^3 mm². A defect was made using a 1-mm diameter drill bit. After exposure, specimens were removed from the cell and allowed to dry. The PPS coating was removed by cutting, revealing a delaminated region that appeared as a light gray area adjacent to the defect.

To evaluate the durability of the PPS/substrate interfacial bond, the lap-shear tensile strength of substrate-to-substrate PPS adhesive specimens was determined after exposure to H_2SO_4 solution (pH ≈ 3) containing 0.1 M NaCl for up to 8 days at 80°C. The lap-shear tensile strength was estimated in accordance with the modified ASTM Method D-1002. Before overlapping the substrate strips, (50 mm long and 15 mm wide), the 10 \times 15 mm lap area was coated with PPS adhesive. The thickness of the overlapped PPS film ranged from 1–3 mil. The bond strength of the lap-shear specimens is the maximum load at failure divided by the total bonding area of 150 mm².

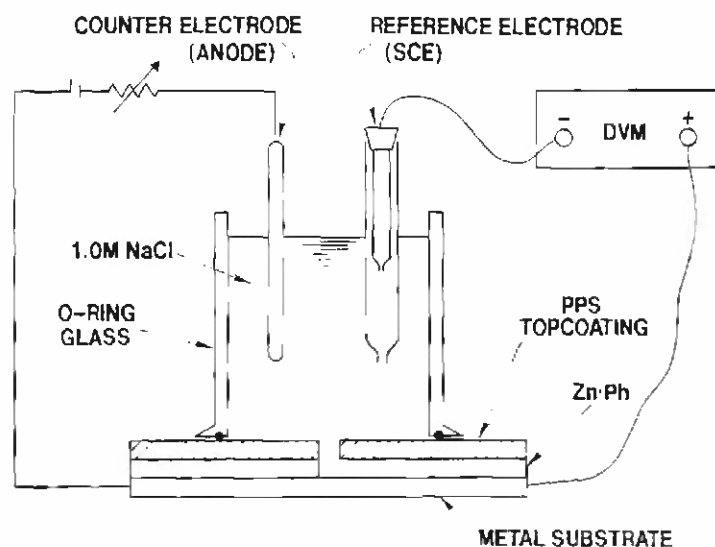


Figure 1 Schematic diagram of cathodic delamination test.

RESULTS AND DISCUSSION

Cathodic Delamination

As discussed in the introduction, it is very important to identify the species of phase present in the anhydrous Zn·Ph layers that greatly influence the vulnerability to alkali attack. The degree of alkali dissolution of the α - $\text{Zn}_3(\text{PO}_4)_2$ phase was considerably lower than that of the γ -phase. To ascertain whether the dehydration phase of Zn·Ph derived from this zinc phosphate solution is α -phase, the Zn·Ph crystal layers were scraped from the steel surfaces before and after thermal dehydration at 350°C in the air and then ground to a size of 325 mesh (0.044 mm) for X-ray powder diffraction (XRD).

Figure 2 illustrates two XRD tracings: the original Zn·Ph, denoted as sample a, and the anhydrous Zn·Ph (sample b) prepared by heating the original sample at 350°C. Two hydrous crystal phases were distinguishable in the original Zn·Ph layers, namely, zinc orthophosphate dihydrate [$\text{Zn}_3(\text{PO}_4)_2 \cdot 2\text{H}_2\text{O}$] present as the major component and hopeite [$\text{Zn}_3(\text{PO}_4)_2 \cdot 4\text{H}_2\text{O}$] as the minor one. The predominating phase of the anhydrous samples is identical to α - $\text{Zn}_3(\text{PO}_4)_2$, and γ - $\text{Zn}_3(\text{PO}_4)_2$ is present as a secondary phase. This result was in agreement with that obtained in our previous investigation,⁶ that is, $\text{Zn}_3(\text{PO}_4)_2 \cdot 2\text{H}_2\text{O}$ was converted into the α - $\text{Zn}_3(\text{PO}_4)_2$ phase during dehydration and the $\text{Zn}_3(\text{PO}_4)_2 \cdot 4\text{H}_2\text{O} \rightarrow \gamma$ - $\text{Zn}_3(\text{PO}_4)_2$ phase

transition is favored. Hence, we can predict that the anhydrous Zn·Ph layers prepared in this study will have a minimum rate of alkali dissolution.

Figure 3 shows the delaminated area of PPS film

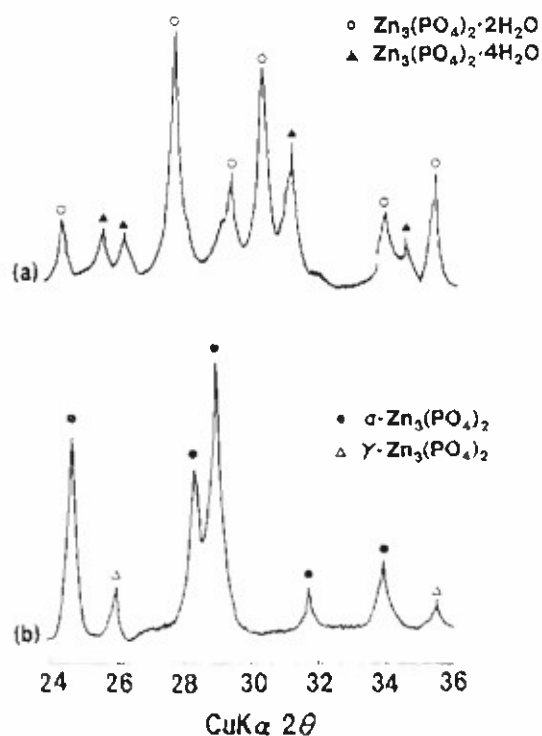


Figure 2 XRD tracings for (a) the original Zn·Ph samples and (b) the 350°C dehydrated Zn·Ph samples.

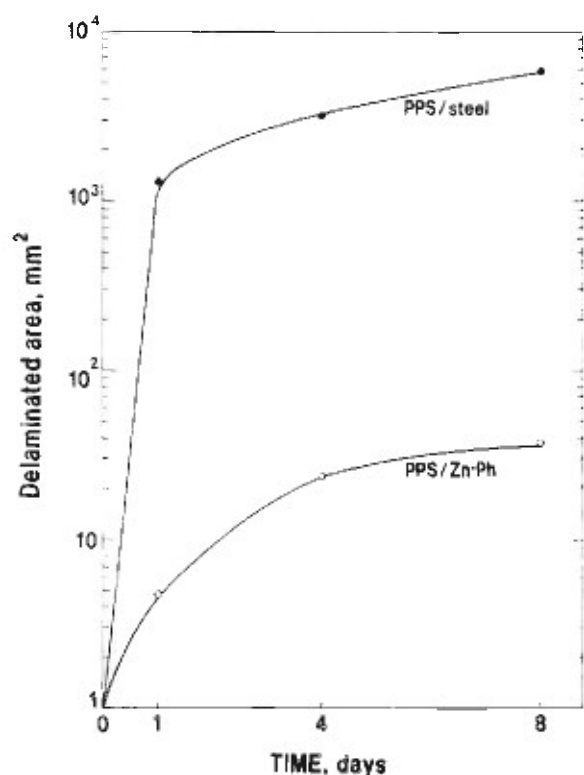


Figure 3 Cathodic delamination of PPS film from steel and Zn·Ph-deposited steel substrates in 1.0M NaCl.

from the substrates after up to 8 days of cathodic testing. For PPS/steel joint systems in the absence of Zn·Ph, the resulting curve indicates that there is a significantly large area of delamination of PPS after only 1 day's exposure. Further exposure up to 8 days resulted in an extensive delamination of $\approx 6 \times 10^3 \text{ mm}^2$. The rate of delamination of this PPS/steel system was considerably reduced when Zn·Ph was deposited onto the steel surfaces. The value of $\approx 4 \times 10^2 \text{ mm}^2$ for the PPS/Zn·Ph system obtained after 8 days was $\approx 10^2$ times lower than that of the PPS/steel system after the same exposure. Why such a high rate of delamination occurs at the critical interfacial zones of the PPS/steel systems is of particular interest. To gain this information, we explored by XPS both cathodically failed PPS and steel interfaces for 8-day-exposed PPS/steel systems. For purposes of comparison, both failure sides for the unexposed control systems were investigated. The control samples were prepared by pulling the PPS films from the steel and Zn·Ph substrate surfaces at sites of tension failure. Table I summarizes the chemical compositions of the cross-section samples before and after the cathodic experiments. For

the controls, the interface chemistry of the PPS side removed from the steel substrate consists of 3.5% S, 42.1% C, 44.0% O, and 10.4% Fe. The S element refers to S originating from the fundamental formula, $[-S-]_n$, of PPS. The C belongs both to carbons in the PPS and in the contaminants. As reported in our previous paper,¹ the Fe and O elements remaining on the PPS side are associated with the interfacial reaction products formed by interaction between the PPS coating and Fe_2O_3 existing at the outermost surface site of steels. No S atom was found on the failed steel sides. Thus, it appears that the locus of failure occurs through the reaction product layers close to PPS. A striking difference from the control was observed in the cathodically delaminated samples. The differences are as follows: (1) A large amount of Fe and O was removed from the interfacial PPS sides, while the concentrations of S and C were markedly increased; (2) a small amount of S remained on the steel sides; and (3) a certain amount of Na from the NaCl electrolyte was detected on both the delaminated PPS and steel sides. There was no evidence for the presence of the Cl atom. The first two results show that the cathodic reaction, $\text{H}_2\text{O} + \frac{1}{2}\text{O}_2 + 2\text{e}^- = 2\text{OH}^-$, occurring at the defect in the PPS film leads to the elimination of Fe-related reaction products. Since the ionic reaction between the OH^- ions generated by cathodic reaction and the Na^+ ions dissociated from NaCl electrolyte yields a high concentration of NaOH in the area of the defect,⁸ it is reasonable to assume that creation of such an alkali environment at the interfacial regions cause NaOH-catalyzed hydrolysis of the interfacial reaction products. Thus, as a result of difference 3, the detection of Na atom at the delaminated interfaces could be due to the penetration of the NaOH solution through the interfacial layers.

To support this hypothesis, we inspected the high-resolution S_{2p} core-level spectra of the PPS and steel

Table I Chemical Composition of Both Interfacial Failure Sides Before and After Cathodic Delamination Tests for PPS/Steel Joint Systems

Cathodic Test	Failed Side	Atomic Concentration, %					
		S	C	O	Mn	Fe	Na
Before	PPS	3.5	42.1	44.0	—	10.4	—
Before	Steel	—	31.3	55.5	0.7	12.6	—
After	PPS	10.7	80.9	6.1	—	1.5	0.8
After	Steel	1.3	23.3	59.6	1.3	13.3	1.2

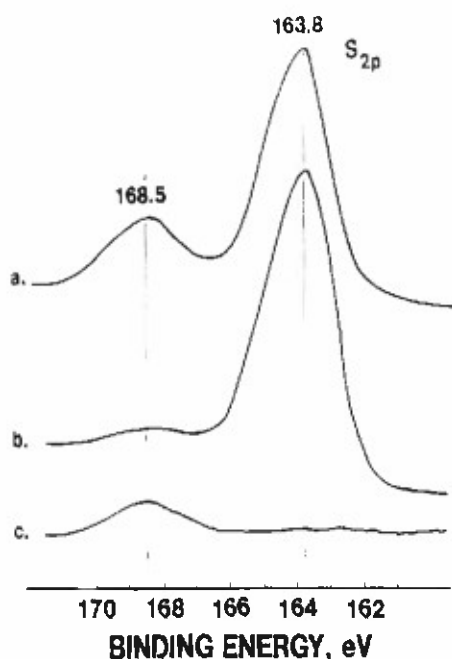


Figure 4 S_{2p} core level spectra for (a) the PPS side removed from the steel before cathodic delamination tests and (b) the delaminated PPS and (c) steel sides after cathodic tests.

interfacial sides of the specimens before and after cathodic tests (Fig. 4). The S_{2p} region for the PPS interface of the control samples reveals two major components at 163.8 and 168.5 eV. The former peak, the principal component, is attributable to the S in the PPS, while the latter reflects the S in the ferrous sulphate ($FeSO_4$) formed by the interfacial gas-solid reaction between Fe_2O_3 and SO_2 and SO_3 gases emitted from PPS in air at a high temperature.¹ By comparison with the control, the remarkable attenuation of peak intensity at 168.5 eV originating from the Fe in the $FeSO_4$ reaction product can be observed on spectrum (h) of the cathodically delaminated PPS side. In the spectrum (c) of the delaminated steel side, the presence of weak line at 168.5 eV verifies that a small amount of intermediate $FeSO_4$ adhering to the steel remains at the interfacial steel side, while there are no signals for the peaks of 163.8 eV corresponding to the PPS. Therefore, the major reason for the more extreme cathodic delamination at PPS/steel interfaces was the NaOH-catalyzed hydrolysis of $FeSO_4$ adjacent to the steel surfaces.

Table II gives the elemental compositions for both interfacial failure sides in the PPS/Zn-Ph joint systems before and after cathodic tests for 8 days.

The interfacial PPS surface of control samples had a composition closely resembling that of the Zn-Ph interface except that there was no S element. The detection of a certain amount of P, Fe, and Zn on the PPS interface demonstrated that these elements migrate from the Zn-Ph-covered steel substrate to the coating sides during the failure of the bond. These results show that there is a good interfacial bond between PPS and Zn-Ph. Hence, failure must occur through the Zn-Ph layer. In other words, the PPS-to-Zn-Ph bond strength is much greater than that of Zn-Ph itself. A dramatic change in composition can be seen on both of the cathodically delaminated areas of the interfacial PPS and Zn-Ph sides, namely, a remarkable amount of P, O, Fe, and Zn has vanished from the delaminated areas, while additional amounts of Na atom have been incorporated into the interfaces. The data also suggested that the rate of elimination of Fe atom is much higher than that of any other elements. The removal of P and Zn may be mainly due to the dissolution of Zn-Ph layers caused by the attack of alkali solution generated by the oxygen reduction reaction ($H_2O + \frac{1}{2}O_2 + 2e^- = 2OH^-$) at the site of the defect. Since the evolved OH^- ions ionically react with Na^+ dissociated from NaCl, the incorporation of Na can be directly related to the penetration of NaOH yielded by this charge balance into the failure zones. Such alkali dissolution of the Zn-Ph layers is reflected in the increase in concentration of S and C atoms in the PPS. But an important question still remains to be answered. Why is the rate of elimination of Fe-related compounds considerably higher than that of the Zn-Ph? To answer this question, we inspected the high-resolution P_{2p} , $Zn_{2p3/2}$, $Fe_{2p3/2}$, and S_{2p} spectra of the cathodically delaminated PPS side and the PPS failure surface that was made by pulling the PPS film from the Zn-Ph before the

Table II Chemical Composition of Both Interfacial Failure Sides Before and After Cathodic Delamination Tests for PPS/Zn-Ph Joint Systems

Cathodic Test	Failed Side	Atomic Concentration, %						
		P	S	C	O	Fe	Zn	Na
Before	PPS	8.5	2.5	32.0	47.1	6.1	3.8	—
Before	Zn-Ph	5.3	—	35.9	47.7	8.1	3.0	—
After	PPS	3.4	4.1	56.2	26.9	0.4	2.1	6.9
After	Zn-Ph	2.1	1.5	56.8	31.5	0.9	2.5	4.7

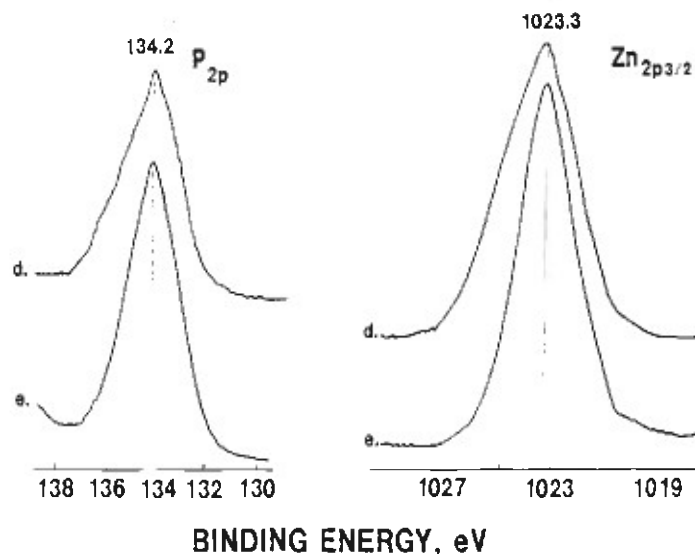


Figure 5 P_{2p} and Zn_{2p_{3/2}} regions for (d) the interfacial PPS sides before cathodic test and (e) at the cathodically delaminated PPS interface.

cathodic tests. Figure 5 illustrates the resultant P_{2p} and Zn_{2p_{3/2}} regions of these samples. The control sample (before cathodic tests), denoted as d, had a main line at 134.2 eV for P_{2p} and at 1023.3 eV for Zn_{2p_{3/2}} spectra, reflecting the P and Zn atoms in Zn·Ph.⁹ Peak features and intensity similar to those of the control was observed in both the P_{2p} and the Zn_{2p_{3/2}} region for the sample (e) after cathodic tests. In the Fe_{2p_{3/2}} region (Fig. 6), the control sample (d)

displays a strong signal emerging at the BE position of 710.7 eV, corresponding to the formation of ferric oxide (Fe₂O₃).¹⁰ Since the electrochemical reaction between the steel and Zn·Ph solution at an early stage of Zn·Ph precipitation leads to the liberation of the free Fe ions from the steel surface,¹¹ it is not surprising that Fe₂O₃ forms by the oxidation of free Fe present in the Zn·Ph layers during the Zn₃(PO₄)₂·2H₂O → α-Zn₃(PO₄)₂ phase conversion

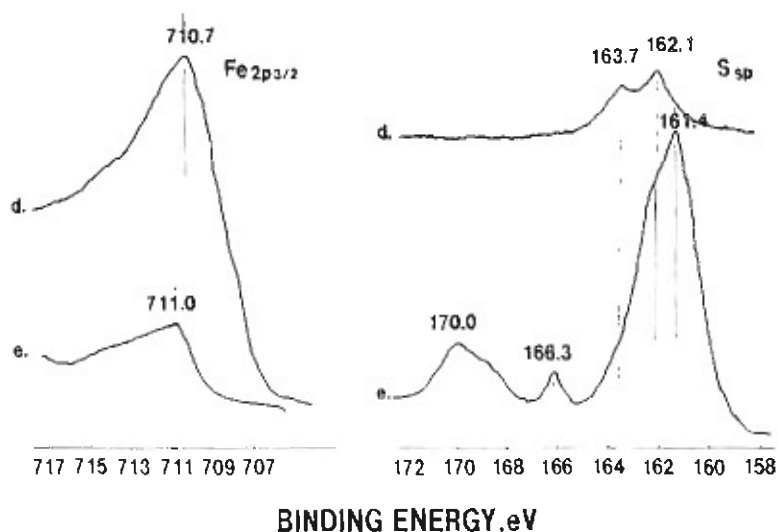


Figure 6 Fe_{2p_{3/2}} and S_{2s} regions for (d) the interfacial PPS side before cathodic test and (e) at the cathodically delaminated PPS interface.

in air at 350°C before the PPS coating is deposited. In fact, we observed color changes in Zn·Ph coating, from a dark gray at 100°C to a light brown at 350°C. A striking decay in the $\text{Fe}_{2p3/2}$ signal intensity was observed from the cathodically delaminated PPS interface (e) (the reason will be discussed later). The S_{2p} region (Fig. 6) for the control (d) reveals two resolvable components at 163.7 and 162.1 eV. The former peak is attributable to the S in the PPS, and the latter belongs to the S in the FeS.¹² This information seems to suggest that the SO_2 gas emitted from the PPS in the vicinity of Zn·Ph layer preferentially reacts with Fe_2O_3 in the Zn·Ph layers, rather than the α - and γ - $\text{Zn}_3(\text{PO}_4)_2$ phases. To confirm that SO_2 was taken up by Fe_2O_3 , anhydrous Zn·Ph coatings were exposed in SO_2 gases at 350°C (flow rate ≈ 200 cc/min) for up to 120 min. The chemical compositions of the exposed coating surfaces were investigated by XPS, and then the internally generated P_{2p} , S_{2p} , Fe_{2p} , and $\text{Zn}_{2p3/2}$ peak areas were used to calculate the atomic percent ratios. Figure 7 shows the variation in P/Zn, S/Zn, and Fe/Zn ratios as a function of exposure times. The data indicate that the value of the S/Zn ratio increases with longer exposure time, while the Fe/Zn

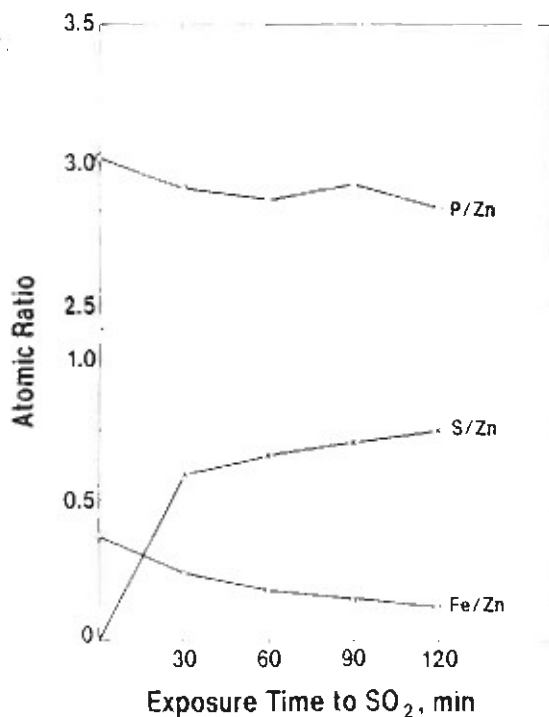


Figure 7 Changes in P/Zn, S/Zn, and Fe/Zn atomic ratios as a function of exposure time to SO_2 .

Zn ratio value monotonously decreases as a function of time. In contrast, the P/Zn ratio does not express any changes in value for the exposure periods up to 120 min. Thus, these data strongly support the idea that SO_2 is taken up by the Fe_2O_3 present in the Zn·Ph layers.

Returning to the S_{2p} spectrum in Figure 6, the drastic changes in spectral features occur as the cathodic reaction is initiated at the defect. In particular, the S_{2p} signal at the cathodically delaminated PPS side (e) was characterized by the appearance of three new peaks, the most intense peak being at 161.4 eV, with two prominent lines at 166.3 and 170.0 eV. Considering that there is little residual Fe atom at the delaminated PPS side, these new lines do not reflect the formation of Fe-related sulfur compounds. However, since a large amount of Na remains on the delaminated PPS interface, these lines possibly could be assigned to the Na-related sulfur compounds derived from the cathodic reaction. Assuming that these predicted assignments are correct, other authors¹³ suggested that the predominating line at 161.4 eV is due to the S in the sodium sulphide (Na_2S) as the major by-product of the cathodic reaction; the other lines at 166.3 and 170.0 eV were ascribed to the sodium sulphite (Na_2SO_3) and sulphate (Na_2SO_4), respectively. The striking decay of $\text{Fe}_{2p3/2}$ signal [Fig. 6(e)] at the cathodically delaminated PPS side can be interpreted as follows: The Fe_2O_3 in Zn·Ph layers favorably reacts with PPS to form FeS, which is one of several S-related iron reaction compounds. However, it was very difficult to distinguish the photoelectron line of FeS from the Fe_2O_3 line in the $\text{Fe}_{2p3/2}$ region because the signal originating from Fe in FeS emerges at only ≈ 0.3 eV lower BE position than that of Fe_2O_3 .¹⁴ Nevertheless, the decay of $\text{Fe}_{2p3/2}$ signal was implicated in the loss of a great deal of FeS caused by NaOH-catalyzed hydrolysis.

Using SEM and EDX, we also investigated the morphology and the elemental distribution of cathodically failed Zn·Ph side (Fig. 8). As seen in the bottom left photograph of Figure 8, SEM topography reveals the existence of two distinctive areas: site A represents an area approximately 1000 μm in diameter surrounding the defect, while site B is at the edge of the delaminated PPS. The C area in the top photograph, an enlargement of site A, discloses the presence of the PPS adhering locally to the substrate. As is evident from the EDX elemental data from this region, a small part of the PPS film remaining on the substrate contains not only the S atom but also has other elements such as Na, Fe,

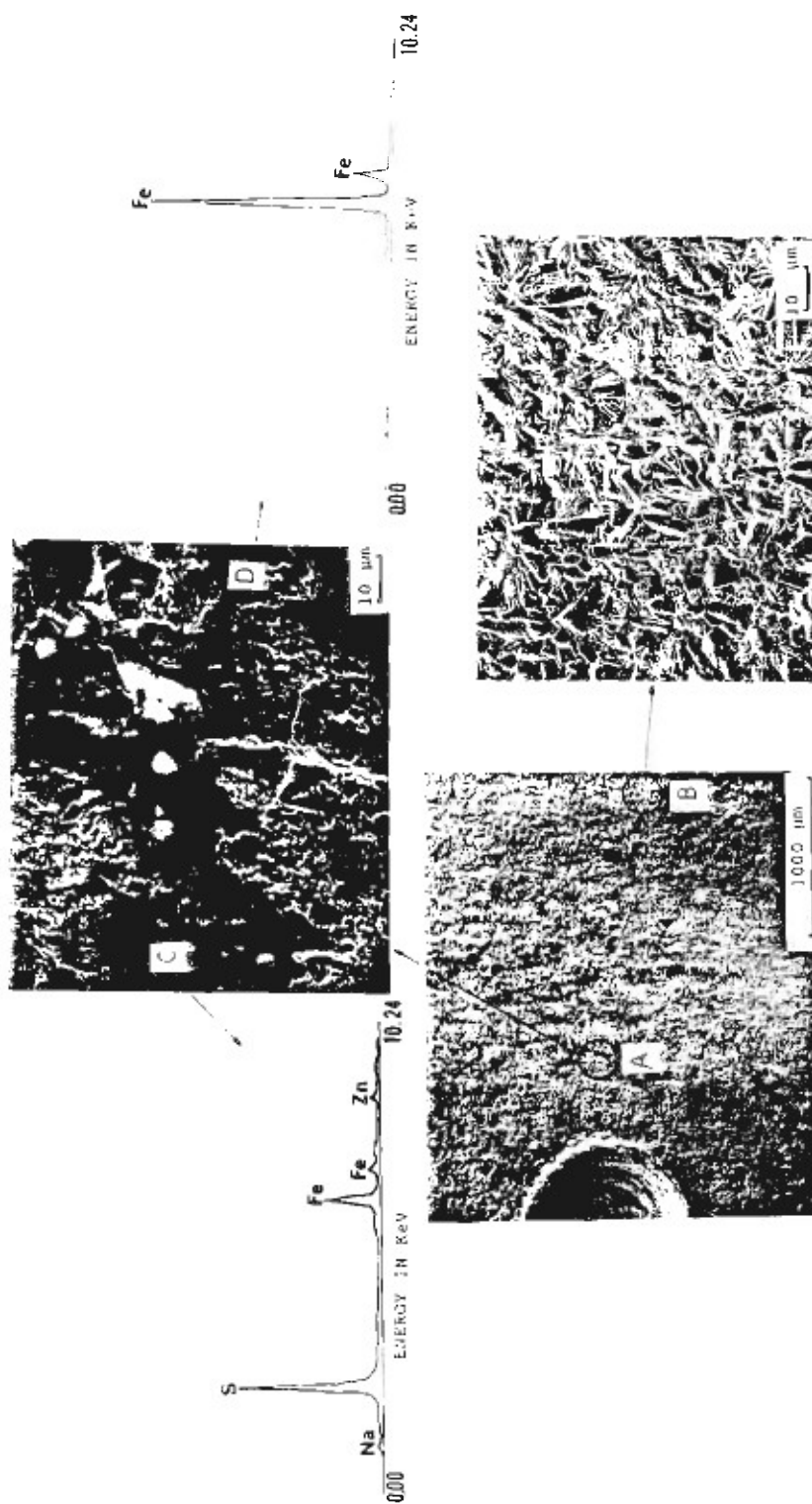


Figure 8 SEM microprobe and EDX spectra of the cathodically delaminated area (A) near a defect and (B) at the delaminated front of anhydrous Zn·Ph coating after PPS was removed from the PPS/Zn·Ph joint.

and Zn. The EDX spectrum of area D in the same photograph, representing the presence of the Fe atom alone, relates to the steel substrate. These findings strongly suggested that almost all the crystalline conversion coating surrounding the defect was dissolved in the NaOH solution resulting from the cathodic reaction occurring beneath the PPS film. The right-bottom SEM microstructure (an enlargement of site B) is an image of the morphology of a normal Zn·Ph crystal coating, which has not been attacked by NaOH.

A certain amount of p(AA) polyelectrolyte incorporated during crystal growth into the zinc phosphate solution is present at the outermost surface sites of Zn·Ph layers.¹⁵ Thus, we should consider whether there is an interaction between p(AA) and PPS. In an attempt to obtain this information, samples were prepared in the following way: First, the steel plate was dipped for 5 min into the 1.0% p(AA) aqueous solution, and then dried in an oven at 350°C for 1 h to transform the p(AA) macromolecule from the poly(acid), having COOH pendent groups, to

the poly(acid)anhydride having

$$\begin{array}{c} \text{C} & & \text{C} \\ // & \backslash & / & // \\ \text{O} & & \text{O} & \text{O} \end{array}$$

and COOH groups.¹⁶ A PPS slurry was then deposited on the poly(acid)anhydride macromolecule film surfaces, followed by curing in air at 350°C. Finally, the PPS site removed from the poly(acid)anhydride-primed steel was inspected by XPS. Fig-

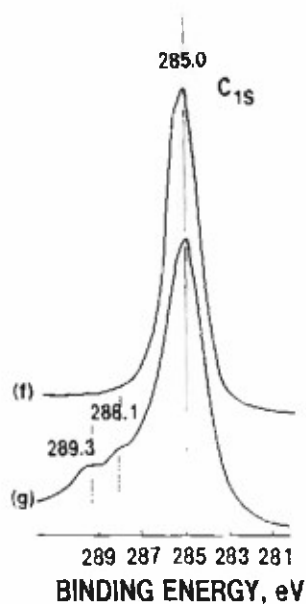


Figure 9 C_{1s} spectra for (f) bulk PPS and (g) PPS interface removed from poly(acid)anhydride-primed steel.

ure 9 shows the XPS spectra for the C_{1s} region of the bulk PPS film (f) and for the interfacial PPS site (g). For the bulk PPS, the single peak at 285.0 eV reveals the aromatic hydrocarbon in PPS. By comparison with the symmetry of the curve of bulk PPS, the shape of the peak of the samples from the interfacial PPS site has an asymmetric tailing toward the high BE sides. This tail, which separates from the primary peak of aromatic hydrocarbon at 285.0 eV, reveals the presence of at least two resolvable peaks. Based upon published data,¹⁷ the assignments of the lines at 288.1 and 289.3 eV are due to the carbon in the carboxyl ($C=O$) group and the carboxylic acid (COOH) group, respectively, thereby suggesting that bond failure occurs through the mixing layers of PPS and poly(acid)anhydride. Although there is no evidence about the interfacial bond structure and the chemical or physical interactions, it appears that the poly(acid)anhydride macromolecule has a strong affinity for PPS. On the other hand, the rough surface structure of crystalline Zn·Ph was one factor contributing to the increased mechanical interlocking forces associated with the mechanical anchoring of the PPS polymer, resulting from the penetration of the melted polymer into the open-surface microstructure and microfissures of Zn·Ph layers. Consequently, the combination of such chemical and physical bond structures plays a major role in the good adhesion performance at PPS-to-Zn·Ph joints.

Durability of Adhesive Bond

As discussed, the cathodic delamination of PPS film from a zinc-phosphated steel was due primarily to the alkali dissolution of Zn·Ph and FeS underneath the PPS coatings. We investigated the durability of the steel/ and Zn·Ph/PPS adhesive bonds after exposure at 80°C to H_2SO_4 solution ($pH \approx 3$) containing 0.1 M NaCl. All edges on the PPS adhesive/adhered joints were unprotected to evaluate the susceptibility of the interfacial bonding to the hot acid. Figure 10 shows the changes in the value of lap-shear bond strength as a function of exposure time; each value in the figure represents the average of three measurements. For the unexposed control specimens, the bond strength of the PPS/Zn·Ph joint was much higher than that of the PPS/steel joint. The deposition of Zn·Ph layer on the steel surface appears to provide a strong adhesive bonding of PPS/steel joints. The data for the PPS/Zn·Ph specimens indicated that a reduction in strength gradually occurs during exposures of up to 4 days; beyond this, there is very little reduction in strength.

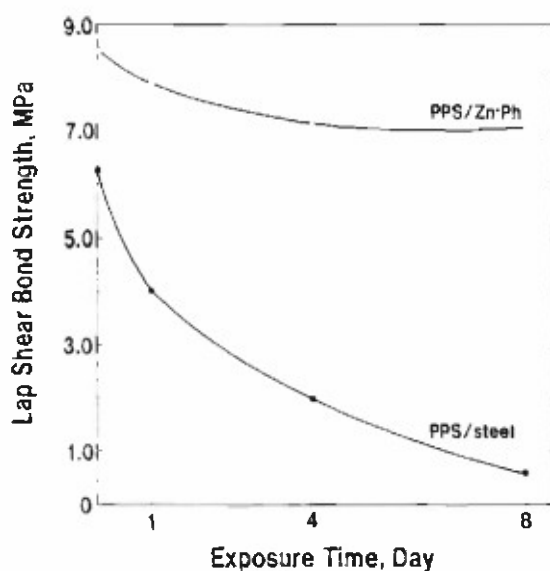


Figure 10 Lap-shear bond strength vs. exposure time to 80°C H_2SO_4 solution.

This fact is reflected in the considerable durability of the PPS/Zn·Ph joint in hot-acid environments. The SEM image (not shown) of peeled PPS interface for the 8-day-exposed specimens showed the presence of a large amount of Zn·Ph, suggesting that the mode of delamination can be defined as cohesive failure that occurs through the Zn·Ph layer. In contrast, the strength of the PPS/steel specimens after exposure for 8 days dropped dramatically to a value of 0.6 MPa, a reduction of $\approx 89\%$. There was a partial separation of the PPS film from the steel surface, thereby implying that the bond durability of PPS/steel joints is very poor.

To elucidate the failure mode of acid-damaged PPS/steel joints, the PPS-coated steel specimens were exposed for 8 days at 80°C in H_2SO_4 solution ($\text{pH} \approx 3$) containing 0.1M NaCl. After exposure, the chemical composition of the separated PPS and steel interfaces was inspected by XPS; the quanti-

tative data are given in Table III. Compared with the control specimens, the interfaces of the exposed specimens were characterized by representing the migration of S atom from the PPS to the steel sides and the interfacial diffusion of Cl. There was no signal for Na from the formation of Na-related sulfur reaction compounds, which are induced by the diffusion of Na ions into the interfacial boundary zones. Nevertheless, the locus of failure appears to occur through the S-incorporated reaction product layers as means of the adhesive failure at the interface.

To identify the reaction product that causes the bond failure in hot acid, we inspected S_{2p} core-level spectra for both the separated PPS and the steel sides (Fig. 11). The S_{2p} region for both sides showed the emergence of a single peak at the position of 169.0 eV, which corresponds to a shift of 0.5 eV to the higher BE site than that of FeSO_4 , formed by interaction between PPS and the steel [see Fig. 4(a)] before exposure. A shift of 0.5 eV is reasonable to distinguish the formation of ferric sulphate $[\text{Fe}_2(\text{SO}_4)_3]$,¹³ which may be generated by H_2SO_4 -catalyzed oxidation of FeSO_4 . Thus, the cause for the bond failure of PPS/steel joints after exposure to hot-acid solution was the interfacial $\text{FeSO}_4 \rightarrow \text{Fe}_2(\text{SO}_4)_3$ phase transition.

CONCLUSIONS

When high-temperature performance PPS polymer coatings were directly applied to cold-rolled steel surfaces, the chemical reaction at 350°C between the Fe_2O_3 at the outermost surfaces of the steel and

Table III Atomic Concentrations of Failed PPS and Steel Sides Before and After Exposure for 8 Days to 80°C H_2SO_4 Solution

Exposure to H_2SO_4	Failed Side	Atomic Concentration, %					
		S	Cl	O	Mn	Fe	Cl
Before	PPS	3.5	42.1	44.0	—	10.4	—
Before	Steel	—	31.3	55.5	0.7	12.6	—
After	PPS	6.7	20.9	63.0	—	7.8	1.6
After	Steel	3.1	18.4	65.0	—	11.2	2.3

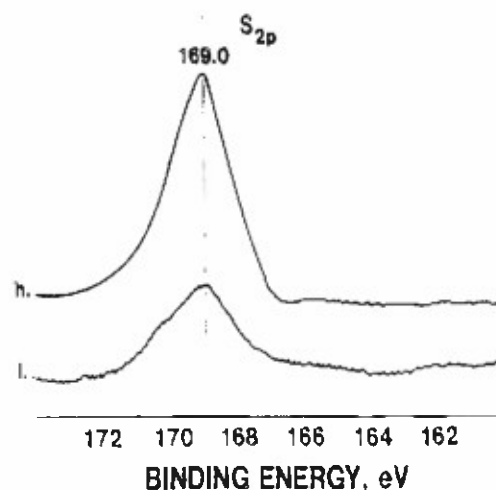


Figure 11 S_{2p} region for (h) PPS and (i) steel interfaces separated by the attack of hot-acid solution on the PPS-steel joint.

the PPS in air led to the formation of FeSO_4 at the critical interfacial zones. Although the intermediate FeSO_4 layers, as interfacial reaction products, play an important role in developing bond strength at the PPS/steel joint, the alkali-catalyzed hydrolysis of FeSO_4 caused by the cathodic reaction, $\text{H}_2\text{O} + \frac{1}{2}\text{O}_2 + 2\text{e}^- = 2\text{OH}^-$, at any defects in the coating film caused catastrophic cathodic delamination of the PPS film from the steel. Therefore, to avoid the direct contact of PPS with steel, a p(AA)-modified $\text{Zn} \cdot \text{Ph}$ conversion coating was deposited on the steel surfaces. Before applying the PPS, the $\text{Zn}_3(\text{PO}_4)_2 \cdot 2\text{H}_2\text{O}$ as major phase of the $\text{Zn} \cdot \text{Ph}$ layers was converted into an $\alpha\text{-Zn}_3(\text{PO}_4)_3$ phase by thermal dehydration at 350°C . This thermal treatment also promoted the transformation of the poly(acid) structure within the p(AA) into the poly(acid)anhydride and the oxidation of free Fe atoms dissociated from the steel surfaces during the precipitation of the crystalline $\text{Zn} \cdot \text{Ph}$ coating. We found that SO_2 emitted from the PPS at the PPS-to- $\text{Zn} \cdot \text{Ph}$ boundary regions preferentially reacts with the oxidized Fe compounds rather than with Zn and P atoms in the $\text{Zn} \cdot \text{Ph}$ crystals. Such a gas-solid interaction between SO_2 and the oxidized Fe compound at 350°C caused the formation of an FeS reaction product. In addition, two different interactions were recognized: One was the polymer-to-polymer reaction between the PPS and the poly(acid)anhydride existing at the outer surface of the $\text{Zn} \cdot \text{Ph}$ layers; the other was the mechanical interlocking associated with the mechanical anchoring of the PPS polymer, which resulted from the penetration of the melted polymer into the open surface microstructure of the $\text{Zn} \cdot \text{Ph}$ layers. These physicochemical factors, contributing to the development of adhesion force at the PPS/ $\text{Zn} \cdot \text{Ph}$ interfaces, were essentially responsible for the high lap-shear bond strength on the phosphated metal-to-phosphated metal PPS specimens.

Once a cathodic reaction occurs at a defect in the PPS/ $\text{Zn} \cdot \text{Ph}$ system, the action of NaOH derived from the cathodic reaction results in the dissolution and hydrolysis of the anhydrous $\text{Zn} \cdot \text{Ph}$ and FeS interaction product. Such an alkali-induced dissociation resulted in the formation of the Na-related sulfur compounds, such as Na-sulphide, Na-sulphite, and Na-sulphate. However, the rate of cathodic delamination of PPS for the PPS/ $\text{Zn} \cdot \text{Ph}$ system was considerably lower than that for the PPS/steel system.

The adhesive bonds of the PPS/ $\text{Zn} \cdot \text{Ph}$ systems displayed an outstanding bond durability against attack by a hot H_2SO_4 solution containing NaCl. In

contrast, the bonds of the PPS/steel systems failed after exposure for only 8 days to this hot-acid solution. The major reason for this failure was due to $\text{FeSO}_4 \rightarrow \text{Fe}_2(\text{SO}_4)_3$ phase transformation in the intermediate layers. The formation of $\text{Fe}_2(\text{SO}_4)_3$ may be deduced from the acid-catalyzed oxidation of the FeSO_4 reaction product formed at the PPS/steel interfaces.

This work was performed under the auspices of the U.S. Department of Energy under Contract No. DE-AC02-76CH00016 and supported by the U.S. Army Research Office Program MIPR-ARO-119-91 and the Physical Sciences Department of the Gas Research Institute under Contract No. 5090-260-1948.

REFERENCES

1. T. Sugama and N. R. Carciello, *Int. J. Adhesion Adhesives*, **11**, 97 (1991).
2. J. B. Sardisco and R. E. Pitls, *Corrosion*, **21**, 245 (1965).
3. C. Milton, *Corrosion*, **22**, 191 (1966).
4. A. L. Martin and R. R. Annand, *Corrosion*, **36**, 297 (1981).
5. T. Sugama and J. Pak, *Adv. Mater. Manuf. Proc.*, **6**, 227 (1991).
6. T. Sugama, L. E. Kukacka, N. Carciello, and J. B. Warren, *J. Mater. Sci.*, **26**, 1045 (1991).
7. M. P. Seah and W. A. Dench, *Surf. Interface Anal.*, **1**, 2 (1979).
8. H. Leidheiser Jr. and W. Wang, in *Corrosion Control By Organic Coatings*, H. Leidheiser, Jr. (ed.), NACE, Houston, TX, 1981, pp. 70-77.
9. T. Sugama, L. E. Kukacka, N. Carciello, and J. B. Warren, *J. Coat. Tech.*, **61**, 43 (1989).
10. N. S. McIntye and D. G. Zetaruk, *Anal. Chem.*, **49**, 1521 (1977).
11. T. Sugama, L. E. Kukacka, N. Carciello, and J. B. Warren, *J. Mater. Sci.*, **22**, 722 (1987).
12. H. Binder, *Z. Naturforsch.*, **B28**, 255 (1973).
13. B. J. Lindberg, K. Hamrin, G. Johanson et al., *Phys. Scr.*, **1**, 277 (1970).
14. J. C. Carver, G. K. Schweitzer, and T. A. Carlson, *J. Chem. Phys.*, **57**, 973 (1972).
15. T. Sugama, L. E. Kukacka, N. Carciello, and J. B. Warren, *J. Mater. Sci.*, **23**, 101 (1988).
16. T. Sugama, L. E. Kukacka, C. R. Clayton, and H. C. Hua, *J. Adhes. Sci. Tech.*, **1**, 265 (1987).
17. D. Briggs and M. P. Seah, *Practical Surface Analysis by Auger and X-ray Photoelectron Spectroscopy*, John Wiley, New York, 1985, p. 385.

Received March 25, 1991

Accepted September 3, 1991

APPENDIX B

POLYMETALLOSILOXANE - RELATED PUBLICATIONS

POLYTITANOSILOXANE COATINGS DERIVED FROM Ti(OC₂H₅)₄-MODIFIED ORGANOSILANE PRECURSORS*

T. SUGAMA, L. E. KUKACKA and N. CARCIELLO

Process Sciences Division, Department of Applied Science, Brookhaven National Laboratory, Upton, NY 11973 (U.S.A.)

(Received August 22, 1989; in revised form November 24, 1989)

Summary

Amorphous polytitanosiloxane (PTS) was formed by hydrolysis-polycondensation and hydrolysis-polycondensation-pyrolysis reaction mechanisms of precursor sol solutions consisting of monomeric organosilanes, Ti(OC₂H₅)₄, methanol, water and hydrochloric acid, over the temperature range 100 - 500 °C. These reaction processes which are responsible for the assemblage of PTS networks were found to depend mainly on the species of organosilane used.

The PTS was applied as a coating on aluminum substrates and the factors which play an important role in providing corrosion protection were investigated. Three major findings are as follows: (1) the addition of HCl, which was used as a hydrolysis accelerator for the organosilanes and Ti(OC₂H₅)₄, acts to produce a clear sol solution, thereby aiding in the formation of smooth and uniform coating layers; (2) the organosilane to Ti(OC₂H₅)₄ ratios are critical for the fabrication of PTS films; and (3) moderate densification of the Si—O—Ti bond in PTS networks is needed to produce a good film.

Introduction

The use of titanium alkoxide, Ti(OR)₄ (where R is CH₃, C₂H₅, C₃H₇ or C₄H₉), as a means of enhancing the network connectivity and, hence, the extent of three-dimensional crosslinking of polymeric organosilanes synthesized using sol-gel techniques in terms of hydrolysis-polycondensation processes, has been investigated previously [1, 2]. These authors reported that the incorporation of Ti(OR)₄ into the organosilane system improved mechanical properties such as the modulus of elasticity and tensile strength of the organosiloxane polymer. It has also been reported that the addition of excessive amounts of Ti(OR)₄ to the systems results in large

*This work was performed under the auspices of the U.S. Department of Energy, Washington, D.C. under Contract No. DE-AC02-76CH00016, and supported by the U.S. Army Research Office Program MIPR-ARO-102-89.

reductions in the elongation at the failure point of the polymers [3]. All of these studies were performed at temperatures up to 220 °C.

Apparently an inorganic polysilane formed by a sol-gel polycondensation process involving tetraethylorthosilicate, $\text{Si}(\text{OC}_2\text{H}_5)_4$, is presently used as a binder in inorganic zinc-rich primers which act to inhibit the corrosion of metals [4]. The major characteristics of these cured inorganic zinc primer films are their excellent adhesion to metallic substrates, thermal stability, resistance to ultraviolet light and weathering, and abrasion. As a result, they appear promising for use as reliable underlying structures to which organic topcoats can be applied. From the standpoint of adhesion to metals, it has been emphasized that hydroxy-terminated end groups in the assembled polysilane macromolecules react favorably with hydroxylated metals to form strong covalent bonds [5, 6]. This formation of interfacial bonds is primarily responsible for adhesion durability at metal-polysilane joints.

On the basis of the above information, our attention was focused on the characteristics of polymeric materials synthesized through hydrolysis-condensation reactions of $\text{Ti}(\text{OR})_4$ -incorporated organosilane monomeric mixtures over the temperature range 100 - 500 °C. When film fabrication temperatures ≥ 300 °C are considered, it can be assumed that a large number of carbon-containing groups will be eliminated pyrolytically from the polymer network structures as a result of elevated temperature. Hence, attention was given to the pyrolytic changes in the conformation of Ti compound-modified organosilane polymers. Of course, such conformational changes and their processes, as a function of temperature, may be different depending on the species of organosilane and the proportions of organosilane to $\text{Ti}(\text{OR})_4$ used as original starting materials.

As an approach to obtaining such information, it was decided to examine three topics. First, emphasis was placed on the pyrolytic conformational changes and the mechanisms of Ti compound-modified organosilane polymers formed at various $\text{Ti}(\text{OR})_4$ to organosilane monomer ratios. In this study, the 3-glycidoxypropyltrimethoxysilane (GPS) examined by previous investigators [1, 2] was used. The observed conformational changes were correlated with alterations in the surface morphology, changes in surface chemical composition and chemical states of the Ti compound-modified GPS coating films overlayed on aluminum substrates at temperatures up to 500 °C. The ability of the coatings formed at temperatures ranging from 100 °C to 500 °C to inhibit the pitting corrosion of aluminum was studied secondly. Finally, based upon fundamental knowledge obtained from the above studies, efforts were then focused on the fabrication of good coating films and evaluation of their corrosion protective performance.

Experimental

Materials

The six different monomeric organoalkoxysilanes listed in Table 1 were used in this study. Sources of these silanes which served as network-

TABLE 1
Organosilanes used in the present study

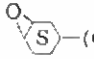
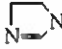
Organosilane	Chemical formula
tetraethoxysilane (TS)	$\text{Si}(\text{OC}_2\text{H}_5)_4$
1,2-bis(trimethoxysilyl)ethane (BTSE)	$(\text{H}_3\text{CO})_3\text{Si}(\text{CH}_2)_2\text{Si}(\text{OCH}_3)_3$
β -(3,4-epoxycyclohexyl)ethyltrimethoxysilane (ECS)	 $-(\text{CH}_2)_2-\text{Si}(\text{OCH}_3)_3$
3-glycidoxypropyltrimethoxysilane (GPS)	$\text{CH}_2-\text{CH}(\text{O})-\text{CH}_2-\text{O}-(\text{CH}_2)_3-\text{Si}(\text{OCH}_3)_3$
3-aminopropyltrimethoxysilane (APS)	$\text{H}_2\text{N}-(\text{CH}_2)_3-\text{Si}(\text{OCH}_3)_3$
<i>N</i> -[3-(triethoxysilyl)propyl]-4,5-dihydroimidazole (TSPI)	 $\text{N}-(\text{CH}_2)_3-\text{Si}(\text{OC}_2\text{H}_5)_3$

TABLE 2
Compositions of clear precursor solutions used for various GPS/Ti(OC₂H₅)₄ ratios

GPS/Ti(OC ₂ H ₅) ₄ (wt. ratio)	GPS (wt.%)	Ti(OC ₂ H ₅) ₄ (wt.%)	CH ₃ OH (wt.%)	Water (wt.%)	HCl (wt.%) / [GPS + Ti(OC ₂ H ₅) ₄]
100/0	50	0	30	20	10
80/20	40	10	30	20	10
60/40	30	20	30	20	20
40/60	20	30	30	20	30
30/70	15	35	30	20	40

forming materials were the Aldrich Chemical Company, Inc. and Petrarch Systems Ltd. The titanium alkoxide was titanium(IV) ethoxide, Ti(OC₂H₅)₄, supplied by Alfa Products.

The film-forming mother liquor which served as the precursor solution was prepared by incorporating the organoalkoxysilane/Ti(OC₂H₅)₄ mixture into a methyl alcohol/water mixing medium containing an appropriate amount of hydrochloric acid. In order to produce a clear precursor solution, it was found to be very important to add the HCl as a hydrolysis accelerator to the blending material, thereby forming a uniform coating film on the metal substrates (see Table 2).

The aluminum substrate used in the experiments was 2024-T3 clad aluminum sheet containing the following chemical constituents: 92 wt.% Al, 0.5 wt.% Si, 0.5 wt.% Fe, 4.5 wt.% Cu, 0.5 wt.% Mn, 1.5 wt.% Mg, 0.1 wt.% Cr, 0.25 wt.% Zn and 0.15 wt.% other elements.

Oxide etching of the aluminum was carried out in accordance with a well-known commercial sequence called the Forest Products Laboratory

(FPL) process [7]. As the first step in this preparation, the surfaces were wiped with acetone-soaked tissues to remove any organic contamination. They were then immersed in chromic-sulfuric acid ($\text{Na}_2\text{Cr}_2\text{O}_7 \cdot 2\text{H}_2\text{O}:\text{H}_2\text{SO}_4:\text{water} = 4:23:73$ by weight) for 10 min at 80 °C. After etching, the fresh oxide surfaces were washed with deionized water at 30 °C for 5 min, and subsequently dried for 15 min at 50 °C.

Coating of the aluminum surfaces using the sol system was performed in accordance with the following sequence. The FPL-etched aluminum substrate was dipped into the precursor solution at ambient temperature. The substrate was then withdrawn slowly from the soaking bath, after which the substrate was heated in an oven for 20 h at a temperature of 100 °C to yield a solid coating. The samples were subsequently heated for 20 min at temperatures ranging from 200 °C to 500 °C.

Measurements

The combined techniques of infrared (IR), X-ray powder diffraction (XRD) and X-ray photoelectron spectroscopy (XPS) were used to obtain fundamental data regarding the changes in conformation, chemical components and states induced by pyrolysis, as well as the degree of network crosslinking for the Ti compound-modified organosilane polymers at temperatures up to 500 °C. Alterations to the surface microstructure of the films after deposition on the aluminum substrate were observed using scanning electron microscopy (SEM).

Electrochemical testing for data on corrosion was performed using an EG & G Princeton Applied Research Model 362-1 corrosion measurement system [8]. The electrolyte was a 0.5 M sodium chloride solution made from distilled water and reagent grade salt. The specimen was mounted in a holder and then inserted into an EG & G Model K47 electrochemical cell. Tests were conducted in an aerated 0.5 M NaCl solution at 25 °C with the exposed surface area of the specimens being 1.0 cm². The polarization curves containing the cathodic and anodic regions were measured at a scan rate of 0.5 mV s⁻¹ over a corrosion potential range of -1.2 V to -0.3 V.

Results and Discussion

Ti(OC₂H₅)₄-modified GPS system

The mix compositions for the GPS/ $\text{Ti}(\text{OC}_2\text{H}_5)_4$ -based precursor solution systems used in the conformational change and mechanistic experiments (study 1) are given in Table 2. For each formulation, the GPS to $\text{Ti}(\text{OC}_2\text{H}_5)_4$ ratio was varied so that the concentration of HCl needed to produce a clear precursor solution was mainly dependent upon the GPS/ $\text{Ti}(\text{OC}_2\text{H}_5)_4$ ratio. As the proportion of $\text{Ti}(\text{OC}_2\text{H}_5)_4$ increased, the required amount of HCl was increased to form Ti compounds which were susceptible to hydrolysis. The HCl-catalyzed hydrolysis of $\text{Ti}(\text{OC}_2\text{H}_5)_4$ may be depicted as follows:

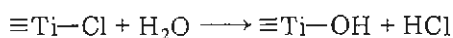
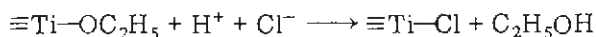


Figure 1 depicts the IR absorption spectra for powder samples containing GPS to $\text{Ti}(\text{OC}_2\text{H}_5)_4$ ratios varying between 100/0 and 30/70 by weight heated at 200 °C. The IR analyses were conducted using the KBr method which incorporates the powder samples into KBr pellets. In the spectrum for the $\text{Ti}(\text{OC}_2\text{H}_5)_4$ -free bulk GPS polymer samples [see Fig. 1(a)], it appears that the broad peak at *ca.* 3450 cm^{-1} and the weak peak at 1615 cm^{-1} are due to the O—H stretching vibration of hydroxy groups and the H—O—H bending vibration of H_2O molecules, respectively. The strong peaks at 2950 and 2880 cm^{-1} are ascribed to the C—H stretching mode in the methyl groups in conjunction with the C—H bending mode at 1460 and 1390 cm^{-1} . The stretching of the Si—CH₂— bond in the Si-joined propyl groups is confirmed by the pronounced peak at 1115 cm^{-1} [9, 10]. It is well known that the peak at 1040 cm^{-1} identifies the Si—O—Si bond in the polymeric organosilane formed by condensation reactions between neighboring silanol functions in the hydrolyzed GPS. Thus, the peak in the vicinity of 800 cm^{-1} corresponds to the bending mode of the O—Si—O bond [11]. The bands at 3030, 1265, 917 and 837 cm^{-1} which were assigned to the terminal epoxide rings, $\text{CH}_2-\text{CH}-$, in the monomeric GPS, no longer

exist since the GPS monomer was heated to 200 °C. Also, the peak at 700 cm^{-1} reveals the C—Cl stretching frequency [12]. This is likely to be asso-

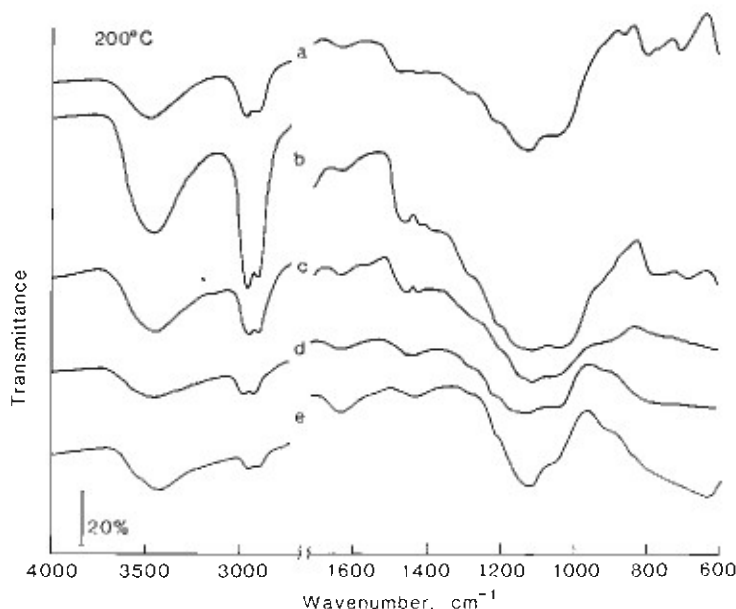


Fig. 1. IR absorption spectra for powder samples heated at 200 °C and having the following GPS/ $\text{Ti}(\text{OC}_2\text{H}_5)_4$ ratios: (a) 100/0; (b) 80/20; (c) 60/40; (d) 40/60; and (e) 30/70.

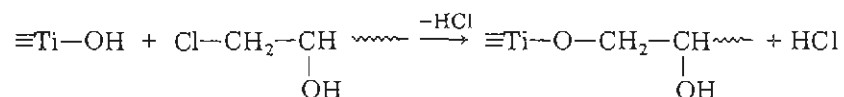
ciated with cleavage of epoxide rings caused by the HCl-catalyzed hydrolysis resulting in the transformation of $\text{CH}_2-\text{CH} \begin{smallmatrix} \diagup \\ \text{O} \end{smallmatrix} \diagdown$ groups into $\text{CH}_2-\text{CH} \begin{smallmatrix} | \\ \text{Cl} \end{smallmatrix} \begin{smallmatrix} | \\ \text{OH} \end{smallmatrix}$

groups [13].

When compared with the spectral features of the sample containing a GPS/ $\text{Ti}(\text{OC}_2\text{H}_5)_4$ ratio of 100/0, the spectrum [see Fig. 1(b)] for that with the 80/20 ratio is characterized by a broad doublet peak in the absorption range 1150–1000 cm^{-1} . The major assignments of this doublet relate directly to the Si–CH₂ and Si–O–Si bonds.

With the exception of those in the wavenumber region 800–600 cm^{-1} , spectral features similar to those for the 80/20 ratio material were observed with the samples containing 60/40 and 40/60 ratios. Changes occurred in the peak intensity at 700 cm^{-1} which corresponds to the C–Cl bond in the $\text{Cl}-\text{CH}_2-\text{CH} \begin{smallmatrix} | \\ \text{OH} \end{smallmatrix}$ groups. Thus, the intensity of this peak di-

minished as a higher proportion of $\text{Ti}(\text{OC}_2\text{H}_5)_4$ was added to the GPS. As is evident from the appearance of a peak at *ca.* 625 cm^{-1} for the 30/70 ratio sample [Fig. 1(c)], the addition of an excessive amount of $\text{Ti}(\text{OC}_2\text{H}_5)_4$ seems to result in the production of a crystalline titania (TiO_2) in the polymeric organosilane layers. It is very surprising that a prominent peak near 930 cm^{-1} , which would be attributable to the Si–O–Ti bond arising from the formation of the polytitanosiloxane (PTS), is not apparent in any of the spectra for the $\text{Ti}(\text{OC}_2\text{H}_5)_4$ -modified organosilane polymer samples heated at 200 °C. This suggests strongly that, at this temperature, a substantial amount of the PTS polymer was not present in these material systems. Thence, the hydroxylated titania derived from the hydrolysis of $\text{Ti}(\text{OC}_2\text{H}_5)_4$ appears to react preferentially with the C–Cl groups rather than with the silanol groups, Si–OH, formed by hydrolysis of the methoxysilane groups in GPS. A possible reaction occurring between the C–Cl groups in the polymeric organosilanes and the hydroxy groups in the hydrated Ti compounds may be written as:



This suggests that the shoulder absorption bands detected at *ca.* 1290 cm^{-1} in the Ti compound-modified GPS polymer systems may be attributed to the Ti–O–C linkages in the $\equiv\text{Ti}-\text{O}-\text{CH}_2-\text{CH} \begin{smallmatrix} | \\ \text{OH} \end{smallmatrix}$ compounds.

Figure 2 illustrates the IR spectra for the series of samples heat-treated at 300 °C. At a 100/0 ratio [Fig. 2(a)] the major differences observed in the spectrum to that previously described for the sample heat-treated at 200 °C are as follows: (1) a slight shift of the absorption corresponding to

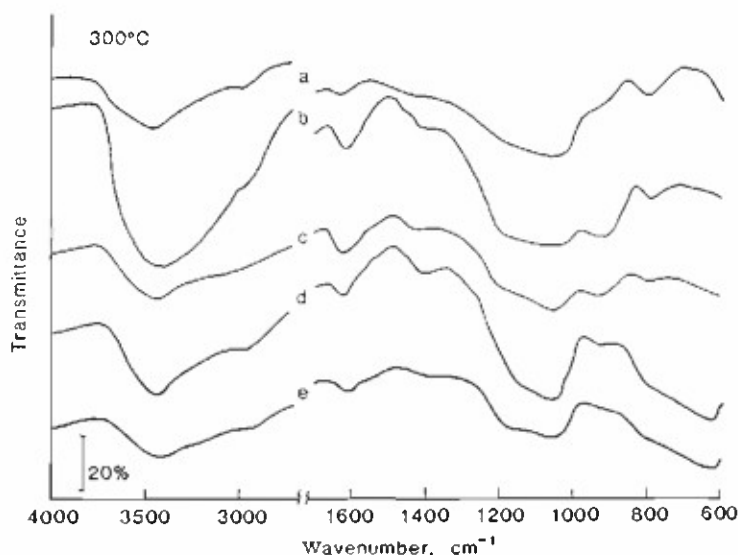
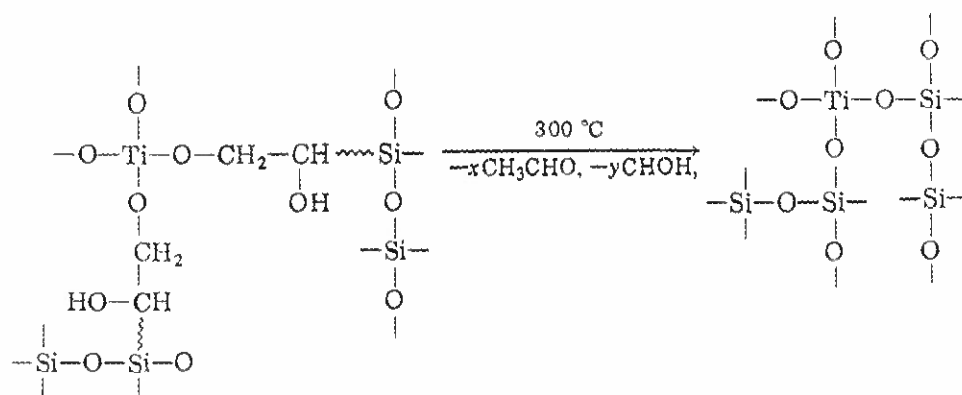


Fig. 2. IR absorption spectra for powder samples heated at 300 °C and having the following GPS/Ti(OC₂H₅)₄ ratios: (a) 100/0; (b) 80/20; (c) 60/40; (d) 40/60; and (e) 30/70.

the Si—O—Si bonds at 1040 cm⁻¹ toward a higher wavenumber (1055 cm⁻¹); (2) disappearance of the peaks at 1115 cm⁻¹ and 700 cm⁻¹ which correspond to the Si—CH₂ and C—Cl bands, respectively; and (3) a considerably diminished intensity for the peaks at 2950, 2880, 1460 and 1390 cm⁻¹. This implies that heating to 300 °C leads to the elimination of a large number of carbonaceous groups such as CH₂O and CH₃CHO from the polymeric organosilane networks. The conversion of the polymeric organosilane into the inorganic polysiloxane network structure occurs around this temperature. It is also evident from the weak peak at 1615 cm⁻¹ that the samples treated at 300 °C still contained traces of water. This may have been due to the presence of water adsorbed from the atmosphere at ambient temperature during the preparation of the IR samples.

Attention was then focused on the spectra for samples containing 80/20 and 60/40 ratios, since the appearance of the Si—O—Ti linkage in the vicinity of 930 cm⁻¹ indicates the formation of PTS networks. In conjunction with the Si—O—Si band at ca. 1050 cm⁻¹, it is possible that PTS can be produced at 300 °C through the network transition processes shown below.

At high temperature, pyrolytic changes in conformation appear to occur while numerous organic groups are eliminated from the Ti-incorporated organopolysilane network structures. Once the transition is completed the Ti elements located in the networks act as a crosslinking agent which connect directly between the polysiloxane chains. The extent of Ti crosslinking depends mainly on the GPS/Ti(OC₂H₅)₄ ratio. This is evident from the absorption intensity at ca. 930 cm⁻¹ which becomes weaker as the



proportion of $\text{Ti}(\text{OC}_2\text{H}_5)_4$ is increased. As seen from the spectrum for the 40/60 ratio sample [Fig. 2(d)], a very weak band is present at 930 cm^{-1} . The strong peak near 625 cm^{-1} reveals the formation of a large amount of TiO_2 . From the above information, it can be concluded that to assemble highly crosslinked PTS networks at 300°C , it is essential that the proper ratio of GPS to $\text{Ti}(\text{OC}_2\text{H}_5)_4$ be employed.

When the heat-treatment temperature was increased to 400°C , the peak in the 2900 cm^{-1} region of the IR spectra disappeared for all the samples. This is shown in Fig. 3 and suggests that the residual organic compounds

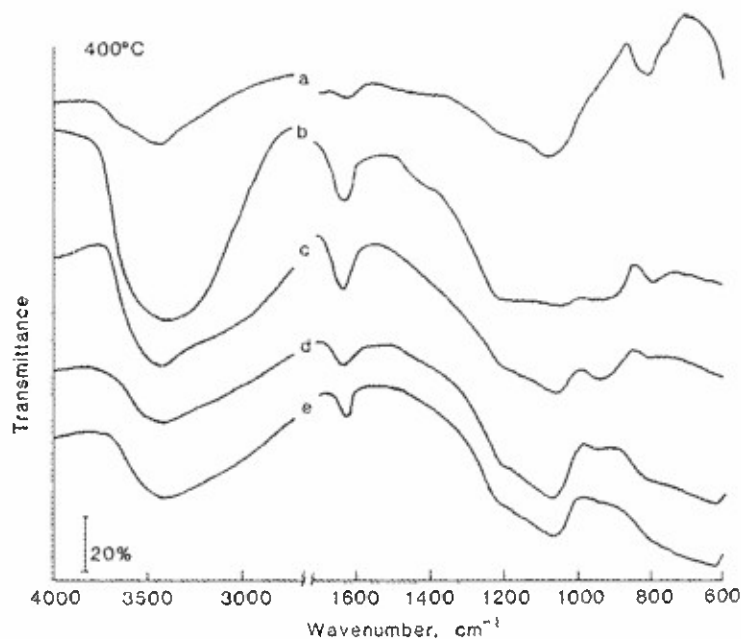


Fig. 3. IR absorption spectra for powder samples heated at 400°C and having the following GPS/ $\text{Ti}(\text{OC}_2\text{H}_5)_4$ ratios: (a) 100/0; (b) 80/20; (c) 60/40; (d) 40/60; and (e) 30/70.

were virtually removed completely from the PTS networks. With that exception, the spectral features for the samples heat-treated at 400 °C were similar to those for the samples heat-treated at 300 °C. On comparing the results for samples heated at 500 °C (see Fig. 4) with those for samples heated at 400 °C, no specific changes and shifts in the absorption bands can be seen for any of the samples.

In order to obtain information supplementary to the above findings, X-ray powder diffraction (XRD) analyses were performed on the 100/0, 60/40 and 40/60 ratio samples heat-treated at 200 °C and 500 °C, respectively. The resulting XRD patterns extending over the diffraction range 0.163 - 0.404 nm are depicted in Fig. 5. No spacing lines were detected over this

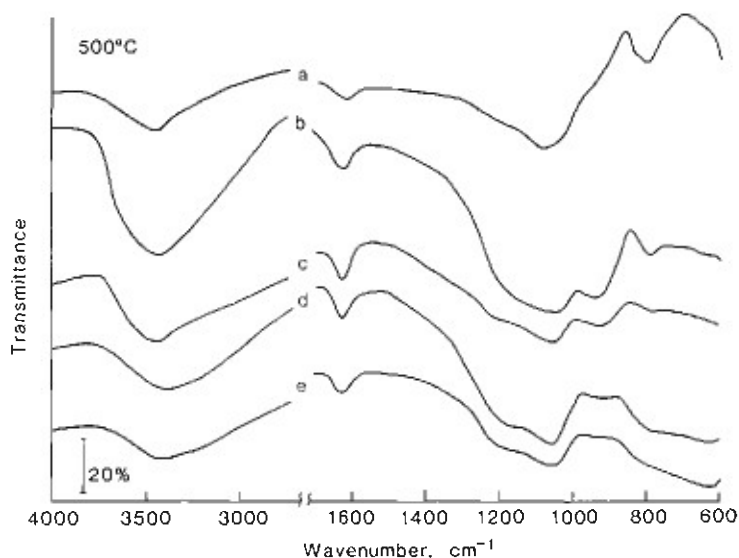


Fig. 4. IR absorption spectra for powder samples heated at 500 °C and having the following GPS/Ti(OC₂H₅)₄ ratios: (a) 100/0; (b) 80/20; (c) 60/40; (d) 40/60; and (e) 30/70.

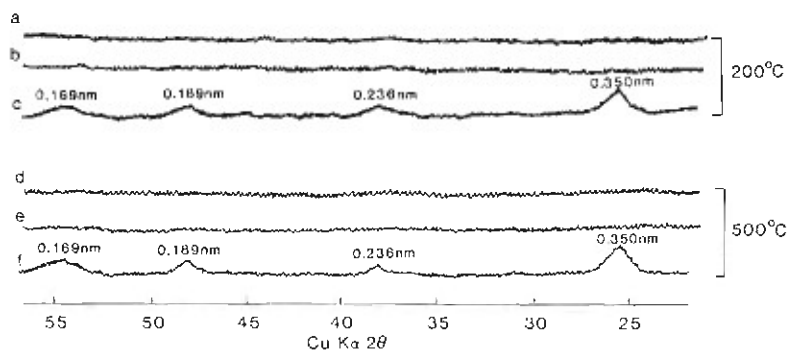


Fig. 5. XRD traces for (a) 100/0, (b) 60/40, (c) 40/60 GPS/Ti(OC₂H₅)₄ ratio samples heated at 200 °C, and for (d) 100/0, (e) 60/40 and (f) 40/60 GPS/Ti(OC₂H₅)₄ ratio samples heated at 500 °C.

diffraction range for the 100/0 and 60/40 ratio samples heated at 200 °C and 500 °C, indicating that these polymeric organosilanes are substantially amorphous. In contrast, the reflections observed at 0.169, 0.189, 0.236 and 0.350 nm for the 40/60 ratio sample heated at 200 °C indicate the presence of anatase (TiO_2) crystallites in the organopolysilane layers. Based upon the growth of the anatase line intensities upon heating to 500 °C, the amount of anatase crystals formed in the amorphous network structure seems to increase with temperature. Hence, it appears that high proportions of $\text{Ti}(\text{OC}_2\text{H}_5)_4$, as in the 40/60 and 30/70 ratio samples, result in the formation of crystalline anatase particles in the amorphous polymeric layers at temperatures as low as 200 °C.

On the basis of the above findings, our interest then focused on the influence of pyrolysis-induced changes in the conformational and chemical states of Ti compound-incorporated organosilane polymers on the ability to fabricate coating films as a function of temperature. Films were prepared by first dipping the FPL-etched aluminum substrate into the film-forming precursor solution and then heating it in an oven at 100 °C for 20 h. The thickness of the films adhering to the substrate was determined using a surface profile measuring system; thus for coatings preheated to 100 °C it was found that such thicknesses were in the 7–12 μm range. The morphological and topographical alterations in the coating surface as a function of both the GPS/ $\text{Ti}(\text{OC}_2\text{H}_5)_4$ ratio and the heating temperature were investigated using SEM methods.

Figure 6 depicts the SEM images for coatings treated at 200 °C. The surface microtexture views of the 100/0 [Fig. 6(a)] and 60/40 [Fig. 6(b)] ratio coatings reveal a continuous film over the entire surface including small and large pits. In comparison to these smooth surface morphologies, a rough surface texture containing a microcrack was observed for the 40/60 ratio coating [Fig. 6(c)]. Increasing the $\text{Ti}(\text{OC}_2\text{H}_5)_4$ concentration to produce a 30/70 ratio sample resulted both in an increased number and size of the cracks [see Fig. 6(d)]. Partial separation of the film from the substrate was also apparent. The cause for the crack development encountered during drying of the sol-derived coatings is primarily the generation of stresses within the film layers brought about by differences in thermal expansion and/or differential shrinkage between the film and substrate. Such stresses generated at the film–substrate interface result in the disbondment of the film from the substrate [14–16]. As a result, it can be rationalized that the introduction of *in situ* sintered crystalline anatase particles into the amorphous polymer layers leads to the formation of poor coating films of a fragile nature. When the film-treatment temperature was raised to 300 °C, samples containing a GPS/ $\text{Ti}(\text{OC}_2\text{H}_5)_4$ ratio of 100/0 experienced severe damage. This is shown in Fig. 7(e). The failure appears to be due to pyrolytic changes in conformation of polymeric organosilane resulting from the elimination of organic species from the network structure. These conformational changes eventually result in excessive shrinkage of the film. Although the elimination of carbonaceous compounds occurs

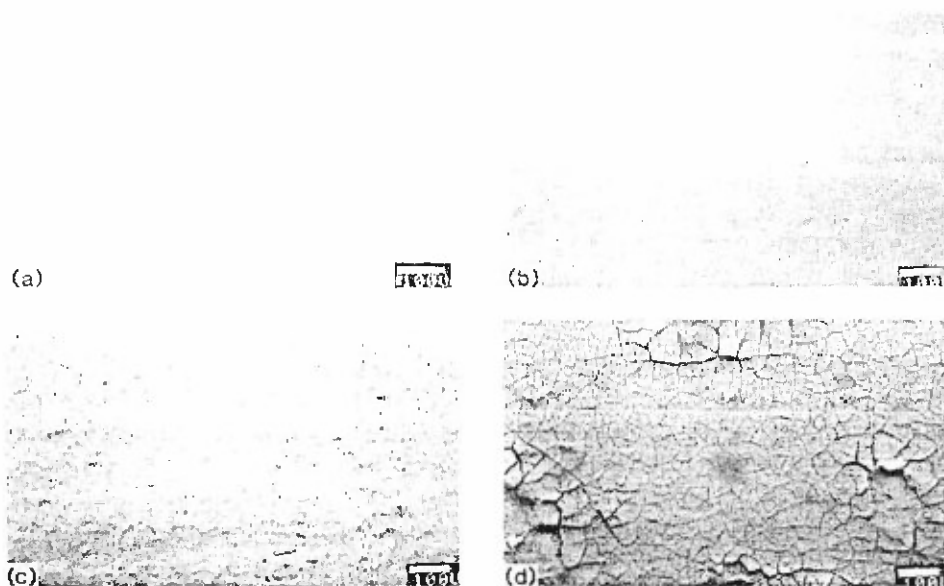


Fig. 6. Scanning electron micrographs for coating films derived from GPS/Ti(OC₂H₅)₄ systems heat-treated at 200 °C. The micrographs correspond to the following GPS/Ti(OC₂H₅)₄ ratios: (a) 100/0; (b) 60/40; (c) 40/60; and (d) 30/70.

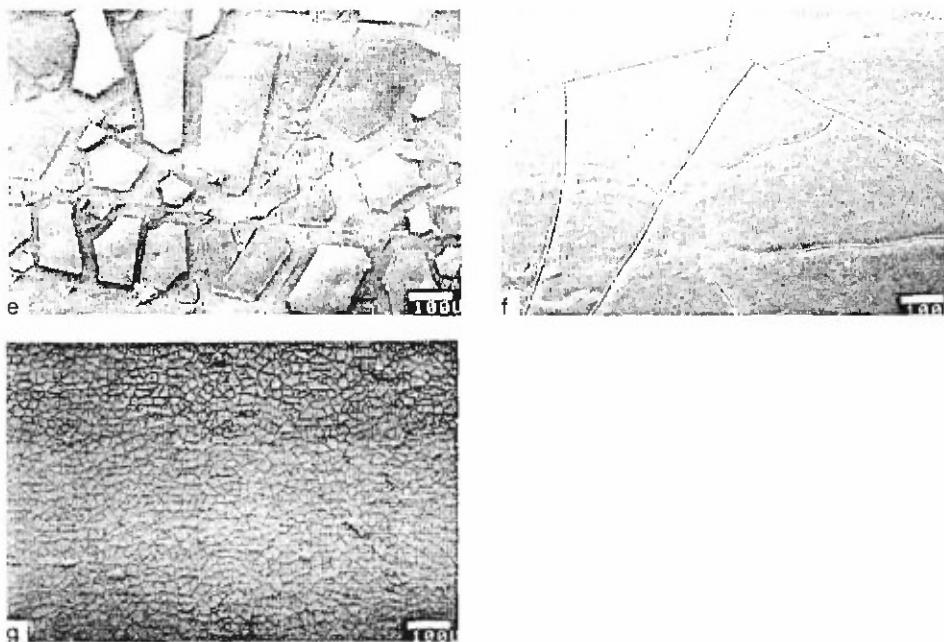


Fig. 7. Comparison of film surface morphologies for GPS/Ti(OC₂H₅)₄ coatings heat-treated at 300 °C. The micrographs correspond to the following GPS/Ti(OC₂H₅)₄ ratios: (e) 100/0; (f) 60/40; and (g) 40/60.

progressively at this critical temperature, the SEM microstructure view of the 60/40 ratio film [Fig. 7(f)] discloses a much lower magnitude in shrinkage and/or stress cracks. This strongly suggests that the crosslinking ability of the Ti compounds, which connect directly between the polysilane chains, acts significantly to suppress the development of stress cracks. Thus, it is inferred that the network structure of PTS polymers formed by pyrolytically induced conformational changes in Ti compound-modified organosilane polymers contributes to the maintenance of film shape at high temperatures. In contrast, the 40/60 ratio film [Fig. 7(g)] developed numerous cracks probably because of the increased amount of sintered anatase crystallites in the amorphous polymer layers.

SEM images coupled to energy-dispersive X-ray (EDX) data for a 60/40 ratio coating heat-treated at 500 °C are given in Fig. 8. The general method for preparing specimens for the SEM study was to deposit a gold film onto the sample surface. Hence the gold indicated by EDX arose from that source. As expected, an increase in flaw width with respect to the direction of crack propagation is visible in the microstructures. Upon enlargement of a portion of the crack areas, EDX examination of site No. 1, which was at a distance of ca. 15 μm from the edge of a crack, revealed

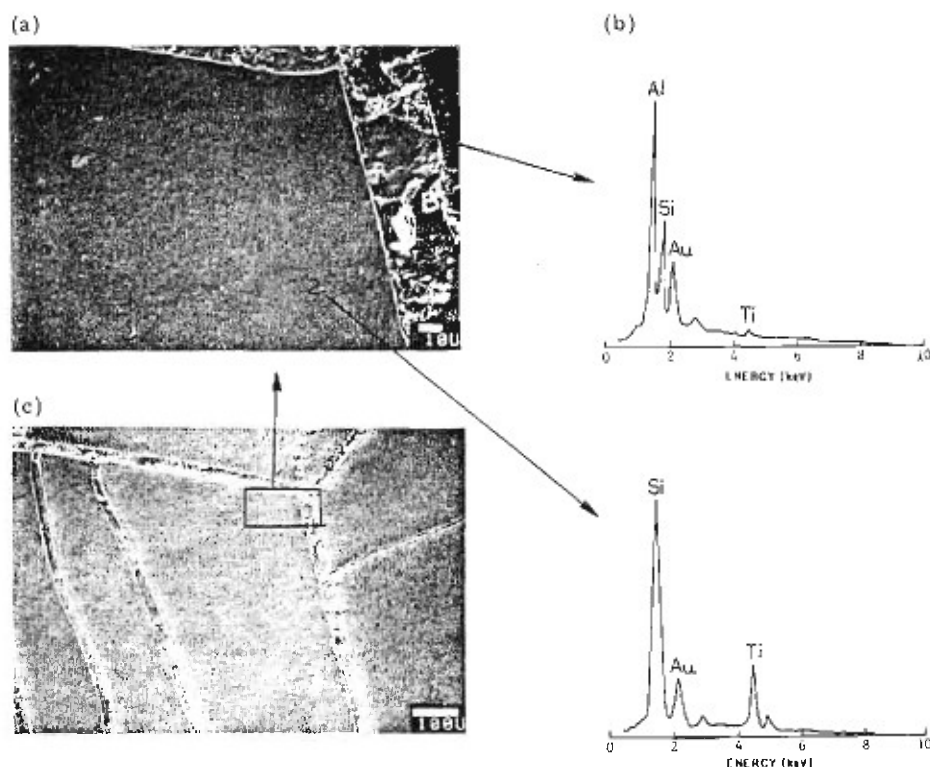


Fig. 8. SEM images and EDX analyses of 60/40 GPS/Ti(OC₂H₅)₄ ratio coating films heat-treated at 500 °C.

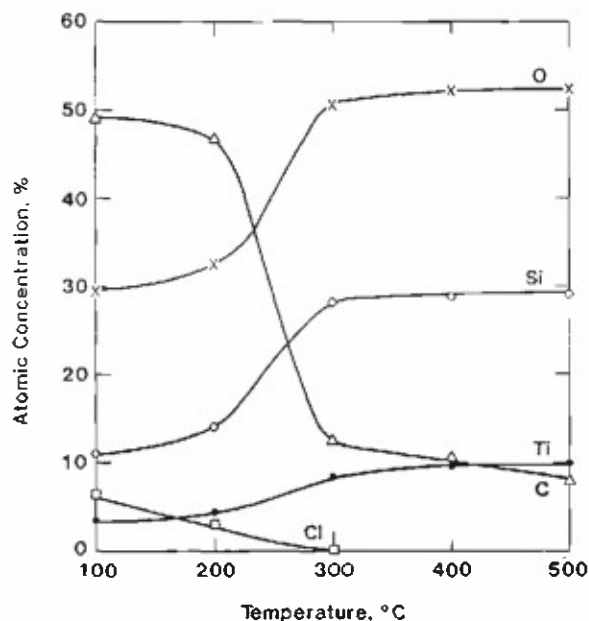


Fig. 9. Changes in XPS elemental composition at the outermost surface sites of a 60/40 coating film as a function of film-treatment temperature.

excitation of weak peaks corresponding to the elements Si and Ti in conjunction with the principal peak of Al associated directly with the substrate. A possible reason for the presence of small quantities of Si and Ti in the crack region could be that the surfaces in the crack zone contained a thin film of PTS polymer adhering to the substrate. This would indicate a strong adhesive force at the interface between PTS and aluminum.

Figure 9 illustrates the changes in elemental composition at the surface sites of 60/40 ratio coating films arising as a function of temperature. These quantitative data were obtained by comparison of the XPS peak areas which were then converted into the elemental concentrations by using the differential cross-sections for core level excitation. For the coating surfaces preheated at 100 °C, the principal element at the outermost surface sites was carbon originating from carbonaceous groups in the Ti compound-incorporated organosilane polymer. The secondary predominant element was oxygen. The percentages of detected silicon, titanium and chlorine atoms were 11.4%, 3.2% and 6.6%, respectively. After heating to temperatures between 200 °C and 300 °C, the XPS signal intensity for carbon decreased rapidly, thereby revealing a considerable loss in the concentration of this element. Above 300 °C this concentration appears to diminish further only slowly. At this point, it should be noted that at ≥ 300 °C the detected carbon arises not only from the residual carbonaceous groups on the PTS surface but also from carbon contaminants adsorbed from the atmosphere. A similar trend for the variation in concentration of the Cl

atom was also observed. This relates to $\text{Cl}-\text{CH}_2-\underset{\text{OH}}{\text{CH}}$ which is completely

eliminated at 300 °C from the sample surfaces. In contrast, marked increases in atomic concentrations were noted for O, Si and Ti between 200 °C and 300 °C. Further increases in temperature had little, if any, effect on these atomic concentrations. The above XPS results are in agreement with the IR data discussed earlier in this paper, *viz.* conformational changes to the inorganic PTS polymer from Ti compound-modified organosilane polymers occur over the temperature range 200 - 300 °C.

The Ti oxide-organosilane polymer \rightarrow PTS transitions can also be identified from the spectra in the Si_{2p} and Ti_{2p} core level regions which are of particular interest. The binding energy (BE) scale for these spectra were calibrated with the C_{1s} peak of the carbonaceous and contaminated hydrocarbon peak fixed at 285.0 eV as an internal reference standard. Figures 10 and 11 represent the Si_{2p} photoemission and Ti_{2p} doublet separation

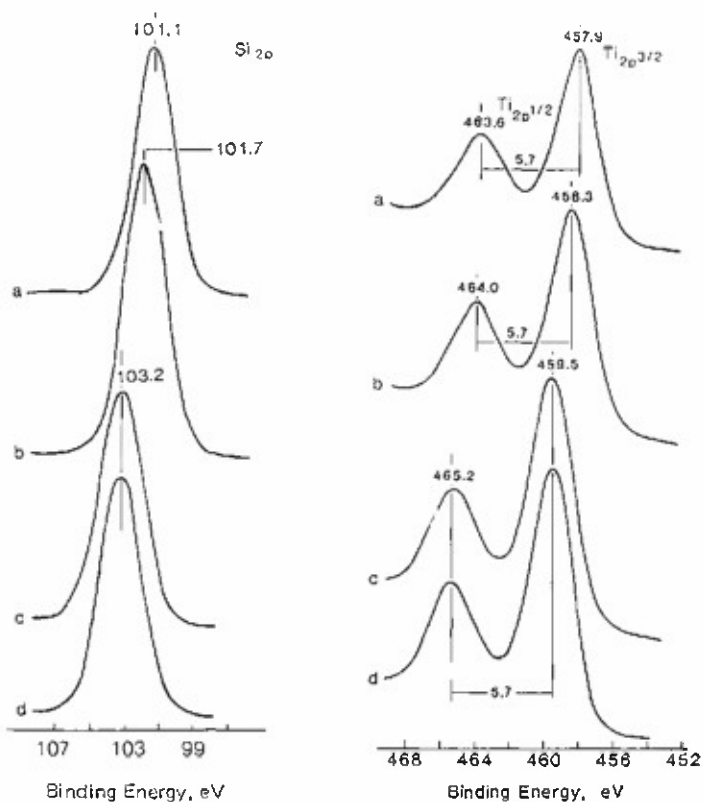


Fig. 10. Si_{2p} spectra for GPS/ $\text{Ti}(\text{OC}_2\text{H}_5)_4$ 60/40 ratio coating surfaces thermally treated at (a) 100 °C, (b) 200 °C, (c) 300 °C and (d) 400 °C, respectively.

Fig. 11. Ti_{2p} separation spectra for GPS/ $\text{Ti}(\text{OC}_2\text{H}_5)_4$ 60/40 ratio coating surfaces thermally treated at (a) 100 °C, (b) 200 °C, (c) 300 °C and (d) 400 °C, respectively.

spectra for thermally treated 60/40 ratio coating surfaces. In the Si_{2p} region, the peak at 101.1 eV for the coating surfaces pretreated at 100 °C [Fig. 10(a)] may be assigned to the Si originating from the polymeric organosilane. The spectrum [Fig. 10(b)] for the sample heat-treated at 200 °C exhibits a shift in the peak to a higher BE site. A further shift in the peak to a BE of 103.2 eV occurred when the coating was treated at 300 °C [Fig. 10(c)]. No further shift occurred for the coating surface heat-treated at 400 °C [see Fig. 10(d)].

Trends similar to those for the Si_{2p} signal were observed in the separation spectra for the $\text{Ti}_{2p_{3/2}}$ and $\text{Ti}_{2p_{1/2}}$ lines. These are shown in Fig. 11. Specifically, the Ti_{2p} peak remained at a separation distance of 5.7 eV between the $2p_{3/2}$ and the $2p_{1/2}$ energy shifts to higher BE sites as the treatment was increased from 100 °C to 300 °C. Likewise, a further increase in temperature to 400 °C induced no further shift in the 2p doublet line arising from the sample heat-treated at 300 °C [Fig. 11(d)]. Based upon these observations, the shifts in the Si_{2p} and Ti_{2p} peaks to higher BE levels at ≤ 300 °C seem to be associated with the silicon and titanium originating from the PTS polymers.

All of the above data were correlated with the effectiveness of the pyrolytically transferable coating materials in providing corrosion protection to FPL-etched aluminum. The corrosion data were obtained from the polarization curves for coated aluminum samples upon exposure in an aerated 0.5 M NaCl solution at 25 °C. The typical cathodic-anodic polarization curves of $\log(\text{current density})$ versus potential for all of the coated sample studied in this work were similar to those reported for other materials by several investigators [17 - 19] and were characterized by a rapid increase in the current density at a particular voltage in the anodic region. This voltage is commonly described as the critical pit initiation potential. The curves also exhibited a short Tafel region for cathodic polarization, but no Tafel region was found at the anodic sites.

Literature data [19] indicate that the electrochemical procedure used to evaluate the corrosion protective performance of coatings involves measuring the corrosion current I_{corr} by extrapolation of the cathodic Tafel slope. This has been undertaken for all the specimens studied in this work, and the variation in the I_{corr} value has been plotted as a function of the treatment temperature. The results obtained are depicted in Fig. 12. As shown in the figure, the protective ability of the coatings depends primarily on the GPS/ $\text{Ti}(\text{OC}_2\text{H}_5)_4$ ratio and the treatment temperature. For the coating series preheated at 100 °C, the highest I_{corr} value measured was 2.6 μA for the 30/70 ratio coating. Since a low I_{corr} value is predictive of good corrosion protection, the 30/70 ratio coating should yield poor protection. SEM micrographs for this coating surface revealed numerous stress cracks probably caused by the conversion of *in situ* sintered crystalline titania in the amorphous coating layers. As expected, the I_{corr} value for the 30/70 coatings treated at higher temperatures remained essentially constant. In contrast, the 100/0, 80/20 and 60/40 ratio coatings pretreated at 100 °C exhibited

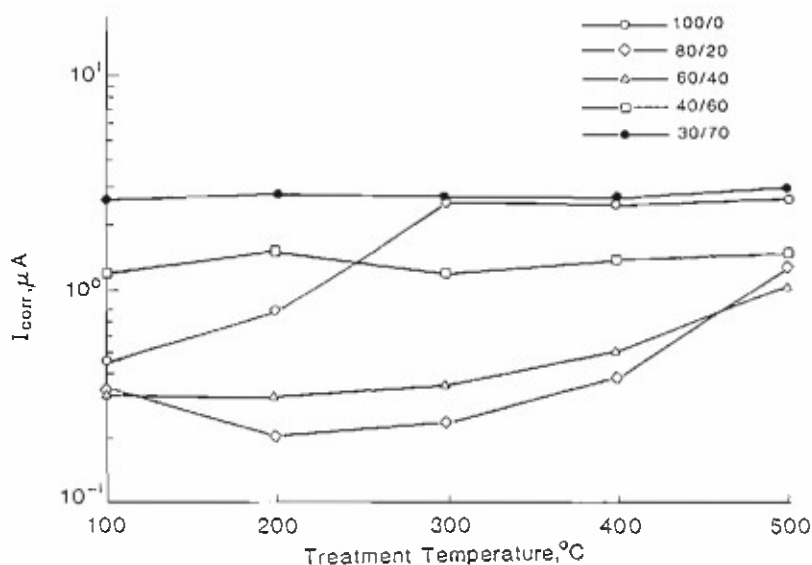


Fig. 12. Variation in the corrosion current i_{corr} for aluminum substrates coated with various GPS/Ti(OC₂H₅)₄ ratio systems as a function of the film-treatment temperature.

i_{corr} values approximately one order of magnitude lower than that for the 30/70 coating. Thus, good corrosion protection is predicted. However, when the 100/0 ratio coatings pretreated at 100 °C were heated at higher temperatures for 20 min, the i_{corr} values increased with temperature up to 300 °C and then leveled off at a value approximately equal to that for the 30/70 ratio sample. It is reasonable to interpret that this is due mainly to damage caused by pyrolytic changes in the conformation of polymeric organosilanes. Hence the coatings no longer protect the aluminum substrates from corrosion. The i_{corr} -temperature relations for the 80/20 and 60/40 ratio coatings indicate that although microcracks form on the film surfaces at ≥ 300 °C, the i_{corr} values after treatment at 400 °C are almost equal to those for the coatings pretreated at 100 °C. This suggests that PTS coating films formed from *in situ* conformational changes at 400 °C provide corrosion protection for aluminum. In the case of PTS coatings heat-treated at 500 °C, the protective ability for both the 80/20 and 60/40 ratio samples appears poor.

Ti(OC₂H₅)₄-modified organosilanes

On the basis of the above information obtained from the Ti(OC₂H₅)₄-GPS system, work was initiated to define the role of the monomeric organosilane structure in promoting and retarding the densification and/or network connectivity of the Si—O—Ti bonds formed in PTS as a function of temperature. These findings were then related to the corrosion protective performance in order to develop an advanced PTS coating system.

With the exception of GPS, all of organosilanes listed in Table 1 were used in these studies. A film-forming precursor solution composed of 30 wt.% of the particular organosilane, 20 wt.% $\text{Ti}(\text{OC}_2\text{H}_5)_4$, 30 wt.% CH_3OH and 20 wt.% water was employed to produce the PTS polymers. The required concentrations of the HCl hydrolysis promoter needed to prepare clear precursor solutions were dependent upon the species of organosilane, and for the TS, BTSE, ECS, APS and TSPI systems were 40%, 50%, 40%, 50% and 30% by weight of total mass of organosilane and $\text{Ti}(\text{OC}_2\text{H}_5)_4$, respectively.

Since the presence of Si-O-Ti linkages in the PTS can be readily identified from the IR absorption peak at $\text{ca. } 930 \text{ cm}^{-1}$, the extent of the densification of this linkage was estimated by comparing the absorbances at $\text{ca. } 930 \text{ cm}^{-1}$ for the PTS samples derived from the various organosilane- $\text{Ti}(\text{OC}_2\text{H}_5)_4$ systems. As previously discussed, samples for IR analyses were prepared by incorporating the powdered samples into KBr pellets. Figure 13 summarizes the resulting variations in absorbance plotted as a function of treatment temperature. It is evident from the data that the extent of densi-

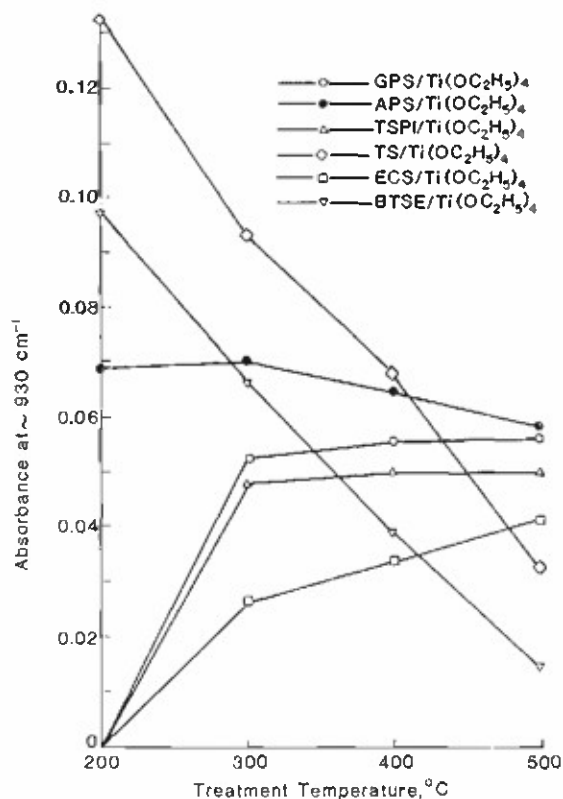
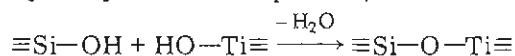


Fig. 13. Changes in the IR absorbance corresponding to the Si-O-Ti bond at $\text{ca. } 930 \text{ cm}^{-1}$ for Ti compound-incorporated organosilanes preheated at temperatures within the range 200 - 500 °C.

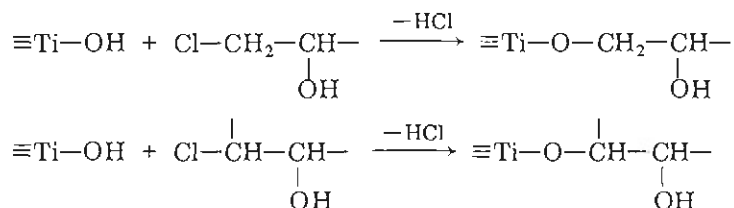
fication of Si—O—Ti bonds is dependent upon the reactive organic functional groups attached to the terminal carbon of the methylene chains within the monomeric organosilane structures. For instance, TS and BTSE can be classified as organosilanes having only hydrolyzable alkoxy groups (OCH_3 and OC_2H_5) bound to silicon, but they do not have any terminal functionalities. Both materials exhibited high absorbance values at *ca.* 930 cm^{-1} after pretreatment at the relatively low temperature of 200°C . This implies that a PTS containing a highly densified Si—O—Ti bond was formed at this temperature. However, at temperature above 200°C the absorbance values decreased significantly. This suggests that the Si—O—Ti bonds in PTS networks derived from the $\text{Ti}(\text{OC}_2\text{H}_5)_4$ -TS and -BTSE systems decompose at elevated temperatures. The processes for Si—O—Ti bond breakage at high temperature are not clear. For the $\text{Ti}(\text{OC}_2\text{H}_5)_4$ -APS systems, the measured absorbances for samples pretreated at 200°C and 300°C were about 0.069, a value approximately 50% lower than that for the TS system after pretreatment at 200°C . Hence this value was assumed to be representative of a moderate densification of Si—O—Ti bonds. Increasing the pretreatment temperature above 300°C resulted in a decrease in absorbance, but the extent of reduction was considerably less than that for the TS and BTSE systems. This demonstrates the greater stability of the Si—O—Ti bond at high temperatures. From the above results, it can be inferred that condensation reactions occurring at low temperatures between silanol groups in hydrolyzed organosilanes containing an amino, *i.e.* $-\text{NH}_2$, group or no reactive terminal groups, and the OH groups in hydroxylated Ti compounds, lead to the formation of Si—O—Ti bonds:



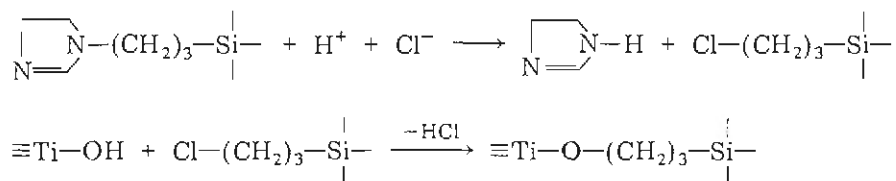
In contrast, an absorption peak at 930 cm^{-1} was not detected for GPS-, ECS- and TSPI- $\text{Ti}(\text{OC}_2\text{H}_5)_4$ systems pretreated at 200°C . These

organofunctional silanes contain acyclic, $\text{CH}_2-\overset{\text{O}}{\text{---}}-\text{CH}-$, and alicyclic, $-\text{CH}-\overset{\text{O}}{\text{---}}-\text{CH}-$, oxirane rings and a dihydroimidazol, $\begin{array}{c} \diagup \\ \text{N} \\ \diagdown \end{array}$ ring, and they

appear to have little, if any, affect on the formation of PTS at 200°C . A possible explanation for this is that the OH groups in the hydroxylated Ti compounds react preferentially with the Cl in the Cl-terminated end groups derived from the cleavage of the oxirane rings brought about by the nucleophilic attack of Cl^- and H^+ , rather than the silanol formed by acid-catalyzed hydrolysis of alkoxy silane in the organofunctional silane structures:



Since the imidazol group acts as a strong base by accepting a proton [20], nucleophilic attack of H^+ on the dihydroimidazol nitrogen results in bond breakage at the $N-CH_2$ linkage [21 - 23]. This breakage leads to the formation of a Cl-substituted end group which then reacts with the hydroxylated Ti compounds:



As reported earlier, a prominent IR peak at *ca.* 930 cm^{-1} was observed for these systems when the samples were heated at 300°C for 20 min. Above this temperature, the absorbance value increased slowly. This suggests that the *in situ* conversion of the Ti compound-incorporated organosilane polymers into PTS occurs progressively at temperatures ranging from 200°C to 300°C .

When the formation and the decomposition of PTS associated with breakage of the $Si-O-Ti$ bonds are considered, the monomeric organosilane materials used as precursors for PTS can be categorized into the following types: (1) alkoxysilanes, such as TS and BTSE which do not contain organic functionaries, produce a highly densified $Si-O-Ti$ linkage in PTS at a temperature of 200°C ; however, breakage of the $Si-O-Ti$ bond occurs above 200°C ; (2) APS containing an amino functionary yields moderate densification of $Si-O-Ti$ linkages at 200°C , and the degree of bond breakage is small over temperatures ranging from 300°C to 500°C ; (3) as far as GPS and TSPI are concerned, organofunctional silanes having acyclic oxirane and imidazole rings act to promote *in situ* conversion into PTS over the temperature range $200 - 300^\circ\text{C}$, but above these temperatures the rate of $Si-O-Ti$ densification increases slowly; and (4) ECS having an alicyclic oxirane ring yields a low rate of conformational change in PTS at 300°C , but the extent of $Si-O-Ti$ linkage increases markedly with increased temperature.

Since the emphasis of this part of our study was to evaluate the coating film formability of PTS and to determine its corrosion protective performance, films overlaid on FPL-etched aluminum surfaces were prepared using a procedure similar to that for the $GPS-Ti(OC_2H_5)_4$ system. The film thicknesses of the TS-, ECS-, APS- and TSPI- $Ti(OC_2H_5)_4$ systems, precured at 100°C for 20 h, were 9.0, 12.5, 11.8 and $11.0\text{ }\mu\text{m}$, respectively.

Figure 14 depicts the SEM images obtained for coating film surfaces preheated at 200°C . The surface microtexture of the TS coating system [Fig. 14(h)], which can be classified as a PTS polymer having a highly densified $Si-O-Ti$ bond, displays numerous cracks which are indicative of the creation of large stresses. Although not shown in the figure, the BTSE

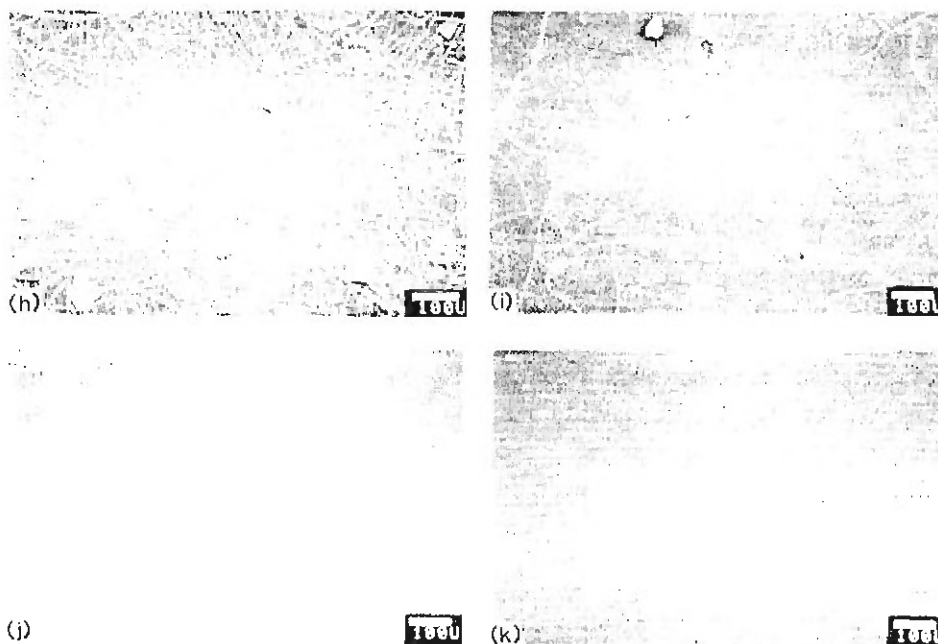


Fig. 14. SEM images for (h) TS, (i) ECS, (j) APS and (k) TSPI system coating films heat-treated at 200 °C.

system produced a similar surface morphology. This suggests that the use of PTS polymers which have excessively densified Si—O—Ti bonds produces poor coating films. Compared with the TS system, the ECS coating system produced much less cracking. This is shown in Fig. 14(i). Except for the development of few microcracks, the APS and TSPI coatings [Fig. 14(j) and (k)] exhibit excellent surfaces.

The SEM micrographs of these coating systems after exposure for 20 min in air at 300 °C are shown in Fig. 15. As expected, the surface of the TS coating [Fig. 15(l)] displays newly developed and propagated cracks. The crack width in the ECS coating pretreated at 200 °C increased upon heating to 300 °C [Fig. 15(m)]. This led to the local separation of the film from the substrate. In contrast, the APS and TSPI coatings [Fig. 15(n) and (o)] showed no film damage other than the appearance of a clear crack line.

Significant cracking occurred when the APS coatings were heated at 500 °C [see Fig. 16(p)]. Heat damage and distortion of the aluminum substrate was apparent, but after heating for 20 min at 500 °C the TSPI coating was not damaged. This is shown in Fig. 16(q). Accordingly, PTS coating films derived from the $\text{Ti}(\text{OC}_2\text{H}_5)_4$ -TSPI system appear to have the best stability at elevated temperature, possibly due to moderate densification of the Si—O—Ti bonds in the PTS network structure.

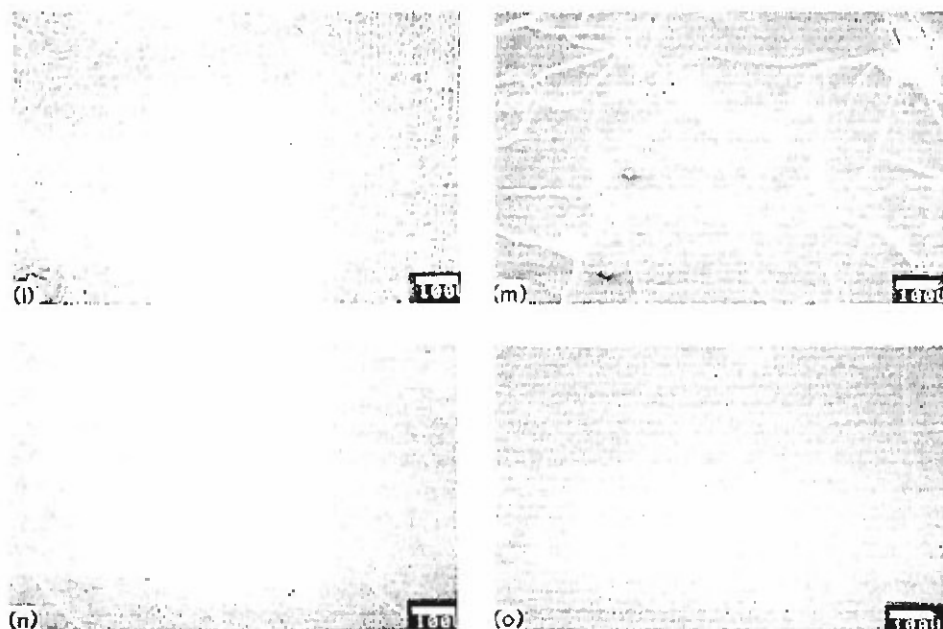


Fig. 15. Surface morphologies for (l) TS, (m) ECS, (n) APS and (o) TSPI system coatings heat-treated at 300 °C.

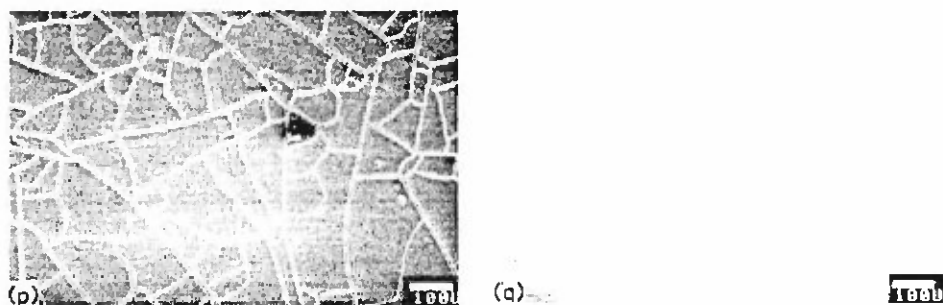


Fig. 16. SEM micrographs for (p) APS and (q) TSPI system coatings heat-treated at 500 °C.

The corrosion protective performance of PTS coatings derived from various organosilane- $\text{Ti}(\text{OC}_2\text{H}_5)_4$ systems has been determined by comparing the corrosion current (I_{corr}) values determined from the cathodic Tafel slopes. Although some coating systems such as TS and APS are pyrolytically converted into PTS networks at 200 °C, the corrosion tests in this study were performed on PTS coatings formed on the FPL-etched aluminum at 300, 400 and 500 °C, respectively. The resultant changes in I_{corr} (μA) for these coating specimens are listed in Table 3. After heat treatment at 300 °C, the lowest I_{corr} value ($2.0 \times 10^{-2} \mu\text{A}$) was measured on the PTS coatings derived from the TSPI system. The APS system produced the next lowest

TABLE 3

Comparison of corrosion current (I_{corr}) values for PTS coatings derived from various organosilane-Ti(OC₂H₅)₄ systems preheated for 20 min at 300, 400 and 500 °C, respectively

Coating system	I_{corr} values (μA) obtained after pretreatment at		
	300 °C	400 °C	500 °C
TS-Ti(OC ₂ H ₅) ₄	2.3	2.5	2.8
ECS-Ti(OC ₂ H ₅) ₄	2.6×10^{-1}	9.1×10^{-1}	1.5
GPS-Ti(OC ₂ H ₅) ₄	3.5×10^{-1}	6.0×10^{-1}	0.5
APS-Ti(OC ₂ H ₅) ₄	8.5×10^{-2}	5.8×10^{-1}	1.2
TSPI-Ti(OC ₂ H ₅) ₄	2.0×10^{-2}	4.6×10^{-1}	9.8×10^{-1}

I_{corr} value. These values were approximately two orders of magnitude less than that for the TS system. The data also indicate that the I_{corr} values for all of the PTS coatings formed after pretreatment above 300 °C increased as the film-treatment temperature was raised, probably as a result of the increased size and number of cracks in the films. For all treatment temperatures, PTS coatings derived from the TSPI system imparted the best corrosion protection, and after preheating at 500 °C the I_{corr} value was still of the order of 10^{-1} μA . Hence, the findings indicate that a most effective PTS protection coating can be derived pyrolytically from the TSPI/Ti(OC₂H₅)₄ precursor system by heating at temperatures ≥ 300 °C.

Conclusions

Polytitanosiloxane (PTS) polymers containing Si—O—Ti linkages have been synthesized through hydrolysis-polycondensation or hydrolysis-polycondensation-pyrolysis reactions involving clear precursor sol solutions consisting of monomeric organosilanes, Ti(OC₂H₅)₄, methanol, water and hydrochloric acid. The purpose of the HCl in the precursor solution was to promote the hydrolysis of organosilane and Ti(OC₂H₅)₄, thereby producing the clear sol solution necessary for the fabrication of uniform and smooth coating films. The ratios of organosilane to Ti(OC₂H₅)₄ in the compositions play a major role in forming the PTS polymer, *viz.* an excessive amount of Ti(OC₂H₅)₄ leads to the formation of *in situ* sintered anatase crystallite in the amorphous organosilane polymer layers rather than forming amorphous PTS. The sol-derived coating films were prepared by dipping FPL-etched aluminum substrates into the film-forming precursor solutions. When the quality of corrosion protection provided to aluminum by the application of PTS coating was considered, this was found to depend upon the PTS film-forming processes or mechanisms, as well as the extent of Si—O—Ti bond densification in PTS networks. All of these factors were dependent on the species of organosilane reacted with the hydroxylated Ti oxide compounds.

functional groups, such as triethoxysilyl)ethane (BTSE), produced PTS networks at relatively low temperatures ($\leq 200^\circ\text{C}$). This network structure was formed by condensation reactions occurring between OH groups in hydroxylated Ti oxide compounds and the silanol groups in hydrolyzed organosilanes.

It was found that when such PTS networks were derived from TS- and BTSE-Ti(OC₂H₅)₄ systems, the extent of Si-O-Ti densification was considerably higher than when they were derived from other systems. However, PTS polymers containing a highly densified Si-O-Ti bond yielded coating films containing numerous stress cracks and thus provided poor corrosion protection. In addition, breakage of the Si-O-Ti bonds occurred progressively when the PTS films were heated at temperatures above 200°C .

At film-treatment temperatures of 200°C no PTS formation was observed in materials produced through hydrolysis-polycondensation reactions involving β -(3,4-epoxycyclohexyl)ethyltrimethoxysilane (ECS)-, 3-glycid-oxypropyltrimethoxysilane (GPS)- or *N*-[3-(triethoxysilyl)propyl]-4,5-dihydroimidazole (TSPI)-Ti(OC₂H₅)₄ precursor systems. This indicates that the OH groups in hydroxylated Ti oxide compounds react preferentially with the Cl-terminated or -substituted end groups formed by HCl-induced hydrolysis of oxirane rings in ECS and GPS (or the dihydroimidazole groups in TSPI) rather than with the silanol groups in hydrolyzed organosilanes. Amorphous Ti compound-incorporated organosilane polymer was identified as a reaction product. The *in situ* transition of this reaction product into PTS networks occurred progressively at treatment temperatures between 200°C and 300°C . In other words, PTS networks were formed by the pyrolytic changes in conformation of the Ti-incorporated organosilane polymers involving the elimination of a large number of carbonaceous species from the original polymer structures at elevated temperature. Thus, the smaller number and short length of the hydrocarbon chains connecting between the Ti and Si atoms in the precursor Ti-organosilane polymer resulted in less shrinkage of the pyrolyzed film. This PTS network was characterized by moderate densification of Si-O-Ti bonds. Further increases in pretreatment temperature to 400°C resulted in slight increases in densification. Although some stress cracks were observed on the surfaces of coating films fabricated at 300°C and 400°C , PTS coatings possessing moderate Si-O-Ti densification provided good corrosion protection for aluminum. Finally, the most effective organosilane for use in the fabrication of PTS coatings leading to good corrosion protection was *N*-[3-(triethoxysilyl)propyl]-4,5-dihydroimidazole.

References

- 1 G. Philipp and H. Schmidt, *J. Non-Cryst. Solids*, 63 (1984) 283.
- 2 H. Schmidt, *J. Non-Cryst. Solids*, 73 (1985) 681.

- 3 H. H. Huang, R. H. Glaser and G. L. Wilkes, in M. Zeldin, K. J. Wynne and H. R. Allcock (eds.), *Inorganic and Organometallic Polymers*, ACS Symp. Ser. No. 360, Am. Chem. Soc., Washington, DC, 1988, p. 354.
- 4 R. F. Brady, Jr., *J. Protect. Coat. Linings*, 4 (1987) 42.
- 5 H. Schroeder, in G. Hass and R. E. Thun (eds.), *Physics of Thin Films*, Vol. 5, Academic Press, New York, 1969, p. 87.
- 6 B. Arkles, *Chemtech.*, 7 (1977) 766.
- 7 H. W. Eichner and W. E. Schowalter, *Forest Products Lab. Rep. 1813*, Madison, WI, 1950.
- 8 T. Sugama, L. E. Kukacka, N. Carciello and J. B. Warren, *J. Coat. Technol.*, 61 (1989) 43.
- 9 A. L. Smith, *Spectrochim. Acta*, 16 (1960) 87.
- 10 D. R. Anderson, in A. L. Smith (ed.), *Analysis of Silicones*, Wiley-Interscience, New York, 1974, Chapter 10.
- 11 N. P. Bansal, *J. Am. Ceram. Soc.*, 71 (1988) 666.
- 12 S. Mizushima, T. Shimanouchi, K. Nakamura, M. Hyashi and S. Tsuchiya, *J. Chem. Phys.*, 26 (1957) 970.
- 13 C. K. Ingold, *Structure and Mechanism in Organic Chemistry*, Cornell University Press, New York, 1953, p. 344.
- 14 G. W. Scherer and T. Garino, *J. Am. Ceram. Soc.*, 68 (1985) 216.
- 15 R. K. Bordia and R. Raj, *J. Am. Ceram. Soc.*, 68 (1985) 287.
- 16 J. C. Huling and G. L. Messing, *J. Am. Ceram. Soc.*, 71 (1988) C-222.
- 17 G. A. Dibari and H. J. Read, *Corrosion*, 27 (1971) 483.
- 18 Z. A. Foroulis and M. J. Thubriker, *Electrochim. Acta*, 21 (1976) 225.
- 19 A. V. Pocius, in K. L. Mittal (ed.), *Adhesion Aspects of Polymeric Coatings*, Plenum Press, New York, 1983, pp. 173 - 192.
- 20 N. V. Sidgwick, *The Organic Chemistry of Nitrogen*, Clarendon Press, Oxford, 1966, p. 782.
- 21 S. Torkelson and C. Ainsworth, *Synthesis*, (1976) 722.
- 22 A. B. Bocarsly, E. G. Walton and M. S. Wrighton, *J. Am. Chem. Soc.*, 102 (1980) 3390.
- 23 R. A. Simon, A. J. Ricco and M. S. Wrighton, *J. Am. Chem. Soc.*, 104 (1982) 2031.

Pyrogenic polygermanosiloxane coatings for aluminum substrates *

T. Sugama and N. Carciello

*Brookhaven National Laboratory, Department of Applied Science, Energy Efficiency and Conservation Division,
Upton, NY 11973, USA*

C. Taylor

University of Virginia, Chemistry Department, Charlottesville, VA 22901, USA

Received 23 August 1990

Revised manuscript received 11 March 1991

The factors governing the film-forming performance of pre-ceramic polygermanosiloxane (PGS) coatings for aluminum (Al) substrate surfaces were investigated. The coatings were prepared through the hydrolysis-dehydrochlorinating and dehydrating condensations-pyrolysis reactions of a sol-precursor solution consisting of N-[3-(triethoxysilyl)propyl]-4,5-dihydroimidazole, $\text{Ge}(\text{OC}_2\text{H}_5)_4$, water, CH_3OH , and HCl . Six factors were important in obtaining a good film: (1) the high spreadability of the sol solution on the Al surfaces; (2) the formation of organopolygermanosiloxane at sintering temperatures of 150°C ; (3) the pyrolytic conversion at 350°C into an amorphous PGS network structure in which the Si–O–Ge linkages were moderately enhanced; (4) the persistence of only minimum amounts of organic by-products; (5) the non-crystalline phases; and (6) the formation of interfacial oxane bond between PGS and aluminum oxide.

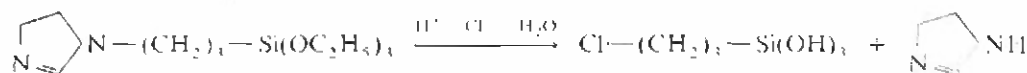
1. Introduction

Ceramic coatings have not yet been widely employed on aluminum and magnesium alloys, and on other low melting-point metal substrates. There are two main reasons for this. First, coatings must adhere well and have an appropriate expansion coefficient, especially during temperature cycling, otherwise the coating will separate from the substrate. Second, many ceramic coatings must be applied and processed at high temperature ($> 1000^\circ\text{C}$), using expensive and time-consuming methods, such as chemical vapor deposition.

To solve these problems with conventional ceramic coatings, our previous work [1,2] focused

upon the synthesis of pre-ceramic inorganic poly-metallosiloxane (PMS) polymers, and upon the characteristics of the synthesized PMS as corrosion-protective coatings on aluminum substrates. The polymers were synthesized through the hydrolysis-dehydrochlorinating and dehydrating condensations-pyrolysis reactions of sol-gel 'paint' precursor solutions, consisting of N-[3-(triethoxysilyl)propyl]-4,5-dihydroimidazole (TSPI), the metal alkoxides, $\text{M}(\text{OR})_4$, (where M is Ti or Zr, and R is C_2H_5 or C_3H_7), with hydrochloric acid as a hydrolysis accelerator, and methanol, and water. We suggested that this reaction occurs in the following sequence.

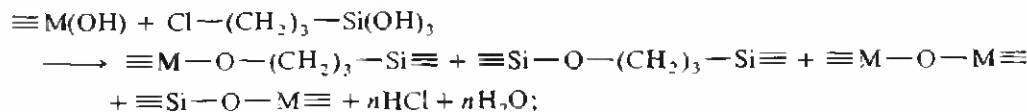
(1) HCl-catalyzed hydrolysis of TSPI and $\text{M}(\text{OR})_4$ at room temperature,



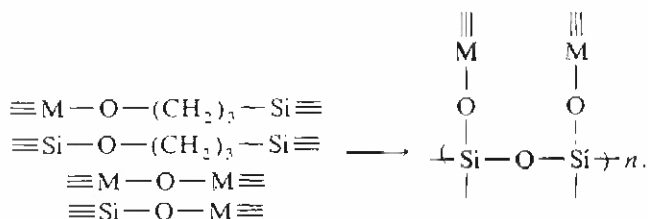
* This work was performed under the auspices of the US Department of Energy, Washington, DC under Contract No. DE-AC02-76CH00016, and supported by the US Army Research Office Program MTPR-ARO-103-90.



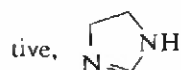
(2) dehydrochlorinating and dehydrating condensation at the sintering temperature of 150 °C,



(3) pyrolysis at 350 °C,



In the first reaction stage, the HCl-catalyzed hydrolysis of TSPI promotes the cleavage of the N-CH₂- linkage, and then breakage of this bond leads to the formation of the imidazoline deriva-



and the organosilanol compounds containing Cl-substituted end groups. At the same time, the hydrolysis of the metal alkoxides forms hydroxylated metal compounds. The dehydrochlorinating and dehydrating condensation reactions between these hydrolysis-induced compounds occur in the 150 °C-sintering processes of sol-precursor solution. The pyrolytic treatment of the sintering organometallosiloxane as a final stage induces the formation of PMS network structures, while causing the volatilization of carbonaceous species from the sintered compounds. When this PMS was used as a corrosion-protective coating for aluminum substrates, we found that two factors were important in making uniform, continuous coatings on the substrates: (1) the degree of densification of metal-O-Si linkage, and (2) the bond formation at the PMS-aluminum interfaces.

As part of our work to develop the advanced PMS coatings, our objectives were to examine the characteristics of polygermanosiloxane (PGS) derived from the sol-gel solution containing two main film-forming components, TSPI and germanium ethoxide [Ge(OC₂H₅)₄], and to investi-

gate the ability of such films to protect the aluminum substrate from the attack of corrosive fluids.

2. Experiments

2.1. Materials

N-[3-(triethoxysilyl)propyl]-4,5,-dihydroimidazole (TSPI), supplied by Petrarch Systems Ltd., was used as a network-forming monomeric organoalkoxysilane. The germanium (IV)-ethoxide [Ge(OC₂H₅)₄] obtained from Alfa Products was employed as a cross-linking agent.

The film-forming mother liquor which served as the precursor solution was prepared by incorporating the TSPI-Ge(OC₂H₅)₄ mixture into a medium of methyl alcohol/water containing HCl as a hydrolysis accelerator. To produce a clear precursor solution, it was very important to add the HCl to the blending material, thereby forming a uniform coating film on the metal substrates. Table 1 shows the compositions of the precursor solutions used in this study.

The metal substrate used was 2024-T3 clad aluminum sheet, containing the following chemical constituents: 92 wt% Al, 0.5 wt% Si, 0.5 wt% Fe, 4.5 wt% Cu, 0.5 wt% Mn, 1.5 wt% Mg, 0.1 wt% Cr, 0.25 wt% Zn, and 0.15 wt% other.

The oxide etching of the aluminum was carried out in accordance with a well-known commercial

Table 1
Compositions of clear precursor solutions used in $\text{Ge}(\text{OC}_2\text{H}_5)_4$ -TSPI systems

TSPI/ $\text{Ge}(\text{OC}_2\text{H}_5)_4$ (wt ratio)	TSPI (wt%)	$\text{Ge}(\text{OC}_2\text{H}_5)_4$ (wt%)	CH_3OH (wt%)	Water (wt%)	HCl (wt%)/ TSPI + $\text{Ge}(\text{OC}_2\text{H}_5)_4$
100/0	50	-	30	20	15
90/10	45	5	30	20	15
80/20	40	10	30	20	15
70/30	35	15	30	20	15

sequence called the Forest Products Laboratory (FPL) process [3]. As the first step in the preparation, the surfaces of the sheets were wiped with acetone-soaked tissues to remove any organic contamination. They were then immersed in chromic-sulfuric acid ($\text{Na}_2\text{Cr}_2\text{O}_7 \cdot 2\text{H}_2\text{O} : \text{H}_2\text{SO}_4 : \text{water} = 4 : 23 : 73$ by weight) for 10 min at 80°C . After etching, the fresh oxide surfaces were washed with deionized water at 30°C for 5 min, and subsequently dried in air for 15 min at 50°C .

Coating of the aluminum surfaces using the sol system was performed in the following sequence. The FPL-etched aluminum substrates were dipped into the precursor solution at ambient temperature. The substrates then were withdrawn slowly from the soaking bath, after which they were preheated in an oven for 20 h at 150°C to yield a sintered coating. The samples were subsequently annealed for 30 min at temperatures up to 350°C .

2.2. Measurements

The combined techniques of thermogravimetric analysis (TGA), differential thermal analysis (DTA), infrared (IR), and X-ray powder diffraction (XRD) were used to examine the changes in conformation, the degree of Ge-O-Si linkage, and the in situ phase transformation of the $\text{Ge}(\text{OC}_2\text{H}_5)_4$ -modified organosilane polymers at temperatures up to 350°C .

The extent to which the precursor solutions wetted the FPL-etched Al surfaces was estimated from the values of contact angle measured within the first 20 s after dropping the solution on the surfaces.

The surface microstructure of the films formed on Al surface at 350°C were observed with scanning electron microscopy (SEM). The surface-interface chemical components and states of the PGS-coated Al substrate samples were also investigated using X-ray photoelectron spectroscopy (XPS).

The electrochemical testing for data on corrosion was performed with an EG & G Princeton Applied Research Model 362-1 corrosion measurement system. The electrolyte was a 0.5M sodium chloride solution, made from distilled water and reagent grade salt. The specimen was mounted in a holder and then inserted into a EG & G Model K47 electrochemical cell. The tests were conducted in an aerated 0.5M NaCl solution at 25°C , on an exposed surface area of 1.0 cm^2 . The polarization curves containing the cathodic and anodic regions were measured at a scan rate of 0.5 mV/s in the corrosion potential range of -1.2 to -0.3 V .

3. Results

3.1. Thermal characteristics of Ge-incorporated organosilane compounds

Before surveying the properties of the pyrogenic polygermanosiloxane (PGS) films deposited on the aluminum (Al) substrates, we investigated the thermal behaviors of the Ge-incorporated organosilane sinters derived from the sol-gel precursor solution using TGA-DTA, IR, and XRD. These measurements gave us data on thermal decomposition, phase transformation, and pyrolysis.

is-induced change and rearrangements in molecular conformation.

A thermal analysis, combining TGA and DTA, revealed the decomposition characteristics during pyrolysis of 150°C-sintered powder samples (fig. 1). The TGA data for the control, a sample with a ratio 100/0 of TSPI/ $\text{Ge}(\text{OC}_2\text{H}_5)_4$, showed a slight decrease between 0 and 100°C followed by a large decrease between 300 and 450°C, and a smaller decrease between 500 and 700°C. At temperatures > 700°C, no further changes were seen in the TGA and DTA data. The weight loss occurring at each individual stage in the three-step decomposition process gave the following values: $\approx 3\%$ at temperatures up to 200°C, $\approx 27\%$ between 200 and 500°C, and $\approx 9\%$ between 500 and 600°C. Compared with the TGA data of the controls, changes in the shape of the curve can be seen in the samples in which $\text{Ge}(\text{OC}_2\text{H}_5)_4$ was incorporated: the addition of $\text{Ge}(\text{OC}_2\text{H}_5)_4$ to TSPI shifts the temperature of onset of thermal decomposition on the second and third stages to a lower value. As the DTA curves show, the temperature of the two prominent peaks between 300 and 500°C decreases as the $\text{Ge}(\text{OC}_2\text{H}_5)_4$ concentration increases.

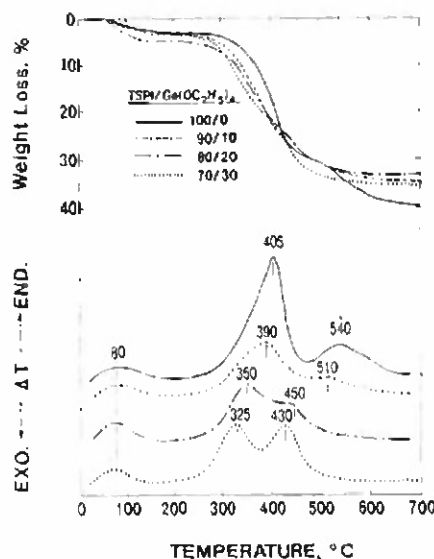


Fig. 1. TGA and DTA curves for the pyrolysis of samples heated in an oxygen atmosphere at a rate of 10°C/min.

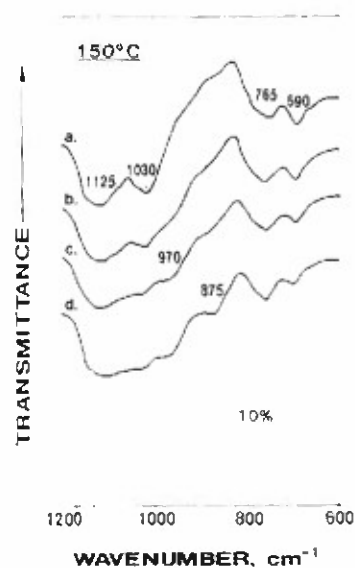


Fig. 2. IR absorption spectra for the 150°C-sintered samples having (a) 100/0, (b) 90/10, (c) 80/20, and (d) 70/30 ratios of TSPI/ $\text{Ge}(\text{OC}_2\text{H}_5)_4$.

To verify our findings, the IR spectra of samples sintered at 350°C and 500°C were measured. Figure 2 shows the IR absorption spectra over the wavenumber region of 1200 to 600 cm^{-1} for 150°C-sintered powder samples having 100/0, 90/10, 80/20, and 70/30 ratios of TSPI/ $\text{Ge}(\text{OC}_2\text{H}_5)_4$. The spectrum for the bulk TSPI (a) had four pronounced bands. As described in the previous paper [2], the respective bands are assigned to the following absorbing species: the Si-C bond stretching in the Si-joined propyl groups at 1125 cm^{-1} , the antisymmetric bond stretching of the Si-O-Si linkage at 1030 cm^{-1} , the symmetric stretching of the Si-O-Si linkage at 765 cm^{-1} , and the C-Cl stretching in the Cl-substituted end groups at 690 cm^{-1} .

When 20 parts of the total weight mass of TSPI were replaced by $\text{Ge}(\text{OC}_2\text{H}_5)_4$, a new peak appeared at 970 cm^{-1} in the absorption spectrum (c). This peak is attributed to Si-O-Ge linkages [4]. The peak intensity of the C-Cl band at 690 cm^{-1} decreases as the proportion of $\text{Ge}(\text{OC}_2\text{H}_5)_4$ increases. The data also indicated that Cl in the Cl-substituted end groups preferentially reacts

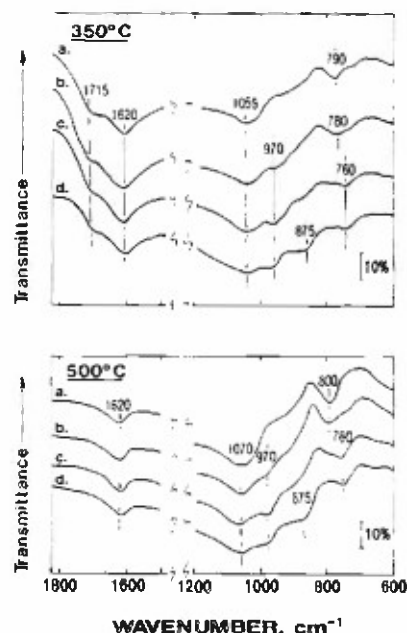


Fig. 3. IR spectra for the 350°C- and 500°C-pyrolyzed (a) 100/0, (b) 90/10, (c) 80/20, and (d) 70/30 TSPT/ $\text{Ge}(\text{OC}_2\text{H}_5)_4$ ratio samples.

with OH groups in the hydroxylated Ge compounds derived from the HCl-catalyzed hydrolysis of $\text{Ge}(\text{OC}_2\text{H}_5)_4$. With a further increase in the proportion of $\text{Ge}(\text{OC}_2\text{H}_5)_4$ to 30 parts, another new peak at 875 cm^{-1} appeared (see fig. 2(d)), which is attributed to the Ge-O stretching mode of GeO_2 [5]. Figure 3 shows the comparisons and changes in the IR spectral features of the 350°C- and 500°C-pyrolyzed samples. At 350°C, the changes in the spectra of the samples with 100/0 ratio (a), compared with that of a 150°C-preheated sample, can be described as follows: (1) the peaks at frequencies of 1125 and 690 cm^{-1} originating from the Si-C and C-Cl bonds, respectively, are eliminated; (2) there is a slight shift of the absorption due to the Si-O-Si linkage at 1030 and 765 cm^{-1} ; and (3) a new band emerges at 1715 cm^{-1} . The first result is indicative of the removal of many carbonaceous groups from the polymeric organosilane networks. Such a pyrolytic phenomenon will lead to the third result, namely, the new absorption band at 1715 cm^{-1} is due to

the C=O stretching absorption in the aldehyde yielding pyrogenic by-products [6]. The peak intensity of the by-products decreased with an increase in proportion of $\text{Ge}(\text{OC}_2\text{H}_5)_4$.

There was no evidence for Si-O-Ge linkage at 150°C for the 90/10 ratio sample. However, when this sample was pyrolyzed at 350°C, the spectrum (fig. 3(b)) contained a component at 970 cm^{-1} which we attribute to Si-O-Ge, corresponding to the formation of polygermanosiloxane (PGS). The most intense band at 970 cm^{-1} in the spectrum of 350°C-pyrolyzed series was observed in the samples with 80/20 ratio (fig. 3(c)). By contrast, the incorporation of a certain amount of $\text{Ge}(\text{OC}_2\text{H}_5)_4$ is associated with the formation of GeO_2 , rather than the Si-O-Ge linkages. The formation of GeO_2 is deduced from the increase in intensity of a band at 875 cm^{-1} , compared with that at 970 cm^{-1} (see fig. 3(d)). The peak absorbance of the Si-O-Ge band at 970 cm^{-1} in the 90/10 ratio sample was almost the same as that of the 80/20 ratio sample, indicating that the extent of densification of Si-O-Ge linkage in the PGS films is similar in both. The spectra for all samples exhibit a band, ranging from 800 to 750 cm^{-1} , that is due to the symmetric stretching mode of the Si-O-Si. When these samples were treated at 500°C, there was no evidence of the bands at 1715 cm^{-1} in the spectra of any sample. Thus, the volatilization of the organic species is completed at 500°C. The shift of Si-O-Si band at 1055 cm^{-1} toward a higher wavenumber was also apparent in the spectra of the 500°C-pyrolyzed samples.

There are no diffraction peaks detected by XRD over the diffraction ranges of 0.59 to 0.201 nm for the 350°C-pyrolyzed 90/10 and 80/20 ratio samples. This finding indicates that the PGS derived from these systems is essentially amorphous. By contrast, reflections at 0.236 , 0.215 , and 0.204 nm in the same diffraction range were observed from the 70/30 ratio sample. These spacings belong to crystalline GeO_2 [7]; therefore, the 70/30 ratio-derived amorphous PGS layers contain some GeO_2 crystalline particles.

On the basis of this knowledge, the study then focused upon the properties of PGS coating films as a barrier against corrosion of Al substrates.

3.2. Properties of PGS coating films

In dealing with the formation of uniform-continuous PGS coating films, the magnitude of wettability and spreadability of the Forest Products Laboratory (FPL)-etched Al surfaces by sol precursor liquids are among the most important factors governing good protective-coating performance. As we have shown [8], FPL treatment of Al substrates introduces an amorphous oxide layer into the outermost surface sites of Al. One significant feature of a fresh Al_2O_3 surface is its extremely high susceptibility to moisture: the aging FPL-etched surface layer which was used in this study consisted of the phases of anhydrous and hydrous aluminum oxides. Therefore, the magnitude of the sol liquid-wettability of the oxide surface was estimated from the average value of the advancing contact angle, θ (in degrees), on this surface. The sol-precursor solution systems, as shown in table 1, were also used in this study. A plot of θ as a function of the TSPI/ $\text{Ge}(\text{OC}_2\text{H}_5)_4$ ratios, for the FPL-etched Al surface, is given in fig. 4. Since a low contact angle implies better wetting, the resultant θ -ratio data exhibited an interesting feature; namely, the wetting behavior was improved by increasing the proportion of $\text{Ge}(\text{OC}_2\text{H}_5)_4$ in the precursor systems. The θ value for the 80/20 ratio solution was considerably lower (2.0° vs. 29.3°) than that for the 100/0 ratio. In fact, the 80/20 and 70/30 ratio solutions had such a great affinity for the oxide surfaces that complete coverage over the whole oxide face by sol solutions, thereby producing uniformly sintered coating films under the pre-heat treatment at 150°C , was observed.

Figure 5 shows SEM micrographs for the 150°C -sintered 100/0, 80/20, and 70/30 ratio samples after pyrolysis for 30 min at 350°C . As expected, the surface microstructure of the 100/0 ratio-coating film (fig. 5(a)) is discontinuous. Improvements in the film of the 80/20 ratio sample can be seen in the SEM micrograph (fig. 5(b)). Although there were a few propagated microcracks with a flow width of $\approx 2\ \mu\text{m}$, there was no evidence of film discontinuity, nor of the separation of the film from the substrate. By contrast, the surface microstructure for the 70/30 ratio-re-

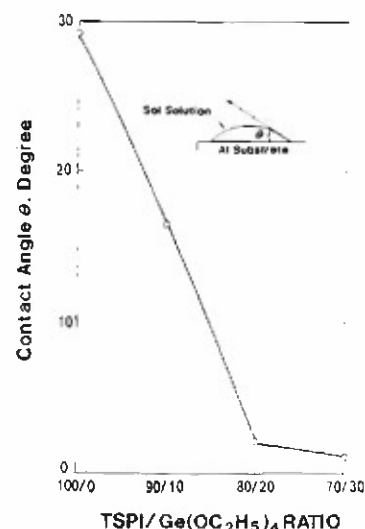


Fig. 4. Effect of $\text{Ge}(\text{OC}_2\text{H}_5)_4$ on improvement of sol solution-wettability of Al surfaces. The line is drawn to connect data symbols.

lated PGS coatings (fig. 5(c)) had developed numerous and wide cracks which are indicative of large stresses.

The adhesion at the interface and/or inter-phase between the PGS and the aluminum oxide is also an important factor contributing to good film-forming behavior and to protection against corrosion. Since adhesion is a local phenomenon involving only a few atom layers of film and substrate, the high-resolution XPS spectrum of the Ge_{3d} signal was obtained. To set a scale in the XPS spectra, the binding energy (BE) was calibrated with the C_{1s} hydrocarbon-type carbon peak fixed at 285.0 eV. A curve deconvolution technique was employed to find the respective chemical components from the high-resolution spectrum of element, and to determine the relative quantity of each particular chemical state. The 80/20 ratio-PGS films suitable for XPS analyses were prepared on etched substrates in the following way: a 0.2% sol-precursor solution in de-ionized water was deposited over the substrate surfaces by spin-coating at 1000 rpm and then the samples were heated for 20 h at 150°C to produce a sintered film. The pyrolytic conversion of the

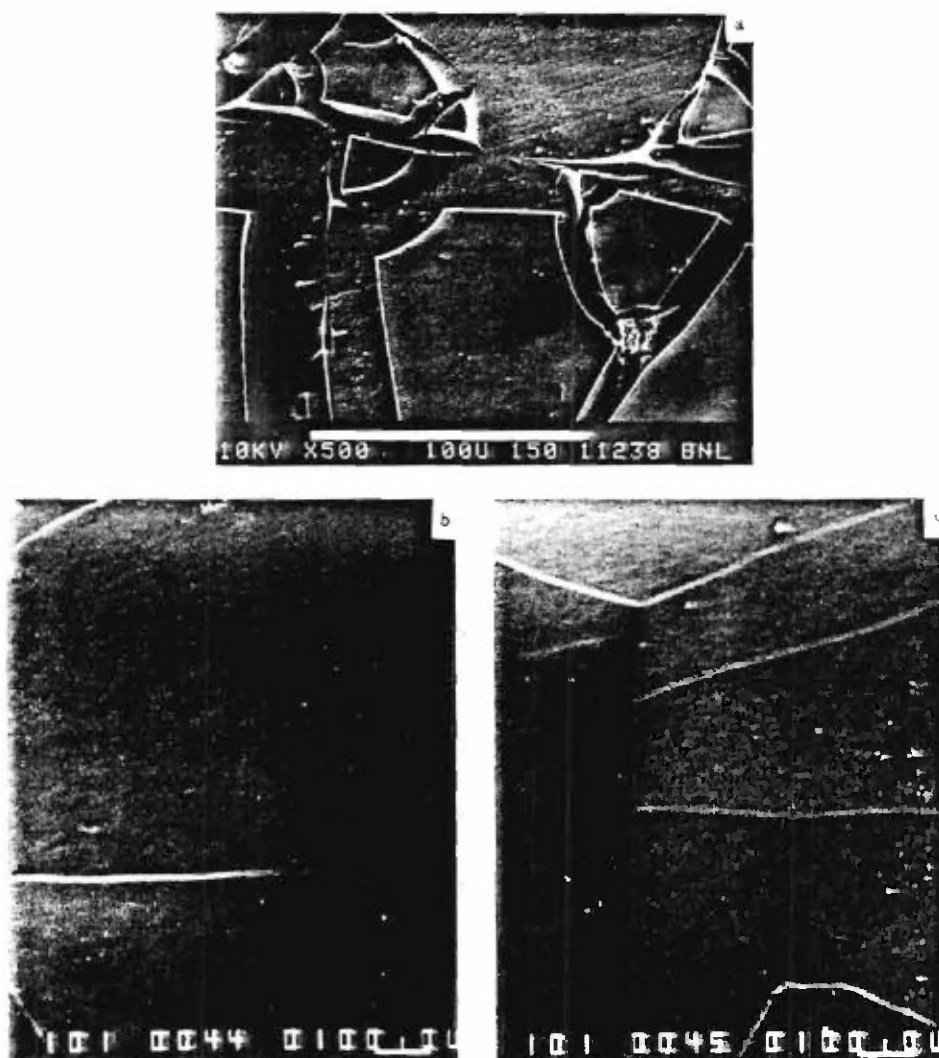


Fig. 5. SEM micrographs for 350°C-pyrolyzed (a) 100/0, (b) 80/20, and (c) 70/30 TSPI/ $\text{Ge}(\text{OC}_2\text{H}_5)_4$ ratio coating films.

sintered film into the PGS film was accomplished by annealing for 30 min at 350°C; the resulting interfaces were examined using XPS. For the purposes of comparison, a 0.2% $\text{Ge}(\text{OC}_2\text{H}_5)_4$ -sol solution in deionized water without TSPI was deposited on the Al oxide surfaces, and then pyrolyzed at 350°C to produce a thin Ge-based compound film.

The thickness of PGS and Ge-compound films made by this method were thin enough to permit

the photoemission signal from the underlying aluminum substrates to be detected. Figure 6 gives the germanium 3d spectra for the PGS film surface, and PGS/aluminum oxide and Ge compound/aluminum oxide interfaces. The Ge_{3d} region for the PGS film (fig. 6(a)) reveals two resolvable Gaussian components at BE of 33.0 and 31.9 eV, corresponding to the Ge originating from the Si-O-Ge linkages as the major component, and the Ge in germanium oxides as a minor phase, respec-

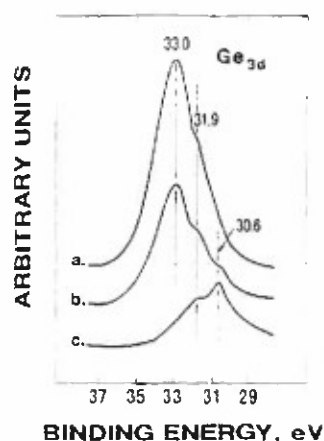


Fig. 6. Ge_{3d} spectra originating from (a) PGS surface, and (b) PGS/aluminum oxide, and (c) Ge compound/aluminum oxide interfaces. The vertical lines are drawn to indicate the positions of peaks of spectral components.

tively [9]. By comparison, the Ge_{3d} signal feature (fig. 6(b)) emerging from the critical interfacial zones of PGS/Al oxide indicated the appearance

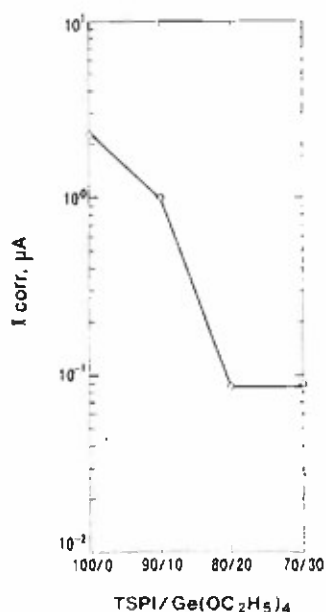


Fig. 7. Changes in corrosion current, I_{corr} , of PGS-coated aluminum substrates as function of TSPI to $\text{Ge}(\text{OC}_2\text{H}_5)_4$ ratios. The line is drawn to connect data symbols.

of new component at a low BE site of 30.6 eV, with the principal and shoulder lines of Si-O-Ge and germanium oxide germaniums still present. To assign this new peak, we investigated the Ge compound/ Al_2O_3 interface induced by the pyrolytic interaction between the hydroxylated Ge compounds (sol-precursor solution) and the Al_2O_3 substrates (fig. 6(c)). The resulting curve contains a major line at 30.6 eV and a minor one at 31.9 eV. We suggest that the new peak at 30.6 eV is due to $\equiv\text{Ge-O-Al}$ (on the Al_2O_3 surfaces) in the interaction products.

The PGS coatings were derived from the sol composition systems (see table 1). The corrosion data were obtained from the polarization curves for PGS-coated aluminum samples exposed in an aerated 0.5M sodium chloride solution at 25°C. The typical cathodic-anodic polarization curves exhibited a short Tafel region in the cathodic polarization, but no Tafel region was found at the anodic sites. To evaluate the protective performance of coatings, the corrosion current, I_{corr} , was measured by extrapolation of the cathodic Tafel slope.

Figure 7 illustrates the variation in I_{corr} value of Al substrate as a function of the ratio of TSPI/ $\text{Ge}(\text{OC}_2\text{H}_5)_4$ in the precursor sol solution. The I_{corr} values decrease with increased proportion of $\text{Ge}(\text{OC}_2\text{H}_5)_4$ up to 20 wt%; beyond this fraction, there was a slight increase in I_{corr} on the 70/30 ratio coating sample. The I_{corr} value of 8.7×10^{-2} for the 80/20 ratio PGS coatings was

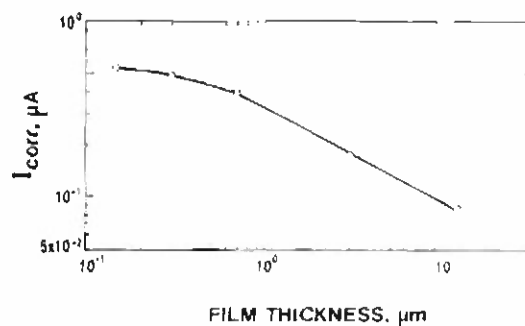


Fig. 8. I_{corr} vs. film thickness of 80/20 TSPI- $\text{Ge}(\text{OC}_2\text{H}_5)_4$ ratio-related PGS coating deposited on aluminum. The line is drawn to connect data symbols.

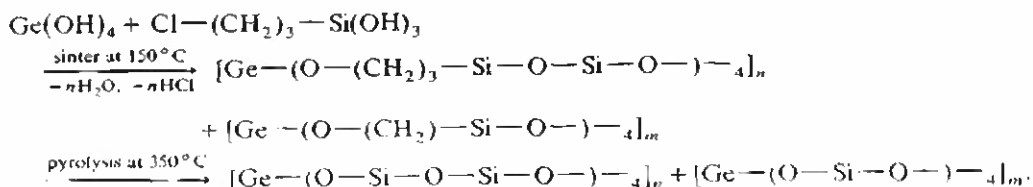
approximately two orders of magnitude less than that for the germanium oxide-uncross-linked polysiloxane coatings (100/0 ratio). The effect of film thickness of 80/20 ratio coatings on the decrease in I_{corr} value was also investigated. The I_{corr} values for the PGS coatings ranging from $1.5 \times 10^{-1} \mu\text{m}$ to $10 \mu\text{m}$ are shown in fig. 8.

4. Discussion

From the results of the IR analyses (see figs. 2 and 3), the following points can be made. In sintering sol systems consisting of organosilanols containing Cl-substituted end groups and $\text{Ge}(\text{OH})_4$ in alcoholic aqueous media, the OH groups in $\text{Ge}(\text{OH})_4$ preferentially react with Cl in the chlorinated organosilanol to promote dehydrochlorinating condensation, rather than with OH in $\text{Ge}(\text{OH})_4$ and $-\text{Si}(\text{OH})_3$ [1]. Since the Si-O-Si linkages also form in 150°C -sintered samples, the dehydrating condensation reactions between neighboring silanol in the chlorinated organosilanol yield a polymeric siloxane structure [2]. The combination of such condensation reactions lead to the conformation of network structures of germanium oxide-cross-linked organosiloxane. At the pyrolytic temperature of 350°C , the removal of carbonaceous groups from these cross-linked structures contributes to their conversion into the inorganic PGS network structures containing aldehydes as pyrogenic by-products. The amount of aldehyde-type by-products remaining in the pyrolysis-induced inorganic phase depends primarily on the proportion of TSPI. This finding is reflected directly in the results of TGA-DTA analysis; namely, the weight loss of the $\text{Ge}(\text{OC}_2\text{H}_5)_4$ -modified TSPI samples during pyrolysis was much

lower than that of unmodified TSPI. The complete elimination of aldehyde by-products can be achieved by increasing the temperature to 500°C . On the other hand, although a high proportion of $\text{Ge}(\text{OC}_2\text{H}_5)_4$ in the $\text{Ge}(\text{OC}_2\text{H}_5)_4$ -TSPI systems produces a low amount of aldehydes, the incorporation of a large amount of $\text{Ge}(\text{OC}_2\text{H}_5)_4$ resulted in the formation of the crystalline GeO_2 as a pyrogenic by-product in the amorphous PGS layers.

We propose the hypothetic model of sintering-pyrolyzing processes for the formation of a PGS network, as shown at the bottom of this page. When the sol precursor system is applied as a practical sol 'paint' to the surface of the Al substrate, good wettability of the Al surface becomes an important factor in fabricating a continuous, uniform sintered coating film. As described in the TSPI/ $\text{Ge}(\text{OH}_2\text{H}_5)_4$ ratio-contact angle relations (see fig. 4), an increase in proportion of $\text{Ge}(\text{OC}_2\text{H}_5)_4$ in the precursor systems resulted in better spreading of the sol solution over the aluminum oxide surfaces. With regard to the acid-base interactions of surface hydroxyl groups, Bolger [10] and Fowkes [11] report that hydrous aluminum oxides existing at the outermost surface layer of FPL-etched Al substrates have a strong chemical affinity with the polar OH groups in the adhesive, so forming hydrogen bonds. Because the HCl-catalyzed hydrolysis of $\text{Ge}(\text{OC}_2\text{H}_5)_4$ induces the formation of hydroxylated Ge sol, a possible interpretation for the enhanced wetting of the Al substrate by sols with a high proportion of $\text{Ge}(\text{OC}_2\text{H}_5)_4$ is that there is an increase in total OH groups in the precursor solutions. However, once all available functional groups of aluminum oxide faces are occupied by polar OH groups in the sol, the presence of ad-



The hypothetic model of sintering-pyrolyzing processes for the formation of a PGS network.

ditional OH groups do not promote wetting and spreading of the sol solution. In fact, we found no significant difference between the contact angles of 80/20 ratio and 70/30 ratio sols (fig. 4).

An inspection of 350°C pyrolysis-induced coating films using SEM revealed discontinuities in the 100/0 ratio coating. These discontinuities were not only caused by the poor diffusive behavior of the 100/0 ratio precursor solution on aluminum oxide, but was also due to the presence of large amounts of pyrogenic by-products. The incorporation of excessive amount of Ge, especially GeO_2 -related Ge, into the PGS films caused the development of a large number of cracks in the films. This finding agrees with that of our previous study on polytitanosiloxane coating [1]; the growth of crystalline GeO_2 particles in the amorphous polymer phases has a detrimental effect on the formation of the film coating. Further, such films have a thermal expansion which differs from that of the Al substrate, and adheres poorly to aluminum oxides. Thus, it is clear that the proper proportions of TSPI to $\text{Ge}(\text{OC}_2\text{H}_5)_4$ are an important factor in forming a good film. We found that the 80/20 was the most effective ratio of TSPI to $\text{Ge}(\text{OC}_2\text{H}_5)_4$ for the sol-precursor system.

The structure of the PGS-aluminum oxide interfacial bond is one of the important parameters contributing to better protection of Al substrates against corrosion. For the purpose of supporting the results obtained from the XPS Ge_{3d} spectra (fig. 6), the additional Si_{2p} , Al_{2p} , and O_{1s} core level spectra were also explored. In our assignments of the peaks in the Si_{2p} , Al_{2p} and O_{1s} regions, we used the polysiloxane (PS), polyaluminosiloxane (PAS) and $\text{GeO}_2\text{-Al}_2\text{O}_3$ compounds, as reference samples. PS was synthesized by the condensation-pyrolysis reaction of the sol-precursor solution consisting of 47 wt% TSPI, 28 wt% CH_3OH , 19 wt% water and 6 wt% HCl. Using the same synthesis methods, the pyrogenic PAS and $\text{GeO}_2\text{-Al}_2\text{O}_3$ compounds were derived from the following different precursor systems: (1) 20 wt% TSPI, 20 wt% $\text{Al}(\text{OC}_2\text{H}_5)_3$, 25 wt% CH_3OH , 17 wt% water and 18 wt% HCl, and (2) 20 wt% $\text{Ge}(\text{OC}_2\text{H}_5)_4$, 20 wt% $\text{Al}(\text{OC}_2\text{H}_5)_3$, 25 wt% CH_3OH , 17 wt% water and 18 wt% HCl.

Table 2
Positions of XPS reference peaks in Si_{2p} , Al_{2p} , and O_{1s} regions for the standard compounds

Compound	Active group	Si_{2p} (eV)	Al_{2p} (eV)	O_{1s} (eV)
PS	Si-O-Si	102.8	-	532.4
PAS	Si-O-Al	101.6	74.0	531.3
$\text{GeO}_2\text{-Al}_2\text{O}_3$	Ge-O-Al	-	73.2	530.9
GeO_2	-	-	-	529.4
Al_2O_3	-	-	74.5	531.7

respectively. In addition, the aluminum oxide (Al_2O_3) and germanium (IV) oxide (GeO_2) of chemical reagent grades (supplied by Alfa) were also employed as reference compounds. The principal peak positions from the Si_{2p} , Al_{2p} and O_{1s} spectra of the main group in these reference compounds are summarized in table 2. Thus, the chemical components and the groups for each peak in the XPS curve were identified in accordance with the reference peaks and with published data. The observational error between the peak positions of reference and test samples was ± 0.2 eV.

The Si_{2p} region of the spectrum from the surface of bulk PGS (fig. 9(d)) indicates the presence of the major peak at 102.8 eV and the shoulder at 101.6 eV. The principal line at 102.8 eV reveals Si

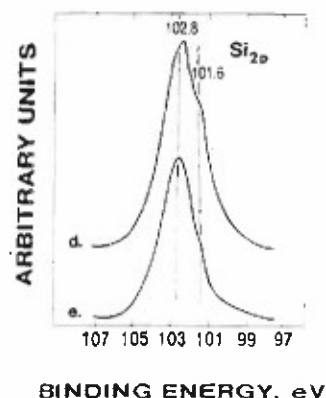


Fig. 9. Si_{2p} spectra originating from (d) PGS surface, and (e) PGS/aluminum oxide interface. The vertical lines are drawn to indicate the positions of peaks of spectral components.

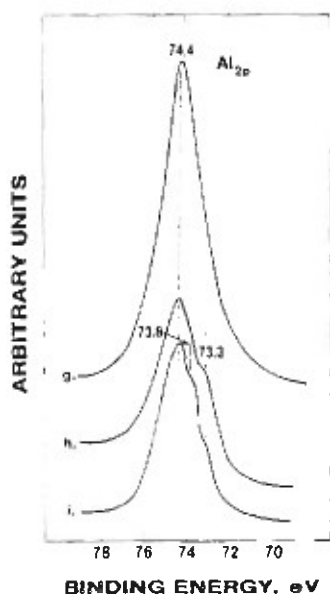


Fig. 10. Al_{2p} region of (g) FPL-etched aluminum substrate surface, (h) Ge compound/aluminum oxide, and (i) PGS/aluminum oxide interfaces. The vertical lines are drawn to indicate the positions of peaks of spectral components.

in the siloxane bonds [12]. Since the line around 101.6 eV is due to the Si in the Si–O–metal linkages [2,13], it is reasonable to assume that the shoulder at the position of 101.6 eV is due to the Si belonging to Si–O–Ge bonds. Although a spectral feature similar to that of the bulk PGS was observed in a PGS–aluminum oxide interfacial boundary (fig. 9(e)), the peak at 101.6 eV, emerging from some interfacial areas may be due to two Si components joined to the metal oxides; one is Si bonded to the aluminum oxide substrates, and other is that of the Si–O–Ge in PGS. For the Al_{2p} core level spectra (fig. 10), the Al substrate in fig. 10(g) reveals only a symmetric single peak at 74.4 eV, corresponding to the Al in Al_2O_3 . The Al_{2p} feature (fig. 10(h)) emitted from the Ge compound/aluminum oxide interphase regions is characterized by an emerging shoulder at 73.3 eV. According to the reference peaks, this shoulder is attributed to Al from the Ge–O–Al linkages. Following the deposition of a thin PGS film on the

Al_2O_3 surfaces, the Al_{2p} regions (fig. 10(i)) indicate the presence of three resolvable components at 74.4, 73.8, and 73.3 eV, due to Al in Al_2O_3 , Si–O–Al, and Ge–O–Al linkages, respectively. From comparisons between the intensities of two shoulder peaks at 73.8 and 73.3 eV, the bond structure formed at the PGS/ Al_2O_3 interfaces is the Si–O–Al linkage, rather than with the Ge–O–Al. By comparison with the O_{1s} spectral feature of Al_2O_3 (fig. 11(j)), a broad spectral feature which obviously contains at least three components can be seen in the oxygen 1s region of Ge compound/ Al_2O_3 interfaces (fig. 11(k)). The secondary intense peak at 531.0 eV is assigned to the bridging oxygen in the Ge–O–Al linkages; by contrast, the weak line at the position of 529.4 eV, which is 1.6 eV lower than that of the bridging oxygen, is due to the non-bridging oxygen in the germanium oxides. The O_{1s} spectrum of the PGS surfaces (fig. 11(l)) contains three components which are attributed to three oxygen compounds at 532.5, 531.5, and 529.4 eV. The two strong lines at 532.5 and 531.5 eV are due to the bridging oxygens in the Si–O–Si and Si–O–Ge [14], respectively. Although the number of components is very small, it is evident from the weak shoulder at 529.4 eV that the non-bridging oxygen in the GeO_2 is present on PGS surfaces. For the PGS/ Al_2O_3 interfaces (fig. 11(m)), the intensity of the non-bridging oxygen peak is conspicuously reduced, while a new peak appears at 531.2 eV, representing oxygen in an interfacial oxane bond bridging between the PGS and Al_2O_3 . The formation of an interfacial oxane bond involves both $\equiv\text{Si}-\text{O}-\text{Al}$ as a major structure and $\equiv\text{Ge}-\text{O}-\text{Al}$ as a minor one. Thus, the interfacial covalent bond structure such as $\equiv\text{M}(\text{Si and Ge})-\text{O}-\text{Al}$ (on the surface of substrate) forms at the interfaces between PGS and aluminum. Also, we note that the peak near 531.5 eV is due to oxygen in either the Al_2O_3 or the Ge–O–Si bond.

Three major factors are responsible for minimizing the development of stress cracks by shrinkage of pyrolyzed PGS films: (1) spreadability and mobility of $\text{Ge}(\text{OCH}_3)_4$ -modified TSPI sol solution on aluminum oxide surfaces, (2) cross-linking of germanium oxides between polysiloxane chains, and (3) formation of PGS–aluminum in-

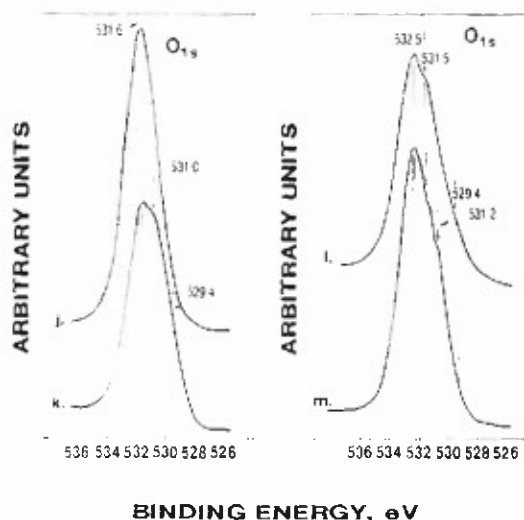


Fig. 11. O_{1s} core level spectra for (j) etched aluminum substrate, (k) Ge compound/aluminum oxide interface, (l) PGS, and (m) PGS/aluminum oxide interface. The vertical lines are drawn to indicate the positions of peaks of spectral components.

terfacial chemical bonds. These factors not only contribute to good film-forming behavior, but also directly affect the corrosion protection of aluminum substrates.

As reported by several investigators [15–17], the localized corrosion (pitting-type corrosion) of Al alloys in aqueous media containing NaCl electrolyte occurs in three steps: (1) adsorption of reactive anions such as Cl^- and OH^- , on the aluminum oxides; (2) chemical reaction of the adsorbed anions with Al ion in the aluminum oxide lattice; and (3) dissolution of the colloidal reaction products. Particularly, the low rate of adsorption of reactive anions plays an essential role in inhibiting the corrosion of Al substrate. Since OH^- ions are generated by cathodic reaction of Al with atmospheric reactants such as O_2 and H_2O , $2H_2O + O_2 + 4e^- \rightarrow 4OH^-$, the corrosion current, I_{corr} , determined on the cathodic curve for PGS-coated Al samples was evaluated to estimate the rate of OH^- adsorption into aluminum oxides; a decrease in I_{corr} corresponds

to a low rate of adsorption of OH^- ions. In other words, good coverage of PGS coating films over Al is shown by a decrease in I_{corr} , because of the low penetration rate of O_2 and H_2O reactants which pass through the PGS film. The lowest I_{corr} for the Al samples coated with various ratios of TSPI/ $Ge(OC_2H_5)_4$ was observed for the 80/20 PGS sample. The reason for the slight increase in the 70/30 ratio sample (see fig. 7) is mainly associated with the presence of many microcracks in the film, compared with that of the 80/20 sample, thereby reducing protection against corrosion. It is clear that a PGS coating derived from the proper ratio of TSPI to $Ge(OC_2H_5)_4$ provides an effective barrier to the corrosion of Al substrate. The film thickness of PGS also influences the rate of penetration of reactants. The I_{corr} of thick PGS coating (see fig. 8), around 13 μm , was approximately one order of magnitude less than that for the thin film of $1.5 \times 10^{-1} \mu m$.

5. Conclusions

We can make the following generalized conclusions from our study. At the interfacial contact zones between the sol-precursor solution and the FPL-etched aluminum (Al) substrate, the magnitude of wetting of Al surfaces by the sol solution consisting of N-[3-(triethoxysilyl) propyl]-4,5-dihydroimidazole (TSPI), HCl, CH_3OH , and water was improved by incorporating a proper amount of $Ge(OC_2H_5)_4$ into the sol media; this selection resulted in a uniform covering of the substrate surfaces by the sol phase. During sintering of the sol phases, a particular characteristic of $Ge(OC_2H_5)_4$ -modified TSPI coating materials was the formation of organo polygermanosiloxane structures containing Si–O–Ge bonds at the relatively low temperature of 150°C. The 350°C-treatments of these organic–inorganic structures produced an amorphous polygermanosiloxane (PGS) network that had a good coating performance. Further, the interaction between the PGS and the Al substrate induced the formation of covalent oxane bonds at the interfaces. PGS coating provides good corrosion protection to Al against salt solutions.

References

- [1] T. Sugama, L.E. Kukacka and N. Carciello, *Prog. Org. Coat.* 18 (1990) 173.
- [2] T. Sugama and C. Taylor, *J. Mater. Sci.*, in press.
- [3] H.W. Eichner and W.E. Schowalter, *Forest Products Laboratory Report No. 1813*, Madison, WI (1950).
- [4] D.R. Anderson, in: *Analysis of Silicones*, ed. A. Lee Smithe (Wiley-Interscience, New York, 1974) ch. 9.
- [5] S.P. Mukherjee, A.S. Glass and M.J.D. Low, *J. Am. Ceram. Soc.* 73 (1990) 242.
- [6] L.J. Bellamy, *The Infra-red Spectra of Complex Molecules*, 3rd Ed. (Chapman and Hall, London, (1975) ch. 9.
- [7] Joint Committee on Powder Diffraction Standards, Card 34-1089 JCODS, Pennsylvania (1984).
- [8] T. Sugama, L.E. Kukacka, C.R. Clayton and H.C. Hua, *J. Adhes. Sci. Tech.* 1 (1987) 265.
- [9] G. Hollinger, P. Kumurdjan, J.M. Mackowski, P. Pertosa, L. Porte and T. Minhduc, *J. Electron Spectrosc. Relat. Phenom.* 5 (1974) 237.
- [10] J.C. Bolger, in: *Adhesion Aspects of Polymeric Coatings*, ed. K.L. Mittal (Plenum, New York, 1981) p. 3.
- [11] F.M. Fowkes, *J. Adhesion Sci. Tech.* 1 (1987) 7.
- [12] B. Carriere and J.P. Deville, *J. Electron Spectrosc. Relat. Phenom.* 10 (1977) 85.
- [13] T.E. Madey, C.D. Wagner and A. Joshi, *J. Electron Spectrosc. Relat. Phenom.* 10 (1977) 359.
- [14] H. Nasu, J. Heo and J.D. Mackenzie, *J. Non-Cryst. Solids.* 99 (1988) 140.
- [15] W.A. Bell and H.C. Campbell, *Br. Corros. J.* 1 (1965) 72.
- [16] L. Liepina and V. Kadek, *Corros. Sci.* 6 [3] (1966) 177.
- [17] R.T. Foley, *Corros.* 42 [5] (1986) 277.

Chemical degradations of pyrogenic polytitanosiloxane coatings [☆]

T. Sugama and C. Taylor ¹

Energy Efficiency and Conservation Division, Department of Applied Science, Brookhaven National Laboratory, Upton, NY 11973, USA

Received 31 January 1991; in final form 25 March 1991

We investigated the vulnerability of pyrogenic polytitanosiloxane (PTS) coatings to attack by 1.0 M NaOH and 1.0 M H₂SO₄ solutions. Exposure to NaOH caused breakage of the Si-O-Si bond, thereby producing water-soluble Na-related silicate and hydroxylated silicon compounds. The formation of such reaction products severely damaged the coatings. During treatment with H₂SO₄, SO₄²⁻ preferentially reacts with the TiO₂ formed in PTS layers, rather than with the Si-O-Si and Si-O-Ti linkages. The formation of water-soluble titanium sulphate in this reaction led to pitting of the coatings.

1. Introduction

As a pre-ceramic-type polymer, polytitanosiloxane (PTS) can be synthesized through the hydrolysis-dehydrochlorinating and dehydrating condensation-pyrolysis reactions of a sol-gel precursor solution consisting of monomeric organosilanes, such as 3-glycidoxypolytrimethoxysilane, 3-aminopropyltrimethoxysilane, and N-[3-(triethoxysilyl)propyl]-4,5-dihydroimidazole as network-forming materials, the titanium (IV) alkoxides, Ti(OR)₄ (where R is C₂H₅ and C₃H₇), as crosslinking agents, hydrochloric acid as a hydrolysis accelerator, and methanol and water [1]. The assembled PTS conformation was characterized as representing a Ti oxide-crosslinked polysiloxane network, having Si-O-Ti and Si-O-Si bonds.

Because, PTS has a good film-forming performance, excellent adhesion to metal oxides and high-temperature stability, we consider that this polymer is applicable as an oxidation and corrosion resistance coating on the metal substrates, particularly on low-melting-point metals such as aluminum and

magnesium alloys [2]. Ceramic coatings on metal alloys have not yet been widely employed for several reasons: (1) many coatings must be applied and processed at high temperatures (>1000°C), using expensive and time-consuming methods such as chemical vapor deposition, (2) many coatings adhere poorly to metal oxides, and (3) many coatings lack a thermal expansion coefficient. The latter two problems can result in the separation of the ceramic film from the substrate.

Although pre-ceramic PTS coating appears to be suitable as a coating, its susceptibility to acid- and alkali-induced degradations after exposure to an extremely aggressive corrosive fluid at elevated temperature has not been studied. Accordingly, our objective in the present study was to explore the chemical and topographical changes of PTS film surfaces exposed to 1.0 M H₂SO₄ and 1.0 M NaOH solutions at temperatures up to 80°C. Information was obtained using X-ray photoelectron spectroscopy (XPS) and scanning electron microscopy (SEM), in conjunction with energy-dispersive X-ray (EDX) analysis.

2. Experimental

The N-[3-(triethoxysilyl)propyl]-4,5-dihydroimidazole (TSPI), supplied by Petrarch Systems Ltd.,

[☆] This work was performed under the auspices of the U.S. Department of Energy, Washington, D.C. under Contract No. DE-AC02-76CH00016, and supported by the U.S. Army Research Office program MIPR-ARO-103-90.

¹ Also at: Chemistry Department, University of Virginia, Charlottesville, VA 22901, USA.

was selected from several network-forming monomeric organoalkoxysilanes. The titanium (IV) ethoxide employed as crosslinking agent was supplied by Alfa Products. The film-forming mother liquor, which served as the precursor, was prepared by incorporating the TSPI-Ti(OC₂H₅)₄ mixture into a methyl alcohol/water mix containing an appropriate amount of HCl. The composition of the precursor solution expressed in wt% was TSPI, 37; Ti(OC₂H₅)₄, 9; CH₃OH, 28; water, 19; and HCl, 7. The metal substrate used in the experiments was 2024-T3 clad aluminum sheet. We coated the aluminum surfaces with the precursor solution in the following way. The aluminum substrate was dipped into the precursor solution at ambient temperature, then withdrawn slowly from the soaking bath, after which the substrate was preheated in an oven for 20 h at 150°C to yield a sintered coating. Although some thermal distortions of substrate may occur, the samples were annealed for 30 min at 350°C.

X-ray photoelectron spectroscopy (XPS) was used to study the changes in surface chemical components and states for the PTS-coating films after exposure for 20 min to aqueous 1.0 M NaOH and 1.0 M H₂SO₄ at 25 and at 80°C. The surface microstructure and elements of the exposed films were observed with scanning electron microscopy (SEM) in conjunction with energy-dispersive X-ray (EDX) analysis.

3. Results and discussion

Table 1 summarizes the changes in elemental compositions for the PTS surfaces after exposure to NaOH and H₂SO₄ solutions. By comparison with unexposed controls, the chemical changes in NaOH-

exposed samples were characterized by the removal of a certain amount of Si atoms from the PTS surfaces, while the concentration of Ti increased. The rate of elimination of Si for the 80°C NaOH-treated samples was slightly higher than that of sample at 25°C. The data also showed that a remarkable number of Na atoms was incorporated into the outermost surface sites. The H₂SO₄-exposed PTS film surfaces showed distinct differences from the NaOH-treated surfaces, namely, a decrease in Ti concentration, and the inclusion of the S atom as an additional component, while maintaining around 20% Si. A further decrease and increase in Ti and S atom concentrations, respectively, occurred when the film was exposed to H₂SO₄ solution at 80°C. These data clearly verified that the mechanism of alkali-induced decomposition of PTS surfaces is quite different from that caused by acid.

To obtain more detailed information on the mechanisms of degradation, we examined the XPS high-resolution core-level spectra of the Si_{2p}, Ti_{2p_{2/3}}, O_{1s}, and S_{2p} regions on the PTS coating surfaces exposed to NaOH and H₂SO₄ solutions at 80°C. To set a scale in all the XPS spectra, the binding energy (BE) was calibrated with the C_{1s} of the principal hydrocarbon-type carbon peak fixed at 285.0 eV as an internal reference standard. A curve-deconvolution technique was employed to find the respective chemical components from the high-resolution spectra of each element, and to determine the relative quantity of each chemical.

Fig. 1 shows the core-level photoemission spectra of the respective elements for the NaOH-exposed samples, together with the spectra of the control for comparison. The Si_{2p} signal denoted as curve (a) for the control could be resolved into two Gaussian

Table 1
Changes in XPS atomic composition of PTS surface after exposure to NaOH and H₂SO₄ solutions

Environment	Atomic concentration (%)						
	Si	C	N	Ti	O	Na	S
control	22.2	26.1	5.8	3.2	42.8	-	-
25°C NaOH	15.4	28.2	4.5	6.6	40.0	5.3	-
80°C NaOH	15.2	26.7	4.1	6.8	41.5	5.7	-
25°C H ₂ SO ₄	21.0	27.9	6.0	2.8	41.6	-	0.7
80°C H ₂ SO ₄	20.7	27.5	6.0	2.4	42.1	-	1.3

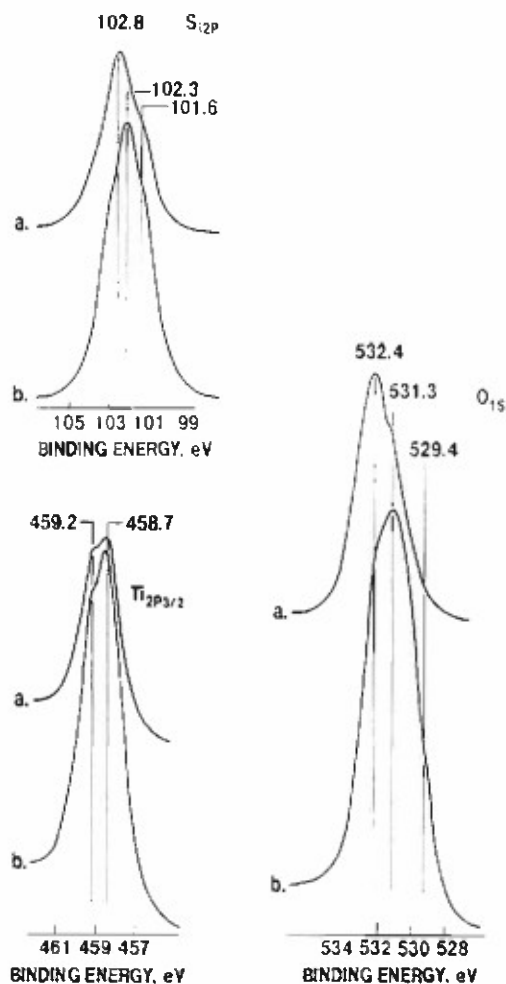
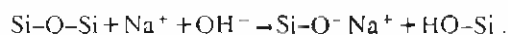


Fig. 1. Si_{2p}, O_{1s} and Ti_{2p_{3/2}} core-level spectra for PTS coating surfaces before (a) and after (b) exposure to NaOH solution at 80°C.

components at 102.8 and 101.6 eV. The former peak, the principal surface chemical component, reveals the Si in the siloxane bonds (Si-O-Si) [2,3], while the latter is attributable to the Si belonging to the Si-O-Ti linkages [2,4]. The signal feature (b) of the NaOH-exposed sample is strikingly different from that of the control: namely, a new principal peak has appeared at the position of 102.3 eV, while the peak representing the Si-O-Si bond at 102.8 eV has markedly decayed. According to the literature [5], this new peak is associated with the formation of sil-

icates. Relating this to the fact that a certain amount of Na is incorporated into the NaOH-exposed PTS surfaces, it is possible to assume that the silicates formed correspond to the Na-related silicate compounds as a reaction product, yielded by the attack of NaOH on the Si-O-Si linkages. The asymmetric feature of O_{1s} spectrum for the control (a) can be deconvoluted into at least three components situated at 532.4, 531.3, and ≈529.4 eV. The major component at 532.4 eV belongs to the bridging oxygens binding two Si atoms (the siloxane bond), while the Ti-bound oxygen in the Ti-O-Si linkages relates to the peak emerging at 531.3 eV [6]. Assuming that the non-bridging oxygens such as the hydroxylated silicon (Si-OH) are present at the PTS surface, the weak peak at ≈529.4 eV, which is about 3.0 eV lower than that of the bridging oxygens in the Si-O-Si, is attributable to non-bridging oxygens [7]. The intensity of this non-bridging oxygen peak increased remarkably as the coating film was exposed to NaOH (see O_{1s} (b) curve).

The curve of the NaOH-exposed sample (b) also showed that the line intensity at 532.4 eV, originating from the bridging oxygen in Si-O-Si bonds, conspicuously decayed, while the other bridging O line (531.3 eV) in the Ti-O-Si linkages was converted into the major oxygen component. In the Ti_{2p_{3/2}} region, the control (a) has two peaks: the main line at 458.7 eV, corresponding to the titanium in the Ti-O-Si linkages, and the minor line at 459.2 eV, reflecting the titanium oxide Ti [8]. The shape of the curve of the NaOH-exposed samples (b) resembled that of the control. From these data, we conclude that the hot NaOH solution preferentially reacts with the Si-O bond rather than the Ti-O bond. As described by several investigators [9-11], such a chemical reaction breaks the Si-O-Si linkages. The mechanism of bond breakage can be represented as follows:



Some of Na-related silicate compounds generated may be dissolved in the NaOH aqueous media, because a marked elimination of Si atom from the PTS surface was observed for the NaOH-exposed samples (see table I).

On the other hand, earlier XPS survey scans of the H₂SO₄-exposed sample surfaces suggested, on the basis of the changes in atomic compositions, that the

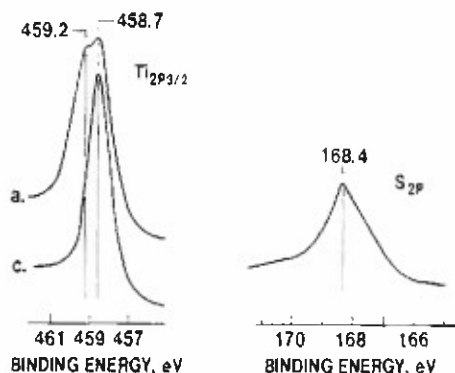
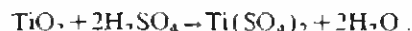


Fig. 2. $Ti_{2p_{3/2}}$ and S_{2p} regions for H_2SO_4 -treated (c) and untreated (a) PTS surfaces.

noteworthy elements are Ti and S atoms. Therefore, we closely inspected the $Ti_{2p_{3/2}}$ and S_{2p} regions, shown in fig. 2. In the $Ti_{2p_{3/2}}$ region, the peak feature (c) of H_2SO_4 -treated PTS surfaces, compared with that of the control (a), was characterized by a considerable attenuation of the line at 459.2 eV originating from Ti in the TiO_2 . The S_{2p} region for H_2SO_4 -

treated surfaces indicated the presence of the peak emerging at the BE position near 168.4 eV. We believe that the assignment of this peak is due to the formation of sulphate-related compounds [12]. In correlation with a decline in the intensity of the TiO_2 titanium line, it is reasonable to assume that the sulphate-related compounds formed by the attack of H_2SO_4 to the TiO_2 are associated with titanium sulphate $[Ti(SO_4)_2]$:



This finding can be supported by Tanabe and Yamaguchi's [13] observations of the role of the catalytic activity between the SO_4^{2-} and the metal oxides. They reported that a high catalytic reaction can be observed from the SO_4^{2-}/ZrO_2 , $/TiO_2$, and $/Fe_2O_3$ systems; by contrast, the SO_4^{2-}/SiO_2 and $/B_2O_3$ systems show no catalytic behavior.

Fig. 3 is a SEM micrograph of the PTS coatings before exposure to the NaOH and H_2SO_4 solutions. The thickness of coating film determined with a surface profile measuring system was $\approx 10 \mu m$. As seen in the SEM image, such a thick film adhering to the

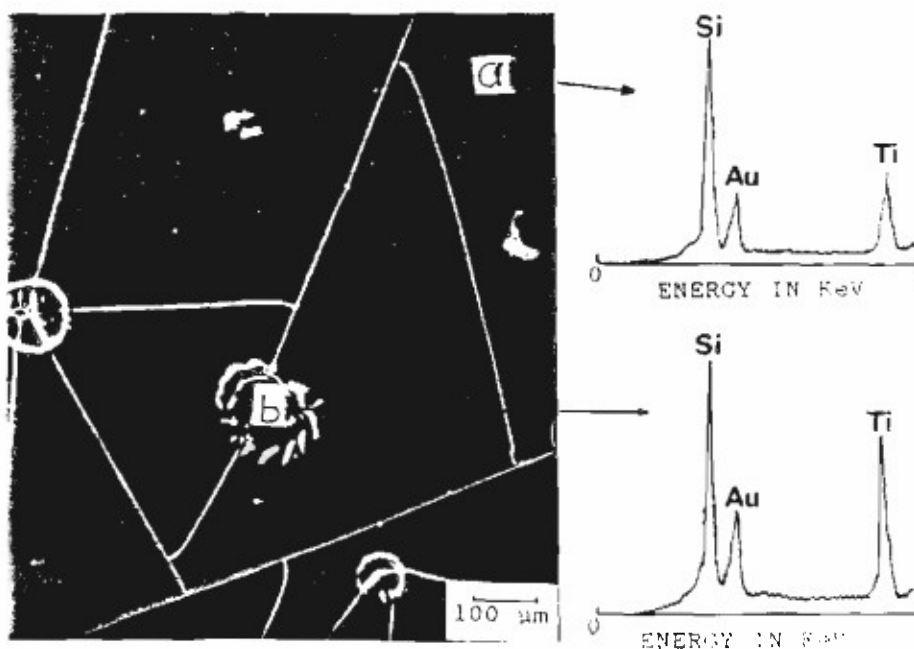


Fig. 3. SEM micrograph coupled with EDX spectra for PTS coating deposited to aluminum substrate.

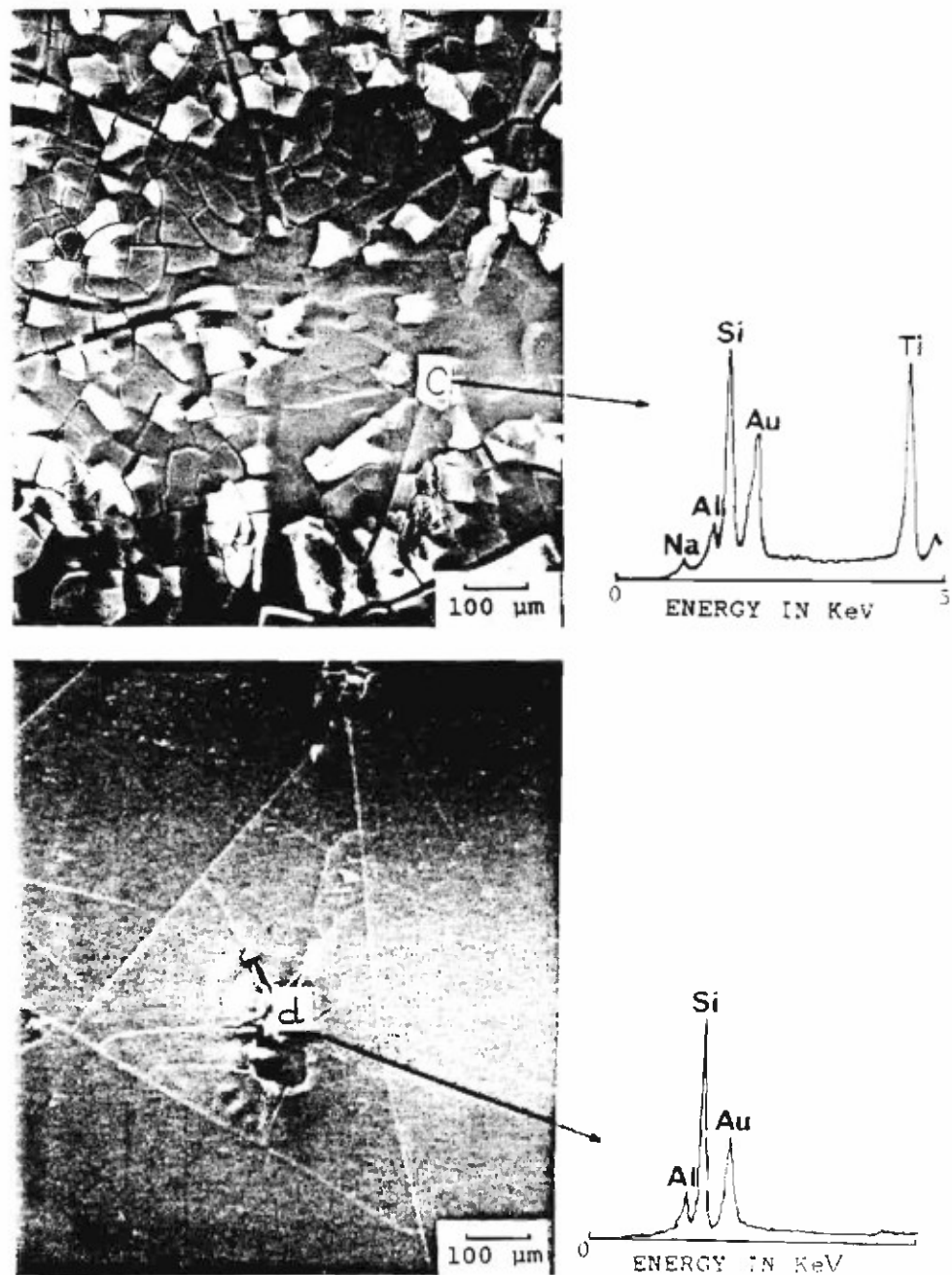


Fig. 4. SEM-EDX inspections for NaOH-exposed (top) and H_2SO_4 -exposed (bottom) PTS coatings.

substrate causes the development of stress micro-cracks as the film shrinks during the volatilization of carbonaceous species of the sintering coating film at the pyrolytic temperature. However, a crack-free coating film can be formed if the film thickness is designed to be under 2.0 μm . EDX data coupled to SEM showed the presence of two distinctive phases in the surface: (1) a smooth area (a), and (2) a rough area (b) which encompasses a circular shape isolated from the body of the film. Comparing with that of area (a), the EDX spectrum of area (b) was characterized by showing an increased intensity of the Ti peak, suggesting that area (b) has a higher concentration of Ti than area (a). Thus, the segregated rough area is explicable as an amorphous PTS layer containing a certain amount of TiO_2 .

Dramatic changes in the surface texture of the film were observed from coatings exposed to 80°C –1.0 M NaOH solution (see fig. 4, top). The alkali metal-induced bond breakages of Si–O–Si linkages in the PTS structure not only result in a significantly increased number and size of the cracks, but also in the partial separation of the chipped film from the substrate. EDX inspection of damaged area (c) shows the presence of a large number of Si and Ti atoms and few Na and Al atoms. Since the Al signal comes from the substrate, NaOH-damaged PTS films display discontinuous features. By comparison, no significant damage of the film was observed in the 30°C –1.0 M H_2SO_4 exposed sample surfaces (see fig. 4, bottom), except for the appearance of localized pits. The EDX spectrum in the pitted areas (d) indicated no signal of Ti and S. We believe that these elements were removed due to the dissolution of water-soluble titanium sulphate formed by the reaction of TiO_2 with H_2SO_4 .

4. Conclusions

Pre-ceramic-type polytitanosiloxane (PTS) coating films, synthesized through the hydrolysis–dehy-

drochlorinating–pyrolysis, were exposed to solutions of NaOH and H_2SO_4 to investigate the chemical degradation of the PTS film. The magnitude of susceptibility of the Si–O link to NaOH-induced bond breakages was significantly higher than that of Ti–O in the PTS network structure consisting of Ti-cross-linked polysiloxane. The formation of water-soluble Na-related silicate compounds and hydroxylated silicon compounds from the reaction of NaOH with Si–O–Si linkage severely damaged the PTS film. Although the PTS films displayed a great resistance in H_2SO_4 , SO_4^{2-} ions preferentially reacted with TiO_2 formed locally into the amorphous PTS body, rather than with the Si–O–Si and Si–O–Ti linkages. The water-soluble Ti sulphate compounds yielded in this reaction led to pitting of the PTS film.

References

- [1] T. Sugama, L.E. Kukacka and N. Carciello, *Progr. Organic Coat.* 18 (1990) 173.
- [2] T. Sugama and C. Taylor, Brookhaven National Laboratory, Upton, New York (1990) BNL 44752.
- [3] B. Carriere, J.P. Deville, D. Brionn and J. Escard, *J. Electron Spectry, Related Phenom.* 10 (1977) 85.
- [4] T.E. Madey, C.D. Wagner and A. Joshi, *J. Electron Spectry, Related Phenom.* 10 (1977) 359.
- [5] C.D. Wagner, D.E. Passoja, H.F. Hillery, T.G. Kinisky, H.A. Six, W.T. Jansen and J.A. Taylor, *J. Vacuum Sci. Technol.* 21 (1982) 933.
- [6] H. Nasu, J. Heo and J.D. Mackenzie, *J. Non-Cryst. Solids* 99 (1988) 140.
- [7] R. Caracciolo and S.H. Gofalimi, *J. Am. Ceram. Soc.* 71 (1988) C-346.
- [8] M. Murata, K. Wakino and S. Ikeda, *J. Electron Spectry, Related Phenom.* 6 (1975) 459.
- [9] S.W. Feriman, *Ceram. Bull.* 67 (1988) 392.
- [10] H. Hirayama, T. Kawakubo, A. Goto and T. Kaneko, *J. Am. Ceram. Soc.* 72 (1989) 2049.
- [11] T. Uchino, T. Sakka, K. Hotta and M. Iwasaki, *J. Am. Ceram. Soc.* 72 (1989) 2173.
- [12] B.J. Lindberg, K. Hamrin, G. Johansson, U. Gelius, A. Fahlman, C. Nordling and K. Siegbahn, *Physica Scripta* 1 (1970) 286.
- [13] K. Tanabe and T. Yamaguchi, *Crit. Rev. Surface Chem.* 1 (1990) 1.

Pyrolysis-induced polymetallosiloxane coatings for aluminium substrates

T. SUGAMA

Process Sciences Division, Department of Applied Science, Brookhaven National Laboratory, Upton, NY 11973, USA

C. TAYLOR

University of Virginia, Chemistry Department, McCormick Road, Charlottesville, VA 22901, USA

Inorganic amorphous polymetallosiloxane (PMS) coating films on aluminium substrate were produced through the polycondensation-pyrolysis reaction mechanisms of a sol-precursor solution. The precursor solution was formed by HCl-catalysed hydrolysis of a mixture of *N*-[3-(triethoxysilyl)propyl]-4,5-dihydroimidazole (TSPI) and $M(OC_3H_7)_n$ ($M = Zr, Ti$ and Al , $n = 3$ or 4). The TSPI/ $Zr(OC_3H_7)_4$ or $Ti(OC_3H_7)_4$ precursor systems formed higher quality thin coating films, compared to the $Al(OC_3H_7)_3$ system. This was because of the critical formation of the polyorganosiloxane terminated by end groups containing zirconium and titanium oxides. These end groups were derived by a dechlorinating reaction between the Cl, bonded to the propyl C in organosilane, and the hydroxylated Zr or Ti compounds in the sintering stages of the film production. Good film-forming performance resulted from moderate degrees of cross-linking of metal oxides to polysiloxane chains and of the densification of metal -O-Si linkages in the pyrolysis-induced PMS network. In addition to these factors, the formation of an oxane bond at the interface between PMS and aluminium provided corrosion protection for the aluminium substrate.

1. Introduction

In the previous work [1], the inorganic polytitanosiloxane (PTS) polymers were synthesized by a polycondensation-pyrolysis reaction processes of sol-precursor solution systems consisting of monomeric organosilanes, $Ti(OC_2H_5)_4$, methanol, water and hydrochloric acid. These PTS polymers were investigated for applicability as corrosion-resistant inorganic polymer coatings for aluminium substrates. A simple dip-coating method was used to deposit the sol-precursor solution layers on the substrates in this investigation. The precursor layer was converted into a sintered coating film by pre-heating in air at 100°C , and then annealing at 300°C to form the pyrolysed PTS film. Simple dip-coating technology, a practical application method, offered the following two major advantages: (1) the possibility of placing high-temperature-performing inorganic polymeric coatings on low melting point metal substrates, and (2) the ability to coat substrates with a large surface area by a simple, inexpensive, and efficient method which is compatible with a large-scale, integrated, continuous process run at relatively low temperatures of less than 400°C . On the other hand, a serious disadvantage is the shrinkage of PTS films caused primarily by the release of carbonaceous species during the annealing processes. This led to the development of stress cracks and pits, thereby resulting in poor protection behaviour by the coatings.

Although the cross-linking ability of the hydroxylated Ti compounds, which connect polysiloxane chains, suppresses the development of these cracks, it was found that the degree of the shrinkage depends upon several factors: (1) the species of monomeric organosilane used as a starting material, (2) the organosilane to $Ti(OC_2H_5)_4$ ratio, (3) the densification of Ti-O-Si linkages, and (4) the number and length of the hydrocarbon chains connecting Ti and Si in the sintered polyorganosilane that contains titanium oxide terminated and substituted end groups. The most effective organosilane precursor for forming PTS coating films containing fewer stress microcracks, was *N*-[3-(triethoxysilyl)propyl]-4,5-dihydroimidazole (TSPI). Thick PTS coatings (thickness, $> 10\ \mu\text{m}$) derived from the appropriate ratio of TSPI/ $Ti(OC_2H_5)_4$ displayed good corrosion protection for aluminium upon exposure to NaCl solutions.

Detailed studies regarding the hydrolysis activity of the HCl catalyst which plays an important role in forming the metal oxide cross-linked polysiloxane networks and in altering the conformation over the temperature range 100 – 400°C for the TSPI-titanium alkoxide precursor systems, have not yet been performed. Our research focused on the use of other metal alkoxide species such as $Al(OR)_3$ and $Zr(OR)_4$ ($R = C_3H_7$). In addition, the fabrication of thin film (thickness $< 1\ \mu\text{m}$), which may form a microcrack-

free coatings, because of lower rates of volatility and pyrolysis, was also considered.

Accordingly, the objectives in the present study concerned essentially two research areas. One was to study the thermal behaviour, polycondensation-pyrolysis reaction mechanisms, and the reaction products of the sintered TSPI-metal alkoxide systems. In the second, the surface and interface characteristics of sol-derived thin films as a corrosion-protective coatings on aluminium substrates were evaluated.

2. Experimental procedure

2.1. Materials

The *N*-[3-(triethoxysilyl)propyl]-4,5-dihydroimidazole (TSPI), was used as a network-forming monomeric organoalkoxysilane. The metal alkoxides employed as cross-linking agent were aluminium, titanium(IV), and zirconium(IV) isopropoxides.

The film-forming mother liquor, which served as the precursor solution, was prepared by incorporating the TSPI- $M(OC_3H_7)_n$ ($M = Al, Ti$ and Zr , $n = 3$ or 4) mixture into a methyl alcohol/water mixing medium containing an appropriate amount of HCl. In order to produce a clear precursor solution, it was very important to add the HCl, as a hydrolysis accelerator, to the blending material, thereby forming a uniform coating film on the metal substrates. The mix compositions for the precursor solution systems used in this study are given in Table I.

The metal substrate used in the experiments was 2024-T3 clad Al sheet containing the following chemical constituents: 92 wt % Al, 0.5 wt % Si, 0.5 wt % Fe, 4.5 wt % Cu, 0.5 wt % Mn, 1.5 wt % Mg, 0.1 wt % Cr, 0.25 wt % Zn, and 0.15 wt % others.

The oxide etching of the Al was carried out in accordance with a well-known commercial sequence called the Forest Products Laboratory (FPL) process [2]. As the first step in the preparation, the surfaces were wiped with acetone-soaked tissues to remove any organic contamination. They were then immersed in chromic-sulphuric acid ($Na_2Cr_2O_7 \cdot 2H_2O : H_2SO_4$: water = 4:23:73 by weight) for 10 min at 80°C. After etching, the fresh oxide surfaces were washed with deionized water at 30°C for 5 min, and subsequently dried for 15 min at 50°C.

Coating of the Al surfaces using the sol system was performed in accordance with the following sequence. The FPL-etched Al substrate was dipped into the precursor solution at ambient temperature. The sub-

strate was then withdrawn slowly from the soaking bath, after which the substrate was preheated in an oven for 20 h at a temperature of 150°C to yield a sintered coating. The samples were subsequently annealed for 30 min at 350°C.

2.2. Measurements

The combined techniques of thermogravimetric analysis (TGA), infrared (IR), X-ray powder diffraction (XRD), and X-ray photoelectron spectroscopy (XPS) were used to obtain fundamental data regarding the condensational and pyrolytic changes in conformation, surface and interface chemical components and states, as well as the degree of network cross-linking for the metal alkoxide-modified organosilane polymers at temperatures up to 350°C.

The surface microstructure and elements of the films after deposition on the Al substrate were observed using scanning electron microscopy (SEM) in conjunction with energy-dispersive X-ray (EDX) analysis.

The electrochemical testing for data on corrosion was performed with an EG&G Princeton Applied Research Model 362-1 Corrosion Measurement System. The electrolyte was a 0.5 M sodium chloride solution made from distilled water and reagent grade salt. The specimen was mounted in a holder and then inserted into a EG&G Model K47 electrochemical cell. The tests were conducted in an aerated 0.5 M NaCl solution at 25°C, on an exposed surface area of the 1.0 cm². The polarization curves containing the cathodic and anodic regions were measured at a scan rate of 0.5 mV s⁻¹ in the corrosion potential range of -1.2 to -0.3 V.

3. Results and discussion

3.1. Characteristics of sintered organometallicsilane compounds

Before assessing the properties of polymetallosiloxane (PMS) coating films deposited on Al substrates, the thermal and chemical characteristics of the metal alkoxide-modified organosilane compounds were explored using TGA, IR, and XRD techniques. The specific areas of study were the thermal decomposition process, phase-related transitions, pyrolytic changes and rearrangements in conformation, and the crystallization of the sol-gel derived organometallicsilane compounds.

TABLE I Compositions of clear precursor solutions used in various $M(OC_3H_7)_n$ -modified TSPI systems. ($M = Zr, Ti, Al$, $n = 3$ or 4)

TSPI/ $M(OC_3H_7)_n$ (wt ratio)	TSPI (wt %)	$Zr(OC_3H_7)_4$ (wt %)	$Ti(OC_3H_7)_4$ (wt %)	$Al(OC_3H_7)_3$ (wt %)	CH_3OH (wt %)	Water (wt %)	HCl (wt % of TSPI + $M(OC_3H_7)_n$)
100/0	50				30	20	12
70/30	35	15			30	20	20
50/50	25	25			30	20	30
70/30	35		15		30	20	15
50/50	25		25		30	20	25
70/30	35			15	30	20	40
50/50	25			25	30	20	50

The aim in this broad exploration was to understand the thermal decomposition process and the transition of the sintered organometallicsilane to its inorganic polymer phase by pyrolysis in an air environment. From the mix compositions given in Table I, 150 °C sintered powder samples with 100/0 and 50/50 TSPI/M(OC₃H₇)_{4 or 3} weight ratios were selected. Their TGA curves are depicted in Fig. 1. The onset temperatures of decomposition were obtained by finding the intersection point of the two linear extrapolations. As one can see, the onset temperature depends upon the species of metal alkoxide reagent added to the TSPI. The beginning of thermal decomposition for all of the samples, with the exception of the Al(OH₃H₇)₃-TSPI system, is likely to occur over the temperature range 300–350 °C. Decomposition of the TSPI/Al(OC₃H₇)₃ system started at a lower temperature (200 °C) than the other metal alkoxide systems. The weight loss curve of bulk TSPI exhibited the two step decomposition process: the first step occurring at a temperature between 350 and 430 °C and the second step ranging from 430–600 °C. The former change might be associated with the liberation of hydrocarbon and chemisorbed water; the latter may be caused by the removal of excess carbon in the samples. Beyond the annealing temperature of 600 °C, the curve levels off, implying that the conversion into inorganic phases is essentially complete. Although the curve shapes of the TSPI/M(OC₃H₇)_{4 or 3} systems are unlike that of the bulk TSPI, the final transition temperature to the inorganic phase was almost the same as the bulk TSPI. When compared to the weight loss (approximately 42%) of TSPI at 600 °C, less of a weight loss was observed for the Ti(OC₃H₇)₄ system, whereas the Al(OC₃H₇)₃ system had considerable mass loss, approximately 68%. This large weight loss caused by the pyrolysis could be associated with an enhanced degree of shrinkage of the precursor coating films that results in cracking and delamination of the films from the substrates.

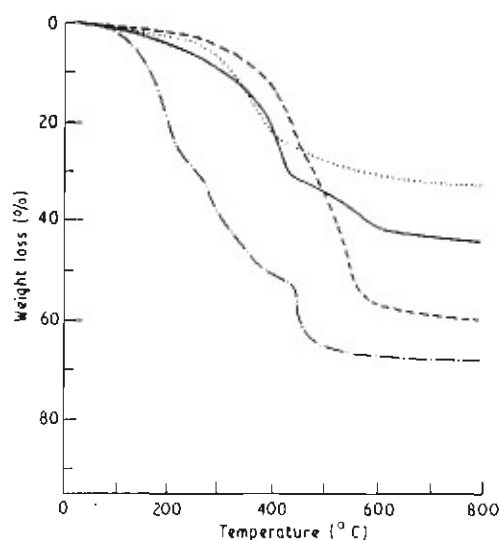


Figure 1 TGA curves of metal isopropoxide-modified and unmodified TSPI powders after sintering at 150 °C: (—) TSPI, (---) Zr(OC₃H₇)₄-TSPI, (·····) Ti(OC₃H₇)₄-TSPI, (- · - ·) Al(OC₃H₇)₃-TSPI.

Based upon TGA data, the pyrolytic changes and rearrangements in conformation at 350 °C were studied with IR. Fig. 2 shows the IR absorption spectra for 150 °C-preheated powder samples of bulk TSPI and the TSPI/metal alkoxide, 50/50 ratio samples. The IR analyses were conducted using the KBr method which incorporates the powder samples of 2–3 mg into KBr pellets of approximately 200 mg. For the metal alkoxide-TSPI samples and the TSPI bulk sample, the various absorption peaks and their assignments are shown in Fig. 2 and Table II. In the TSPI bulk sample (Fig. 2a), the shoulder peak due to the superposition of physically absorbed water and hydrogen-bonded O–H stretching in silanol Si–OH groups is located at 3450 cm⁻¹ [3]. Because no N–H bond exists in the monomeric TSPI used as a starting material, the peak assignment at 3240 cm⁻¹ seems to reveal a newly developed N–H stretching mode in the dihydroimidazole [4]. The bands around 2930 and 2880 cm⁻¹ are attributed to absorptions due to the C–H stretching mode in the methylene chains and dihydroimidazole rings. The C–H bending mode peaks appear at 1435 and 1395 cm⁻¹. An intense absorption peak, observed at 1655 cm⁻¹, is ascribed to the imine, C=N–, stretching vibration in the five-membered dihydroimidazole rings [5]. Five-membered heterocycles commonly have two other fundamental ring stretching bands at frequencies ranging from 1670–1400 cm⁻¹ [6]. Thus, the weak peak near 1525 cm⁻¹ could reflect on the ring-stretching modes. The other peak corresponding to the heterocyclic rings may be masked by strong C–H absorption in the vicinity of 1430 cm⁻¹. The pronounced peak at 1135 cm⁻¹ verifies the existence of the stretching mode of the Si–O–C bond in the Si-joined alkoxy groups [7]. As is well known [3], the peaks at 1035 and 775 cm⁻¹ are associated with the stretching of Si–O–Si and the bending of Si–O–Si bonds, respectively. These bonds in the polymeric organosilane are formed by the condensation reactions between neighbouring silanol functions. The new peak developed at 695 cm⁻¹ can be assigned to the C–Cl stretching band in the chlorinated compounds [8]. The development of this C–Cl band can be

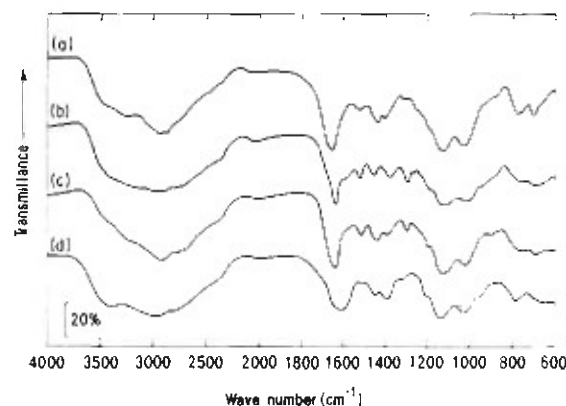
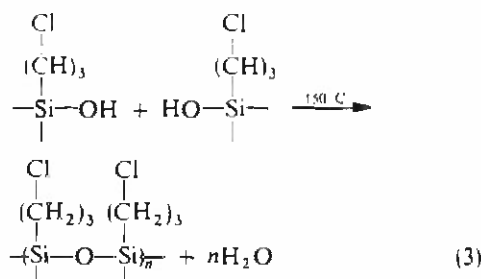
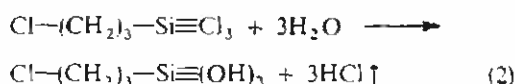


Figure 2 IR adsorption spectra for 150 °C-sintered powder samples having 100/0 and 50/50 TSPI M(OC₃H₇)_{4 or 3} ratios: (a) TSPI, (b) TSPI/Zr(OC₃H₇)₄, (c) TSPI/Ti(OC₃H₇)₄, and (d) TSPI/Al(OC₃H₇)₃.

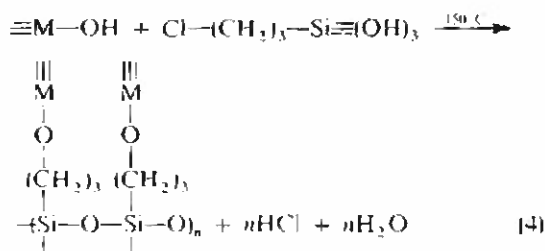
explained if the emergence of the N-H peak at 3240 cm^{-1} is taken into consideration. Because the imidazole group in TSPI acts as a strong base by accepting a proton [9], the nucleophilic attack of H^+ to the dihydroimidazole N bonded to the propyl group in the HCl media leads to the cleavage of the N- CH_2 linkage [10]. Then this bond breakage forms the imidazoline as derivative of dihydroimidazole,



and polymeric organosilane containing Cl-substituted end groups. This HCl-catalysed hydrolysis-polycondensation reaction will occur according to the following sequence



On the basis of the information, the spectral features of the metal alkoxide-modified TSPI samples were investigated to identify the reaction products of TSPI with metal alkoxides at a low temperature, 150°C . Compared with the spectrum for bulk TSPI, characteristics noted for the $\text{Zr}(\text{OC}_3\text{H}_7)_4$ - and $\text{Ti}(\text{OC}_3\text{H}_7)_4$ -systems spectra (Fig. 2b and c) are as follows: (1) the appearance of a notable peak near 1300 cm^{-1} which corresponds to metal (Zr and Ti) -O-C linkages [11], (2) the loss in C-Cl peak intensity at 695 cm^{-1} , and (3) no remarkable peak present around 950 cm^{-1} which would be attributable to the Zr- or Ti-O-Si linkages [3, 12] in the PMS formed. As a result, it is believed that the hydroxyl groups derived from the HCl-catalysed hydrolysis of $\text{Zr}(\text{OC}_3\text{H}_7)_4$ and $\text{Ti}(\text{OC}_3\text{H}_7)_4$, react preferentially with the Cl in Cl-substituted end groups in the silane compound, rather than the silanol groups which are formed by hydrolysis of the ethoxysilyl groups in the TSPI. The proposed reaction mechanism for this is shown below



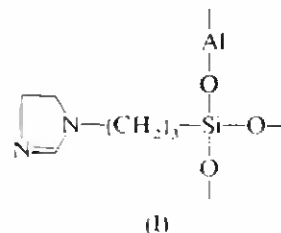
where M = Zr or Ti.

At 150°C , the two major components, polymeric organosilane containing oxygen-bridged metal compounds and isolated dehydroimidazole derivative, appear to be present in the pre-heated materials.

To support the proposed reaction mechanism, the absorbance ratios between the M-O-C peak at 1300 cm^{-1} and the C-Cl peak at 695 cm^{-1} were computed as a function of the TSPI/ $\text{M}(\text{OC}_3\text{H}_7)_4$ ratio. As expected, the resultant data (see Fig. 3) indicate that the absorbance ratios increase with an increase in the proportion of $\text{M}(\text{OC}_3\text{H}_7)_4$. This, thereby, implies that the reaction of the halide with the OH in the hydroxylated metals favours the elimination of

hydrogen chloride. The formation of Cl-terminated end groups plays an important role in creating the M-O-C linkages.

On the other hand, the introduction of $\text{Al}(\text{OC}_3\text{H}_7)_3$ reagent into the TSPI results in many different features being present in the spectrum (Fig. 2d). Specifically, no peaks from the N-H stretching and ring-stretching modes in the dihydroimidazole derivative at 3240 and 1525 cm^{-1} , the M-O-C linkage band at 1300 cm^{-1} and the C-Cl bond peak at 695 cm^{-1} , were found. However, two new absorption frequencies around 1590 and 945 cm^{-1} did emerge. Because dihydroimidazole ring stretching in monomeric TSPI is discernible from a strong peak in the vicinity of 1610 cm^{-1} (not shown), the first of the new peaks may reveal the presence of the original dihydroimidazole attached to the propyl C of TSPI. The formation of Al-O-Si linkages possibly explains the new absorption band at 945 cm^{-1} [13, 14]. Therefore, compared to the $\text{Zr}(\text{OC}_3\text{H}_7)_4$ - and $\text{Ti}(\text{OC}_3\text{H}_7)_3$ -TSPI systems, a different reaction process occurs in the $\text{Al}(\text{OC}_3\text{H}_7)_3$ -TSPI system. Questions as to why this system does not produce heterocyclic derivatives and the Cl-substituted end groups still remain. It is evident that polymeric organoaluminosilane network structures containing Al-O-Si linkages do form at 150°C . The conformation of this hypothetical reaction product may be as follows:



The IR studies were further extended in an attempt to understand and clarify the pyrolytic conformation changes in inorganic PMS produced by annealing in air at high temperatures. All of the 150°C pre-heated samples were heated for 12 h in air at 350°C . Fig. 4

TABLE II Summary of the assignments of IR absorption detected in the spectra of bulk TSPI sample at 150 °C

Wave numbers (cm ⁻¹)	Vibration ^a	Absorbing species
3450	νOH	H-O-Si and H ₂ O
3240	νNH	H-N in dihydroimidazole derivative
2930	νCH	-CH ₂ - and dihydroimidazole derivative
2880	νCH	-CH ₂ - and dihydroimidazole derivative
1655	νCN	-C=N- in dihydroimidazole derivative
1525	ν ring	in dihydroimidazole derivative
1435	δCH and ν ring	-CH ₂ - and dihydroimidazole derivative
1395	δCH	-CH ₂ - and dihydroimidazole derivative
1135	νSi-O-C	Si-O-C ₂ H ₅
1035	νSi-O-Si	Si-O-Si
775	δSi-O-Si	Si-O-Si
695	νC-Cl	Cl-CH ₂ -

^a ν denotes stretching vibration. δ denotes bending vibration.

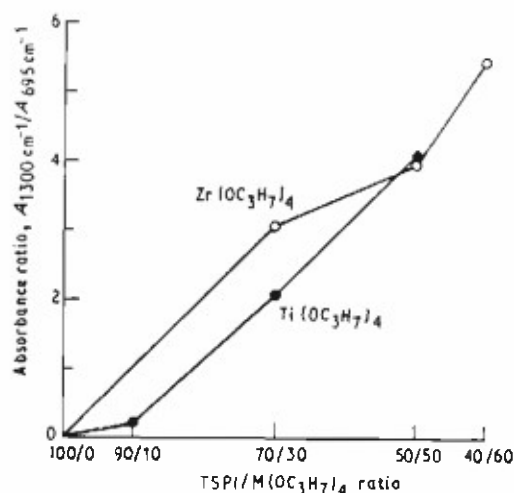


Figure 3 Variations in absorbance ratio of M-O-C at 1300 cm⁻¹ to C-Cl at 695 cm⁻¹ as a function of TSPI/M(OC₃H₇)₄ ratios.

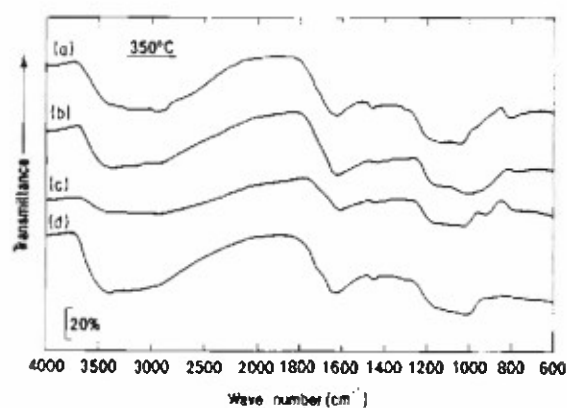
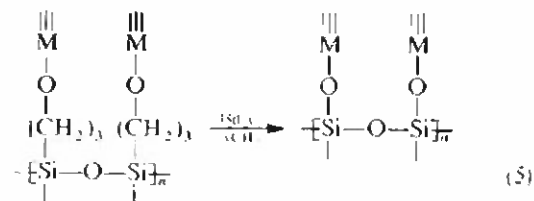


Figure 4 IR spectra for 350 °C annealed 100/0 and 50/50 TSPI/M(OC₃H₇)₄ systems: (a) TSPI, (b) TSPI/Zr(OC₃H₇)₄, (c) TSPI/Ti(OC₃H₇)₄, and (d) TSPI/Al(OC₃H₇)₄.

illustrates the IR spectra for the 350 °C annealed sample series. The bulk TSPI sample spectrum (Fig. 4a) changed markedly, compared with the 150 °C treated sample spectra. These changes are as follows: (1) a considerable loss in intensity of the peaks at 2930,

2880, 1435 and 1395 cm⁻¹, (2) a slight shift of the C=N- band at 1655 cm⁻¹ toward lower wave numbers (1620 cm⁻¹), (3) a decrease in intensity of the peak around 1135 cm⁻¹ corresponding to a decrease in Si-CH₂- bonds, and (4) a disappearance of the C-Cl peak at 697 cm⁻¹. Changes (1), (3) and (4) result directly from the elimination of a large amount of carbonaceous groups such as CH₂O and CH₃CHO from the polymeric organosilane networks. The absorption band near 3400 cm⁻¹ and a weak band around 1450 cm⁻¹, are due to the superposition of ring stretching and H-O-H bending vibrations. Thus, around 350 °C the polymeric organosilane is believed to be pyrolytic converted into the inorganic polysiloxane network. Nevertheless, some residual imidazole derivative still remains in the polysiloxane network.

Attention was then focused on the spectra for the TSPI/Zr(OC₃H₇)₄ (Fig. 4b) and TSPI/Ti(OC₃H₇)₄ (Fig. 4c) systems. The depicted spectrum features of annealed samples were characterized by the development of new peaks at 950 cm⁻¹ (b) and 930 cm⁻¹ (c). These absorption bands signify the formation of Zr-O-Si or Ti-O-Si linkages, respectively. The predominance of the Si-O-Si band around 1020 cm⁻¹, proves that the inorganic PMS structures can be formed at 350 °C through the pyrolytic *in situ* transformation processes shown below



Where M = Zr or Ti. Under annealing conditions, these pyrolytic conformation changes occur with the elimination of numerous organic groups. Once the organopolysilane inorganic PMS transition is completed, the Zr and Ti metal oxides located in the networks act as cross-linking agents which connect the polysiloxane chains.

In contrast, the spectrum for the postannealed TSPI/ $\text{Al}(\text{OC}_3\text{H}_7)_3$ system indicated the shift in the Si-O-Si band at 1035 cm^{-1} to a lower position of 1000 cm^{-1} and the disappearance of the 950 cm^{-1} peak corresponding to the Al-O-Si linkages. The shifting and disappearance of these peaks render the thermal decompositions of 150°C -formed organopolyaluminosilane as a means of the bond breakages of Al-O-Si linkages. This strongly suggests that the Al-O-Si bond-based network structures, which are formed readily at a low temperature of 150°C , are vulnerable to pyrolysis. However, conformation of the pyrolytically assembled PMS, which is represented by the metal oxide cross-linked polysiloxane networks, is responsible for the development of high-temperature-performance inorganic polymer structures.

In addition to TGA and IR analyses, an XRD study was considered necessary to determine whether the pyrolysed materials had crystallized. Fig. 5 represents the XRD patterns of the 350°C annealed metal alkoxide-TSPI systems, over the diffraction range $0.444\text{--}0.182\text{ nm}$. For the $\text{Zr}(\text{OC}_3\text{H}_7)_4$ (a) and $\text{Al}(\text{OC}_3\text{H}_7)_3$ (b) systems, no spacing lines were detected over this diffraction range. Hence, this indicates that the PMS in these systems is essentially amorphous. In contrast, the reflections at 0.353 , 0.236 and 0.190 nm for the TSPI/ $\text{Ti}(\text{OC}_3\text{H}_7)_4$ system are attributable to the presence of a certain amount of anatase, TiO_2 , crystalline particles in the amorphous polytitanosiloxane layers.

3.2. Characteristics of PMS coating films

On the basis of the above findings, the investigations were focused on understanding the physico-chemical factors governing the formation and fabrication of high-quality PMS coating films. Uniformity and continuity were studied using surface and interface analytical tools such as SEM-EDX, and XPS. As described earlier in Section 1, thin PMS films with a thickness of up to $0.5\text{ }\mu\text{m}$ are of particular interest to this study. To obtain a thin coating film, 20 g of the original precursor sol solution (shown in Table I) was diluted with 80 g deionized water. First the FPL-etched Al substrate was dipped into the diluted film-forming precursor solution, and then sintered in an oven at 150°C for 20 h . In order to form the pyrolysis-

induced PMS coating films, the 150°C sintered samples were subsequently annealed for 30 min at 350°C . The thickness of the PMS film deposited on the substrate was determined using a surface profile measuring system. The average thickness of the films derived from the precursor solution consisting of 100/0, 70/30, and 50/50 TSPI/ $\text{M}(\text{OC}_3\text{H}_7)_4$ or $_3$ ratios, ranged approximately, from $0.2\text{--}0.4\text{ }\mu\text{m}$.

Fig. 6 shows a scanning electron micrograph for the metal oxide-uncross-linked polysiloxane (PS) originating from the 100/0 ratio precursor. The surface microstructure of this pyrolysed film reveals a large number of pits and microcracks. The EDX spectrum (not shown) accompanying the SEM image indicated Si to be a principle component of the film, but Cl was not detected in the film. Thus, the HCl which was used as a hydrolytic catalyst of TSPI was probably eliminated from the sintered precursor films during the pyrolysis at 350°C . Therefore, possible attack to the Al substrate by corrosive dissociated Cl ions was disregarded. Although some microcracks were present, the polyzirconosiloxane (PZS) film derived from the 70/30 TSPI/ $\text{Zr}(\text{OC}_3\text{H}_7)_4$ ratio precursor (Fig. 7a), exhibited far better coating features and no pits. EDX quantitative evaluation of this film indicated that no Cl was present and that the Zr to Si intensity count ratio was 0.17 . Compared with the 70/30 ratio sample, the 50/50 ratio-derived PZS film had numerous microcracks (Fig. 7b). Hence, the incorporation of an excessive amount of $\text{Zr}(\text{OC}_3\text{H}_7)_4$ in TSPI leads to the generation of stresses within the film brought about by differences in the thermal expansion and/or the differential shrinkage between the film and substrate during pyrolysis.

In the case of the polyaluminosiloxane (PAS) derived from TSPI- $\text{Al}(\text{OC}_3\text{H}_7)_3$ systems, SEM images for either 70/30 (Fig. 8a) or 50/50 (Fig. 8b) ratios indicate film discontinuity and non-uniform features, and partial delamination from the substrate. These

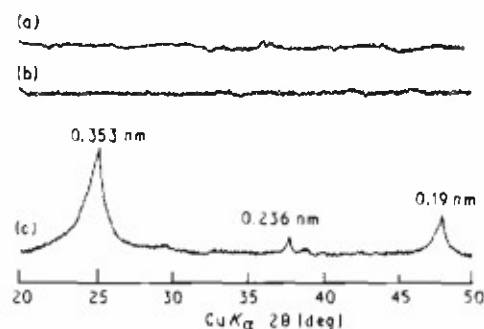
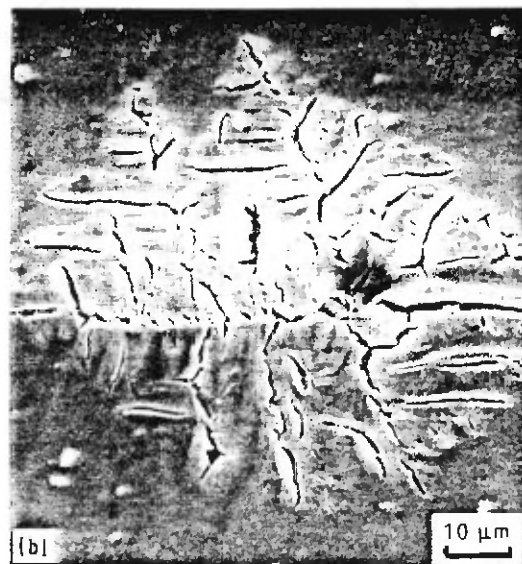
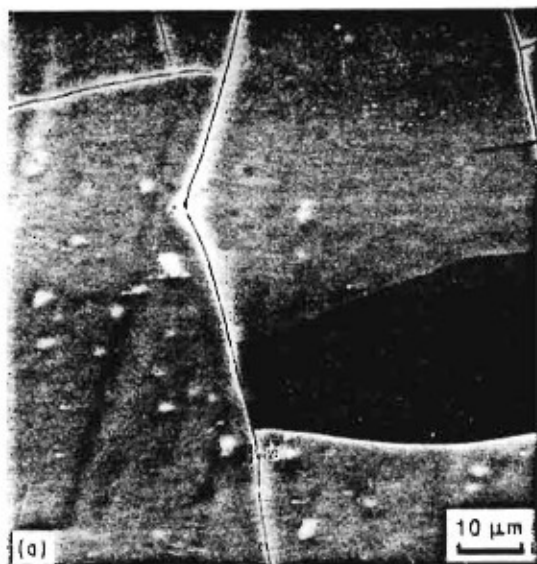


Figure 5. XRD tracings for 350°C annealed 50/50 (a) TSPI/ $\text{Zr}(\text{OC}_3\text{H}_7)_4$, (b) TSPI/ $\text{Al}(\text{OC}_3\text{H}_7)_3$ and (c) TSPI/ $\text{Ti}(\text{OC}_3\text{H}_7)_4$ systems.



Figure 6. Scanning electron micrograph of PS coating film derived from 100% TSPI at 350°C .



(c)

Element	Intensity (counts, 30s)	Intensity ratio Si
Zr	239	0.17
Si	1407	1.00
Cl	0	0.00

undesirable film-forming characteristics, in connection with the results of TGA and IR, are due presumably to great stresses generated at the film-substrate interface caused by the large weight loss and thermal decomposition of the film due to Al-O-Si linkages breaking. The most ideal PMS coating surface consists of a uniform film free of cracks and pits over large dimensions. These characteristics were observed in the 50/50 TSPI/ $\text{Ti}(\text{OC}_3\text{H}_7)_4$ ratio (Fig. 9b)-derived polytitanosiloxane (PTS). However, in the 70/30 ratio film, a few microcracks developed (Fig. 9a). It appears that the use of a proper TSPI to $\text{Ti}(\text{OC}_3\text{H}_7)_4$ proportion is one of the important factors

Figure 7. SEM (a, b) images and (c) EDX analysis of PZS coatings formed by annealing at 350 °C for 70/30 and (b) 50/50 TSPI/ $\text{Zr}(\text{OC}_3\text{H}_7)_4$ ratio precursor films.

leading to the formation of high-quality inorganic PTS amorphous coatings containing crystalline anatase particles.

Further experimental work focused on identifying the chemical components and states at the outermost surface of the various PMS coatings. XPS was used to obtain this information for coatings derived from a 70/30 TSPI/ $\text{M}(\text{OC}_3\text{H}_7)_4$ or Zr ratio precursor solution. For the scale in all the XPS spectra, the binding energy (BE) was calibrated with the C_{1s} of the principal hydrocarbon-type C peak fixed at 285.0 eV as an internal reference standard. The C_{1s} core level spectrum of the PMS surfaces was not taken into consideration, because the concentration of hydrocarbon impurities on pyrolysis-induced surfaces was negligible compared to the intensity of the signal from the

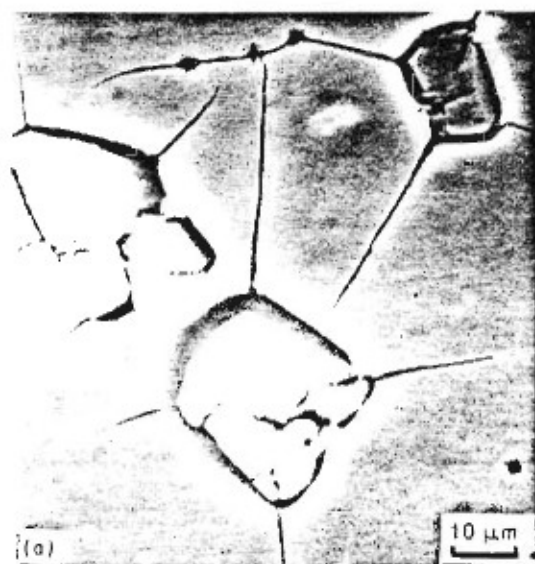
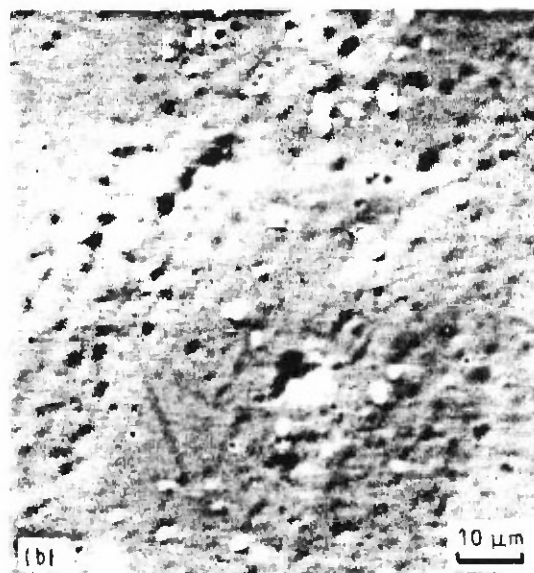
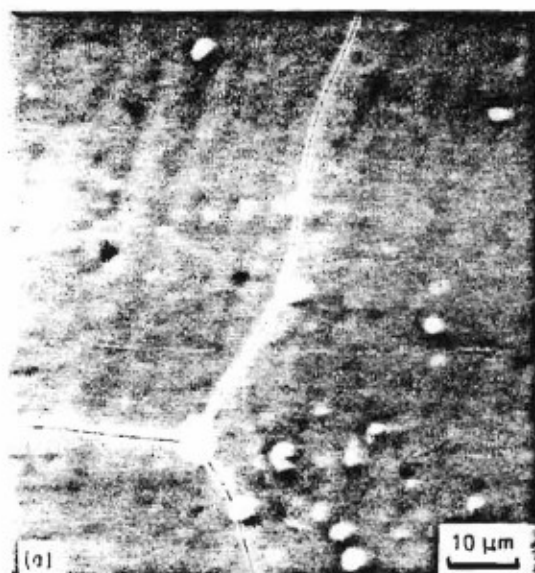


Figure 8. SEM images of 350 °C pyrolysed (a) 70/30 and (b) 50/50 TSPI/ $\text{Al}(\text{OC}_3\text{H}_7)_2$ ratio coating films.



(c)

Element	Intensity (counts, 30s)	Intensity ratio Si
Ti	2692	2.38
Si	1132	1.00
Cl	0	0.00

(d)

Element	Intensity (counts, 30s)	Intensity ratio Si
Ti	3330	7.38
Si	451	1.00
Cl	0	0.00

Figure 9 (a, b) Surface features and (c, d) EDX data of pyrolysis-induced PTS coating films; (a) 70/30 and (b) 50/50 TSPI:Ti (OC_3H_7)₄ ratio systems.

unpyrolysed samples. A curve deconvolution technique was employed to find the respective chemical components from the high-resolution spectra of each element, and to determine the relative quantity of a particular chemical state.

The Si_{2p} and O_{1s} core level photoemission spectra for the PS (derived from 100% TSPI), PZS, PTS, and PAS films are shown in Figs 10 and 11, respectively. The Si_{2p} region for the PS coating (Fig. 10a) reveals only a single peak at 102.8 eV, corresponding to the silicon in the siloxane bonds, Si-O-Si [15, 16]. Drastic changes in the position, intensity, and shape of the Si_{2p} peak were induced when zirconium, titanium and aluminium oxides were incorporated in the PS network as cross-linking agents. The Si_{2p} signal for the PZS surface (Fig. 10b) could be resolved into two Gaussian components at 101.6 and 102.8 eV. The former peak as the principal component corresponds to the silicon in the Zr-O-Si linkages [17, 18]; and the latter ascribes the siloxane Si as a minor component. The peak shape of the PTS film (Fig. 10c) is strikingly different from that of the PZS. The peak of siloxane Si emerged at 102.8 eV is of a principal component, while a shoulder peak at 101.6 eV, interpreted as the Si in the Ti-O-Si bonds, is of a minor component. This infers that the extent of cross-linking of titanium oxides in the PTS coating is lower than that of the zirconium oxides in PZS. Peak features similar to those of PZS were observed on the PAS film (Fig. 10d), suggesting that, like PZS, the surface contains a highly densified Al-O-Si network. The O_{1s} spectrum of PS (Fig. 11a) exhibits an asymmetric

shape containing a main peak at 532.4 eV originating from the bridging oxygen-bonded to two Si atoms (the siloxane bond). Assuming that the nonbridging oxygens are bonded to one Si, and more likely to one H (the hydroxylated Si) are present at the PS surface, the cause of the shoulder at ≈ 529.4 eV can be established. This shoulder, which is about 3.0 eV lower than that of the bridging oxygens in the Si-O-Si, is attributable to nonbridging oxygens [19]. In contrast, O_{1s} spectra for the PMS coatings are characterized by a broad, asymmetric peak which obviously contains at least three components situated at 532.4, 531.5, and ≈ 529.4 eV. The major component at 531.5 eV belongs to the metal-bound oxygen in the M-O-Si linkages [20]. The two shoulders at 532.4 and ≈ 529.4 eV are presumably due to the bridging oxygens in the Si-O-Si and the nonbridging oxygens in the Si-OH, respectively. The intensity of the nonbridging oxygen peak seems to depend on the species of PMS. The quantitative evaluation of Si-OH groups existing at the outermost surface was carried out by comparing the integrated intensity ratio of oxygen in Si-OH peak at approximately 529.4 eV to oxygen in the M-O-Si peak at approximately 531.5 eV. As a result, the PTS surface indicated the highest ratio of 0.53 (Fig. 11). Because the peak of TiO_2 oxygen appears near 529.4 eV [21, 22], this peak will include contributions from both SiOH and TiO_2 oxygens. Nevertheless, the presence of an appreciable number of polar OH groups at the surface of PMS is very important to adhesion. It is believed that the OH in the hydroxylated Si compound promotes the chemical

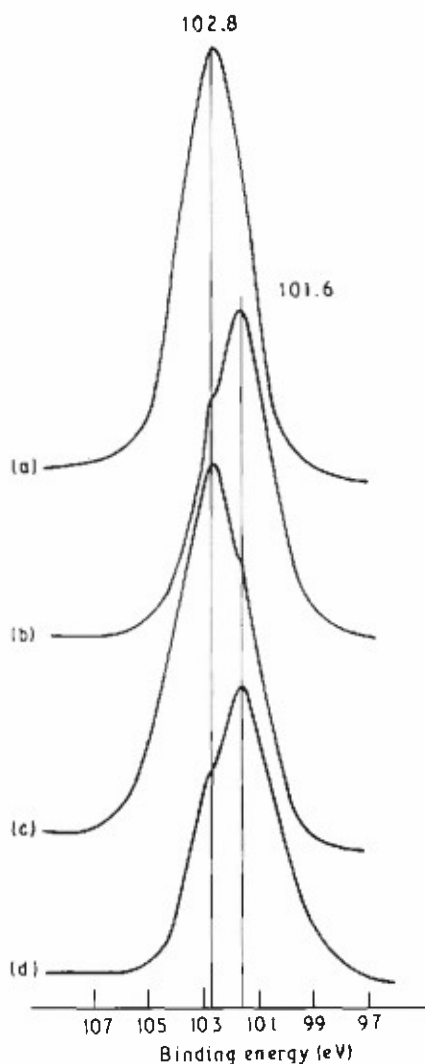


Figure 10 Si 2p spectra originating from (a) PS, (b) PZS, (c) PTS and (d) PAS coating surfaces.

link between the organic and inorganic polymers through covalent or H bonds. Fig. 12 illustrates the Zr 3d and Ti 2p doublet separation spectra for PZS and PTS, respectively, and the Al 2p region for PAS. The $3d_{5/2}$ and the $3d_{3/2}$ lines at 182.3 and 184.2 eV for Zr_{3d} spectrum are assigned to the Zr in the Zr–O–Si linkages. The symmetric peak at 74.1 eV in the Al 2p spectrum corresponds to the Al in the Al–O–Si bonds [17]. For PTS, there are four peaks in the Ti 2p regions. The main $2p_{3/2}$ peak at 458.7 eV and the $2p_{1/2}$ line at 464.5 eV are assigned to the Ti in the Ti–O–Si linkages. The anatase titanium was observed in the $2p_{3/2}$ peak at approximately 459.2 eV and $2p_{1/2}$ peak at approximately 465.1 eV [23].

The adhesive nature at the interface between PMS and the FPL-etched Al substrate is an important factor contributing to a good film-forming behaviour and to subsequent corrosion protection. Therefore, it is worthwhile to assess the bonding structure and mechanism at the PMS/Al interface. For these interface studies, a PTS coating was selected from the other PMS films. The thin PTS films suitable for XPS analyses were fabricated on the etched substrates in accordance with the following procedure: a 0.5% sol-

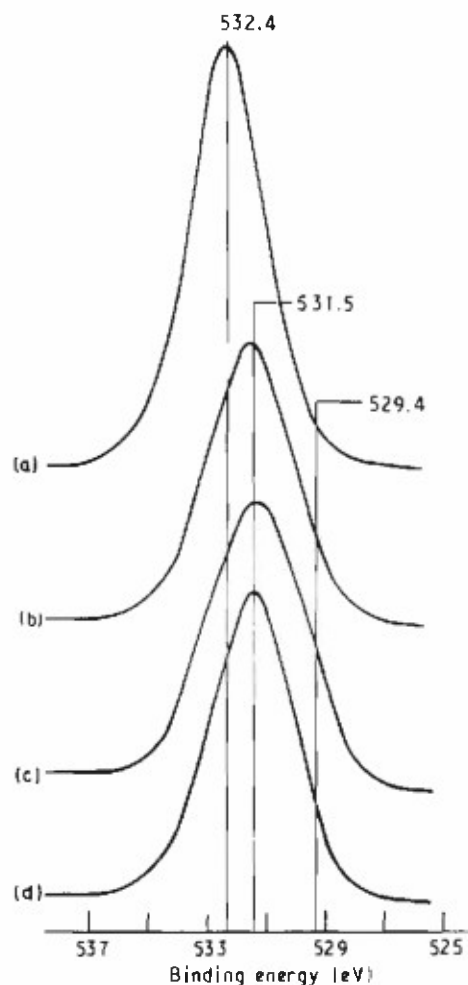


Figure 11 O 1s region of (a) PS, (b) PZS, (c) PTS and (d) PAS. Integrated intensity ratio of $O(SiOH)/O(M-O-Si)$: (b) 0.3, (c) 0.53 and (d) 0.36.

precursor solution in deionized water was deposited over the substrate surfaces by spin-coating at 1000 r.p.m., and then heated for 20 h at 150 °C to produce a sintered film. The pyrolytic conversion of the sintered film into the PTS film was accomplished by annealing for 30 min at 350 °C. Finally, the resulting interfaces were examined using XPS.

The PTS films made by this method were thin enough to permit the photo-emission signal from the underlying Al substrate to be detected. Figs 13 and 14 show the Al 2p and the O 1s core level spectra for the FPL-etched substrate and for the interface between the PTS and the substrate. As is evident from the Al 2p peak at 74.4 eV (Fig. 13a), the main component of the outer surface of Al is aluminium oxide, Al_2O_3 [20]. The Al 2p signal at the PTS/Al interface (Fig. 13b) is composed of two major components at 74.4 and ≈ 74.0 eV. The exciting photoemission at 74.4 eV originates from Al_2O_3 aluminium; however, the new line at ≈ 74.0 eV is of particular interest. As discussed earlier, the aluminium in the Al–O–Si linkages refers to a peak at 74.1 eV. Thus, the possible assignment of this new peak is to the aluminium in the interfacial oxane bond bridging the PTS to the Al_2O_3 . Such

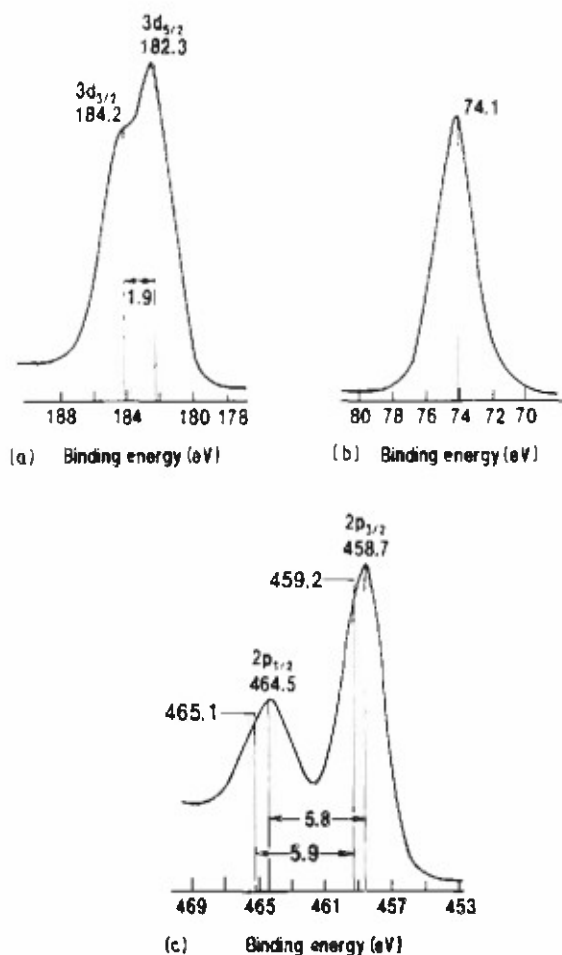
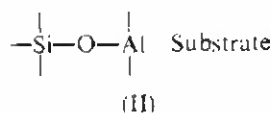


Figure 12 XPS spectra of (a) Zr 3d, (b) Al 2p, and (c) Ti 2p regions for PZS, PAS, and PTS coatings, respectively.

interfacial covalent bond structure may be illustrated as follows



These covalent bonds presumably form through a dehydration–condensation reaction mechanism of the hydroxylated Al_2O_3 with the —Si—OH , in the PTS film. The investigations of the O 1s region appear to support the above-mentioned findings. The new peak at 531.2 eV, emerging at an interfacial boundary, (Fig. 14b) is associated with the oxygen in the Si–O–Al (on the surface of the substrate) bonds; whereas the position of the peak at 531.6 eV corresponds to the Al_2O_3 oxygen (Fig. 14a). The Si 2p signal (Fig. 15) is asymmetric because it consists of three components at 102.9, 101.7, and 99.6 eV. The major line at 101.7 eV can be ascribed to the Si in the M–O–Si linkages, and the weak shoulder at 102.9 eV to the Si in Si–O–Si linkages. The existence of other possible Si-based components could not be established on the basis of the minor peak at 99.6 eV. Apart from a slight broadening of the peak no special spectral features were observed on the Ti 2p doublet separation spectrum (Fig. 15) compared with that of PTS surface

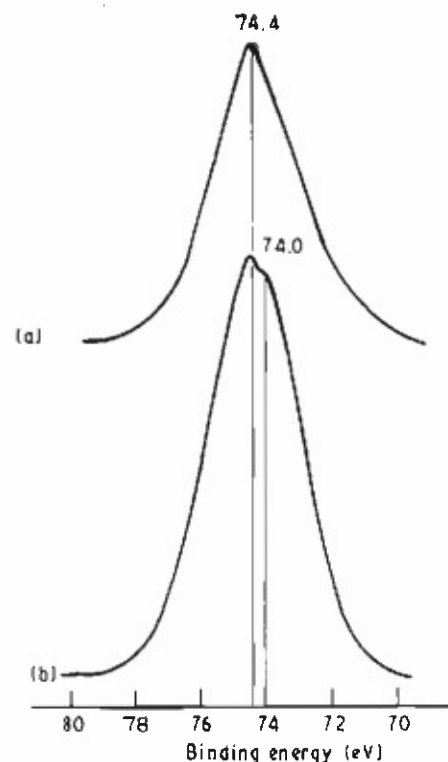


Figure 13 Al 2p spectra from (a) FPL-etched Al substrate surface and (b) critical interfacial zone between PTS and etched Al.

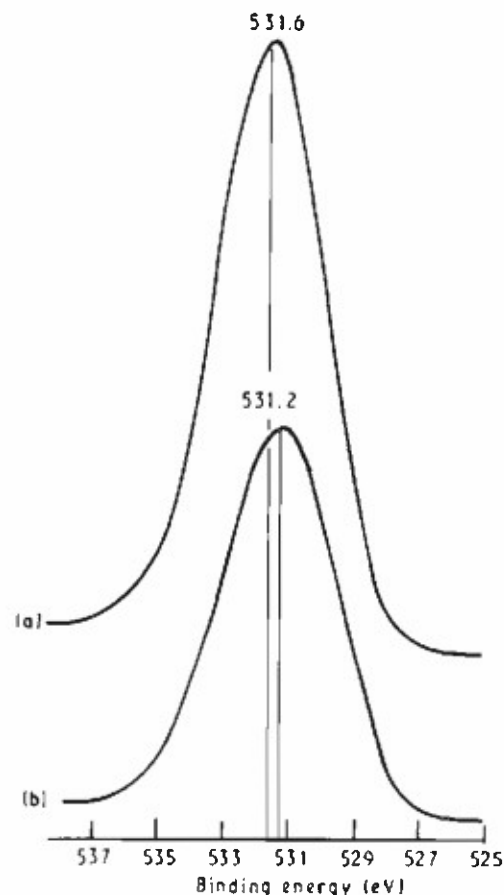


Figure 14 O 1s core level spectra for (a) etched Al surface and (b) PTS–Al interfacial area.

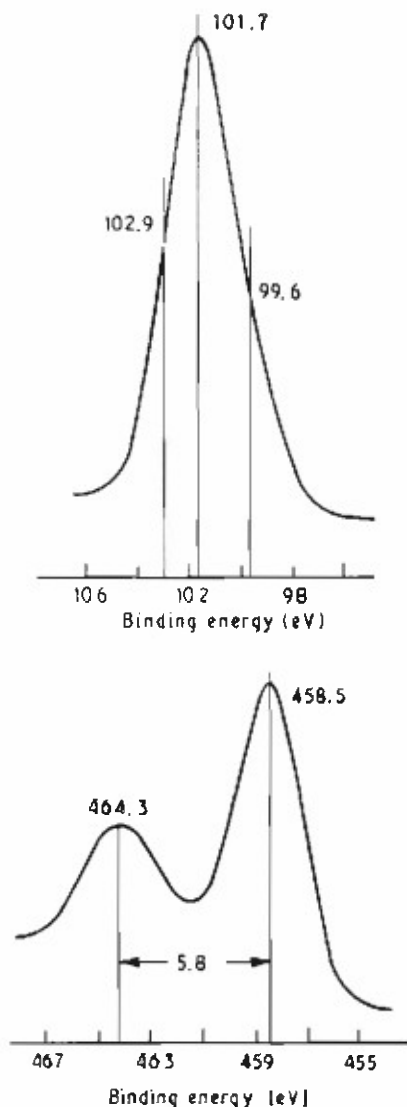


Figure 15 (a) Si 2p and (b) Ti 2p spectra from PTS/etched Al joint.

(Fig. 12). This information suggests that the extent of reactivity of titanium oxide, which acts as a cross-linking agent between the polysiloxane chains, with the Al_2O_3 is very small. Hence, the Al_2O_3 surface formed by FPL treatments of Al substrates preferentially links with the siloxane, rather than with the titanium oxide groups. From the above results, it can be rationalized that two major factors, (1) the cross-linking ability of metal oxides between the polysiloxane chains, and (2) the formation of PMS-Al interfacial chemical bonds, are responsible for greatly minimizing the development of stress cracks by shrinkage of pyrolysed PMS films. These important factors not only contribute to good film-forming behaviour, but also relate directly the affects of the corrosion protection of Al substrates.

All of the above data were correlated with corrosion protection provided by the pyrolysis-induced PMS coatings on FPL-etched Al. The corrosion data were obtained from the polarization curves for PMS-coated Al samples upon exposure in an aerated 0.5 M sodium chloride solution at 25 °C. The typical cathodic

TABLE III Corrosion potential, E_{corr} , and corrosion current, I_{corr} , values for PMS-coated and uncoated Al specimens

Coating systems (TSPI/M(OC_3H_7) _{4 or 3})	E_{corr} (V versus SCE)	I_{corr} (μA)
Uncoated (blank)	-0.725	2.5
PS (100/0)	-0.695	1.8
PZS (70/30)	-0.625	7.8×10^{-1}
PZS (50/50)	-0.710	1.5
PTS (70/30)	-0.589	1.8×10^{-1}
PTS (50/50)	-0.596	1.6×10^{-1}
PAS (70/30)	-0.664	9.0×10^{-1}
PAS (50/50)	-0.700	1.8

anodic polarization curves exhibited a short Tafel region in the cathodic polarization, but no Tafel region was found at the anodic sites. To evaluate the protective performance of coatings, the corrosion potential, E_{corr} , and corrosion current, I_{corr} , were determined for the polarization curves. The former is defined as the potential at the transition point from cathodic to anodic polarization curves. I_{corr} values were measured by extrapolation of the cathodic Tafel slope. Table III summarizes these results. As seen in the table, the major affect of these PMS coatings on the corrosion protection of Al is to move the E_{corr} value to less negative potentials and to reduce the cathodic current, I_{corr} . In particular, the test samples coated with PTS produced significantly higher E_{corr} and lower I_{corr} values than compared with those for the uncoated samples (blanks). This strongly suggests that these PTS coating films will serve to provide good corrosion resistance to sodium chloride solution and in minimizing the corrosion rates of Al. The protective ability of other PMS systems seems to depend on the TSPI/M(OC_3H_7)_{4 or 3} ratios in the precursor sol solution. Coatings derived from a higher ratio of 50/50 displace a lower corrosion resistance in sodium chloride medium. Similarly, the metal oxide-uncross-linked PS coating performed poorly and provided no significant corrosion resistance. The reason for the poor protection performance is, primarily, due to the presence of numerous microcracks and pits in the film layers. In other words, the sodium chloride solution penetrated the blemishes and progressively undermined the coatings.

4. Conclusions

Inorganic amorphous polymetallosiloxane, PMS, can be synthesized through hydrolysis-polycondensation-pyrolysis reaction of sol-precursor solution systems consisting of *N*-[3-(triethoxysilyl)propyl]-4,5-dihydroimidazole (TSPI) and M(OC_3H_7)_n (M = Zr, Ti and Al, $n = 3$ or 4) as a film-forming reagent, the HCl as a hydrolysis catalyst, and CH_3OH and water as a liquor medium. During this study of corrosion-protective thin films for low melting point Al substrates, the following seven items could be conclusively generalized as the major physico-chemical factors governing the film-forming behaviour of PMS under the sol precursor (25 °C) → sintering (150 °C) → annealing (350 °C) processes.

1. During the sol-film forming stage, the addition of HCl to the mixtures of TSPI and $M(OC_3H_7)_n$ induces the formation of hydroxylated metals, the Cl-substituted end groups in the monomeric organosilane and the separation of imidazole derivatives from TSPI.

2. In the sintering process of xerogel films at 150 °C, the formation of metal oxide polyorganosiloxane bond formed by the dechlorinating reaction between the Cl attached to propyl C in organosilane and the proton in the hydroxylated Zr or Ti compounds, played an important role in weight loss of the film.

3. Referring to item 2, the aluminium hydroxide, derived from $Al(OC_3H_7)_3$ in which the trivalent ion is the principal oxidation state, preferentially reacts with hydroxylated organosilane to form the Al-O-Si linkage at a low temperature. However, this linkage was broken when the sintered film was annealed at 350 °C, thereby creating large stress cracks and a high weight loss of the film.

4. The pyrolysis of titanium and zirconium oxides-incorporated polyorganosiloxane compounds led to the formation of titanium and zirconium oxides cross-linked with polysiloxane, while also eliminating carbonaceous groups and Cl compounds from the sintered materials. These cross-linked network structures served to minimize the development of stress cracks in the films pyrolysed at 350 °C.

5. Although a certain amount of crystalline anatase particles were present in the amorphous polytitanosiloxane (PTS) coatings, the moderate cross-linking effects of titanium oxides and the densification of the M-O-Si linkage provided the most effective coating film in this study.

6. The identification of covalent oxane bonds at the interfaces between the PTS and the FPL-etched Al substrate illustrates the possibility of strong adhesive forces.

7. Referring to items 4-6 described above, the integrated assignments of these factors were correlated directly to good corrosion resistance of Al alloys in the NaCl solution.

Acknowledgement

This work was performed under the auspices of the US Department of Energy, Washington, DC, under

Contract no. DE-AC02-76CH00016, and supported by the US Army Research Office Program MIPR-AR0-102-89.

References

1. T. SUGAMA, L. E. KUKACKA and N. CARCIELLO, *Prog. Org. Coat.* **10** (1990) 173.
2. H. W. EICHNER and W. E. SCHOWALTER, Forest Products Laboratory Report no. 1813, Madison, WI (1950).
3. N. P. BANSAL, *J. Amer. Ceram. Soc.* **71** (1988) 666.
4. F. P. ENG and H. ISHIDA, *J. Mater. Sci.* **21** (1986) 1561.
5. C. N. R. RAO, "Chemical Applications of Infrared Spectroscopy" (Academic Press, New York, 1963) p. 323.
6. L. J. BELLAMY, "The Infrared Spectra of Complex Molecules" (Chapman and Hall, London, 1975) p. 318.
7. A. LEE SMITH, *Spectrochim. Acta* **16** (1960) 87.
8. D. H. R. BARTON, J. E. PGAE and C. W. SHOPPEE, *J. Chem. Soc.* (1956) 331.
9. N. V. SIDGWICK, "The Organic Chemistry of Nitrogen" (Clarendon Press, Oxford, 1966) p. 782.
10. R. A. SIMON, A. J. RICCO and M. S. WRIGHTON, *J. Amer. Chem. Soc.* **104** (1982) 2031.
11. G. RAMIS, P. QUINTARD, M. CAUCHATIER, G. BUSCA and V. LORENZELLI, *ibid.* **72** (1989) 1692.
12. S. W. LEE and R. A. CONDRASTE Jr., *J. Mater. Sci.* **23** (1988) 2951.
13. B. E. YOLDAS, *ibid.* **14** (1979) 1843.
14. B. E. YOLDAS and D. P. PARTLOW, *ibid.* **23** (1988) 1895.
15. B. CARRIERE and J. P. DEVILLE, *J. Electron Spectrosc. Relat. Phenom.* **10** (1977) 85.
16. L. J. MATTENZO, *J. Adhes. Sci. Technol.* **3** (1989) 357.
17. T. E. MADEY, C. D. WAGNER and A. JOSHI, *J. Electron Spectrosc. Relat. Phenom.* **10** (1977) 359.
18. R. H. WEST and J. E. CASTLE, *Surf. Inter. Anal.* **4** (1982) 68.
19. R. CARACCILO and S. H. GAROFALINI, *J. Amer. Ceram. Soc.* **71** (1988) C-346.
20. H. NASU, J. IIEO and J. D. MACKENZIE, *J. Non-Cryst. Solids* **99** (1988) 140.
21. C. E. J. NICKERSON, C. ERNSBERGER, J. NICKERSON, A. E. MILLER and J. MOULDER, *J. Vac. Sci. Technol.* **6** (1985) 2415.
22. Y. W. KIM and J. G. LEE, *J. Amer. Ceram. Soc.* **72** (1989) 1333.
23. M. MIURATA, K. WAKINO and S. IKEDA, *J. Elect. Spectrosc.* **6** (1975) 459.

Received 4 January
and accepted 19 November 1990

APPENDIX C

POLYARYL ADHESIVES - RELATED PUBLICATIONS

Interfaces of polyphenylene sulphide-to-metal joints

T. Sugama and N.R. Carciello

(Brookhaven National Laboratory, USA)

High-temperature polyphenylene sulphide (PPS) film was deposited on the surface of cold-rolled, stainless and galvanized steels by slurry coating in N_2 and O_2 gases at $350^\circ C$. The value of the interfacial PPS/steel bond strength depended primarily on the species of sulphur-related iron compounds formed as reaction products at the interfaces. The order of these reaction products, which play an important role in developing bond strength, was $Fe_2(SO_4)_3 > FeSO_4 > FeS$. In contrast, the conversion of ZnS , formed at the PPS/galvanized steel interfaces, into $ZnSO_4$ led to a catastrophic loss of bond strength.

Key words: polyphenylene sulphide; steels; bond strength; interface; X-ray photoelectron spectroscopy

Powdered forms of polyphenylene sulphide (PPS), which is one of a family of high-temperature performance polymers, are commonly used as film-forming materials in slurry-coating systems consisting of solid and liquid phases. The major suitability of PPS powder for such coating processes is that it causes the assembly of a high macromolecule through mechanisms of cross-linking and chain extension at a temperature above the melting point of approximately $290^\circ C^{1-3}$. When the PPS slurry is applied as a corrosion-resistance coating for metallic substrates, it would be expected that the fusing-curing processes of the slurry deposited on the substrates might promote the thermal oxidations of metals beneath the PPS coatings. As reported by Bolger⁴, the high degree of oxidation of the metal surfaces has a strong affinity for the chemisorption of the organic polymers, and by contrast, when the metal surfaces were treated in oxygen-free N_2 gas environments, the chemical reactivity of surfaces having a low degree of oxidation becomes very poor.

Thus, it is of particular interest to explore how the reaction products formed at the critical interfacial contact zones between PPS and metals in oxygen and nitrogen environments influence the adhesive bonding of PPS to the metal substrates. This information was obtained by X-ray photoelectron spectroscopy (XPS) analyses of both failure sides at the interfacial boundaries for PPS/cold-rolled, stainless and galvanized steel joint systems prepared in oxygen or nitrogen environments at a temperature of $350^\circ C$. The

XPS data on the interfacial chemical state and composition were correlated directly with the mechanisms of bonding and bond failure.

Experimental details

Materials

The metallic substrates used were a commercial AISI 1010 cold-rolled steel (CRS), AISI 304 stainless steel (SS) and G-90 galvanized steel (G-S). Before depositing the polyphenylene sulphide (PPS) slurry, the surface of these substrates was wiped with acetone-soaked tissues to remove any gross surface contamination. PPS powder for the slurry coating was supplied by the Phillips 66 Company. The 'as-received' PPS was a finely divided, tan-coloured powder having a high melt flow with a melting point of $288^\circ C$. The PPS film was deposited on the substrate surfaces in the following way. First, the substrates were dipped into a PPS slurry consisting of 45 weight % (wt%) PPS and 55 wt% isopropyl alcohol at $25^\circ C$. Then, the slurry-coated substrates were preheated in oxygen and nitrogen gases at $300^\circ C$ for 3 h, to fuse the PPS powder and allow volatilization of the isopropyl alcohol liquid phase. The flow rate of these gases in a tube furnace with a volume of 1500 cm^3 was $\approx 200\text{ cm}^3\text{ min}^{-1}$. To assemble the cross-linked and extended macromolecular structures, the fused PPS was finally heated in either a 99.5% O_2 or a 99.9% N_2 environment at $350^\circ C$ for 2 h.

Measurements

The chemical compositions and states present on the substrate surface and on bond-failure sides at the interface of the PPS/substrate joint systems prepared in O_2 and N_2 at high temperatures were investigated from the peak areas and from determination of binding energies (BE) deduced from XPS. The spectrometer used was a V.G. Scientific ESCA 3MK II. The excitation radiation was provided by an Al K α (1486.6 eV) X-ray source operated at a constant power of 200 W. The vacuum in the analyser chamber of the instrument was maintained at 10^{-9} torr throughout. The atomic concentrations for the respective chemical elements were determined by comparing the XPS peak areas which can be obtained from the differential cross-sections for core-level excitation⁷. To set a scale in all the high-resolution XPS spectra, the binding energy (BE) was calibrated with the C_{1s} of the principal hydrocarbon-type carbon peak fixed at 285.0 eV as an internal reference. A curve deconvolution technique was employed to find the respective chemical components from the high-resolution spectra of each element.

The lap-shear tensile strength of metal-to-metal joints was determined in accordance with the modified ASTM Method D-1002. Before overlapping the metal strips, 50 mm long and 15 mm wide, the 10 × 15 mm lap area was coated with PPS adhesive. The overlapped metal specimens were then placed in an oven at 350°C for 2 h. The thickness of the overlapped PPS film ranged from 25 to 75 μ m. The bond strength of the lap-shear specimens is the maximum load at failure divided by the total bonding area of 150 mm².

Results and discussion

First, the chemical compositions and states of the bulk PPS, the acetone-cleaned CRS, SS and G-S substrate surfaces were investigated to obtain the XPS reference data (Table 1 and Fig. 1). The S/C atomic ratio of 0.19 for the 350°C-cured bulk PPS surfaces was slightly higher than the value of 0.17 computed from the fundamental formula, $[-C_6H_4-S-]_n$, of PPS. The S_{2p} core-level spectrum (Fig. 1) for the bulk PPS featured a symmetric curve with a peak at the BE position of 163.8 eV, originating from the S of the S-C bond in the PPS structures⁸. CRS surfaces disclosed the presence of a large amount of oxygen, which can be associated with the formation of Fe oxides. In fact, the main core line at 710.9 eV and the shake-up satellite at a high BE site about 8 eV away from the main line in the $Fe_{2p_{3/2}}$ region are assignable to the formation of ferric oxide (Fe_2O_3)⁷. As is evident from a high carbon concentration of 58.3% the SS surface seems to be

covered with carbon-based contaminants which cannot be removed by organic solvents. Regardless of coverage with the C contaminant, the $Fe_{2p_{3/2}}$ spectral feature verified that the underlying Fe compound referred mainly to Fe_2O_3 . The presence of a concentrated P atom suggested that the surface of the galvanized steel used in this study was treated by phosphate. The $Zn_{2p_{3/2}}$ spectrum for the G-S substrates denoted the presence of a single Zn component at the BE position of 1022.1 eV. Since this BE value corresponds to Zn in ZnO formation⁸, the dominant Zn compound formed at the outermost surface of G-S was ZnO.

The results of the lap-shear bond strength of the metal-to-metal PPS adhesive joints are shown in Fig. 2. For CRS and SS substrates, the data clearly demonstrated that the bond strengths depend primarily on atmospheric conditions during the fusing-curing process of the PPS adhesive at high temperature. The strengths of specimens prepared under O_2 are much higher than those for specimens made in N_2 environments. The data also showed that the development of interfacial bond strength for the SS/PPS joint system is better than that of the CRS/PPS system.

Surprisingly, a very poor interfacial bond was recorded for the O_2 -treated G-S/PPS joint system. Although the bond strength value of N_2 -treated G-S/PPS joints is considerably lower than those for other systems, the bonding performance of this joint system was far better, compared with the same joint system made in an O_2 environment.

To clarify the causes of good and poor interfacial bonds, both failure surfaces were explored by XPS. Table 2 shows the elemental compositions for the cross-section samples of the PPS/CRS joint system after exposure to N_2 and to O_2 . In N_2 , the interface chemistry of the PPS side removed from the CRS substrate was characterized by the amount of Fe and a larger amount of O in conjunction with 7.4% S and 42.5% C compared with that of the bulk PPS (Table 1). A 4.3% S, belonging to the PPS, was detected on the interfacial substrate surface. Since the Fe and O elements remaining on the PPS side are associated with Fe_2O_3 and/or the interfacial reaction products, the locus of failure might occur in either the mechanically mixed layer of PPS and Fe_2O_3 , or in the reaction product layer formed by interaction between PPS and Fe_2O_3 . A striking difference from the N_2 samples was observed on the O_2 -treated samples: namely, no S atom was found on the failed CRS sides. Therefore, failure can be figured as a cohesive mode which occurs through the Fe_2O_3 layers close to PPS. In terms of achieving a good bonding performance, it can be assumed that the introduction of O_2 into the interfacial zones promotes the extent of interaction between the

Table 1. XPS elemental analysis of bulk PPS and substrates as reference surfaces

Coating and substrate	Atomic concentration (%)							
	C	S	O	Mn	Fe	P	Cr	Zn
PPS	82.5	15.5	2.0	-	-	-	-	-
CRS	25.8	-	59.9	1.7	12.5	-	-	-
SS	58.3	-	34.4	-	5.5	-	1.8	-
G-S	30.4	-	50.3	-	-	9.1	6.7	3.6

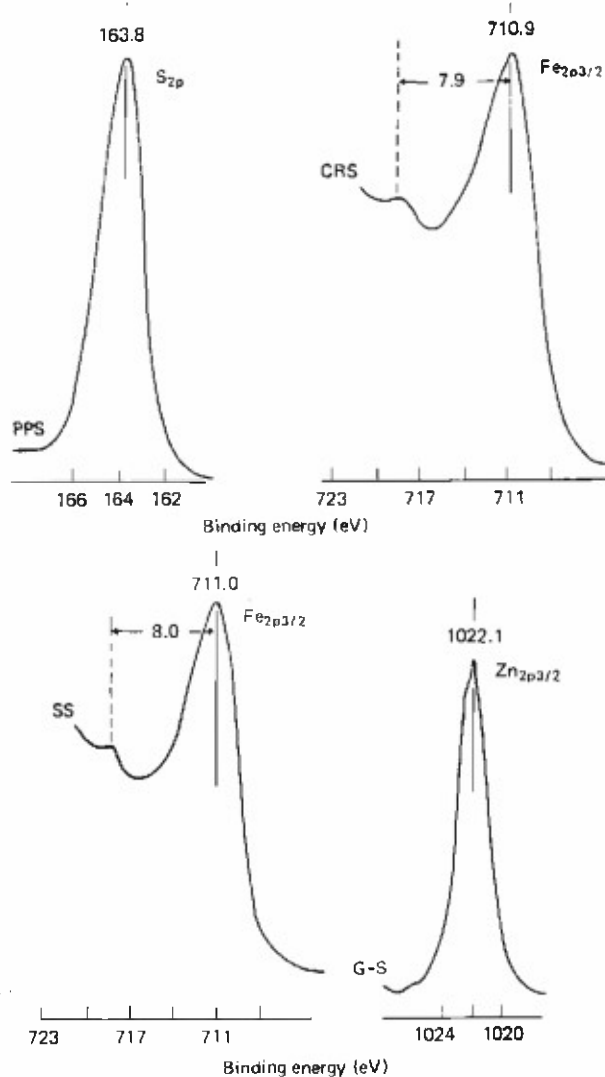


Fig. 1 XPS high-resolution spectra in S_{2p} , $Fe_{2p_{3/2}}$ and $Zn_{2p_{3/2}}$ regions for reference polyphenylene sulphide (PPS), cold-rolled steel (CRS), stainless steel (SS) and galvanized steel (G-S) surfaces

PPS and the Fe_2O_3 . We believe that such reaction products are much stronger than Fe_2O_3 layers.

To support this information, we inspected the high-resolution S_{2p} spectra of both the PPS and CRS interfacial sides for the N_2 -treated samples and the PPS surface for the O_2 -samples (Fig. 3). The asymmetric feature of the resultant S_{2p} region for the N_2 -treated PPS interface reveals two resolvable Gaussian components at 161.8 and 163.8 eV. From the surface

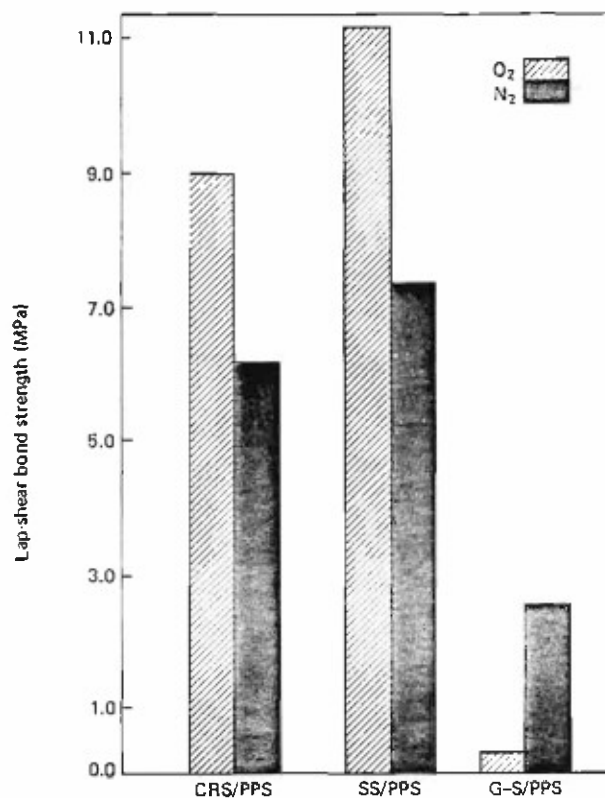


Fig. 2 Lap-shear bond strength at metal-to-metal PPS adhesive joints after exposure in N_2 and O_2 at $350^\circ C$

reference spectra (see Fig. 1), the shoulder peak at 163.8 eV is attributable to the S in the PPS. According to literature⁹, the 161.8 eV principal line, which represents the main chemical component, can be ascribed to the formation of ferrous sulphide (FeS) as the reaction product at the interfaces between the PPS and the Fe_2O_3 in the N_2 environment. The shoulder peak near 710.2 eV, reflecting the Fe in the FeS ¹⁰, was also identified in the $Fe_{2p_{3/2}}$ region (not shown). Since the negative ion mass spectra (not shown) of the oxidized PPS surfaces indicate the presence of intense sulphur trioxide (SO_3) signals, such sulphur-related iron compounds can be formed by the interfacial gas-solid reaction between the Fe_2O_3 and the sulphur dioxide (SO_2) and SO_3 gases emitted from PPS at a high temperature. An additional prominent line was seen at 168.5 eV, corresponding to a shift of about 6.7 eV to the higher BE site than that of FeS from the N_2 -treated CRS interface. A shift of 6.7 eV is reasonable to distinguish the presence of ferrous sulphate

Table 2. Chemical composition of both interfacial failure sides for N_2 - and O_2 -treated PPS/CRS joint systems

Heating environment	Failed side	Atomic concentration (%)				
		S	C	O	Mn	Fe
N_2	PPS	7.4	42.5	41.5	-	8.6
N_2	CRS	4.3	40.8	43.9	0.3	10.7
O_2	PPS	3.5	42.1	44.0	-	10.4
O_2	CRS	-	31.3	55.5	0.7	12.6

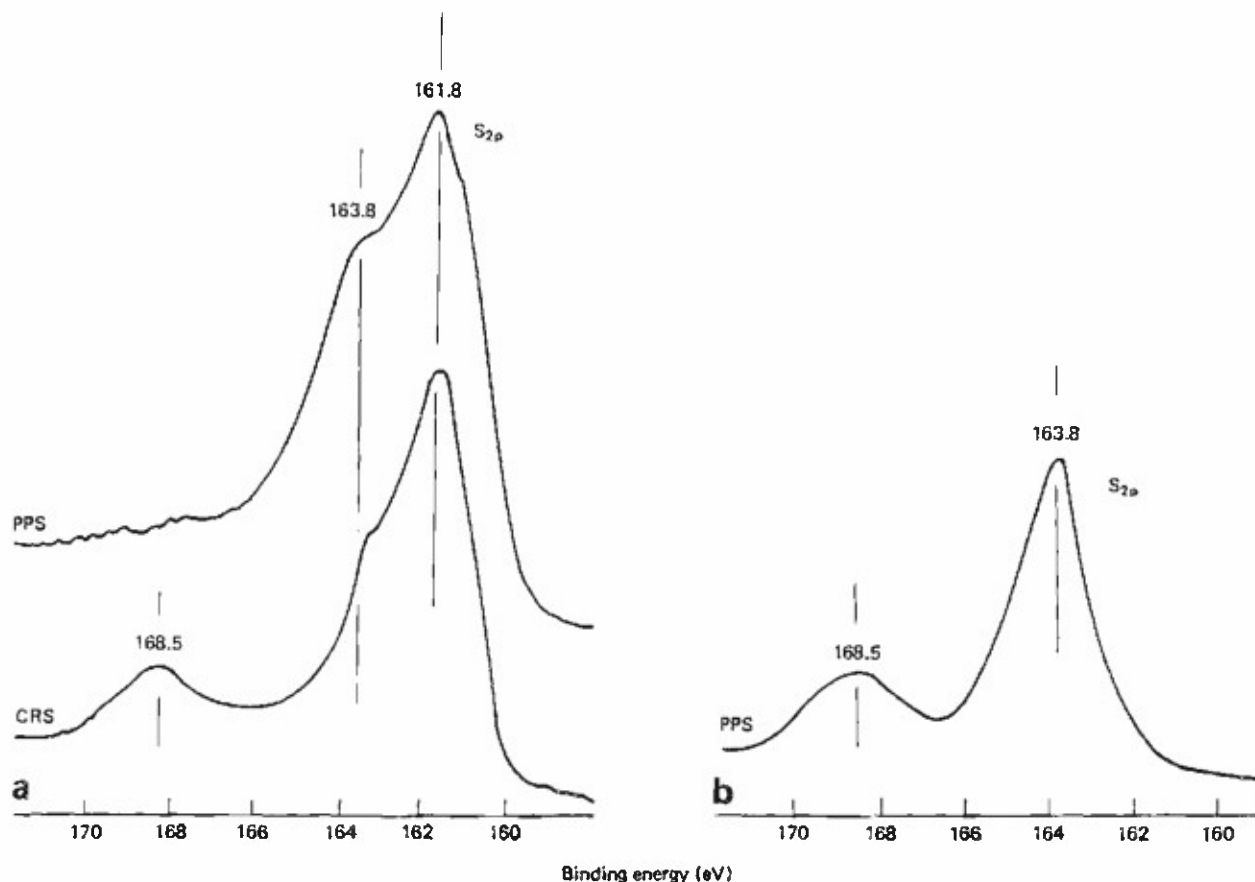


Fig. 3 S_{2p} spectra at failed interfaces of PPS/CRS joint system prepared at 350°C in: (a) N_2 gas and (b) O_2 gas

$(FeSO_4)^{14}$ from FeS . $FeSO_4$ will be formed through the following reaction¹²:



By comparison with that of the PPS side, a distinctive S_{2p} spectral feature could be seen on the O_2 -treated PPS interface. We conclude that there is no evidence for the presence of FeS at 161.8 eV, while the remarkable peak at 168.5 eV, belonging to $FeSO_4$, emerges in the high BE sites. Since the introduction of an abundance of oxygen promotes the conversion of SO_2 to SO_3 ¹³, it is reasonable to rationalize that an enrichment of O_2 catalyst-induced SO_3 gas causes the formation of more $FeSO_4$ than FeS . As a result, the formation of $FeSO_4$ as the interfacial reaction product appears to be responsible for the development of strong interfacial bonds.

Table 3 shows the elemental compositions at the

cross-section areas of the PPS/SS joint system. In N_2 , the PPS interface removed from the SS was characterized by the absence of Fe and the presence of a small amount of O. Compared with the SS reference surface (Table 1), the interfacial SS surface had 4.4% S, a higher C concentration, and a lower O and Fe content. The detection of a certain amount of S and a higher concentration of C reflects good adhesion of PPS to the Fe_2O_3 at the outermost surface of SS.

Concerning the absence of Fe at the PPS side, the cohesive failure mode, which occurs through the PPS layer adjacent to the Fe_2O_3 , can be proposed for this joint system. Of particular interest is the chemical composition at the interfaces of the O_2 -induced PPS/SS joint. The following two chemical characteristics can be described on the interfacial SS surface:

- 1) the presence of S atoms in amounts similar to that observed on the PPS side; and

Table 3. Elemental composition of interfacial PPS and SS surfaces at PPS/SS joint in N_2 and O_2

Heating environment	Failed side	Atomic concentration (%)			
		S	C	O	Fe
N_2	PPS	12.7	83.9	3.4	—
N_2	SS	4.4	82.3	12.7	0.5
O_2	PPS	13.3	81.0	5.6	0.1
O_2	SS	14.3	24.4	56.5	4.8

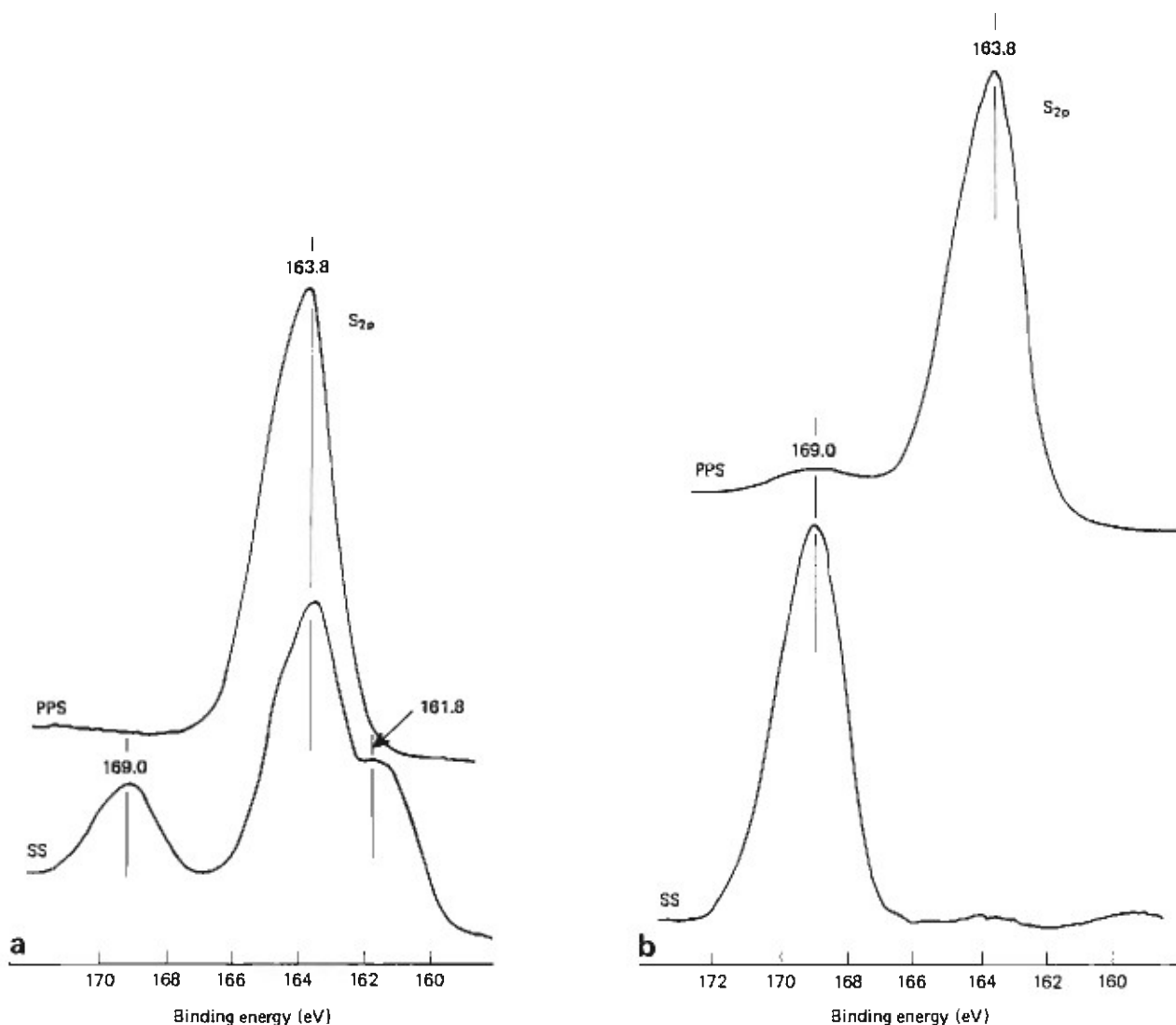


Fig. 4 S_{2p} region at interfacial failure locus of PPS/SS joint system prepared at 350°C in: (a) N_2 gas and (b) O_2 gas

2) the introduction of a large amount of O into the SS side.

This finding suggests that a substantial amount of interaction products containing S, O and Fe atoms remains at the SS side, whereas there are few residual reaction products adhering to the PPS. Thus, the locus of interfacial failure appears to occur through the reaction product layer near the PPS. Fig. 4 shows the S_{2p} region for both interfacial sides after treatment in N_2 and O_2 . The S_{2p} spectrum for the PPS interface in the N_2 -treated joint system features a simple peak containing only a single line at 163.8 eV originating from S in the PPS. There was no indication of peaks at 161.8 and 168.5 eV, which reflect the formation of FeS and FeSO_4 , respectively. In contrast, the emergence of a pronounced line at 161.8 and 169.0 eV, while maintaining the major line at 163.8 eV, was observed from the SS interface, thereby accounting for a certain amount of reaction products remaining on the interfacial SS surface. Regarding the reaction products, the new peak at 169.0 eV, corresponding to ≈ 0.5 eV higher position than that of FeSO_4 , may be associated

with the formation of ferric sulphate $[\text{Fe}_2(\text{SO}_4)_3]^{11}$, which could be generated by the reaction of Fe_2O_3 with three moles of SO_3 on heating¹⁴. We also inspected the $\text{Fe}_{2p3/2}$ region to distinguish between Fe(II) and Fe(III) sulphates. However, it was very difficult to distinguish the photoelectron line of these sulphates, because of the superposition of the strong Fe_2O_3 signal. Striking changes in spectral features occur as O_2 is introduced into the critical interfacial zones. The particular feature of the S_{2p} signal at the SS side was an intense single peak at 169.0 eV, suggesting that only $\text{Fe}_2(\text{SO}_4)_3$ as the interaction product was left on the SS side. A weak line at 169.0 eV was also detected from the PPS interface away from the SS.

Considering that the PPS/SS joint system prepared in O_2 displays the highest bond strength in this series of tests, it can be concluded that the extent of PPS adhesive bonding to metal substrates depends primarily on the species, and on the amount of S-related Fe compounds formed as interaction products at the critical interfacial contact zones between PPS and the substrate. The effective reaction products, which play a major role in the increase in bond strength, have the

Table 4. Atomic concentration of N₂ and O₂-treated PPS/G-S interfaces

Heating environment	Failed side	Atomic concentration (%)					
		P	S	C	O	Cr	Zn
N ₂	PPS	9.3	8.3	51.0	24.9	1.1	5.4
N ₂	G-S	10.5	7.5	48.0	26.0	1.9	6.2
O ₂	PPS	13.6	3.2	36.0	37.0	2.3	7.8
O ₂	G-S	16.0	3.8	35.7	33.8	2.3	8.5

following order: Fe₂(SO₄)₃ > FeSO₄ > FeS. Thus, the O₂-catalysed reaction products at the interfaces are responsible for the improvements in bond strength of PPS/metal joints.

Table 4 gives the elemental compositions for both interfacial failure sides in the PPS/G-S joint system. For the sample made in N₂, the interfacial PPS surface had a composition closely resembling that of the G-S interface. The detection of a certain amount of Cr and Zn on the PPS interface demonstrated that these elements migrate from the substrate to the coating sides during failure of the bond. The amount of Zn detected on the G-S side is considerably greater, and the amount of Cr substantially less than that observed on the reference G-S surface (see Table 1). This finding suggested that the S in PPS preferentially reacts with the Zn in the substrates, rather than with Cr. Hence, failure is certain to occur through the reaction product layers formed at the interfaces between PPS and G-S. A similar locus of failure was observed from the O₂-treated adhesion sample; the chemical compositions of both failure surfaces are close. The only difference was that more P, O, Cr and Zn remained in the cross-section, while the amounts of S and C were reduced. In particular, the increased amounts of residual Zn and O atoms reflect the formation of oxygen-rich zinc compounds at the interfaces.

To identify the interaction products, we inspected the S_{2p} region for both the interfacial PPS and G-S surfaces (Fig. 5). The resultant S_{2p} signal for the N₂-treated cross-sections had at least two resolvable peaks at 163.8 and 161.9 eV. The former, as the major component, reveals the PPS, and the latter is likely to be assigned to the formation of S-related zinc compounds as interfacial reaction products. As reported by several investigators^{9,11,15}, the line emerging in a low BE site, ranging from 160.5 to 162.0 eV, commonly relates to metal sulphide compounds. Hence, zinc sulphide (ZnS), reflected by the peak at 161.9 eV, was formed by the reaction of ZnO with SO₂ and SO₃ gases at the PPS/G-S interfacial regions. Since no Fe from the underlying steel is found on either interfacial sides, we believe that the adhesion of the ZnS phase formed as a reaction product to the zinc layer is much poorer than the adhesion of zinc to the steel substrate. Compared with the N₂ sample, a quite different S_{2p} signal can be seen on both O₂-induced interfacial sides. The distinct spectral features were the growth of a prominent line at the high BE position of 169.5 eV, with a considerable attenuation of peak intensity at 161.9 eV at the interfaces. It is well known¹⁶ that when ZnS is fully exposed to air at an elevated temperature, oxidation leads to the conversion

of ZnS into zinc sulphate (ZnSO₄). Assuming that such oxygen catalysed ZnS → ZnSO₄ conversion occurs at the interfaces, the strong line emerging at 169.5 eV is due to the formation of ZnSO₄. This conversion is correlated directly with the striking decay of the ZnS line at 161.9 eV.

The interfacial ZnS → ZnSO₄ phase transition appears to create detrimental boundary layers which play an active role in the catastrophic loss of bond strength in joint samples exposed to oxygen.

Conclusions

The findings from an XPS study of the interfacial failure sides in polyphenylene sulphide (PPS)-to-metal joint systems prepared in N₂ and O₂ gases at 350°C lead to the following generalized conclusions.

When PPS slurry coatings, consisting of PPS powder and isopropyl alcohol, were deposited on the surfaces of cold-rolled steel (CRS) and stainless steel (SS), the PPS/substrate bond strengths developing in the fusing-cross-linking process of PPS at elevated temperatures depend primarily on the reaction products formed by the solid-gas interaction between the SO₂ and SO₃ emitted from PPS, and the Fe₂O₃ layer at the outermost surfaces. A high rate of SO₂ → SO₃ conversion, which occurs when there is free access to oxygen, resulted in the formation of ferric sulphate [Fe₂(SO₄)₃] as a reaction product, which was responsible for the development of bond strength. The efficacy of sulphur-related iron compounds in improving adhesion force was rated in the following order: Fe₂(SO₄)₃ > FeSO₄ > FeS. Since such interaction-induced Fe-S compounds are generally known as corrosion products of steels¹⁷⁻¹⁹, studies are being made on the influence of these compounds on the cathodic reaction.

In PPS/galvanized steel (G-S) joint systems, the interfacial interaction between the PPS and the ZnO existing at the top surface layers of G-S, in the N₂, induces ZnS as a reaction product. By contrast, a considerable reduction in bond strength was observed in the PPS/G-S joint system prepared in O₂. The reason for the catastrophic loss in strength was due to the formation of weak boundary layers of ZnSO₄, which was derived from the oxygen-catalysed conversion of ZnS.

Acknowledgement

This work was performed under the auspices of the US Department of Energy, Washington, D.C., under Contract No DE-AC02-76CH00016, and supported by

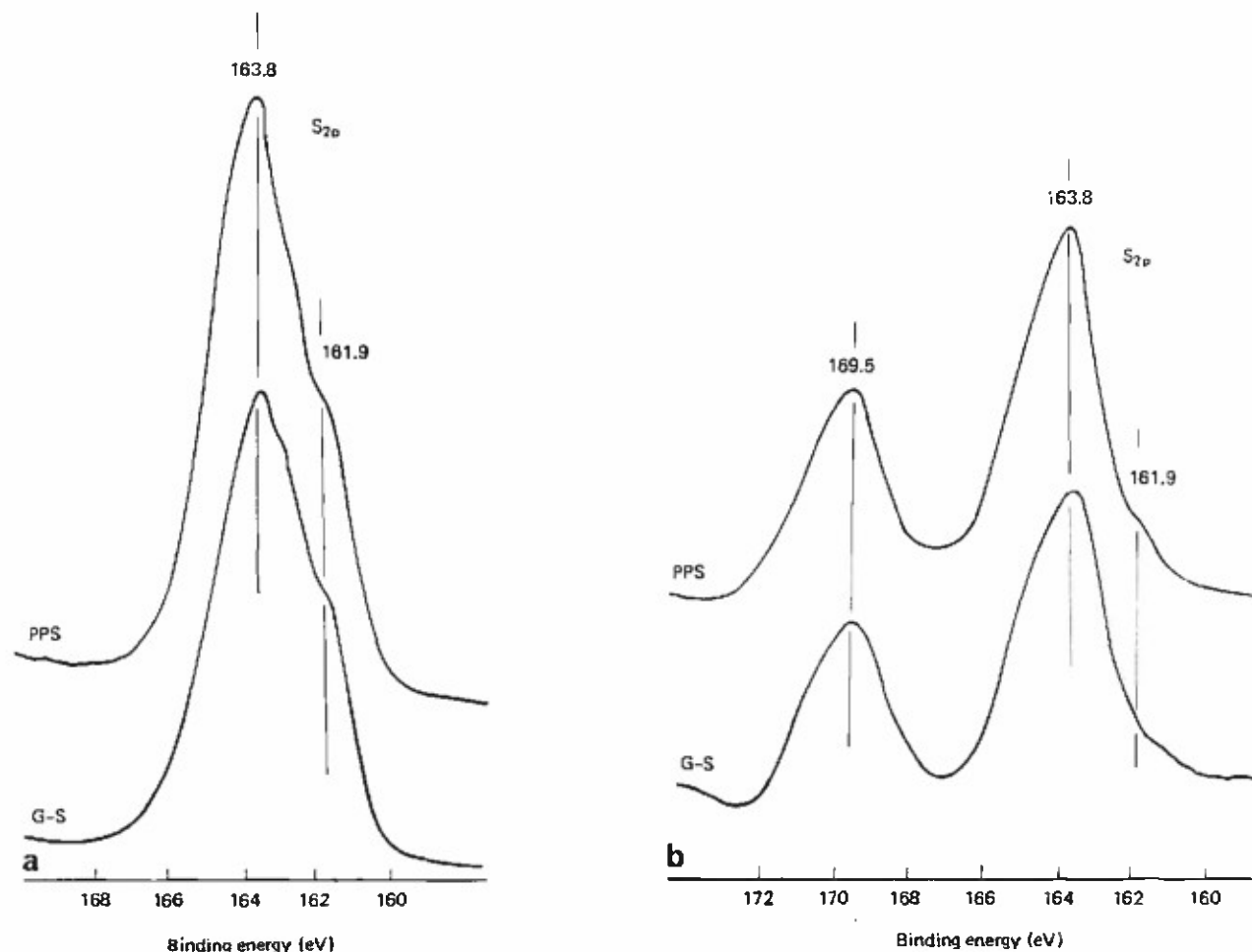


Fig. 5 S_{2p} spectra at failure locus of PPS/G-S joint system prepared at 350°C in: (a) N_2 gas and (b) O_2 gas

the US Army Research Office Program MIPR-ARO-103-90 and the Gas Research Institute under Contract No 5090-260-1948.

References

- 1 Lenz, R.W., Handlovity, C.E. and Smith, H.A. 'Phenylene sulfide polymers. III. The synthesis of linear polyphenylene sulfide' *J Polym Sci* **58** (1962) pp 351-367
- 2 Port, A.B. and Still, R.H. 'Synthesis and characterization of poly(phenylene sulfide), poly(2-methylphenylene sulfide), and poly(2,6-dimethylphenylene sulfide)' *J Appl Polym Sci* **24** (1979) pp 1145-1164
- 3 Lovinger, A.J., Davis, D.D. and Padden Jr, F.J. 'Kinetic analysis of the crystallization of poly(phenylene sulfide)' *Polymer* **28** (1985) pp 1595-1604
- 4 Bolger, J.C. in 'Adhesion Aspects of Polymeric Coatings' edited by K.L. Mittal (Plenum Press, New York, 1983) pp 3-18
- 5 Wagner, C.D., Riggs, W.M., Davis, L.E. and Moulder, J.F. in 'Handbook of X-ray Photoelectron Spectroscopy' edited by G.E. Muilenberg (Perkin-Elmer Corporation, USA, 1979) pp 21-23
- 6 Riga, J., Boutique, J.P., Pireaux, J.J. and Verbist, J.J. in 'Physicochemical Aspects of Polymer Surfaces' edited by K.L. Mittal (Plenum Press, New York, 1983) pp 45-52
- 7 McIntyre, N.S. and Zetaruk, D.G. 'X-ray photoelectron spectroscopic studies of iron oxides' *Anal Chem* **49** (1977) pp 1521-1529
- 8 Gaarenstroom, S.W. and Winograd, N. 'Initial and final state effects in the ESCA spectra of cadmium and silver oxides' *J Chem Phys* **67** (1977) pp 3500-3506
- 9 Binder, H. 'Application of the X-ray photoelectron spectroscopy to the elucidation of the bonding in iron-sulfur compounds' *Z Naturforsch, Teil B* **28** (1973) pp 255-262
- 10 Carver, J.C., Schweitzer, G.K. and Carlson, T.A. 'Use of X-ray photoelectron spectroscopy to study bonding in chromium, manganese, iron, and cobalt compounds' *J Chem Phys* **57** (1972) pp 973-982
- 11 Lindberg, B.J. et al. 'Molecular spectroscopy by means of ESCA [electron spectroscopy for chemical analysis] II. Sulfur compounds. Correlation of electron binding energy with structure' *Phys Scr* **1** (1970) pp 286-298
- 12 Tanabe, K., Hattori, H. and Yamaguchi, T. 'Surface properties of solid superacids' *Critical Rev Surface Chem* **1** (1990) pp 1-25
- 13 Sneed, M.C. and Maynard, J.L. 'General Inorganic Chemistry' (D. Van Nostrand Company, Inc, New York, 1952) p 513
- 14 Moody, B.J. 'Comparative Inorganic Chemistry' (Edward Arnold Publishers Ltd, London, 1965) p 388
- 15 Shelvov, R.B., Fisher, G.B. and Stiles, P.J. 'X-ray photoemission studies of the valence bands of nine [group IV-VI] compounds' *Phys Rev B* **15** (1977) pp 2021-2024
- 16 Sneed, M.C. and Maynard, J.L. 'General Inorganic Chemistry' (D. Van Nostrand Company, Inc, New York, 1952) p 904
- 17 Sordisco, J.B. and Pitts, R.E. 'Corrosion of iron in a hydrogen sulfide-carbon dioxide-water system. Mechanics of sulfide film

formation and kinetics of corrosion reaction' *Corrosion* **21** (1965)
pp 245-253

- 18 **Milton, C.** 'Kansite=Mackinawite, FeS' *Corrosion* **22** (1966)
pp 191-193

- 19 **Martin, A.L. and Annand, R.R.** Accelerated corrosion of steel by
suspended iron sulfides in brine' *Corrosion* **36** (1981)
pp 297-301

Authors

The authors are with the Energy Efficiency and
Conservation Division, Department of Applied Science,
Brookhaven National Laboratory, Upton, NY 11973,
USA. Correspondence should be addressed to
Dr Sugama.

Adhesion of crystalline polyphenyletheretherketone (PEEK) in metal-to-metal joints

T. Sugama, N.R. Carciello and M. Miura

(Brookhaven National Laboratory, USA)

Received 6 September 1991; accepted in revised form 5 November 1991

The characteristics of melt-crystallized polyphenyletheretherketone (PEEK) as an adhesive for steel-to-steel joints have been investigated. Interfacial chemistry, which plays an important role in determining whether adhesion will be poor or good at PEEK/steel interfaces, involved the following reactions. Oxygen-catalysed deformation of PEEK in air led to a low rate of crystallinity, which gave poor adhesion to the steel surfaces. The enrichment of Fe_2O_3 by extensive oxidation of the interfaces also created an undesirable boundary region, thereby indicating that failure occurs cohesively through this weak Fe_2O_3 layer. X-ray photoelectron spectroscopy (XPS) data suggest that there is no chemical interaction of well-crystallized PEEK with Fe_2O_3 at the top surface of steels. In contrast, in nitrogen, interfacial Fe- and Cr-O-C complexes, formed by a charge transfer between elemental Fe or Cr in steel and oxygen in the ketone groups ($C=O$) of crystallized PEEK, contributed significantly to strengthening the PEEK-to-steel bonds.

Key words: adhesion; adhesive-bonded joints; polyphenyletheretherketone; steels; crystallization; interface

Crystalline polyaryl thermoplastics, such as polyphenylenesulphide (PPS), polyphenyletheretherketone (PEEK) and polyphenyletherketone (PEK), have common chemical features consisting of aromatic backbone chains coupled with oxygen, ketone and/or sulphur. When these linear polymers are left in an oven at a temperature above their melting point of $>280^\circ\text{C}$, chain extension of the main phenyl groups caused by melting leads to molecular orientation, which is reflected in the crystallization of the polymers during cooling from the melting temperature to a lower temperature. Such crystallization behaviour of the polyaryls gives them specific, desirable characteristics as adhesives such as high temperature stability, high radiation, chemical and hydrothermal resistance, and good mechanical and dielectric properties. Thus, polyaryls have become of increasing interest for applications in coatings, as adhesives and in composites.

In a previous study, the authors investigated the interfaces of PPS-to-metal joints prepared in oxygen

(O_2) or nitrogen (N_2) environments at 350°C ¹. The results suggested that the strength of the bonds depends primarily on the species of sulphur-related iron compounds formed as reaction products at the interfaces. The formation of oxygen-catalysed reaction compounds by the introduction of oxygen into the interfacial regions gave better adhesion than the bond structure assembled in N_2 gas.

As part of our ongoing research to understand the chemical nature and role of the interfaces contributing to good adhesion of polyaryls to metal substrates, we next focused upon the PEEK compound, studying its adhesion to metal in an air or N_2 environment at high temperature. There were two major objectives: one was to understand the thermal characteristics, crystalline behaviours and changes in chemical conformation for the bulk PEEK polymer; the other was to examine the degree of crystallinity of PEEK adjacent to metals, and to model the interfacial bond structure and the failure mechanisms of the bonds in PEEK-to-metal joint systems. All our results were correlated directly with

the lap-shear bond strength of metal-to-metal specimens with PEEK adhesive bonds.

Experimental details

Materials

The metallic substrates used were commercial AISI 1010 cold-rolled steel (CRS) and AISI 304 stainless steel (SS). Before depositing the PEEK film, the surfaces of these steels were wiped with acetone-soaked tissues to remove any gross contamination. PEEK powder (an average molecule weight of 40 000) used for making a slurry was supplied by Imperial Chemical Industries (ICI). The PEEK slurry consisted of 45 weight % (wt%) PEEK and 55 wt% isopropyl alcohol.

Measurements

Information on the thermal and crystallization properties of bulk PEEK polymer in air or in a 99.9% N₂ environment was gained using the combined techniques of thermogravimetric analysis (TGA), differential thermal analysis (DTA), differential scanning calorimetry (DSC), X-ray diffraction (XRD) and X-ray photoelectron spectroscopy (XPS). These properties included the thermal decomposition temperature and its mechanisms, the melting point, the exothermic crystallization temperature, and the degree of crystallinity. We investigated the chemical composition and states present in the substrate surface and on the bond-failure side at interfaces of the PEEK/substrate joint systems prepared in air or N₂ at high temperatures by examining the peak areas and from determinations of binding energies (BE) deduced from XPS. The atomic concentrations for the respective chemical elements were estimated by comparing the XPS peak areas, which can be obtained from the differential cross-sections for core-level excitation. To set a scale in all the high-resolution XPS spectra, the binding energy was calibrated with the C 1s of the principal hydrocarbon-type carbon peak fixed at 285.0 eV as an internal reference. A curve-deconvolution technique using a DuPont curve resolver revealed the respective chemical components from the high-resolution spectra of each element. To support our XPS data, the PEEK interfaces removed from the substrates were explored with scanning electron microscopy (SEM) and XRD.

The lap-shear tensile strength of metal-to-metal joints was determined in accordance with the modified ASTM Method D-1002. Before overlapping the metal strips (50 mm long and 15 mm wide), a 10 × 15 mm lap-area was coated with PEEK adhesive. The overlapped metal specimens were placed in an oven at 400°C for 2 h, and then cooled to room temperature at the rate of -10°C min⁻¹. The thickness of the overlapped PEEK film ranged from 25 to 75 µm. The bond strength of the lap-shear specimens is the maximum load at failure divided by the total bonding area of 150 mm².

Results and discussion

Properties of bulk PEEK

A thermal analysis, combining TGA and DTA, revealed the decomposition characteristics during pyrolysis of

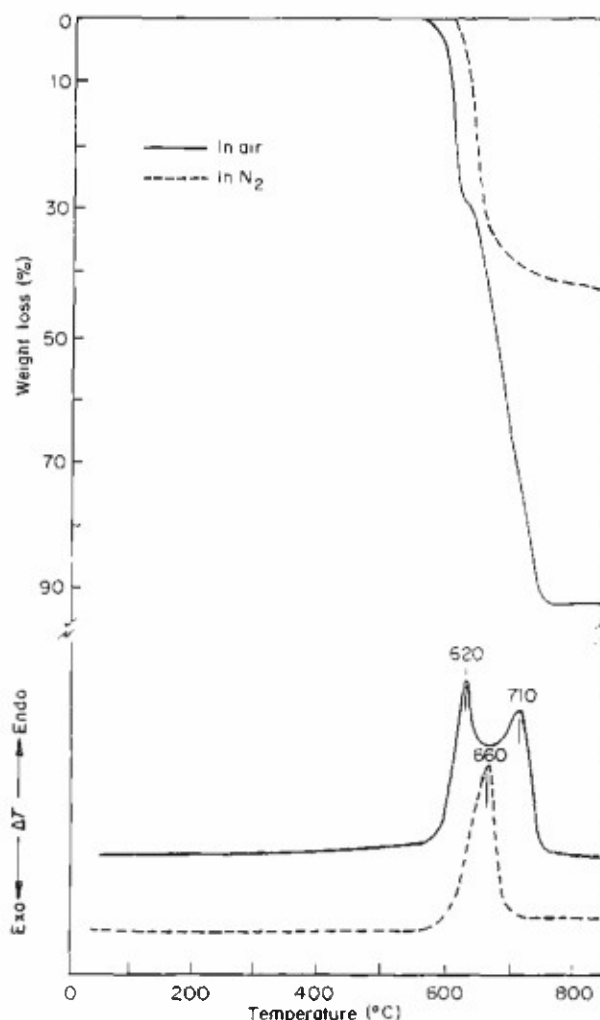


Fig. 1 TGA and DTA curves for the thermal decomposition of bulk PEEK heated in air or N₂ at a rate of 10°C min⁻¹.

'as-received' PEEK powder samples in air or in N₂ gas (Fig. 1). The TGA curve for the N₂ sample (dotted line) indicated that thermal decomposition (*T_d*) starts near 610°C, followed by a weight loss of ~40% between 610 and 700°C. This reduction reflects directly on the DTA endothermic peak at 660°C. Beyond 700°C, weight loss occurs gradually. Distinctive differences are seen between the N₂ sample and the sample pyrolysed in air, namely, the TGA curve has two decomposition stages: the first begins around 570°C and the second occurs between ~610 and ~750°C. These decompositions, reflecting the DTA peaks at 620 and 710°C, represent two different PEEK structures that appear during pyrolysis in air. In addition to these findings, a large weight loss of >90% occurs at ~730°C. This loss is more than double that of the N₂ sample pyrolysed at the same temperature, suggesting that the attack by air at a high temperature significantly promotes the oxygen-catalysed decomposition of PEEK.

Fig. 2 gives the cyclic DSC curves at different heating-cooling rates of ±2, 5 and 10°C min⁻¹ in N₂ at a temperature range from 75 to 400°C. Cooling from 400°C to low temperatures was accomplished using a DuPont Mechanical Cooling Accessory equipped with a DSC. At the lowest rate of ±2°C min⁻¹, the typical

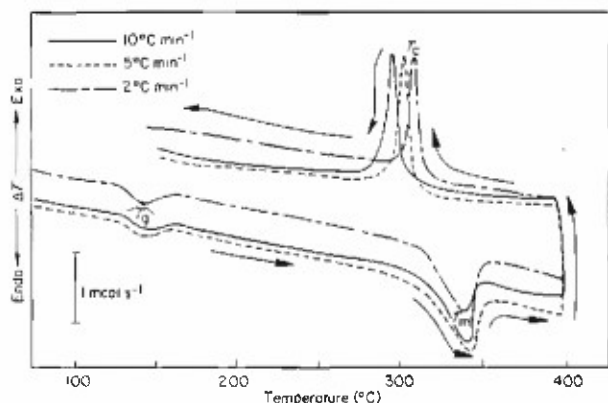


Fig. 2 Cyclic DSC curves of PEEK at heating-cooling rates of ± 2 , 5 and $10^\circ\text{C min}^{-1}$ in the temperature range 75 to 400°C

thermodynamic DSC scan, heated to 400°C , had two endothermic peaks at 145 and 340°C , revealing the glass transition point, T_g , and the melting point, T_m , respectively². On cooling the melted samples, an exothermic peak, which represents the heat evolved by the crystallization of PEEK, was recorded at 308°C . This exothermic crystallization point, T_c , was in good agreement with that reported by Blundell and Osborn³. When the rate of heating-cooling was increased, the thermal transition curves showed that the T_g and T_m temperatures slightly increase, while T_c shifts from 308°C at the rate of $-2^\circ\text{C min}^{-1}$, to 298°C at $-10^\circ\text{C min}^{-1}$. From the above TGA and DSC results, the T_m , T_c and T_d of PEEK in an N_2 environment occur around 340, 300 and 610°C , respectively.

On the basis of this information, a cyclic DSC experiment was planned to find the repeated melting-crystallization characteristics of the same samples at temperatures ranging from 400 to 25°C in air or N_2 . Accordingly, samples were prepared in the following way: DSC aluminium open pans were filled with samples of approximately 5 mg, and then placed in an oven at 400°C in air or N_2 for 2 h. The melted samples were subsequently cooled to room temperature at the rate of $\sim -10^\circ\text{C min}^{-1}$. Then, the PEEK-filled open pans were sealed with aluminium covers. The sealed samples were heated again to 400°C at the rate of $+10^\circ\text{C min}^{-1}$ and immediately cooled to 150°C at the rate of $-10^\circ\text{C min}^{-1}$. The resulting DSC curves are shown in Fig. 3. The figure shows a curve with a feature similar to that recorded on the PEEK sample (Fig. 2) prepared in N_2 (unbroken line). In contrast, the curve of the air-induced sample (dotted line) disclosed two endothermic peaks at temperatures of ~ 310 and $\sim 330^\circ\text{C}$, and a broad-weak exothermic peak near 260°C . The endothermic peak at $\sim 330^\circ\text{C}$ is reasonably thought to be due to the T_m of PEEK. Similarly, the new peak at 310°C seems to reflect the melting point of a new compound formed by the oxidation of PEEK in hot air. The formation of such a new compound might be inferred by the appearance of the weak exothermic peak, reflecting a lower degree of crystallinity compared with that of the N_2 samples.

To visualize the mutuality between poor crystallization behaviours and changes in molecular conformation of the oxidized PEEK polymers, XRD and xps analyses were made of the 400°C air or N_2 film

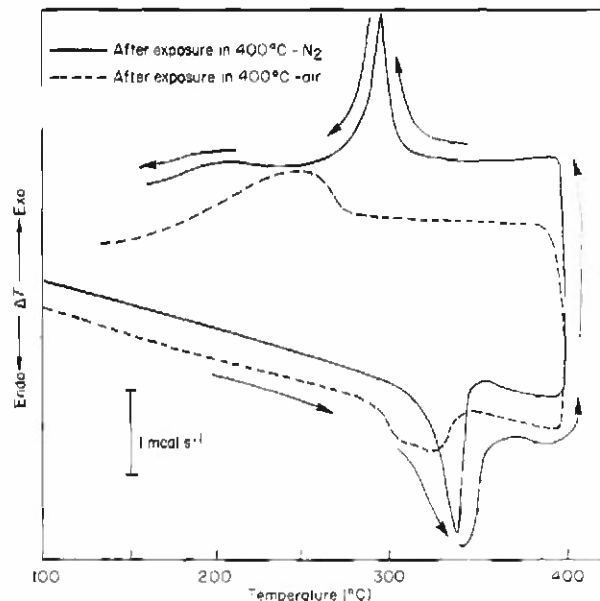


Fig. 3 Cyclic DSC curves for PEEK samples prepared in N_2 or air at 400°C

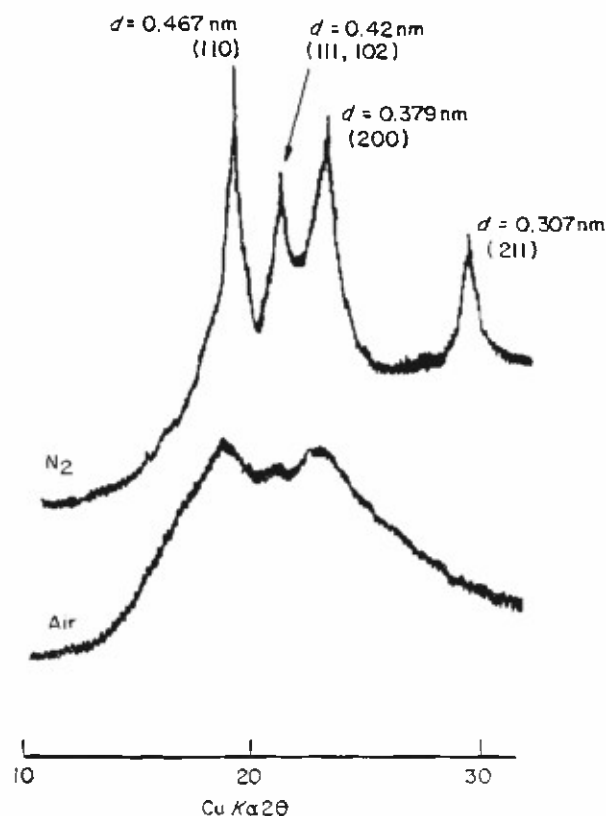


Fig. 4 XRD patterns of PEEK prepared in N_2 or air

samples. Fig. 4 shows the resulting XRD tracings, ranging from 0.884 to 0.279 nm. The XRD pattern of the N_2 sample indicates the presence of four d -spacings, 0.467, 0.42, 0.379 and 0.307 nm, corresponding to the (110), (102) or (111), (200) and (211) planes, respectively⁴. Dramatic changes in the features of the diffraction pattern were seen in the air samples, in which the weak lines at (110) and (200) reflections were still present but

the (211) plane of PEEK had almost disappeared. Thus, we can assume that the oxidation of PEEK inhibits the progression of crystallization, whereas heating in N_2 results in the development of well-crystallized PEEK. To understand the reason for the poor crystallization of the sample treated in air, we inspected the surfaces of PEEK films with XPS after exposing them for up to 24 h in air or N_2 gas at 400°C. The extent of surface oxidation as a function of exposure time was estimated by comparing the ratio of carbon and oxygen on the surface. The data were obtained from the XPS C_{1s} and O_{1s} peak areas, which were converted into elemental concentrations by means of the differential cross-section for core-level excitation. As shown in Fig. 5, the C/O ratio of the 400°C air-treated film surfaces rapidly decreases with increasing exposure time, suggesting that oxidation leads to the incorporation of additional oxygen into PEEK surfaces. However, no significant changes in C/O ratio were found on the 400°C N_2 -treated surfaces. To substantiate this information, we examined the high-resolution spectra of the C_{1s} and O_{1s} core levels for surfaces after exposure for 1, 3 or 24 h to N_2 or air at 400°C. Fig. 6 shows the C_{1s} and O_{1s} regions of N_2 -treated surfaces. Spectral deconvolution in the C_{1s} region for a 1 h-exposed surface showed the presence of four resolvable peaks at BE positions of 285.0, 286.5, 287.6 and 291.6 eV. According to the literature³⁻⁷, the principal component at 285.0 eV reflects carbon in the aryl groups. The assignments of the peaks at 286.5 and 287.6 eV as minor components are due to C in ether (C-O-C) and in ketone (C=O), respectively; the component at 291.6 eV is attributable to the $\pi \rightarrow \pi^*$ shake-up satellite peak of conjugated C=C bonds in the phenyl rings. When the exposure time was extended to 24 h, spectral features similar to those of the 1 h-exposed sample were depicted on the

film surfaces, implying that hot N_2 gas does not cause any conspicuous change in the molecular conformation of PEEK. The O_{1s} spectra of both the 1 h- and 24 h-exposed films had two peaks at 533.6 and 532.2 eV. The former, as the major O-related component, belongs to the ether oxygens in the PEEK, and the latter belongs to ketone oxygens. Although the C_{1s} and O_{1s} regions for the 3 h-exposed films are not presented in the figure, the spectral features of these core levels were similar to those for the 1 h- and 24 h-exposed films. The C_{1s} and O_{1s} regions of a hot air-treated film are given in Fig. 7. In the C_{1s} region of films exposed for 1 h, the spectral structure closely resembled that of the N_2 -treated film. After a 3 h exposure, the spectrum was characterized by a significant attenuation of the $\pi \rightarrow \pi^*$ shake-up peak at 291.5 eV, while maintaining almost the same peak position of the aryl carbons, C-O and C=O at 285.0, 286.5 and 287.6 eV. By comparison with these spectra, there were striking changes in the features of extensively oxidized film surfaces after 24 h treatments: (1) the disappearance of the $\pi \rightarrow \pi^*$ component; (2) the emergence of a new peak at 289.5 eV; and (3) the overall decay of the C_{1s} signal. A possible reason for the first result, the disappearance of $\pi \rightarrow \pi^*$, is the break-up of π bonds in the phenyl rings due to oxygen atoms impinging on the PEEK surfaces. The peak at 289.5 eV (the second change) is assignable to carbon originating from carboxyl groups (-O-C=O). The third result reflects the decay of ether, ketone and aryl groups. Inspection of the O_{1s} spectra provided further insights on the oxygen-catalysed decomposition of PEEK. The O_{1s} spectrum (Fig. 7) for the 1 h-aged films contains two distinct lines, due to ether oxygen atoms at 533.6 eV as the major component and carbonyl oxygen atoms at 532.2 eV as the minor one. After exposure for 3 h, there is a reduction of line intensity at 532.2 eV. Extended oxidation times to 24 h led to the emergence of new peak at 532.7 eV corresponding to the carboxyl oxygen atoms, while the line intensity of C=O continuously diminished. Thus, the high degree of oxidation of PEEK not only promotes the breakage of bonds within the aryl groups and the rupture of ketone, which directly links two phenyl rings, but also results in the formation of carboxyl groups from the incorporation of additional oxygens into the damaged PEEK structure. However, the mechanism of oxygen-induced decomposition of PEEK remains obscure. Overall, these data clearly demonstrate that the decomposition of aryl and ketone groups brought about by the increasing oxidation of PEEK significantly inhibits the rate of crystallinity.

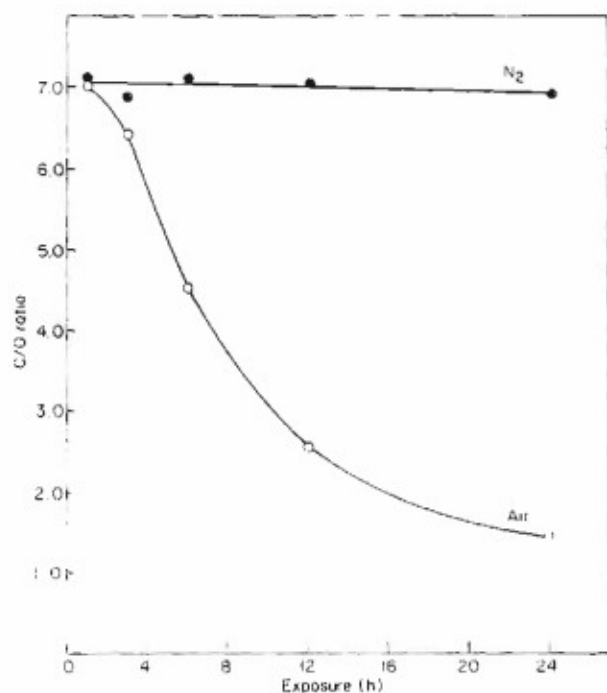


Fig. 5 Changes in the C/O ratio of PEEK film surface as a function of exposure times up to 24 h in air or N_2 at 400°C

Interfaces of PEEK-to-metal joints

In preparing the metal-to-PEEK joints, the cold-rolled steel (CRS) and stainless steel (SS) surfaces were wiped with acetone-soaked tissues to remove any contamination from mill oil. The PEEK film was deposited on the surfaces of the CRS and SS substrates in the following way. First, the substrates were dipped into a PEEK slurry, consisting of 45% wt% PEEK and 55 wt% isopropylalcohol at 25°C. Then the slurry-coated substrates were heated in air or N_2 at 400°C for 3 h to melt the PEEK powder, and, at the same time, to volatilize the isopropylalcohol. To induce crystallization,

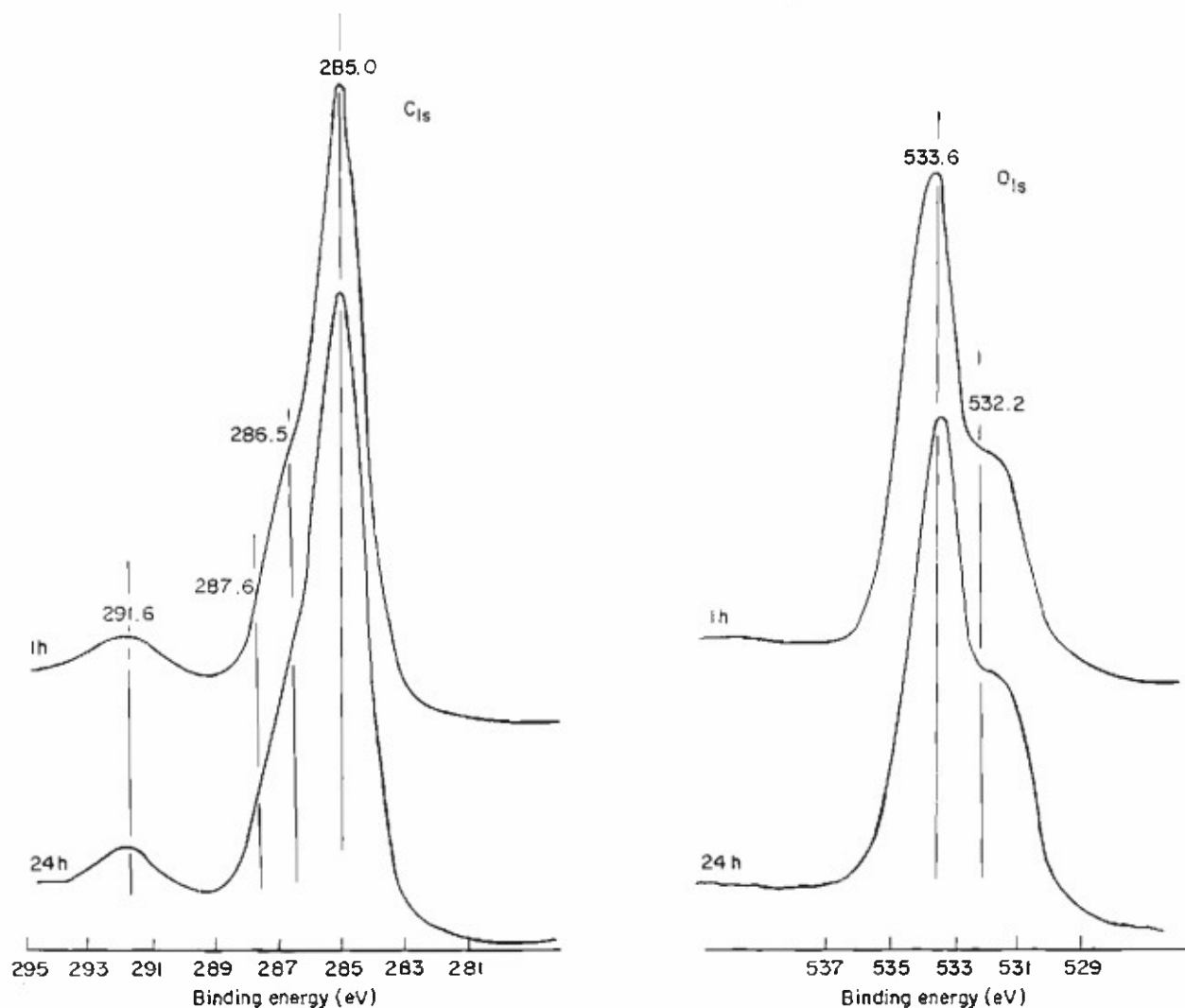


Fig. 6 XPS C_{1s} and O_{1s} core-level spectra for PEEK film surfaces exposed for 1 and 24 h in N₂ at 400°C

the melted PEEK was cooled to room temperature at the rate of $\sim 10^{\circ}\text{C min}^{-1}$.

Fig. 8 shows the lap-shear bond strengths of the metal-to-metal PEEK adhesive joints. The data verified that the bond strengths depend primarily on the ambient atmosphere during the melting-crystallization process, and on the species of substrate. The strengths of specimens prepared under N₂ are much higher than those for specimens made in air. Also, the development of interfacial bond strength in the SS/PEEK joint system is better than that of the CRS/PEEK system.

To clarify the causes of good and poor interfacial bonds, XPS was used to explore failure surfaces. The XPS chemical composition of acetone-cleaned CRS and SS substrate surfaces, and the PEEK surfaces made in N₂ and air at 400°C, are given as reference data in Table 1. Table 2 shows the elemental compositions for the cross-section samples of the PEEK/CRS joint system after exposure to N₂ and to air. In N₂, the interface chemical constituents of the PEEK and CRS sides were similar to those of the bulk PEEK and base CRS surfaces (Table 1), suggesting that failure occurs at the interface between PEEK and CRS. There was a striking difference

between these findings and those from the air-treated samples: namely, a large amount of oxygen, a low amount of carbon and 3.7% Fe, belonging to the CRS, was detected on the PEEK side removed from the CRS substrate. Therefore, failure can be figured as a cohesive mode which occurs through Fe-related oxide compound layers at the top surface of CRS, close to PEEK. This failure mode suggested that the introduction of air into the interfacial zones promotes the extent of interaction between PEEK and Fe oxides. We believe that such reaction products are much stronger than those of Fe oxide layers.

To support this information, we inspected the high-resolution C_{1s} and O_{1s} core-level spectra of both the PEEK and CRS interfacial sides for N₂- or air-treated samples (Figs 9 and 10). In N₂, the spectral feature of the C_{1s} region for the PEEK interface (see Fig. 9) closely resembled those of the bulk PEEK surfaces (Fig. 6) prepared in the same environment. The C_{1s} region of the interfacial CRS side has at least four resolvable Gaussian components at 285.0, 286.5, 287.6 and 289.2 eV, which reflect the C in hydrocarbons, ether or alcohol, aldehyde or ketone, and carboxylic acid or

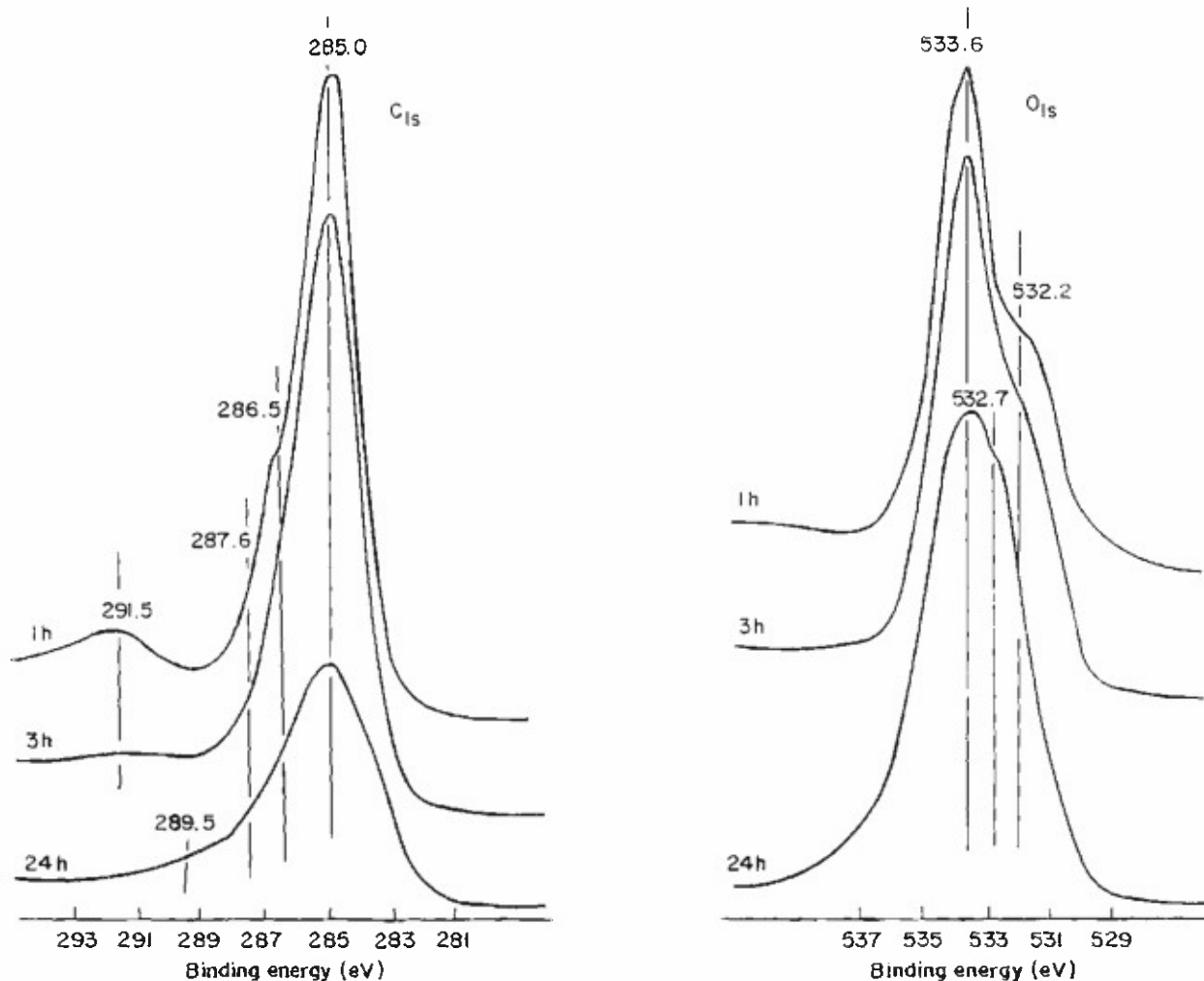


Fig. 7 C_{1s} and O_{1s} regions for PEEK film surfaces after exposure for 1, 3 and 24 h in air at 400°C

ester, respectively⁷. No $\pi \rightarrow \pi^*$ shake-up satellite near 291.5 eV was found on the failed CRS sides. Thus, these carbon species detected from the CRS sides are more likely to be associated with the contaminating carbons in CRS itself, rather than being PEEK-related carbons. As expected, the O_{1s} spectrum for the PEEK interface features a typical PEEK O_{1s} structure containing a major line at 533.6 eV originating from O in ether and a minor line at 532.2 eV from O in ketone. By comparison with the PEEK side, a distinctive O_{1s} signal structure was seen on the CRS interface; namely, a principal component at 530.5 eV, and minor ones at 532.2 and 533.6 eV. The 530.5 eV line can be ascribed to oxygen in the ferric oxide (Fe_2O_3)⁸. In fact, the formation of Fe_2O_3 also was confirmed from the main core line at 710.9 eV in the $Fe_{2p_{3/2}}$ region (not shown). The other lines at 532.2 and 533.6 eV seem to correspond to oxygen in ketone or aldehyde, and ether or ester⁷, as the contaminants of CRS. Fig. 10 gives the C_{1s} and O_{1s} regions for both interfacial sides after treatment in air. As shown, C_{1s} and O_{1s} spectral features similar to those of the CRS interface were observed from the interfacial PEEK side. This finding implied that the Fe_2O_3 compounds and contaminating species are transferred from the CRS to the PEEK side as

the interfacial bond progressively fails. One important factor affecting a better bonding performance is the degree of crystallinity of the PEEK film adjacent to the CRS. Fig. 11 illustrates the XRD tracings for the cross-section PEEK samples of PEEK/CRS joint systems prepared in N_2 or air. The diffraction patterns for (a) the N_2 and (b) the air samples showed features similar to those obtained from hulk PEEK (Fig. 4): namely, a well-crystallized PEEK layer in the vicinity of the CRS substrate is formed when the joint is prepared in N_2 . In contrast, the introduction of oxygen into the critical contact zones of the interface for the air-treated systems resulted in a low degree of crystallinity of PEEK adjacent to the substrates. Such an effect appears to be due to oxygen-catalysed deformation of the PEEK structure, signifying that the major phase of interfacial PEEK layers is the amorphous-type polymer. Although PEEK was damaged by the attack of oxygen, the xps data suggested that oxidized PEEK favourably links to Fe_2O_3 on the top surface of CRS. The bond strength of air-treated specimens is much weaker than that of N_2 -treated specimens, possibly because oxidation at the PEEK/CRS joints results in an extensive production of mechanically weak Fe_2O_3 layers, rather than the loss being caused by the poor crystallization of PEEK. In

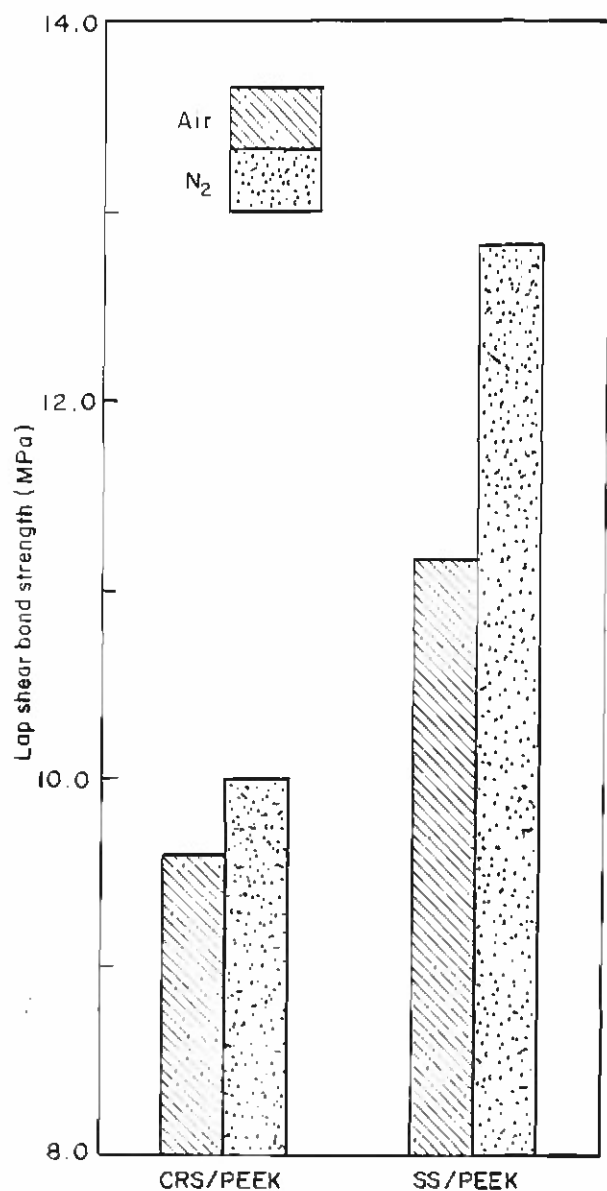


Fig. 8 Lap-shear bond strength for metal-to-metal PEEK adhesive joints prepared in air or N₂ at 400°C

fact, xps inspection of the failing sides showed that they expressed the cohesive mode in which bond failure occurs through the Fe₂O₃ layers.

Table 3 presents the elemental compositions for both interfacial failure sides in the PEEK/SS joint system. For the sample made in N₂, the PEEK interface had a composition closely resembling that of the reference PEEK (see Table 1). The amount of C detected on the ss side was considerably greater, and the amount of O and Fe substantially less than that observed on the reference ss surface, while there was no signal for Cr, thereby accounting for a certain amount of reaction products remaining on the interfacial ss surfaces. This finding suggested that PEEK favourably reacts with the ss surfaces. Hence, failure is certain to occur through the PEEK adhesive layers. On the other hand, a different locus of failure was observed from the air-treated adhesion sample; the

Table 1. XPS elemental analysis of bulk polyphenyletheretherketone (PEEK) and substrates as reference surfaces

Coatings and substrates	Atomic concentration (%)				
	C	O	Mn	Fe	Cr
PEEK made in N ₂	87.5	12.5	—	—	—
PEEK made in air	86.9	13.1	—	—	—
CRS	25.8	59.9	1.7	12.5	—
SS	58.3	34.4	—	5.5	1.8

CRS — 1010 cold-rolled steel; SS — 304 stainless steel

Table 2. Chemical composition of both interfacial failure sides for N₂- and air-treated PEEK/CRS joint systems

Heating environment	Failed side	Atomic concentration (%)			
		C	O	Mn	Fe
N ₂	PEEK	87.9	12.1	—	—
N ₂	CRS	30.7	58.1	1.5	9.7
Air	PEEK	47.8	48.5	—	3.7
Air	CRS	34.3	59.6	0.8	5.3

chemical compositions of the interfacial PEEK and ss sides are similar to those of the reference sample surfaces except that more O was incorporated into the ss side, implying that the interfacial ss was oxidized during exposure to hot air. Thus, an adhesive failure mode, which occurs at the PEEK/ss interfaces, can be proposed for this joint system.

The identification of the reaction products and bond structure at the interfaces of N₂-induced PEEK/ss joints is of particular interest. Again, to obtain this information, we investigated the XPS C_{1s} and O_{1s} core-level spectra for both the interfacial PEEK and ss surfaces (Fig. 12). The C_{1s} region of the interfacial ss side exhibits the $\pi \rightarrow \pi^*$ satellite peak at 291.5 eV, corresponding to a residual amount of PEEK adhering to the ss surfaces, while an additional new peak appears at BE position of 287.1 eV. This new peak, situated between the C-O at 286.5 eV and the C=O at 287.6 eV, may reveal the formation of metal-O-C complexes⁹⁻¹¹. In fact, the O_{1s} core-level spectrum of the interfacial ss side shows a conspicuous peak at 531.6 eV, which we ascribe to metal-O bond formation¹², and the attenuation of the C=O peak in the PEEK at 532.2 eV, while an ether oxygen in the PEEK at 533.6 eV and Fe₂O₃ oxygen at 530.5 eV are present. Unfortunately, information on chemical bonding was difficult to obtain from the Fe and Cr core levels, because these signals were too noisy to analyse by deconvolution. Although further detailed xps studies will be required to ascertain the C_{1s} data, it is possible to assume that the metal-O bond species belongs to the Fe or Cr-O-C model compounds which are generated through a mechanism involving a charge transfer reaction at the interfaces between the C=O in PEEK and the elemental Fe or Cr in ss. Thus, reactive

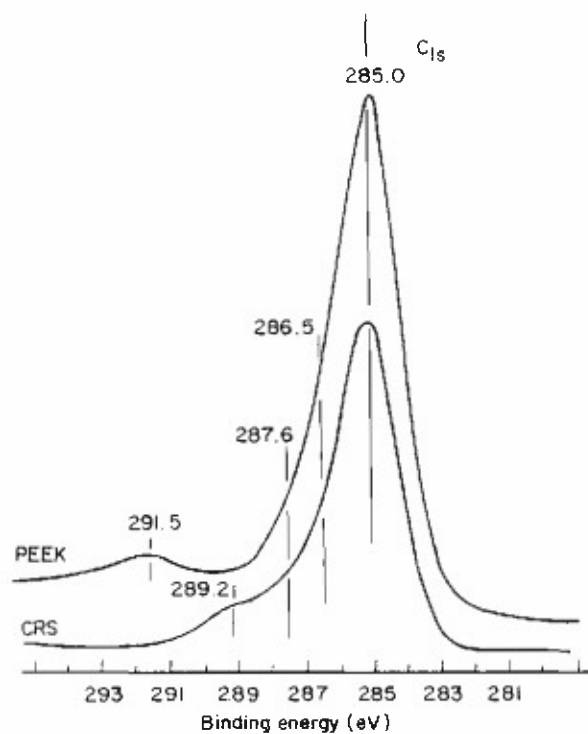


Fig. 9 C_{1s} and O_{1s} spectra at failed interfaces of the PEEK/CRS joint system prepared in N₂ at 400°C

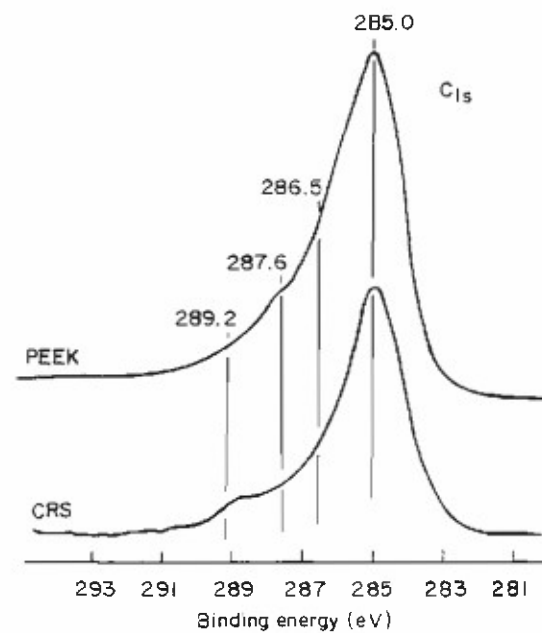
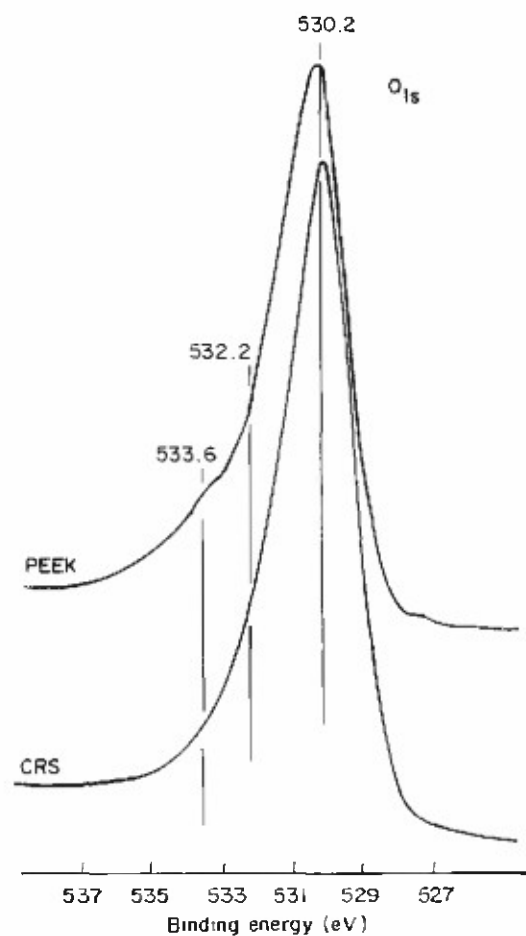
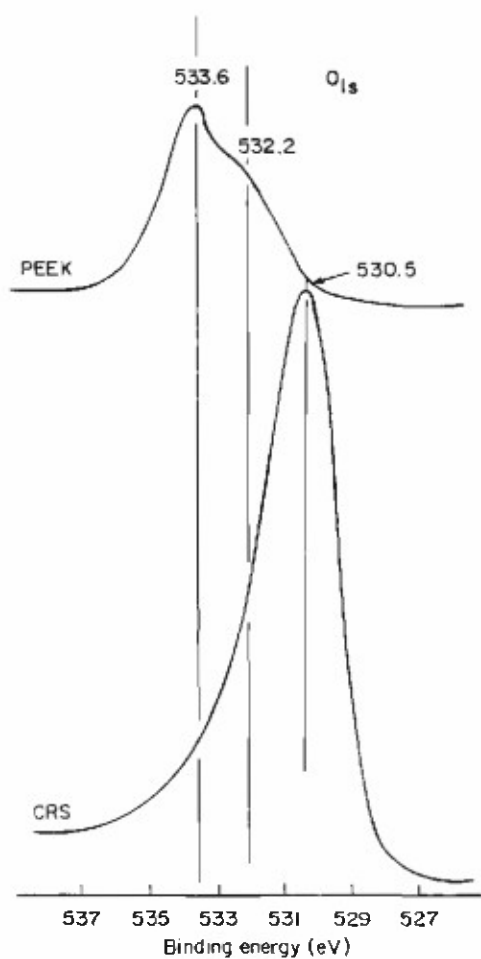


Fig. 10 C_{1s} and O_{1s} regions at the interfacial failure locus of the PEEK/CRS joint system prepared in air at 400°C



Fe and Cr may break the C=O double bond in the PEEK molecules by forming Fe or Cr-O-C complexes where the charge density is transferred from the Fe and Cr to electron-accepting oxygens in functional C=O

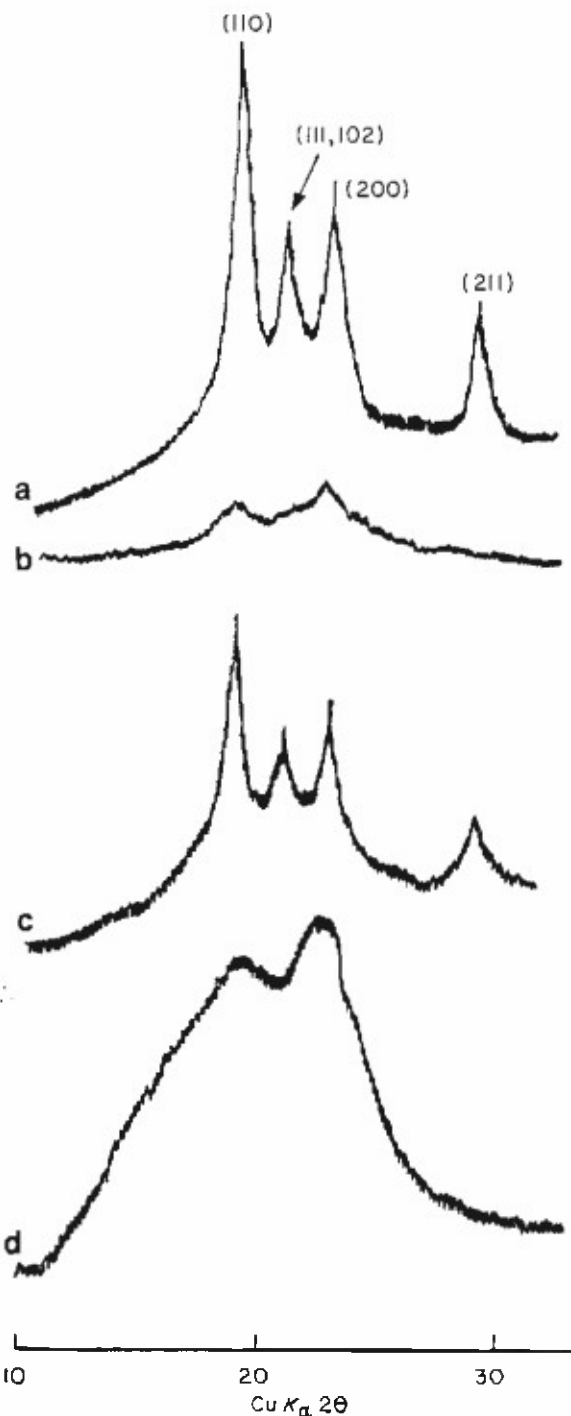


Fig. 11 XRD patterns for interfacial PEEK sides in (a) N_2 - and (b) air-treated PEEK/CRS joints, and in (c) N_2 - and (d) air-treated PEEK/SS joints

groups. Considering that most of the high lap-shear bond strength is conferred by the PEEK-to-SS joint system, such an interfacial Fe or Cr-O-C covalent bond appears to play an active role in improving the strength of this bond. Compared with the N_2 sample, the air-induced SS interface (Fig. 13) shows quite different C_{1s} and O_{1s} signals. Thus, there are no peaks present corresponding to the formation of metal-O-C bonds; otherwise, the spectral signals are similar to those of the CRS interface removed from PEEK in air

Table 3. Atomic concentration of N_2 - and air-treated PEEK/SS interfaces

Heating environment	Failed side	Atomic concentration (%)			
		C	O	Fe	Cr
N_2	PEEK	82.8	17.2	—	—
N_2	SS	76.3	23.1	0.6	—
Air	PEEK	84.5	15.5	—	—
Air	SS	41.1	53.9	3.7	1.3

(see Fig. 10). Therefore, failure is not a cohesive one through the PEEK layer, but may have proceeded through the interface between PEEK and SS.

To further support our findings on the failure mode, we inspected by SEM the microstructure of the interfacial sides of PEEK film removed from SS in the joint system made in air or in N_2 (Fig. 14). The SEM micrograph of the failure surface on the PEEK side obtained from air-induced joints (Fig. 14(a)) shows numerous gutters and grooves, probably caused by being traced out by the profile of SS surface structures (not shown), reflecting the characteristics of the adhesive failure mode. By comparison with this image, a strikingly different one was observed from the PEEK interface in the N_2 -made joints (see Fig. 14(b)). Namely, the failed PEEK side showed very rough surfaces resulting from extensive plastic deformation, which is characteristic of the cohesive failure in ductile PEEK polymers. This failure mode probably explains why these specimens exhibited such high lap-shear bond strengths. Returning to the XRD tracings in Fig. 11, the diffraction patterns of the interfacial PEEK sides for the PEEK/SS joints prepared in N_2 or air clearly verified that, although the species of metals is different, the oxygen-catalysed decomposition of PEEK caused by introducing air into the interfacial contact zones leads to poor crystallinity of PEEK in the vicinity of the SS substrate (see Fig. 11(d)). In contrast, well-formed PEEK crystals are obtained in N_2 -induced joints (Fig. 11(c)).

Conclusions

In N_2 gas, the melted polyphenyletheretherketone (PEEK) polymer can be exothermically crystallized on cooling to $\sim 300^\circ\text{C}$. The thermal decomposition of well-crystallized PEEK begins at temperatures near 610°C . In contrast, PEEK melted in air had a low rate of crystallinity, reflected in a weight loss more than twice that of the N_2 sample at $\sim 730^\circ\text{C}$ and the onset of thermal decomposition at lower temperature. Such poor crystallization behaviour mainly resulted from the decomposition of the PEEK structure caused by oxygen-catalysed breakage of π bonds in the aryl groups and rupture of the ketone groups.

When PEEK was applied as an adhesive material in the metal-to-metal joint systems, generally, the following four items were the major chemical factors governing the bond structure and failure of PEEK/metal joints prepared under air or N_2 at 400°C .

- 1) The bonding failure of N_2 -induced PEEK/cold-rolled steel (CRS) joint was proposed as an adhesive mode,

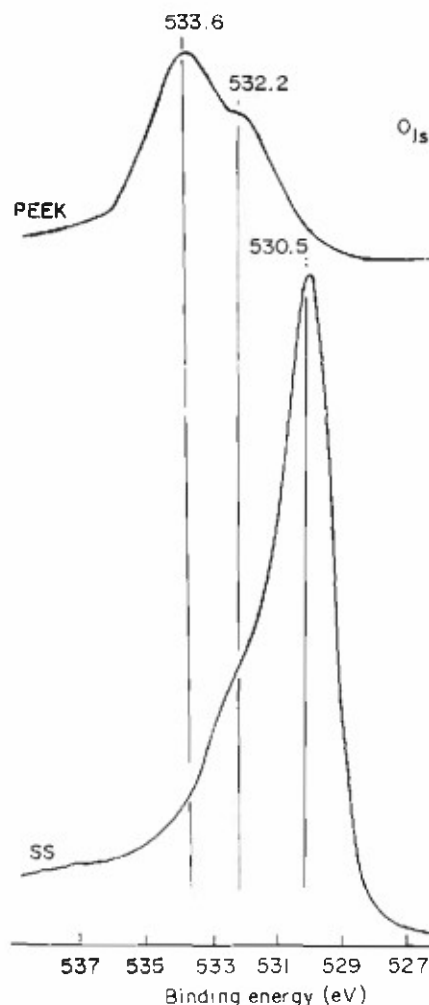
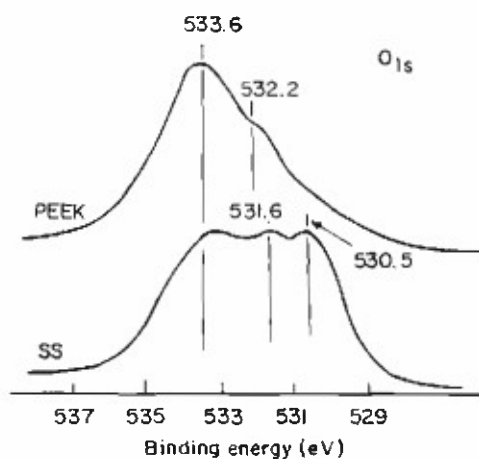
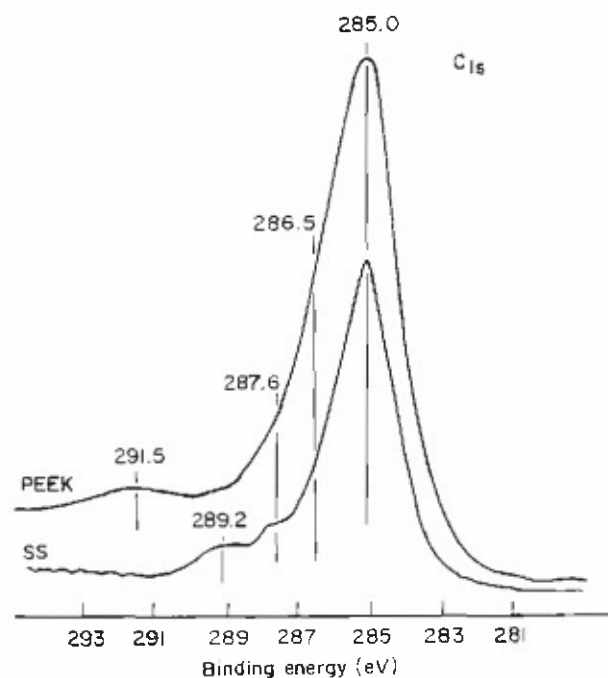
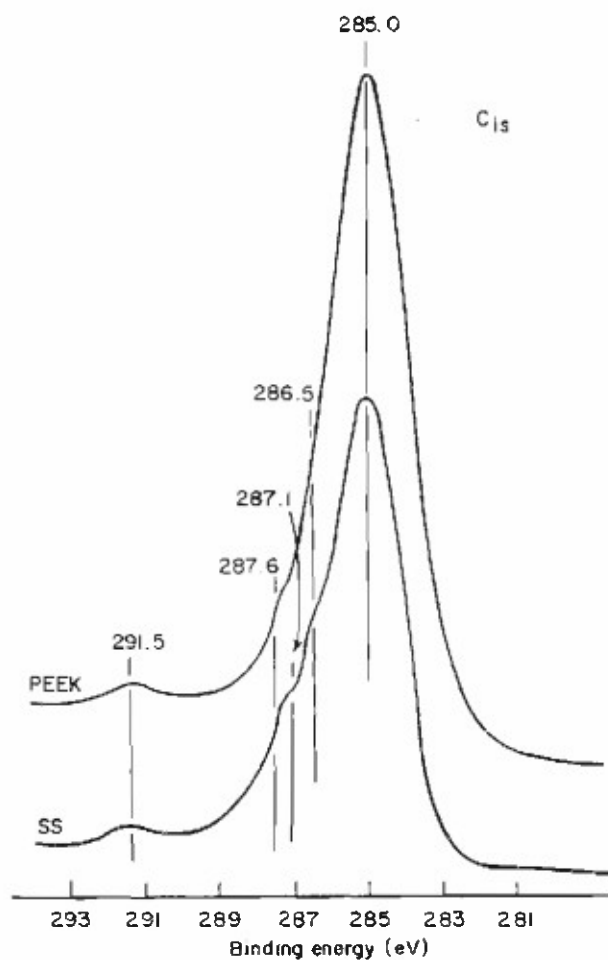


Fig. 12 C_{1s} and O_{1s} spectra at the failure locus in the PEEK/SS joint system prepared in N_2

Fig. 13 C_{1s} and O_{1s} spectra at the failure locus in the PEEK/SS joint system prepared in air

in which delamination of the PEEK film occurs at the PEEK/CRS interface. No clear evidence was found for the chemical interaction of PEEK with an Fe_2O_3 layer at the top surface of CRS by X-ray photoelectron spectroscopy (XPS).

- 2) The lowest bond strength in this test series was from the air-induced PEEK/CRS joint specimens. The lack of strength was more likely to be caused by extensive formation of mechanically weak Fe_2O_3 layers at the

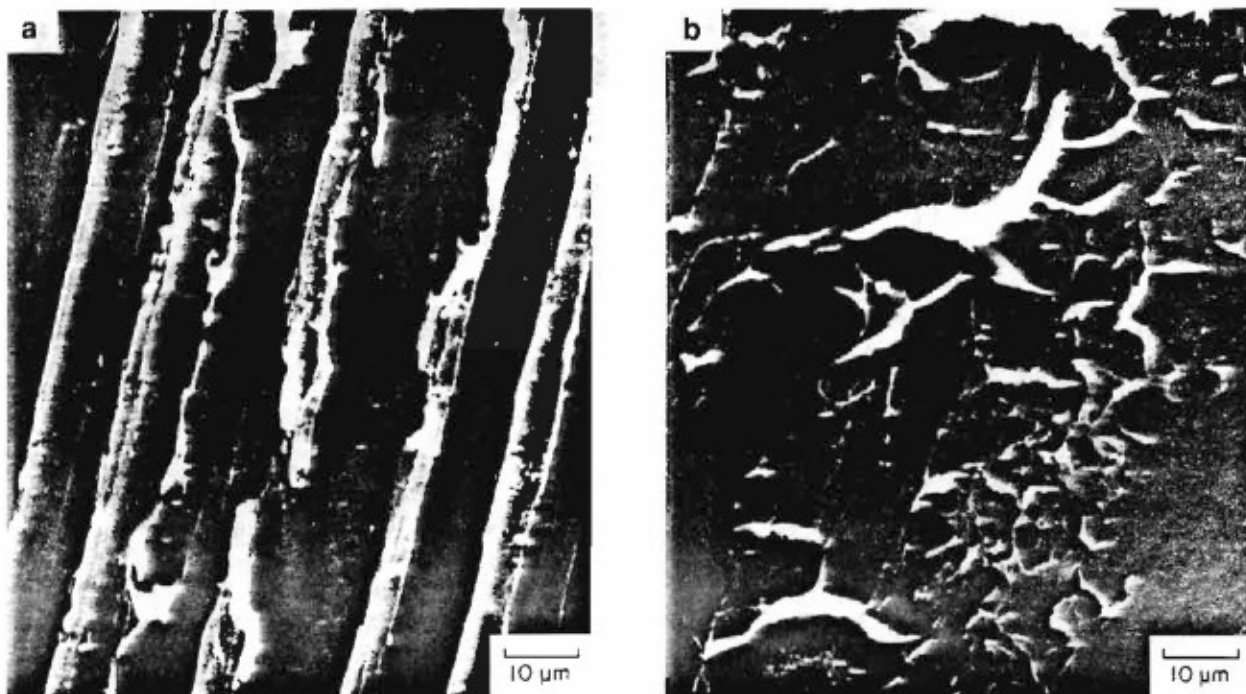


Fig. 14 SEM micrographs of PEEK interfaces removed from the PEEK/SS joint system prepared in: (a) air; and (b) N_2

interfaces, rather than to the poor crystallization of the PEEK film adjacent to the Fe_2O_3 caused by oxidation, because cohesive failure, which occurs through the Fe_2O_3 layer, was observed.

- 3) Three important elements were responsible for a good bond at PEEK/metal joints: (a) the formation of Fe or Cr-O-C complexes bonded covalently by a charge-transferring reaction between oxygen in the ketone groups of PEEK and elemental Fe or Cr in the metals; (b) the formation of a well-crystallized interfacial PEEK; and (c) the presence of a moderate amount of Fe_2O_3 . The N_2 -induced PEEK/stainless steel (SS) joint fully met all of these interfacial requirements, developing maximum bond strength and having a cohesive mode in which failure occurs through the PEEK layer.
- 4) Although the conversion rate of elemental Fe into Fe_2O_3 for interfacial SS is lower than that of CRS in the air-induced PEEK/SS joint, poor crystallization of PEEK caused by oxidation resulted in a lack of interfacial chemical bonds, reflecting failure at the PEEK/SS interfaces.

Acknowledgements

This work was performed under the auspices of the US Department of Energy, Washington, DC, under contract no. DE-AC02-76CH00016, and supported by the US Army Research Office Program MLPR-ARO-119-91 and the Physical Sciences Department of the Gas Research Institute, under contract no. 5090-260-1948.

References

- 1 Sugama, T. and Carciello, N.R. 'Interfaces of polyphenylene sulphide-to-metal joints' *Int J Adhesion and Adhesives* 11 (1991) pp 97-104
- 2 Waddon, A.J., Hill, M.J., Keller, A. and Blundell, D.J. 'On the crystal texture of linear polyaryls (PEEK, PEK, and PPS)' *J Mater Sci* 22 (1987) pp 1773-1784
- 3 Blundell, D.J. and Osborn, B.N. 'The morphology of poly(aryl-ether-ether-ketone)' *Polymer* 24 (1983) pp 935-938
- 4 Dawson, P.C. and Blundell, D.J. 'X-ray data for poly(aryl ether ketones)' *Polymer* 21 (1980) pp 577-578
- 5 Briggs, O., Brewis, D.M. and Konieczko, M.B. 'X-ray photoelectron spectroscopy studies of polymer surfaces' *J Mater Sci* 14 (1979) pp 1344-1348
- 6 Lopez, L.C. and Dwight, D.W. 'Preferential enrichment of chemistry at polymer surfaces' *J Appl Polym Sci* 36 (1988) pp 1401-1415
- 7 Briggs, O. and Seah, M.P. 'Practical Surface Analysis by Auger and X-ray Photoelectron Spectroscopy' (John Wiley & Sons, New York, 1983) pp 359-396
- 8 McIntyre, N.S. and Zetaruk, D.G. 'X-ray photoelectron spectroscopic studies of iron oxides' *Anal Chem* 49 (1977) pp 1521-1529
- 9 Ho, P.S., Hahn, P.O., Barthe, J.W., Rubloff, G.W., LeGoues, F.K. and Silverman, B.O. 'Chemical bonding and reaction at metal/polymer interfaces' *J Vac Sci Technol* 3 (1985) pp 739-745
- 10 Barthe, J.W., Hahn, P.O., LeGoues, F.K. and Ho, P.S. 'Photoemission spectroscopy study of aluminium-polyimide interface' *J Vac Sci Technol* 3 (1985) pp 1390-1393
- 11 Ohuchi, F.S. and Freilich, S.C. 'Metal polyimide interface: a titanium reaction mechanism' *J Vac Sci Technol* 4 (1986) pp 1039-1045
- 12 Geremser, L.J. in 'Metallization of Polymers' edited by E. Sacher, J. Pireaux and S.P. Kowalczyk (ACS Symposium Series 440, Washington, DC, 1990) pp 433-452

Authors

The authors are with the Energy Efficiency and Conservation Division, Department of Applied Science, Brookhaven National Laboratory, Upton, NY 11973, USA. Correspondence should be directed to Dr Sugama.

Synthesis and adhesive properties of some polyurethane dispersions

T. Malavašič, N. Černilec, A. Mirčeva and U. Osredkar

(Boris Kidrič Institute of Chemistry, Slovenia)

Received 6 September 1991; accepted in revised form 12 November 1991

Three different cationic polyurethane dispersions were synthesized and their adhesive properties tested on polyvinyl chloride/polyvinyl chloride, polyurethane/natural leather and rubber/natural leather systems. In some cases the dispersions were cross-linked during bonding. The kinetics of the cross-linking reaction were studied by infra-red spectroscopy and differential scanning calorimetry.

Key words: adhesives; polyurethane dispersions; formulation; cross-linking; reaction kinetics; T-peel strength

Polyurethane solution adhesives are widely used; however, for environmental protection reasons the solvent-borne systems will be gradually replaced by water-borne systems. During the last 20 years the synthesis and properties of polyurethane aqueous dispersions have been extensively studied by many authors¹⁻⁶. Due to the sensitivity of these systems to solvents and water, in some cases of application the linear molecular structure of the polyurethane ionomers could cause problems. This deficiency may be overcome by cross-linking the system during application^{5,6}, for example by using trimerized diisocyanates. The cross-linking reaction can be followed by different methods, with infra-red (IR) spectroscopy⁷ and differential scanning calorimetry (DSC)⁸ being particularly convenient.

In this work the adhesive properties of three cationic polyurethane dispersions to four different materials were examined. In some experiments the polyurethane ionomers were cross-linked during application. The kinetics of the cross-linking reaction were studied by IR spectroscopy and DSC.

Experimental details

Preparation of dispersions

The cationic polyurethane dispersions were synthesized from polycaprolactone (CAPA, $M_n = 2000$ from Solvay), 1,4-butanediol (BD, from Bayer), N-methyl-diethanolamine (NMDEA, from Merck), isophorone

diisocyanate (IPDI, from Huls) and toluene diisocyanate (TDI, 80% of the 2,4 and 20% of the 2,6 isomers, from Soda So) using a standard prepolymer process⁶.

In the first step the isocyanate prepolymer is formed from the polymeric diol (polycaprolactone) and an excess of diisocyanate. The prepolymer is then dissolved in a low boiling solvent (normally acetone) and chain-extended by low molar mass diols, part of them containing ionic groups (1,4-butanediol, N-methyldiethanolamine). In the next step the ionic groups are neutralized and the dispersion is formed by addition of water under vigorous stirring. The solvent is removed by vacuum distillation and a purely aqueous dispersion is obtained, as shown in the reaction scheme illustrated in Fig. 1.

The ionomers differed in their molar ratio of IPDI to TDI — i.e., 3:1 (samples 1 and 3) and 1:1 (sample 2) — and in their molar ratio of CAPA to BD — i.e., 1:4 (samples 1 and 2) and 1:2 (sample 3). The concentration of ionic groups in all cases was 0.30 mmol g^{-1} . Formulations are given in Table 1.

For some of the adhesion tests the 20% dispersions of the polyurethane ionomers were thickened with 2 weight % (wt %) SiO_2 .

During application the dispersions were cross-linked by trimerized hexamethylene diisocyanate (Desmodur N from Bayer, containing 11% of NCO groups) or by isocyanurate trimer (Desmodur DA from Bayer, containing 19.5% of NCO groups). In both cases 10 wt% of the cross-linking agent was added, calculated on the solids content of the dispersion.

APPENDIX D

ISSUED PATENTS

[54] POLYACID MACROMOLECULE PRIMERS

[75] Inventor: Toshifumi Sugama, Mastic Beach, N.Y.

[73] Assignee: Associated Universities, Inc., Washington, D.C.

[21] Appl. No.: 188,974

[22] Filed: May 2, 1988

[51] Int. Cl.⁺ C09J 7/02; B32B 15/08[52] U.S. Cl. 428/343; 428/423.1;
428/425.8; 428/457; 428/463[58] Field of Search 428/343, 423.1, 457,
428/463, 425.8

[56] References Cited

U.S. PATENT DOCUMENTS

4,567,107	1/1986	Rizk et al.	428/425.5
4,610,898	9/1986	Engel et al.	427/379
4,612,236	9/1986	Hsu et al.	428/463 X
4,657,962	4/1987	Brundopke et al.	428/423.1
4,668,588	5/1987	Kishima	428/423.1
4,714,512	12/1987	House et al.	428/423.1 X
4,741,934	5/1988	Terayama et al.	428/457 X

OTHER PUBLICATIONS

Sugama et al.; "Nature of Interfacial Interaction Mechanisms Between Polyacrylic Acid Macromolecules and

Oxide Metal Surfaces". J. Mater. Sci. 19, 4045, Dec. 1983 pp. 1-29.

Sugama et al. (2), "Effects of Polyacrylic Acid Primers on Adhesion and Durability of FPL-Etched Aluminum/Polyurethane Systems", J. of Adhesion Science and Technology, vol. I, No. 4, Jan/1987, pp. 265-280.

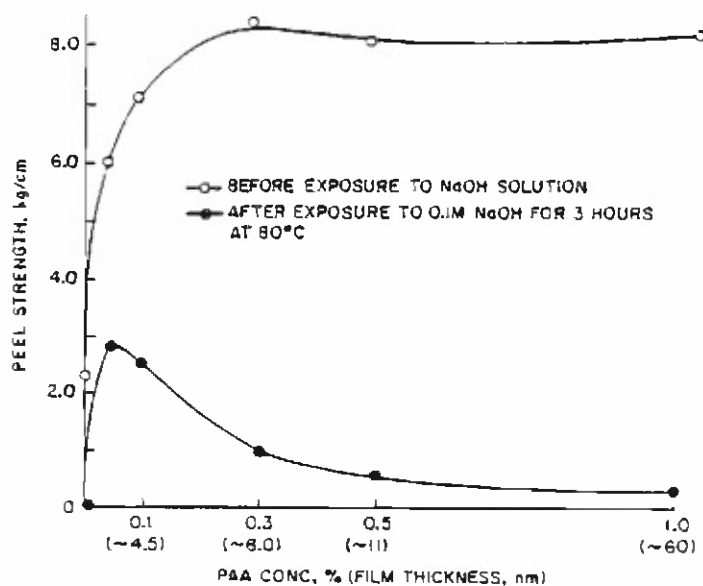
Sugama et al. (3) "Polyitaconic Acid Macromolecule, Primer for Adhesive Bonding and Corrosion Control of Aluminum", TriService Corrosion Conference, May 1987, pp. 1-14.

Primary Examiner—Thomas J. Herbert
Attorney, Agent, or Firm—Margaret C. Bogosian

[57] ABSTRACT

Hydrophylic polyacids, such as macromolecules of polyitaconic acid and polyacrylic acid, where such macromolecules have molecular weights > 50,000 as primers between a polymeric top coating, such as polyurethane, and an oxidized aluminum or aluminum alloy. A near monolayer of primer is used in polymeric adhesive/oxidized aluminum adhered joint systems in 0.05% primer concentration to give superior results in standard peel tests.

12 Claims, 2 Drawing Sheets



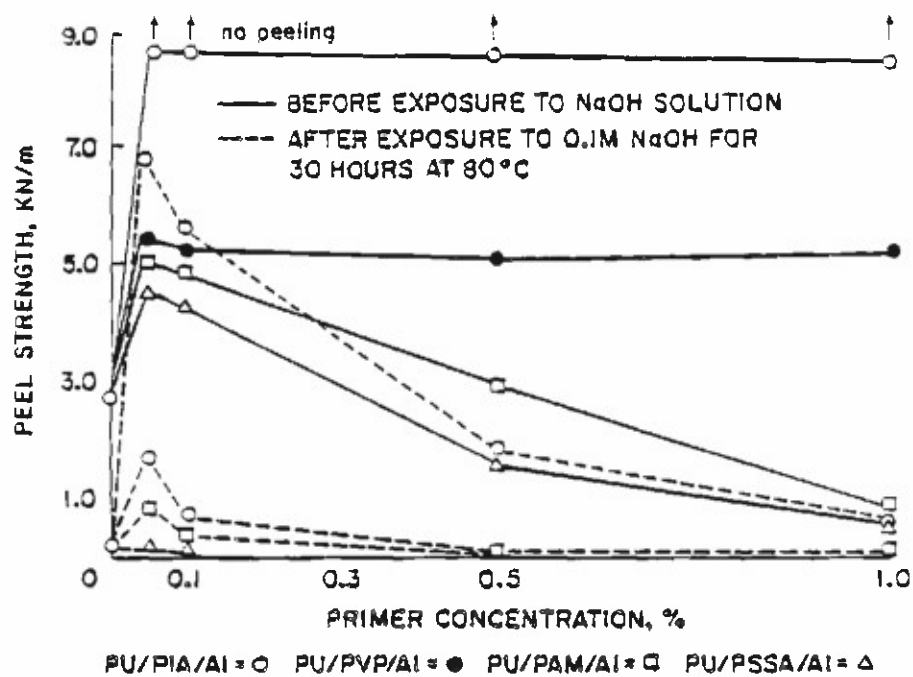


Fig. 1

POLYACID MACROMOLECULE PRIMERS

This invention was made with Government support under contract number DE-AC02-76CH00016 between the U.S. Department of Energy and Associated Universities, Inc. The Government has certain rights in the invention.

BRIEF DESCRIPTION OF THE INVENTION

The present invention describes the formulation and use of hydrophilic-type polyacid macromolecules, usually with molecular weights greater than 50,000, to significantly enhance the surface characteristics of oxidized aluminum and aluminum alloys. When these polyacid macromolecules, which contain functional carboxylic acid pendent groups are used as a coupling or cross-linking primer in polymeric adhesive/oxidized aluminum adherend joint systems, they preferentially interact both with the hydrated oxide aluminum adherend to form hydrogen bonds and with the functional groups in the adhesive to yield polymer-to-polymer chemical bonding. This chemical coupling between the hydrated adherend and the polymeric adhesive acts significantly to promote interfacial adhesive bonds. It appears that a near monolayer of polyacid is enough to occupy all available functional groups at the adhesive and aluminum surface sites. This arrangement plays a key role in governing the adhesion durability of the joint system and the corrosion resistance of aluminum upon exposure to a corrosive fluid. The bond stability and corrosion protective ability are due primarily to the formation of interfacially produced hydrophobic reaction products.

BACKGROUND OF THE INVENTION

The important factors that determine the ability of polymer coatings to protect structural aluminum surfaces from corrosion are the magnitude of the wettability of the Al surface by liquid polymer materials and the stability of the interaction products formed at polymer-to-Al interfaces. In order to achieve enhanced wettability, the Al surface should have a high surface free energy for enhanced surface reactivity and sufficient roughness to provide a large surface area for promoting wetting and mechanical locking. If the chemical interaction at the polymer/Al joint results in the formation of valence bonds, mainly covalent, the interfacially-formed interaction products will not only result in an increase in the basic adhesion, but also contribute to a modification of the chemical composition at the interfacial regions. This modification should be associated with the formation of hydrophobic interaction products which can be expressed as passivating layers.

To date, two commercial surface preparations for Al, the Forest Products Laboratory (FPL) preparation [Eichner et al., Forest Products Laboratory Report No. 1813, Madison, Wis., 1950] and the Phosphoric Acid Anodization (PAA) process [Kabayaski et al., Boeing Corporation Report No. D6-41517, Seattle, Wash., 1974], have been widely applied to promote interfacial bond strength at aluminum adhesive joints. The purpose of these surface treatments is not only to increase the roughness of the Al surface thereby enhancing the mechanical interlocking bonds, but also to modify the surface chemical compositions.

One significant problem that has been encountered with these commercial surface preparations is that

when the freshly etched aluminum surface is exposed to moisture, hydration begins to occur. Considerable attention has been given to the growth and transformation of the FPL oxide to a hydrated oxide Al in the interfacial regions as this interface was exposed at various times to a humid environment. The chemical transformation commences when the moisture penetrates through the polymer layer and reaches the original adherend oxide adjacent to the adhesives. The reaction of Al oxide with moisture results in the formation of the hydrated oxide Al which represents a different morphology from the original oxide. This interfacial conversion of Al oxide to hydroxide leads to the generation of adhesion stress and swelling and the promotion of crack propagation at or near the Al-hydroxide interfaces, thereby resulting in bond failure and the initiation of corrosion. In either the FPL or PAA treatment, an oxide adherend that will resist attack by moisture is the critical element for bond durability.

Prior art approaches to dealing with the moisture problem involve the tailoring of the reactive surface nature using organosilane and titanate derived coupling agents as chemical modifications for Al oxide and hydroxide surfaces. However, oligomers or unreacted mono silanols are still present in the coupling layers. The presence of unreacted functional silanol leads to the hydrolysis of the coupling layer brought about by penetration of moisture through the adhesive, as the adhesive/coupling/adherend joint system is exposed to high humidity environments. This relates directly to the hydrolytic delamination failure mode.

The simplicity of polyacid molecules such as the polyacrylic acid (PAA) and polyitaconic acid (PIA) macromolecules, which consist of $-\text{CH}_2-\text{CH}-$ main chains and functional carboxylic acid pendent groups, makes them very attractive for use in resolving the problems presented by the prior art materials. Work related to the nature of interfacial reactions which play key roles in determining the extent of bonding between PAA/PIA and crystalline hydrate conversion coatings deposited as corrosion protective films on steel surfaces is known [Sugama et al., *J. Mater. Sci.*, 19, 4045, 1984]. Even though the rough surface morphology of the conversion coatings enhances the interfacial mechanical bonding, the regularly oriented pendent carboxylic acid groups at the interface are readily accessible to proton donor-acceptor interactions to form hydrogen bonds with the polar hydroxyl groups which occupy the outermost surface sites of hydrated crystal layers. This interaction behavior of PAA/PIA has been found to play an essential role in promoting good interfacial bond performance.

BRIEF DESCRIPTION OF THE DRAWINGS

FIG. 1 shows the peel strength as a function of primer concentration for: (1) polyurethane (PU)/PIA/Al (○); (2) PU/polyvinylpyrrolidone (PVP)/Al (●); (3) PU/polyacrylamide (PAM)/Al (□); and (4) PU/polystyrenesulfonic acid (PSSA)/Al (Δ) joint systems before and after exposure for 30 hours to hot alkali at 80° C.

FIG. 2 shows the variation in 180° peel strength of PU-PAA-aluminum joints, before and after exposure to hot NaOH solution, as a function of PAA concentration.

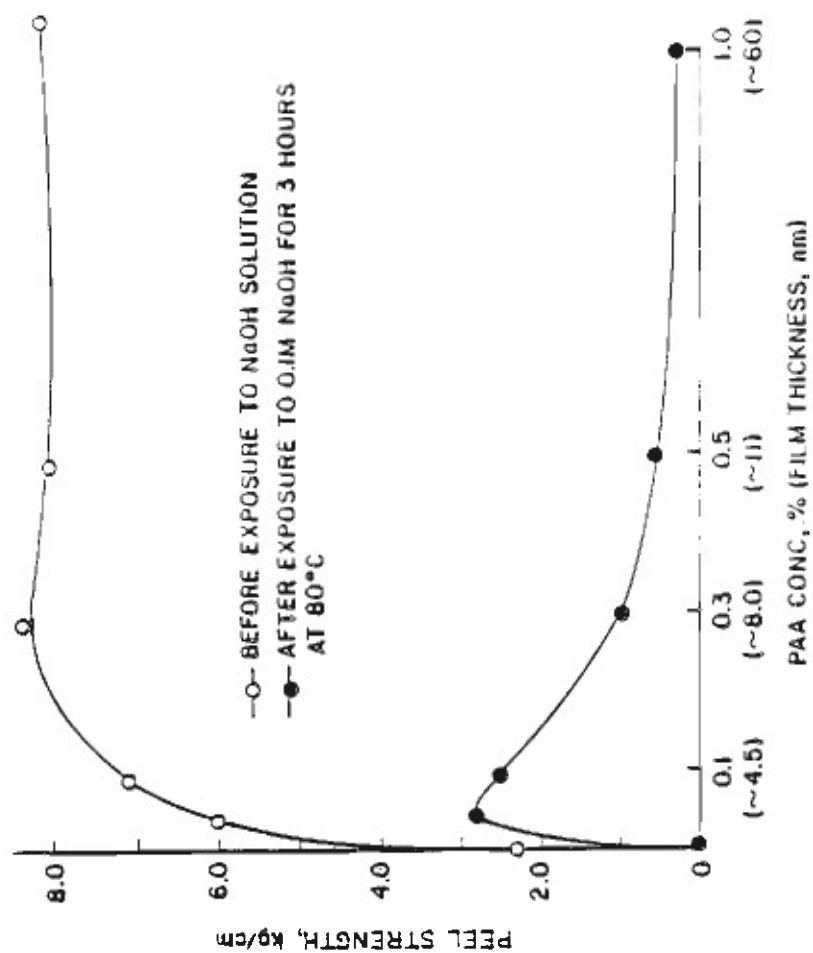


Fig. 2

DETAILED DESCRIPTION OF THE INVENTION

The present invention relates to a polymer topcoat, polyacid primer, and oxidized aluminum or aluminum alloy in a sandwich construction. The polyacid is selected from macromolecules $> 50,000$ M.W., with polyitaconic acid (PIA) and polyacrylic acid (PAA) being preferred. The polyacid is applied in near monolayer depth. This primer technique overcomes the poor bond strength that results from the prior art approaches. Comparative peel strength of one preferred embodiment of the present invention PU/PIA/Al compared with conventional polymeric coats is shown in FIG. 1. As seen in FIG. 1, the peel strength of the unexposed PU/Al control specimens prepared without the use of primers, was increased by more than three times when a PIA intermediate primer layer was applied. In contrast, the use of polyvinylpyrrolidone (PVP), polystyrenesulfonic acid (PSSA), and polyacrylamide (PAM) primers was less effective.

The present invention describes the role and nature of PAA and PIA for use as a primer in adhesive-treated aluminum joint systems. In one embodiment of the present invention, the joint systems can be composed of a Forest Product Laboratory (FPL) process-etched aluminum adherend, polyacid primers, with PAA and PIA primers being preferred, and polyurethane adhesive. The FPL aluminum etching process involves immersing aluminum in a hot chromic acid solution so that the surface is readily oxidized to form a layer of amorphous Al_2O_3 and Gamma- Al_2O_3 during the etching process. One of the most significant features of a fresh Al_2O_3 surface is its extremely high susceptibility to moisture. The reversible physisorption of water is known as a first stage in the hydration process of Al_2O_3 . When a freshly etched surface is immersed in cold water, an amorphous hydroxide is formed at the outermost surface sites, whereas a surface treated with hot water reveals the formation of crystalline boehmite and bayerite outer layers. Therefore, the compositions of aging FPL etched surfaces probably consist of aluminum hydroxide or hydrated aluminum oxide layers covering an aluminum oxide layer.

The objective of the present invention is to use the polyacid primer to promote adhesive bonding of the FPL adherend-PU adhesive joints and to improve the adhesion durability under hot alkaline environments, the type of environments found in geothermal applications among others.

The thin polyacid primer films of a near monolayer ($< 50\text{\AA}$) thickness, which are applied on the oxidized aluminum alloys, are prepared as follows: (1) the acid-treated aluminum substrate is immersed in a $< 0.1\%$ PIA or PAA solution in water for 5 min. at room temperature, and (2) the substrate is then oven heated at a temperature ranging from 100° to 150° C. for approximately 30 min. to solidify the polyacid macromolecules.

In order to achieve good adhesion of polymer adhesive to hydrated aluminum oxide or aluminum hydroxide adherend, water-soluble PAA and PIA macromolecules are applicable as a primer for the adherend-adhesive joints. When the polyacid primer is contacted with FPL-etched aluminum surfaces, macromolecules having regularly oriented functional COOH pendent groups are mobile enough to continuously wet the aluminum oxide hydrate surface sites at which the interfacial chemical affinity is particularly favorable. Subse-

quently, the proton-donating COOH groups form strong hydrogen bonds with the polar hydroxyl groups as proton acceptors which form on the outermost surface sites of oxidized aluminum. The preferred hydrogen bond formation in the interfacial regions is responsible for the development of interfacial bonding in PAA/PIA adherend joints. The presence of discontinuous salt formation at the interface, which results from the presence of nucleophilic Na^+ , Ca^{2+} , and Cu^{2+} ions on the etched surface, results in locally generated disbondment, thereby reducing the bond strength. Thus such salt formation should be avoided.

In addition, the use of a PAA or PIA primer improves the peel strength of the PU polymer/adherend joints because of the interfacial chemical reaction occurring between the carboxylic acid groups of PAA and PIA, and the isocyanate groups in the PU topcoat. Good bond performance and durability brought about by the use of PAA or PIA is associated not only with the chemical crosslinking functions connecting the hydrated oxide aluminum with the PU adhesive but also with the optimum thickness of the intermediate primer layers. The latter means that the PAA/PIA film should have only enough functional groups to occupy all available hydroxyl and isocyanate groups at the adherend and adhesive interface sites. In fact, the presence of a near monolayer of PAA or PIA film, produced using a 0.05% concentration in an aqueous medium, plays a key role in achieving excellent bond durability in hot alkaline solutions. The crosslinking structure of the polyacid primer in the interfacial regions contributes significantly to the formation of a stable interfacial bond which is resistant to moisture because of transformation of hydrophilic COOH to hydrophobic reaction products at the interfaces. The near monolayer application of the polyacid primer is critical. The presence of the additional COOH groups associated with thicker PAA and PIA layers contributes to gel-induced primer failures beneath the PU topcoat.

EXAMPLE I

Materials and Methods Employed In Experimental Work

The aluminum substrate used in the experiments was a clad aluminum sheet (denoted 2024-T3) containing the following chemical constituents: 92 wt % Al, 0.5 wt % Si, 0.5 wt % Fe, 4.5 wt % Cu, 0.5 wt % Mn, 1.5 wt % Mg, 0.1 wt % Cr, 0.25 wt % Zn, and 0.15 wt % other. Commercially available PAA, 0.05 to 5.0% solution in water, having an average molecular weight (M.W.) of 104,000, was employed as a primer coating to promote adhesive bonding. Polyurethane (PU) resin was applied as an elastomeric topcoating. Polymerization of the PU was initiated by incorporating a 50% aromatic amine curing agent.

The oxide etching of the aluminum was prepared in accordance with a well-known commercial sequence called the Forest Products Laboratory (FPL) process. As the first step in the preparation, the surfaces were wiped with acetone-soaked tissues to remove any organic contamination. They were then immersed in chromic-sulfuric acid ($Na_2Cr_2O_7 \cdot 2H_2O$: H_2SO_4 : Water = 4:23:73 by weight) for 10 min at 30° C. After etching, the fresh oxide surfaces were washed with deionized water at 30° C. for 5 min, and subsequently dried for about 15 min at 50° C. After drying, the surfaces were aged in the air at about 80% relative humidity for

7 days. All the etched substrates were stored in a desiccator to avoid adsorption of additional water.

Thin PAA primer films were applied to the treated aluminum surfaces by immersing them in the PAA solutions for about 5 min at room temperature. After immersion, the substrates were left in an oven at 150° C. for about 1 hr. to solidify the PAA macromolecules.

Commercial-grade polyurethane (M313 resin, Lord Corporation) was applied as an elastomeric topcoating. The polymerization of silica-filled PU composite was initiated by incorporating a 50% aromatic amine curing agent M201. The initiated topcoat system was then cured in the oven at a temperature of 80° C.

EXAMPLE 2

Preparation and Testing of Materials

PU polymer was overlaid onto PAA- or PIA-coated aluminum substrates, and then the PU-coated specimens were subjected to a 0.1M NaOH solution at 80° C. for 5 hr. All of the edges on the PU-coated plate specimens used in the tests to estimate the bond durability of the PU/PAA or PIA-10 min-etched aluminum adhesive joints were unprotected. The adhesion durability at the interface was evaluated on the basis of 180° peel strength tests performed at room temperature. For a comparison with the adherend properties of PAA- or PIA-overlaid substrate surfaces, two other substrate surfaces, non-etched plain aluminum and etched aluminum without a PAA or PIA coating, were also examined. The peel strength of the PU/PAA or PIA/etched aluminum joints before and after exposure to the NaOH solution were determined as a function of PAA and PIA film thickness and concentration applied on the etched surfaces. These results are shown in Table I. For the unexposed specimens, a considerable increase in peel strength was noted as the amount of PAA and PIA deposited was increased from 0.05% to 0.5%. The strength of 0.05% PAA- and PIA-containing films was about 70% of the maximum strength. After exposure 0.05% has been found to be the optimum concentration for development of peel strength as is shown in Table I.

In contrast, the intrinsic adhesion mechanism observed at PU-to-etched substrate joints is more likely mechanical interlocking which relates directly to the surface roughness. This was thought to occur when PU resin set in the crater-like pits on the etched surface which gave a mechanical key. However, the physical interlocking formation appears to yield a much stronger bond than that produced with an unetched smooth substrate surface.

TABLE I

Variations in 180° Peel Strength at PU-PAA or PIA-Al Joints, Before and After Exposure to Hot NaOH Solution as a Function of Primer's Thickness and Concentration				
Primers	Concentration %	Film Thickness nm	Peel Strength, kg/cm	
			Before Exposure	After Exposure
non-etched Al	0	0	0.95	*
etched Al	0	0	2.24	*
PIA	0.05	1.0	5.35	4.10
PIA	0.10	3.5	8.21	6.25
PIA	0.50	20.0	8.00	2.10
PIA	1.00	110.0	7.90	0.39
PAA	0.05	1.5	6.10	2.58
PAA	0.10	5.0	7.14	2.57
PAA	0.50	27.0	8.20	0.63
PAA	1.00	150.0	8.26	0.42

* Separation failure of PU film

EXAMPLE 3

Peel Strength

Peel strength measurements were performed on specimens after exposure to hot alkaline solutions. As seen in FIG. 2, although all specimens exhibit strength reduction, the rate of reduction depends upon the PAA concentration and, therefore, the thickness of the primer. The lowest reduction in strength was obtained for specimens containing a 0.05% PAA primer layer which can be described as the formation of a near monolayer. The strength of the 0.1% PAA film which has a thickness of about 4.5 nm drops to about 35% of its original value. At higher concentrations, the rate of reduction increases significantly, ranging from 88% for about 8-nm-thick film to for about 60-nm-thick film.

Films of near monolayer thickness were less susceptible to the hot alkali because of the existence of few hydrolytically sensitive free COOH groups in the primer layers. In this case, most of the functional COOH groups in a monolayer of PAA at the interface between the aluminum substrate and the PU topcoating can react chemically with the available polar groups such as hydroxyl and isocyanate which are present on both the adherend and adhesive surface sites. Thus, for the best alkaline resistance, the PAA primers should have only enough functional groups to occupy all available surface polar sites. A small proportion of functional groups in the primer is optimum. Since the nature of the reaction product formed in the interfacial regions is important in achieving good bond durability, it should be noted that the chemical interactions at the PU-PAA-aluminum interfacial boundaries form new reaction compounds with hydrophobic characteristics less susceptible to the alkaline fluids. This hydrophobic structure formed at the interface plays an important role in achieving long-term bond durability in the chemically aggressive environments.

I claim:

1. A formed polymeric adhesive/polyacid/oxidized aluminum adherend joint system wherein the polyacid is water-soluble has a molecular weight > 50,000 and is applied in near monolayer.

2. The joint system according to claim 1 wherein the polyacid is polyacrylic acid.

3. The joint system according to claim 1 wherein the polyacid is polyitaconic acid.

4. The joint system according to claim 1 wherein the polymeric adhesive is polyurethane.

5. A coupling and crosslinking primer comprising a water-soluble polyacid macromolecule of a molecular weight > 50,000 near monolayer in depth used in a formed polymeric adhesive/oxidized aluminum adherend joint system.

6. A primer according to claim 5 wherein the polyacid is polyacrylic acid.

7. A primer according to claim 5 wherein the polyacid is polyitaconic acid.

8. A primer according to claim 5 wherein the polymeric adhesive is polyurethane.

9. An aluminum/polymer sandwich consisting of an oxidized aluminum base next to a water-soluble polyacid primer of near monolayer thickness and a top polymer layer.

10. A sandwich according to claim 9 wherein the polyacid primer is polyacrylic acid.

11. A sandwich according to claim 9 wherein the polyacid primer is polyitaconic acid.

12. A sandwich according to claim 9 wherein the polymer is polyurethane.



US005110863A

United States Patent [19]

[11] Patent Number: 5,110,863

Sugama

[45] Date of Patent: May 5, 1992

[54] SOLID-GEL PRECURSOR SOLUTIONS AND METHODS FOR THE FABRICATION OF POLYMETALLICSILOXANE COATING FILMS

[75] Inventor: Toshifumi Sugama, Mastic Beach, N.Y.

[73] Assignee: Associated Universities, Inc., Washington, D.C.

[21] Appl. No.: 590,770

[22] Filed: Oct. 1, 1990

[51] Int. Cl.⁵ C08K 3/20; C08K 5/05

[52] U.S. Cl. 524/767; 528/40; 528/41; 528/25; 427/380; 427/387

[58] Field of Search 524/837, 838, 858, 767; 525/475; 528/38, 25, 40, 41, 427/226, 380, 387

[56] References Cited

U.S. PATENT DOCUMENTS

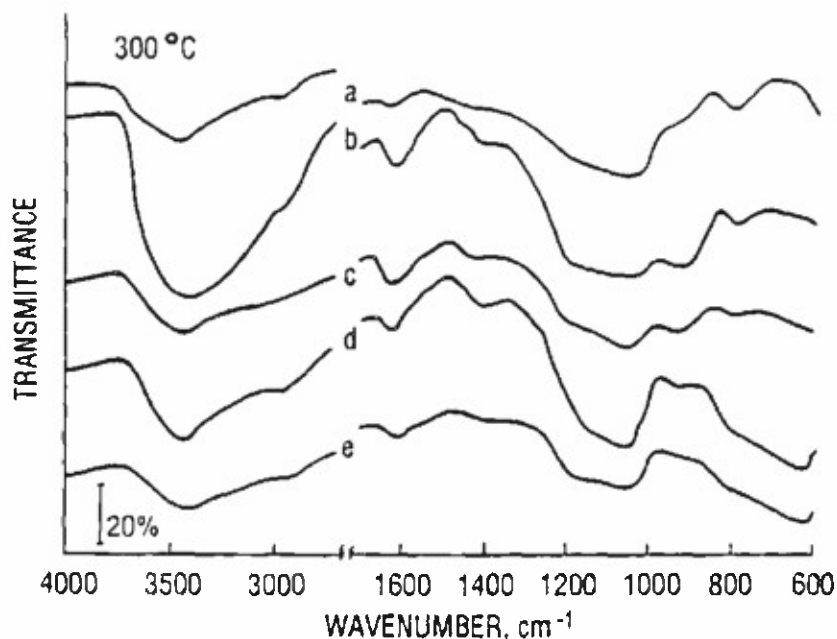
4,028,085	6/1977	Thomas	65/134
4,347,347	8/1982	Yajima et al.	528/30
4,455,414	6/1984	Yajima et al.	528/30
4,584,280	4/1986	Nanao et al.	501/80
4,786,618	11/1988	Shoup	501/12
4,880,851	11/1989	Yamamoto	427/213.34
4,948,843	8/1990	Roberts et al.	525/342

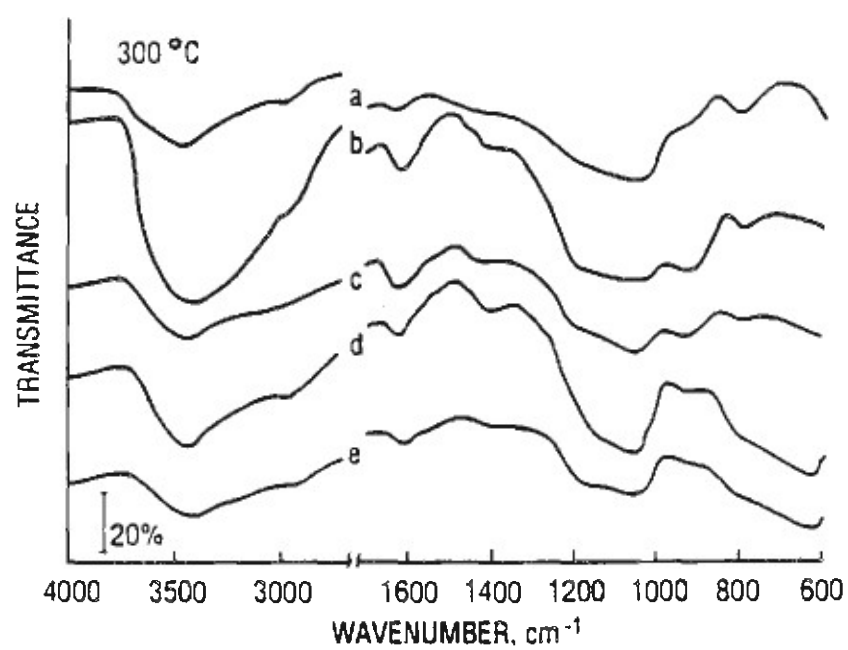
Primary Examiner—Michael Lusignan
Attorney, Agent, or Firm—Margaret C. Bogosian

[57] ABSTRACT

Solutions and preparation methods necessary for the fabrication of metal oxide cross-linked polysiloxane coating films are disclosed. The films are useful in provide heat resistance against oxidation, wear resistance, thermal insulation, and corrosion resistance of substrates. The sol-gel precursor solution comprises a mixture of a monomeric organoalkoxysilane, a metal alkoxide $M(OR)_n$ (wherein M is Ti, Zr, Ge or Al; R is CH_3 , C_2H_5 or C_3H_7 ; and n is 3 or 4), methanol, water, HCl and NaOH. The invention provides a sol-gel solution, and a method of use thereof, which can be applied and processed at low temperatures (i.e., $<1000^\circ C.$). The substrate can be coated by immersing it in the above mentioned solution at ambient temperature. The substrate is then withdrawn from the solution. Next, the coated substrate is heated for a time sufficient and at a temperature sufficient to yield a solid coating. The coated substrate is then heated for a time sufficient, and temperature sufficient to produce a polymetallicsiloxane coating.

27 Claims, 7 Drawing Sheets



**Fig. 1**

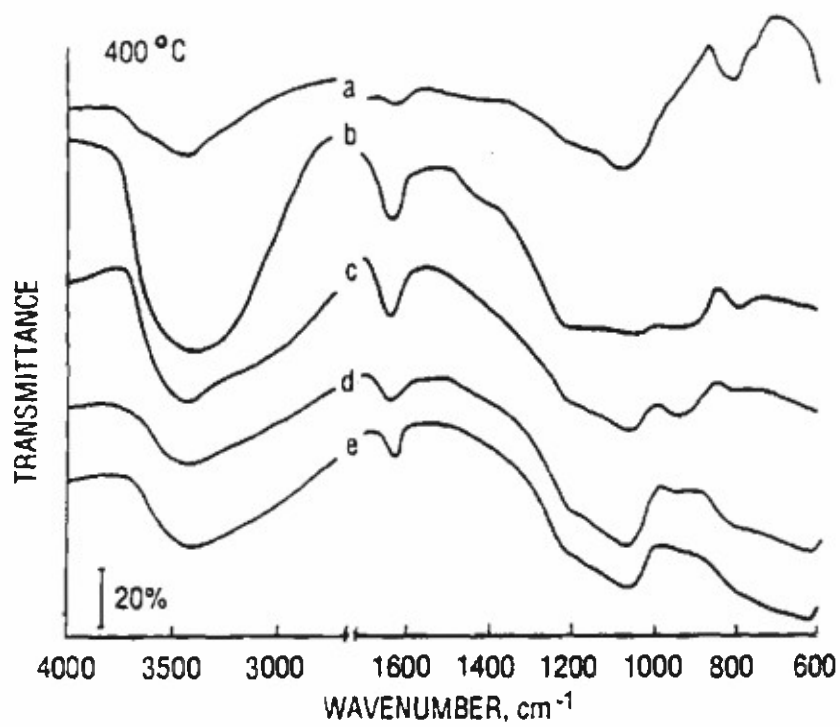


Fig. 2

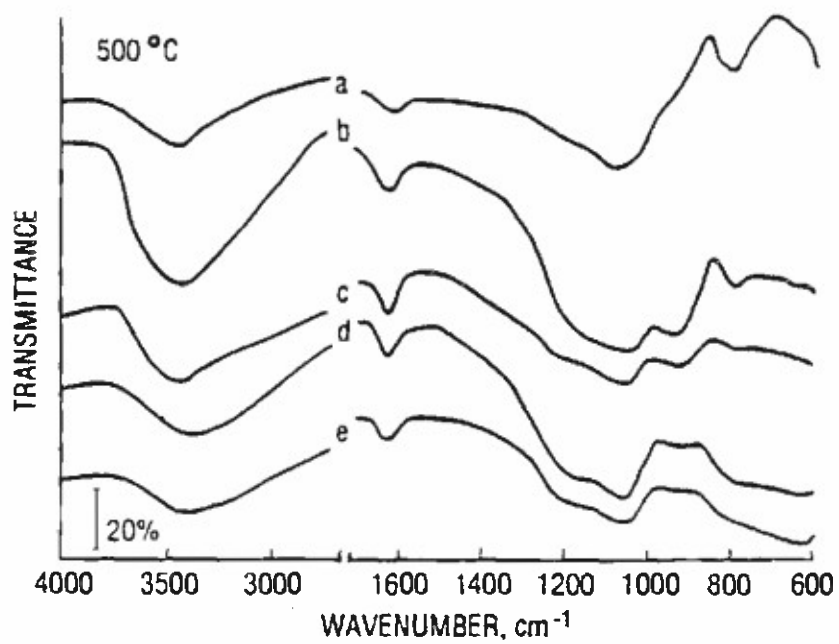


Fig. 3



Fig. 4 (a)

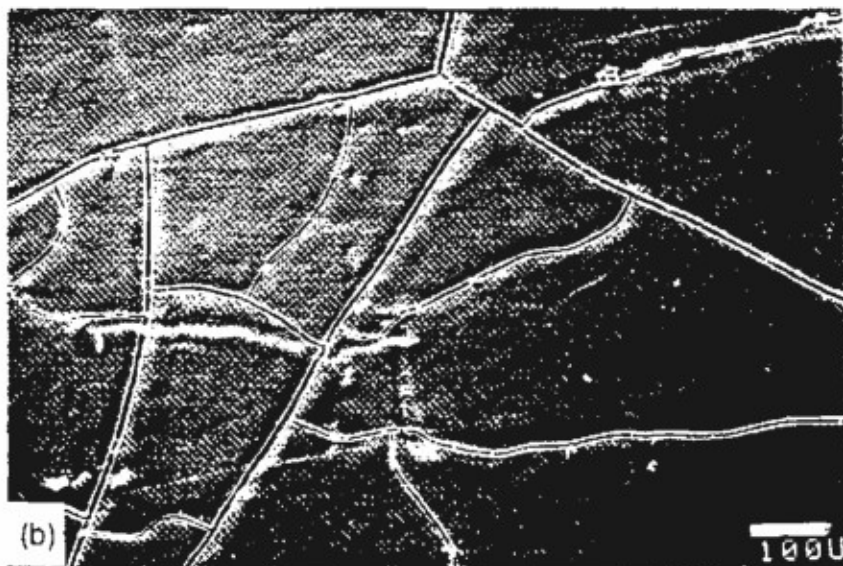


Fig. 4 (b)

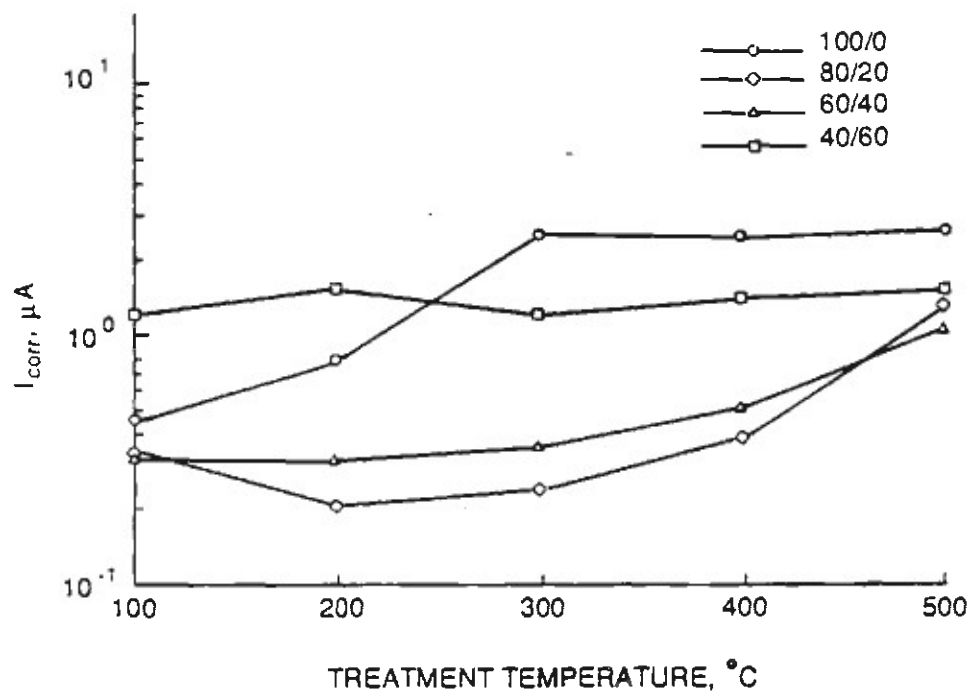


Fig. 5

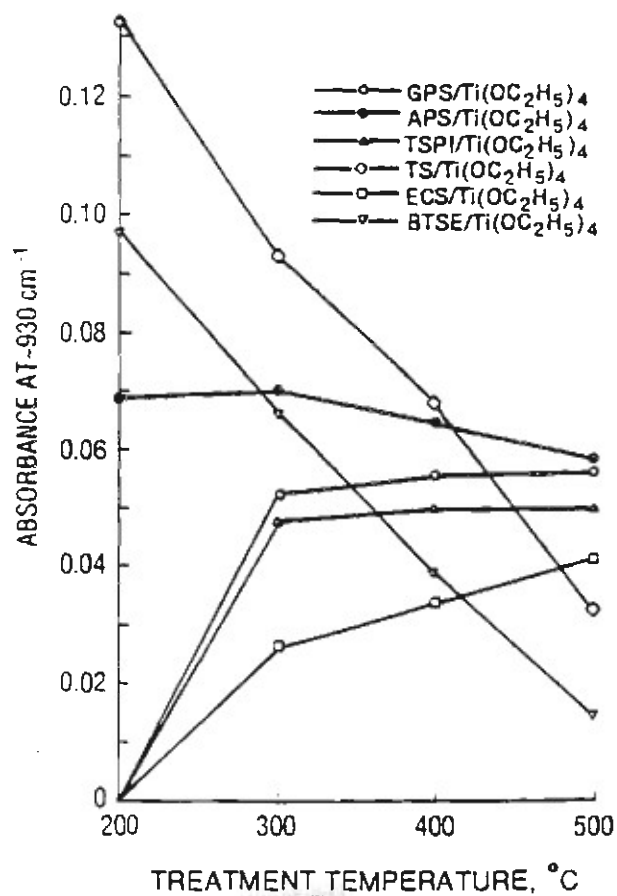


Fig. 6

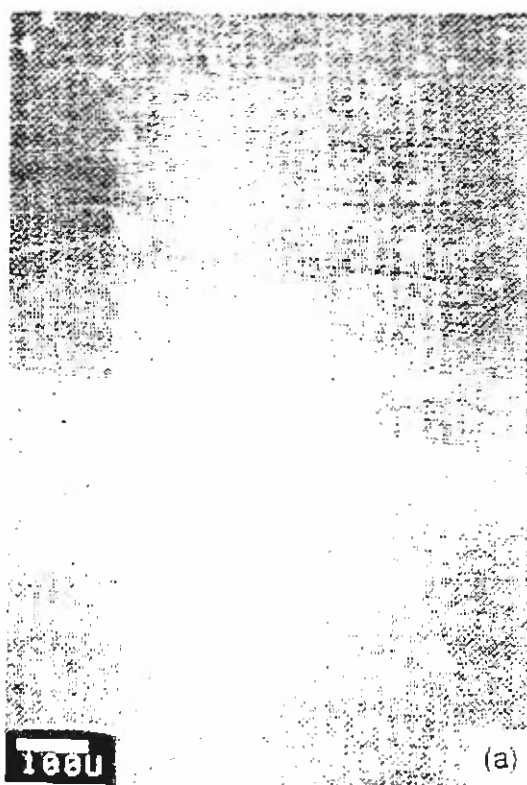


Fig. 7 (a)

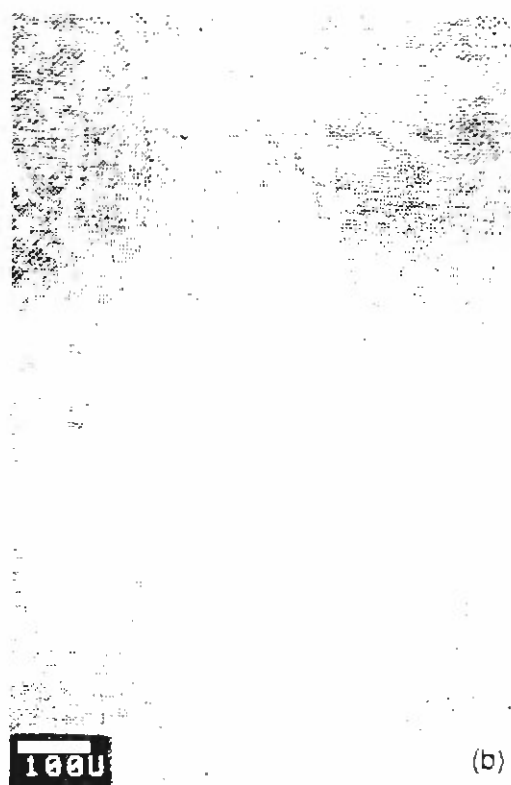


Fig. 7 (b)



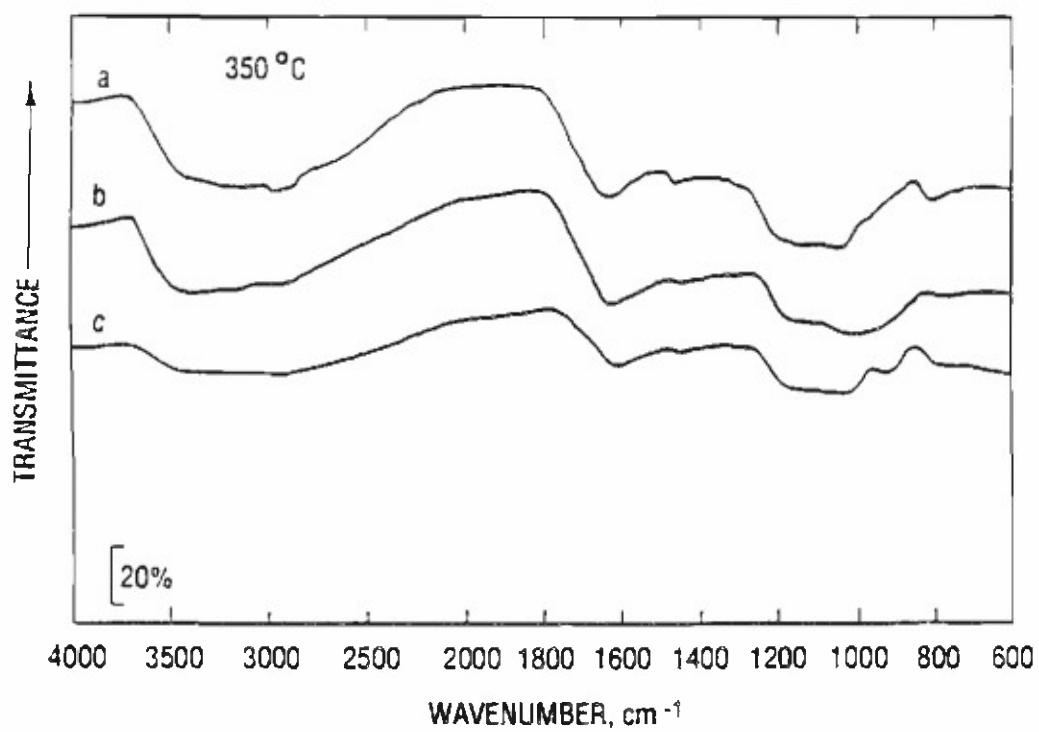
Fig. 9



Fig. 8 (a)



Fig. 8 (b)

**Fig. 10**

SOLID-GEL PRECURSOR SOLUTIONS AND METHODS FOR THE FABRICATION OF POLYMETALLICSILOXANE COATING FILMS

This invention was made with Government support under contract number DE-AC02-76CH00016, between the U.S. Department of Energy and Associated Universities, Inc. The Government has certain rights in the invention.

BACKGROUND OF THE INVENTION

The present invention includes solutions and the preparation methods necessary for the fabrication of metal oxide cross-linked polysiloxane coating films which are useful in providing heat resistance against oxidation, wear resistance, thermal insulation, and corrosion resistance of substrates.

In the past, ceramic coatings on metallic and plastic substrates have not been widely used primarily because many ceramic coatings can be applied and processed only at high temperatures (i.e., only at temperatures above 1000° C.) using expensive and time-consuming methods such as chemical vapor deposition. Therefore, aluminum alloys, plastics and other materials with low melting points were not easily protected.

U.S. Pat. No. 4,584,280 to Nanao discloses a process for preparing a porous ceramic film by applying an anhydrous solution containing an organometallic compound and a multifunctional organic compound to a substrate and thermally decomposing the substrate. The organometallic compound may be titanium alkoxide. Examples of the multifunctional organic compound include such organic compounds as glycerine, 1,4-butanediol, pentaerythritol, dextrin, arginine acid, methyl cellulose, ethyl cellulose, hydroxyethyl cellulose, carboxymethyl cellulose, carboxymethyl starch, hydroxyethyl starch, polyvinylalcohol, and mixtures thereof. The thermal decomposition is conducted at a temperature of not less than 200° C., and then, if necessary, the coated substrate is baked. Nanao does not teach the formation of a polymetallicsiloxane film at low temperatures as does the present invention.

U.S. Pat. Nos. 4,455,414 and 4,347,347, to Yajima, et al. disclose an organic copolymer composed of a polycarbostilane portion and a polymetallicsiloxane portion cross-linked with each other and the process of making it. Neither patent teaches the formation of a polymetallicsiloxane film at low temperature as does the present invention.

U.S. Pat. No. 4,028,085 to Thomas discloses the combination of a hydrolyzable metal alkoxide with a partially hydrolyzed silicon tetraalkoxide to form a metallicsiloxane solution. Thomas does not teach the application of the solution to a substrate nor does it teach the heating of the solution to create a ceramic-type polymetallicsiloxane coating.

It is, therefore, an object of the present invention to provide a polymetallicsiloxane sol-gel precursor solution which can be used in the preparation of metal oxide cross-linked polysiloxane coating films which are useful in providing heat resistance against oxidation, wear resistance, thermal insulation, and corrosion resistance of substrates.

It is an object of the invention to provide a sol-gel solution, and a method of use thereof, which can be applied and processed at low temperatures (i.e., at temperatures of less than 1000° C.).

A further object of the invention is to provide a polymetallicsiloxane sol-gel precursor solution which will adhere well and have an appropriate expansion coefficient, especially during temperature cycling, so that separation of the coating film from the substrate will not occur.

BRIEF DESCRIPTION OF THE INVENTION

This invention relates to the formulation of sol-gel precursor solutions and the preparation methods necessary for the fabrication of the metal oxide cross-linked polysiloxane coating films. The metal oxide cross-linked polysiloxane coating film enhances heat resistance against oxidation, wear resistance, thermal insulation and corrosion resistance of substrates such as aluminum, steel, magnesium, and titanium. The sol-gel precursor solution includes a mixture of a monomeric organoalkoxysilane, a metal alkoxide $M(OR)_n$ (wherein M is a transition metal; R is CH_3 , C_2H_5 or C_3H_7 ; and n is 3 or 4), alcohol, water and a chlorine containing acid. Suitably M can include Ti, Zr, Ge and Al. Preferably the alcohol is methanol, ethanol or propanol. The invention provides a sol-gel solution, which can be applied and processed at low temperatures (i.e., < 1000° C.). Preferably, NaOH is used to adjust the pH of the solution to about 7.5.

Preferably, the monomeric organoalkoxysilane is selected from the group consisting of N[3-(triethoxysilyl) propyl]imidazole (TSPI) and N[3-(triethoxysilyl) propyl]-4,5-dihydroimidazole (TSPDI). In a preferred embodiment the amount of HCl is sufficient to provide a clear solution and acts as a hydrolysis accelerator. In another preferred embodiment the ratio of imidazole containing monomeric organoalkoxysilane to metal alkoxide is in the range of about 80/20 to about 50/50 by weight (i.e., the solution comprises 18-35 wt % TSPI or TSPDI, 9-18 wt % $Ti(OC_2H_5)_4$, 21-26 wt % methanol, 13-29 wt % HCl and 14-17 wt % water). The sol-gel solution is miscible with water and the thickness of the coating films can be adjusted by adding an appropriate amount of water to the solution.

The substrate can be coated by immersing it in the above mentioned solution at ambient temperature. The substrate is then withdrawn from the solution. Next, the coated substrate is heated for a time sufficient and at a temperature sufficient to yield a solid coating. The coated substrate is then heated for a time sufficient, and at a temperature sufficient, to produce a polymetallicsiloxane coating.

To date, ceramic coatings on metallic and plastic substrates have not been widely employed for several reasons. First, coatings must adhere well and have an appropriate expansion coefficient. This is especially true during temperature cycling, otherwise, separation of the coating film from the substrate will occur. Second, many ceramic coatings can be applied and processed as coatings only at high temperatures (i.e., > 1000° C.) using expensive and time-consuming methods such as chemical vapor deposition. Therefore, the instant sol-gel solution, and the preparation methods for the formulation of metal oxide cross-linked polysiloxane coatings films, are advantageous in that they permit the application of an effective polymetallicsiloxane coating at a temperature which more easily permits the use of aluminum alloys and other low melting point materials.

For a better understanding of the invention, together with other and further objects, reference is made to the

following description, and its scope will be pointed out in the appended claims.

BRIEF DESCRIPTION OF THE DRAWINGS

FIG. 1 illustrates the IR absorption spectra for powder samples of various GPS/Ti(OC₂H₅)₄ ratios heat treated at 300° C.

FIG. 2 details the IR absorption spectra for powder samples of various GPS/Ti(OC₂H₅)₄ ratios heated at 400° C.

FIG. 3 details the IR absorption spectra for powder samples of various GPS/Ti(OC₂H₅)₄ ratios heated at 500° C.

FIGS. 4(a) and 4(b) illustrate surface morphologies for GPS/Ti(OC₂H₅)₄ coatings treated at 300°. The micrographs correspond to the following GPS/Ti(OC₂H₅)₄ ratios: FIG. 4(a)—100/0 and FIG. 4(b)—60/40.

FIG. 5 graphically illustrates the variation in corrosion current (*I_{corr}*) for aluminum substrates coated with various GPS/Ti(OC₂H₅)₄ ratio systems as a function of the film-treatment temperature.

FIG. 6 illustrates the changes in IR absorbance corresponding to the Si—O—Ti bond at approximately 930 cm⁻¹ for Ti compound-incorporated organosilanes preheated at temperatures within the range of 200° to 500° C.

FIGS. 7(a) and 7(b) detail SEM images for TSPI 7(a) and APS 7(b) coating films heated at 200° C.

FIGS. 8(a) and 8(b) detail the surface morphologies for TSPDI 8(a) and APS 8(b) system coatings heat treated at 300° C.

FIG. 9 illustrates the SEM micrograph for the TSPDI coating system heat treated at 300° C. The (a) in the corner of the figure was the code used in preparing the SEM micrographs to identify the TSPDI system.

FIG. 10 illustrates the IR spectra for 350° C.-annealed TSPDI/M(OC₂H₅)₄ or 4 for the (a) 100% TSPDI, (b) TSPDI/Zr(OC₂H₅)₄ (50:50 ratio) and (c) TSPDI/Ti(OC₂H₅)₄ (50:50 ratio) systems.

FIG. 11 illustrates the polyzirconosiloxane (PZS) film derived from the 70/30 TSPDI/Zr(OC₂H₅)₄ sol-gel solution.

FIGS. 12(a) and 12(b) illustrate surface features of pyrolysis-induced PTS coating films: FIG. 12(a) illustrates a 70/30 TSPI/Ti(OC₂H₅)₄ ratio system and FIG. 12(b) illustrates a 50/50 TSPI/Ti(OC₂H₅)₄ ratio system.

DETAILED DESCRIPTION OF THE INVENTION

The sol-gel precursor solution of the present invention includes a mixture of a monomeric organoalkoxysilane, a metal alkoxide M(OR)_n (wherein M is a suitable transition metal); R is CH₃, C₂H₅ or C₃H₇; and n is 3 or 4), alcohol (such as methanol, ethanol or propanol), water, and a chlorine containing acid (such as HCl). Suitably, M may be Ti, Zr, Ge or Al. Preferably, the pH of the solution is adjusted to about 7.5 (for reasons of handling safety) by the addition of NaOH. Among the monomeric organoalkoxysilanes which can be used with the present invention are those listed in Table I. In a preferred embodiment, the monomeric organoalkoxysilane contains an imidazole group, for example, N-[3-(triethoxysilyl) propyl]-4,5 imidazole (TSPI) and N-[3-(triethoxysilyl)propyl]-4,5-dihydroimidazole (TSPDI).

TABLE I

Organosilane/Chemical Formula	
3-glycidoxypropyltrimethoxysilane (GPS)	$\text{CH}_2 \begin{array}{c} \diagup \text{O} \diagdown \\ \text{CH} \end{array} \text{CH}_2 \text{O} (\text{CH}_2)_3 \text{Si}(\text{OCH}_3)_3$
3-aminopropyltrimethoxysilane (APS)	$\text{H}_2\text{N}-(\text{CH}_2)_3\text{Si}(\text{OCH}_3)_3$
N-[3-(triethoxysilyl)propyl]imidazole (TSPI)	$\begin{array}{c} \text{N} \\ \diagup \quad \diagdown \\ \text{N} \end{array} (\text{CH}_2)_3 \text{Si}(\text{OC}_2\text{H}_5)_3$
N-[3-(triethoxysilyl)propyl]-4,5-dihydroimidazole (TSPDI)	$\begin{array}{c} \text{N} \\ \diagup \quad \diagdown \\ \text{N} \end{array} (\text{CH}_2)_3 \text{Si}(\text{OC}_2\text{H}_5)_3$

The film-forming precursor solution can be prepared by incorporating an organoalkoxysilane/metal alkoxide M(OR)_n wherein M is a suitable transition metal such as Ti, Zr, Ge or Al; R is CH₃, C₂H₅ or C₃H₇; and n is 3 or 4) into an alcohol/water mixing medium containing an appropriate amount of an acid containing chlorine. Suitably, the alcohol may be methanol, ethanol or propanol. Preferably, the acid is HCl. The acid acts as a hydrolysis accelerator and produces a clear precursor solution. The addition of the acid aids in the formation of a uniform coating film on the metal substrate. When the precursor solution is used as a coating material for a metal substrate, the pH of the solution is preferably adjusted to approximately 7.5 by the addition of an appropriate amount of a suitable base such as, for example, KOH or NaOH. Prior to addition of the base, the solution will be very acidic (i.e., it will have a pH of from about 1.0 to about 3.5). The base makes the solution safer to handle.

The aluminum substrate used in the following examples was 2024-T3 clad aluminum sheet containing the following chemical constituents: 92 wt. % Al, 0.5 wt. % Si, 0.5 wt. % Fe, 4.5 wt. % Cu, 0.5 wt. % Mn, 1.5 wt. % Mg, 0.1 wt. % Cr, 0.25 wt. % Zn and 0.15 wt. % other elements.

The oxide etching of the aluminum was carried out in accordance with a well known commercial sequence called the Forest Products Laboratory (FPL) process. As the first step in the preparation, the surfaces were cleansed with acetone to remove any organic contamination. They were then immersed in chromic-sulfuric acid (Na₂Cr₂O₇·2H₂O:H₂SO₄:Water=4:23:73 by weight) for 10 min at 80° C. After etching, the fresh oxide surfaces were washed with deionized water at 30° C. for 5 min, and subsequently dried for 15 min at 50° C.

The substrate can be coated by immersing it in the above mentioned solution at ambient temperature. The substrate is then withdrawn from the solution. Next, the coated substrate is heated for a time sufficient and at a temperature sufficient to yield a solid coating. The coated substrate is then heated for a time sufficient, and at a temperature sufficient, to produce a polymetallic-siloxane coating.

A thinner polymetallicsiloxane coating may be obtained by diluting the sol-gel precursor solution with water.

C. (FIG. 2), no specific changes or shifts in the absorption bands for any samples can be seen.

When the film treatment temperature was raised to 300° C., samples containing a GPS/Ti(OC₂H₅)₄ ratio of 100/0 experienced severe damage. This is shown in FIG. 4a. The failure appears to be due to pyrolytic changes in conformation of the polymericorganosilane. These pyrolytic changes result from the elimination of organic species from the network structure and result in excessive shrinkage of the film. The SEM (scanning electron microscope) microstructure view of the 60/40 ratio film (FIG. 4b) disclosed a much lower magnitude in shrinkage and/or stress cracks. This strongly suggests that the cross-linking ability of the Ti compounds, which connect directly between the polysilane chains, acts significantly to suppress the development of stress cracks. It is theorized that the network structure of the PTS polymers, formed by pyrolytically induced conformational changes in Ti compound modified organosilane polymers, contributes to the maintenance of film shape at high temperatures. The amount of cracking can be reduced by diluting the sol gel precursor solution with water. The dilution of the sol gel precursor solution results in the formation of a thinner polymetallic-siloxane coating.

Corrosion protection data for the above-coated substrates were obtained from the polarization curves for PMS coated FPL etched aluminum samples upon exposure to an aerated 0.5M sodium chloride solution at 25° C. The typical cathodic-anodic polarization curves of log current density vs. potential for the coated samples were similar to those reported by several investigators for other materials (G. A. Dibari and H. J. Read, *Corrosion*, 27 (1971) 483; Z. A. Foroulis and M. J. Thubriker, *Electrochim. Acta*, 21 (1976) 225; and A. V. Pocius, in K. L. Mittal (ed.), *Adhesion Aspects of Polymeric Coatings*, Plenum Press, New York, 1983, pp. 173-192).

The corrosion protective performance of the coatings was evaluated by an electrochemical procedure involving measurement of the corrosion current, I_{corr} , by extrapolation of the cathodic Tafel slope. The variation in the I_{corr} value was plotted as a function of the treatment temperature. These results are depicted in FIG. 5. As seen in FIG. 5, the protective ability of the coatings depends primarily on the GPS/Ti(OC₂H₅)₄ ratio and the treatment temperature. A low I_{corr} value indicates good corrosion protection.

The I_{corr} -temperature relations for the 80/20 and 60/40 ratio coatings indicate that although microcracks form on the film surface at temperatures $\geq 300^\circ$ C., the I_{corr} values after treatment at 400° C. are almost equal to those for the coatings pretreated at 100° C. This suggests that PTS coating films at 100° C. formed from in-situ conformation changes at 400° C. provided corrosion protection for aluminum.

Ti(OC₂H₅)₄ - Modified Organosilanes

Coating of the aluminum surfaces using the sol-gel system was performed in accordance with the following sequence. First, the FPL-etched aluminum substrate was immersed in the precursor solution at ambient temperature. The substrate was then withdrawn slowly and heated for 20 hr at a temperature of 100° C. to yield a solid coating. The samples were subsequently heated for 20 min at temperatures ranging from 200° to 500° C.

A film-forming precursor solution composed of 30 wt % of the particular organosilane, 20 wt % Ti(OC₂H₅)₄, 30 wt % CH₃OH and 20 wt % water was employed to

produce the PTS polymers. The required concentrations of the HCl hydrolysis promoter needed to prepare clear precursor solutions were dependent upon the species of organosilane, and for the TSPDI system was 30% by weight of total mass of organosilanes and Ti(OC₂H₅)₄.

The presence of Si—O—Ti linkages in the PTS can be readily identified from the IR absorption peak at approximately 930 cm⁻¹. The extent of the densification of the Si—O—Ti linkages was estimated by comparing the absorbencies at approximately 930 cm⁻¹ for the PTS samples derived from the various organosilane-Ti(OC₂H₅)₄ systems. As previously discussed, samples for the IR analysis were prepared by incorporating the powdered samples into KBr pellets. FIG. 6 summarizes the resulting variations in absorbance plotted as a function of treatment temperature. The data indicates that the extent of densification of Si—O—Ti bonds is dependent upon the reactive organic functional groups attached to the terminal carbon of the methylene chains within the monomeric organosilane structures.

An absorption peak at approximately 930 cm⁻¹ was not detected for the 200° C.-treated GPS- and TSPDI-Ti(OC₂H₅)₄ systems. This indicates that a PTS containing a highly densified Si—O—Ti bond was not formed at this temperature. A prominent IR peak at approximately 930 cm⁻¹ was observed for the GPS and TSPDI-Ti(OC₂H₅)₄ systems when the samples were heated at 300° C. for 20 min. An absorption peak at approximately 930 cm⁻¹ was observed for the 200° C. treated APS-Ti(OC₂H₅)₄ system. This indicates that PTS, containing a highly densified Si—O—Ti bond, was formed at these temperatures. This illustrates the formation of a polymetallicsiloxane coating at a low temperature (i.e., less than 1000° C.). Beyond this temperature, the absorbance value increased slowly, suggesting that the in-situ conversion of the Ti compound-incorporated organosilane polymers into PTS progressively occurs at temperatures ranging from about 200° to about 300° C.

FIG. 7 illustrates the SEM images obtained for coating film surfaces preheated at 200° C. Except for the development of few microcracks, the APS and TSPDI coatings [FIG. 7(a) and (b)] exhibit excellent surfaces.

The SEM micrographs of these coating systems after being exposed to air for 20 min at 300° C. are shown in FIG. 8. The APS and TSPDI coatings (FIG. 8(a) and (b)) showed no film damage with the exception of the appearance of a clear crack line.

Heat damage and distortion of the aluminum substrate was apparent, but after heating for 20 min at 500° C., the TSPDI coating was not damaged [See FIG. 9(a)]. Accordingly, PTS coating films derived from the Ti(OC₂H₅)₄-TSPDI system appear to have the most stable Si—O—Ti bonds in the PTS network structure. This may be due to moderate densification of the Si—O—Ti bonds in the PTS network structure.

The corrosion protective performance of PTS coatings derived from various organosilane-Ti(OC₂H₅)₄ systems was determined by comparing the corrosion current, (I_{corr}) values determined from the cathodic Tafel slopes of the various organosilane-Ti(OC₂H₅)₄ systems. The corrosion tests in this study were performed on PTS coatings formed on the FPL-etched aluminum at 300°, 400°, and 500° C. The resultant changes in I_{corr} for these coating specimens are summarized in Table 3.

TABLE 3

Coating system	I_{corr} value (μA) obtained after pretreatment at		
	300° C.	400° C.	500° C.
GPS-Ti(OC ₂ H ₅) ₄	3.5×10^{-1}	6.0×10^{-1}	0.5
APS-Ti(OC ₂ H ₅) ₄	8.5×10^{-2}	5.8×10^{-1}	1.2
TSPDI-Ti(OC ₂ H ₅) ₄	2.0×10^{-2}	4.6×10^{-1}	9.8×10^{-1}
TSP1-Ti(OC ₂ H ₅) ₄	2.5×10^{-2}	4.9×10^{-1}	9.9×10^{-1}

After treatment at 300° C., the lowest I_{corr} value of $2.0 \times 10^{-2} \mu A$ was measured on the PTS coatings derived from the TSPDI system. The APS system produced the next lowest I_{corr} value. These values were approximately two orders of magnitude less than that for the TS system. The data indicates that the I_{corr} values for all of the PTS coatings formed at $\geq 300^\circ C$. increased as the film treatment temperature was raised. This is probably due to the increased size and number of cracks in the films. PTS coatings derived from the TSPDI system imparted the best corrosion protection, and at 500° C., the I_{corr} value was still on the order of $10^{-1} \mu A$.

Ti(OC₃H₇)₄, Zn(OC₃H₇)₄ and Al(OC₃H₇)₃ - Modified Organosilanes

The mix compositions for the Ti(OC₃H₇)₄, Zn(OC₃H₇)₄ and Al(OC₃H₇)₃ sol-gel precursor solutions are listed in Table 4. In order to produce a clear precursor solution it was very important to add a chlorine containing acid such as HCl. The chlorine containing acid acted as a hydrolysis accelerator and aided in the formation of a uniform coating film on the metal substrate.

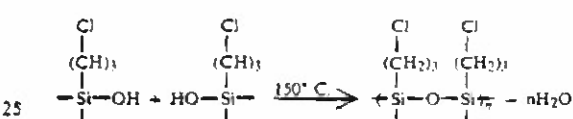
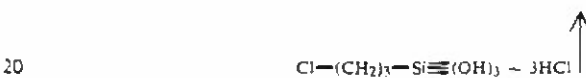
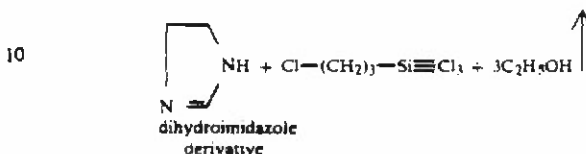
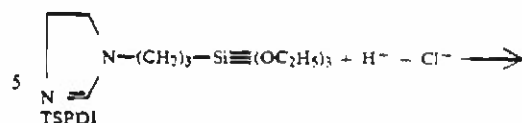
TABLE 4

Compositions of Clear Precursor Solutions Used in Various M(OC ₃ H ₇) _n - Modified TSP1 Systems.								
TSP1/M(OC ₃ H ₇) _n * wt ratio	TSP1 wt %	Zr(OC ₃ H ₇) ₄ wt %	Ti(OC ₃ H ₇) ₄ wt %	Al(OC ₃ H ₇) ₃ wt %	CH ₃ OH wt %	Water wt %	HCl wt %/TSP1 + M(OC ₃ H ₇) ₄ or 3	
100/0	50	—	—	—	30	20	12	
70/30	35	15	—	—	30	20	20	
50/50	25	25	—	—	30	20	30	
70/30	35	—	15	—	30	20	15	
50/50	25	—	25	—	30	20	25	
70/30	35	—	—	15	30	20	40	
50/50	25	—	—	25	30	20	50	

M: Zr, Ti and Al
n: 3 or 4

The substrates were coated by immersing an FPL-etched aluminum substrate into the precursor solution at ambient temperature. The substrate was then withdrawn from the precursor solution. Next, the substrate was heat treated at 150° C. for 20 hrs. The 150° C. heat treatment results in the removal of water and methanol from the precursor solution coating and produces a sintered coating. The substrates coated with the Ti(OC₃H₇)₄ and Zn(OC₃H₇)₄ sol-gel precursor solutions were heated for 30 minutes at 350° C. to form polyzirconosiloxane and polytitanosiloxane coatings. The substrates coated with the Al(OC₃H₇)₃ sol-gel precursor solutions were heated for 30 minutes at 200° C. to form a polyaluminosiloxane coating.

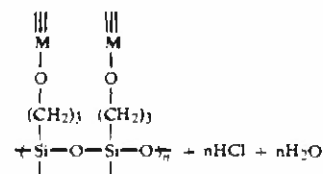
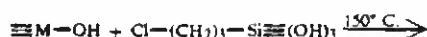
The HCl catalyzed hydrolysis-polycondensation reaction occurred in the following manner:



polymeric organosilane with Cl substituted end groups.

30 It is believed that the hydroxyl groups derived from the HCl-catalyzed hydrolysis of Zr(OC₃H₇)₄ and Ti(OC₃H₇)₄, react preferentially with the Cl in Cl-substituted end groups in the silane compound, rather than

50 the silanol groups which are formed by hydrolysis of the ethoxysilyl groups in the TSPDI. The proposed reaction mechanism for this is shown below:

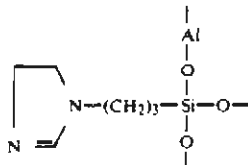


polymeric organosilane with oxygen-bonded Zr or Ti
Where M = Zr or Ti.

It is believed that the reaction of the halide with the OH in the hydroxylated metals favors the elimination of

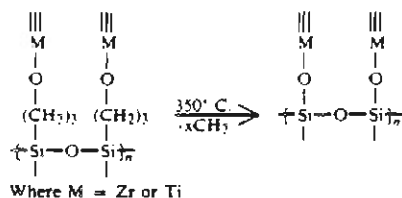
hydrogen chloride. The formation of Cl-terminated end groups plays an important role in creating the M-O-C linkages.

The reaction process for the $\text{Al}(\text{OC}_3\text{H}_7)_3/\text{TSPDI}$ system is different than those of the $\text{Ti}(\text{OC}_3\text{H}_7)_4/\text{TSPDI}$ and $\text{Zr}(\text{OC}_3\text{H}_7)_4/\text{TSPDI}$ systems. A polymeric organoaluminosilane network is formed when the $\text{Al}(\text{OC}_3\text{H}_7)_3/\text{TSPDI}$ system is heated to 150°C . and is believed to have the following structure:



IR studies were performed on the $\text{Ti}(\text{OC}_3\text{H}_7)_4/\text{TSPDI}$ and $\text{Zr}(\text{OC}_3\text{H}_7)_4/\text{TSPDI}$ samples after they had been heated for 30 minutes in air at 350°C . The samples had previously been heated at 150°C . for 20 hours. The IR analyses were conducted using the KBr method which incorporates the powder samples of 2 to 3 mg into KBr pellets of approximately 200 mg. FIG. 10 illustrates the IR spectra for a) 100% TSPDI, b) TSPDI/ $\text{Zr}(\text{OC}_3\text{H}_7)_4$ (in a 50:50 ratio) and c) TSPDI/ $\text{Ti}(\text{OC}_3\text{H}_7)_4$ (in a 50:50 ratio) samples heat treated at 150°C . for 20 hours and 350°C . for 30 minutes. The presence of a polymetallicsiloxane is indicated by an IR peak within the area of about 910 cm^{-1} to about 960 cm^{-1} .

The TSPDI/ $\text{Zr}(\text{OC}_3\text{H}_7)_4$ system (FIG. 10(b)) had an IR peak at 950 cm^{-1} . The TSPDI/ $\text{Ti}(\text{OC}_3\text{H}_7)_4$ system (FIG. 10(c)) had an IR peak at 930 cm^{-1} . These peaks signify the formation of polymetallicsiloxane, at a low temperature (i.e., less than 1000°C .), by the process shown below:



The 350°C . heating results in the elimination of numerous organic groups permitting the Zr and Ti metal oxides to act as crosslinking agents which connect the polysiloxane chains to form polyzirconicsiloxane and polytitanosiloxane.

Characteristics of PMS (Coating Films Derived From TSPDI/ $\text{Ti}(\text{OC}_3\text{H}_7)_4$, TSPDI/ $\text{Zr}(\text{OC}_3\text{H}_7)_4$ and TSPDI/ $\text{Al}(\text{OC}_3\text{H}_7)_3$ Precursor Systems

Thin coating films were obtained by diluting 20 g of the precursor solutions listed in Table 4 with 80 g of deionized water. The FPL-etched aluminum substrate was immersed into the diluted precursor solution. The substrate was withdrawn from the solution and heated for 20 hours at 150°C . The sintered samples were then heated at 350°C . for 30 minutes to form the pyrolysis induced PMS coating films. The thickness of the PMS film deposited on the substrate was determined using a surface profile measuring system. The average thick-

ness of the films derived from the precursor solution consisting of 100/0, 70/30, and 50/50 TSPDI/M- $(\text{OC}_3\text{H}_7)_3$ or 4 ratios, ranged from approximately 0.2 to approximately $0.4\text{ }\mu\text{m}$.

FIG. 11 illustrates the polyzirconicsiloxane (PZS) film derived from the 70/30 TSPDI/ $\text{Zr}(\text{OC}_3\text{H}_7)_4$. This PZS film had relatively few microcracks. The amount of cracking can be reduced by diluting the sol gel precursor solution with water. The dilution of the sol gel precursor solution results in the formation of a thinner polymetallicsiloxane coating.

Ideally, a PMS coating surface will have a uniform film free of cracks and pits. These characteristics were observed in the 50/50 TSPDI/ $\text{Ti}(\text{OC}_3\text{H}_7)_4$ ratio derived polytitanosiloxane (PTS) film illustrated in FIG. 12a. FIG. 12b illustrates the 70/30 TSPDI/ $\text{Ti}(\text{OC}_3\text{H}_7)_4$ ratio derived PTS film. The 70/30 ratio film has a few microcracks. A thinner polymetallicsiloxane coating may be produced by diluting the sol gel precursor solution with water.

Corrosion protection data for the polytitanosiloxane and polyzirconicsiloxane coated substrates were obtained from the polarization curves for PMS coated FPL etched aluminum samples upon exposure to an aerated 0.5M sodium chloride solution at 25°C . To evaluate the protective performance of the coatings, the corrosion potential (E_{Corr}) and corrosion current (I_{Corr}) were determined for the polarization curves. E_{Corr} is defined as the potential at the transition point from cathodic to anodic polarization curves. I_{Corr} values were measured by extrapolation of the cathodic Tafel slope. These results are summarized in Table 5.

TABLE 5

Corrosion Potential, E_{Corr} and Corrosion Current, I_{Corr} Values for PMS-Coated and Uncoated Aluminum Specimens		
Coating Systems, (TSPDI/M($\text{OC}_3\text{H}_7)_4$ or 3)	E_{Corr}^*	I_{Corr} μA
Uncoated (blank)	-0.725	2.5
PS (100/0)	-0.695	1.8
PZS (70/30)	-0.625	7.8×10^{-1}
PZS (50/50)	-0.710	1.5
PTS (70/30)	-0.589	1.8×10^{-1}
PTS (50/50)	-0.596	1.6×10^{-1}

As seen, the major effect of these PMS coatings on the corrosion protection of aluminum is to move the E_{Corr} value to less negative potentials and to reduce the cathodic current (I_{Corr}).

The samples coated with PTS produced significantly higher E_{Corr} values, and significantly lower I_{Corr} values, than the uncoated samples. This strongly suggests that the PTS coating films will serve to provide good corrosion resistance from a sodium chloride solution and will minimize the corrosion rate of the aluminum.

Thus, while there have been described what are the presently contemplated preferred embodiments of the present invention, those skilled in the art will realize that changes and modifications may be made thereto without departing from the scope of the invention, and it is intended to claim all such changes and modifications as fall within the true scope of the invention.

I claim:

1. A coating solution which comprises a monomeric organoalkoxysilane containing an imidazole group, a metal alkoxide and a chlorine containing acid in an alcohol/water medium.

2. The solution of claim 1 wherein the acid is HCl.

3. The solution of claim 1 wherein the alcohol is selected from the group consisting of methanol, ethanol and propanol.

4. The solution of claim 1 comprising 18-35 wt % N[3-(triethoxysilyl)propyl]-4,5-dihydroimidazole, 9-18 wt % $\text{Ti}(\text{OC}_2\text{H}_5)_4$, 21-26 wt % methanol, 13-29 wt % HCl and 14-17 wt % water.

5. The solution of claim 1 wherein the solution has a pH of about 7.5.

6. The solution of claim 5 wherein said pH is adjusted by adding NaOH or KOH.

7. The solution of claim 1 wherein the monomeric organoalkoxysilane is selected from the group consisting of N[3-(triethoxysilyl)propyl] imidazole and N[3-(triethoxysilyl)propyl]-4,5-dihydroimidazole.

8. The solution of claim 1 wherein the metal alkoxide is of the formula $\text{M}(\text{OR})_n$, wherein M is a suitable transition metal; R is CH_3 , C_2H_5 or C_3H_7 and n is 3 or 4.

9. The solution of claim 8 wherein M is selected from the group consisting of Ti, Zr, Ge or Al.

10. The solution of claim 8 wherein the metal alkoxide is selected from the group consisting of $\text{Ti}(\text{OC}_3\text{H}_7)_4$, $\text{Zr}(\text{OC}_3\text{H}_7)_4$, $\text{Ti}(\text{OC}_2\text{H}_5)_4$ and $\text{Al}(\text{OC}_3\text{H}_7)_3$.

11. The solution of claim 1 wherein the amount of acid is sufficient to provide a clear solution.

12. The solution of claim 1 wherein the ratio of monomeric organoalkoxysilane to metal alkoxide is in the range of about 80/20 to about 50/50 by weight.

13. The solution of claim 1 comprising 18-35 wt % N[3-(triethoxysilyl)propyl] imidazole, 9-18 wt % $\text{Ti}(\text{OC}_2\text{H}_5)_4$, 21-26 wt % methanol, 13-29 wt % HCl and 14-17 wt % water.

14. A method for preparing a solution for the fabrication of polymetallicsiloxane coatings which comprises the step of combining a monomeric organoalkoxysilane containing an imidazole group, a metal alkoxide and a chlorine containing acid in an alcohol/water medium.

15. The method of claim 14 wherein the solution has the following weight percentages of substituents 18-35 wt % N[3-(triethoxysilyl)propyl]-4,5-dihydroimidazole, 9-18 wt % $\text{Ti}(\text{OC}_2\text{H}_5)_4$, 21-26 wt % methanol, 13-29 wt % HCl and 14-17 wt % water.

16. The method of claim 14 further comprising adding a pH adjusting agent to the solution.

17. The method of claim 16 wherein the pH adjusting agent is KOH or NaOH.

18. The method of claim 16 wherein sufficient pH adjusting agent is added to adjust the pH to about 7.5.

19. The method of claim 14 wherein the monomeric organoalkoxysilane is selected from the group consisting of N[3-(triethoxysilyl)propyl] imidazole and N[3-(triethoxysilyl)propyl]-4,5-dihydroimidazole.

20. The method of claim 14 wherein the metal alkoxide is of the formula $\text{M}(\text{OR})_n$, wherein M is a suitable transition metal; R is CH_3 , C_2H_5 or C_3H_7 and n is 3 or 4.

21. The method of claim 20 wherein M is selected from the group consisting of Ti, Zr, Ge and Al.

22. The method of claim 14 wherein the alcohol is selected from the group consisting of methanol, ethanol and propanol.

23. The method of claim 14 wherein the acid is HCl.

24. The method of claim 14 wherein the amount of acid is sufficient to provide a clear solution.

25. The method of claim 14 wherein the ratio of monomeric organoalkoxysilane to metal alkoxide is in the range of about 80/20 to about 50/50 by weight.

26. The method of claim 14 wherein the metal alkoxide is selected from the group consisting of $\text{Ti}(\text{OC}_3\text{H}_7)_4$, $\text{Zr}(\text{OC}_3\text{H}_7)_4$, $\text{Ti}(\text{OC}_2\text{H}_5)_4$ and $\text{Al}(\text{OC}_3\text{H}_7)_3$.

27. The method of claim 14 wherein the solution has the following weight percentages of substituents, 18-35 wt % N[3-(triethoxysilyl)propyl] imidazole, 9-18 wt % $\text{Ti}(\text{OC}_2\text{H}_5)_4$, 21-26 wt % methanol, 13-29 wt % HCl and 14-17 wt % water.

* * * * *

40

45

50

55

60

65